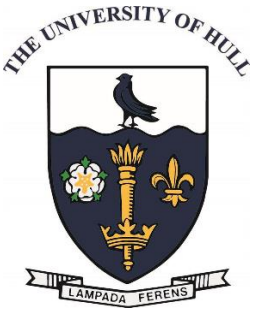

Electrochemical Investigation of Electron-Transfer Cascades for the Development of Solar Energy Conversion Based On Artificial Photosynthesis

Being a Thesis submitted for the Degree of

Doctor of Philosophy (PhD)

In the University of Hull

By

Huda Sami Alhasan

BSc. MSc.

31/10/ 2017

ACKNOWLEDGMENTS

All praises to Allah, who made this thesis possible and gave me the ability to proceed successfully.

I am deeply indebted to my supervisors Dr Jay Wadhawan and Prof. Gillian Greenway for all their advice, provoking thoughts and guidance at every stage of the thesis. I express my heartful thanks to the Iraqi Ministry of Higher Education and Scientific Research (HESR), the Iraqi attaché in London and Ireland, and the University of Babylon for their financial support and encouragement to conduct my study.

I would like to express my sincere gratitude to the Department of Chemistry at the University of Hull for enabling me to pursue postgraduate doctoral training and facilities provided in carrying out this thesis. Special thanks go to Sarah Ord for her constant encouragement and support. I am also thankful to my lab mates for their assistance.

My thanks go to my friends Dr Hassan Al-Kalo, Dr Nadiyah Al-Ahamdy and Nuhu Yidana for their help and advice in all aspects of this work. I owe the deepest appreciation to my best friend Dr Sukinah Al-Husseiny, whose love and encouragement allowed me to complete this hard journey.

I dedicate my thesis to the soul of my father, whose love and inspiration enable me to come out with this work. I would also like to express my gratitude to my mum, my brother Dr Alla, my sisters and all family members for their constant support and encouragement, without their love and support it would have been impossible to complete this work. Finally, I offer my regards and blessings to all those who supported me in any respect during the completion of my PhD study.

ABSTRACT

Natural Photosynthesis process is the source of life; it converts the sunlight into chemical energy. This process takes place in the chloroplast of the green plants in a sophisticated and complex pathway. It involves electron transfer cascades from the photoexcited reaction centre to sustainable energy storage. As a route to develop new chemical systems for artificial photosynthesis in an efficient and fast electron transfer cascade, it is essential to propose three-dimensional molecular ensembles of both electrochemically and photochemically active systems.

This thesis studies the behaviour of using L-cysteine and potassium iodide as electroactive species in a reduction reaction of chlorpromazine hydrochloride on glassy carbon electrodes and rotating glassy carbon disk electrodes with the aid of cyclic voltammetry and linear sweep voltammetry.

The electrochemical characteristics of chlorpromazine hydrochloride (CPZ.HCl) in various concentrations, which induce catalytic oxidation reactions of different concentrations of the electroactive materials, are investigated. The experimental results show that the increase in oxidation peaks current of chlorpromazine hydrochloride depends on the concentrations of L-cysteine and potassium iodide. The current response was enhanced through fast transport *via* a rotating glassy carbon disk electrode. The peak potentials of chlorpromazine hydrochloride in the solution containing L-cysteine shift to more negative values for all concentrations and speeds; similarly for potassium iodide. The electrochemical reaction of chlorpromazine hydrochloride with the electroactive materials determined EC' reactions. The diffusion coefficient for chlorpromazine hydrochloride was found to be 1.28×10^{-6} m^2 s^{-1}. This thesis studies the adsorption and electrochemical investigation of one of the derivatives of chlorophyll – chlorophyllin, at

gold and glassy carbon electrodes. Parameters such as the adsorption time, the electrolyte nature and concentration and chlorophyllin concentration were investigated. The use of chlorophyllin as a redox mediator was examined, with a gold electrode being employed. The importance of gold electrode surface preparation in determining the mechanism of redox was described, and the environment of adsorption process of the different concentrations of chlorophyllin on the surface of the gold electrode had been elucidated in this study. The electrochemical method shows that the cyclic voltammetry responses of studied adsorption chlorophyllin pigment on the gold electrode were more efficient than glassy carbon electrode, with processes being more favourable in aqueous solution.

Third, the oxidation reaction of various concentrations of chlorophyllin is investigated in the bulk solution in the presence of Triton X 100 and potassium iodide. The extraction and identification of chlorophyll in fresh spinach were examined by using thin layer chromatography and UV-visible spectrophotometry techniques. The cyclic voltammetry for this pigment was elucidated in the presence of Triton X 100 and vitamin K_1 at the gold electrode, the mechanism of this reaction was suggested to be EC'.

Lastly, this study has emphasised chlorophyll a and Total chlorophyll (Tchl), based on the effect of electrode materials and diameter, pH, solvent and electrolyte. The inducing of electron transfer of Tchl pigment was examined in presence and absence of vitamin K_1 through light and dark atmosphere. The system of chlorpromazine-lyotropic liquid crystal (CPZ-LLC) was highlighted in this thesis. The effect of parameters such as electrode materials, electrode diameters and CPZ.HCl concentrations in this system have been documented. The self-assembled phase was recorded using polarising optical microscopy and X-ray scattering. The CPZ-LLC system was fabrication into photogalvanic cells. The power conversion efficiency (PCE) of this cell is (0.58%), which is useful and novel.

Table of Contents

LIST OF ABBREVIATIONS

Chapter 1	Abbreviated meaning
AP	Artificial photosynthesis
ATP	Adenosine triphosphate
CVD	Chemical vapour deposition
HER	Hydrogen evolution reaction
HOMO	Highest occupied molecular orbital
LHCII	Light-harvesting complex II
LUMO	Lowest unoccupied molecular orbital
NADPH	Nicotinamide adenine dinucleotide phosphate
NHE	Normal hydrogen electrode
NPS	Natural photosynthesis systems
OER	Oxygen evolution reaction
PEC	Photoelectrochemical
PSI	Photosynthesis I
PSII	Photosynthesis II
PV	Photovoltaic

PVD	Physical vapour deposition
STH	Solar-to-hydrogen
UV	Ultraviolet
Chapter 2	**Abbreviated meaning**
CE	Counter electrode
C_O	Concentration of oxidation
C_R	Reducing concentration
CV	Cyclic voltammetry
EC	Electrochemistry
ET	Electron transfer
IHP	Inner Helmholtz plane
LSV	Linear sweep voltammetry
OHP	Outer Helmholtz plane
RDE	Rotating disk electrode
RE	Reference electrode
WE	Working electrode
Chapter 3	**Abbreviated meaning**
ESR	Electron spin resonance
GCE	Glassy carbon electrode

GPES	General purpose electrochemistry system
SCE	Saturated calomel electrode
SHE	Standard hydrogen electrode
Chapter 4	**Abbreviated meaning**
CPZ.HCl	Chlorpromazine hydrochloride
HPLC	High-performance liquid chromatography
L.Cyst.H	L-cysteine
Chapter 5	**Abbreviated meaning**
CHL	Chlorophyline
Chl a	Chlorophyll a
DI	Deionised water
LHP	Light harvesting pigments
MeCN	Acetonitrile
Chapter 6	**Abbreviated meaning**
DMF	Dimethyl formaldehyde
DMSO	Dimethyl sulfoxide
MWEs	Modified working electron
SWV	Square wave voltammetry
TLC	Thin layer chromatography

TX100	Triton X 100
Chapter 7	**Abbreviated meaning**
AAO	Anodic aluminium oxide
AFM	Atomic force microscopy
CLCs	Calamitic liquid crystals
CLCs	Chiral liquid crystals
CNT	Carbon nanotube
DDR_3	Double data rate type three
$DISP_1$	The first order of disproportion reaction
DLCs	Discotic liquid crystals
DSC	Diffraction scanning calorimetry
DSM	Dynamic scattering mode
emf	electromotive force (V)
FF	Fill factor for PG system
GB	A gigabyte
GM_Z	A gigahertz
ILCs	Ionic liquid crystals
IR	Infra-red
LCD	Liquid crystal display

LCs	Liquid crystals system
LLCPs	Liner liquid crystals
ME	Microelectrode
MHz	Megahertz
MLC	Metallotropic
NMR	Nuclear magnetic resonance
PCE	The power conversion efficiency
POM	Polarising microscopy
PTFE	polytetrafluoroethylene
RAM	Random access memory
SAXS	Small-angle X-ray scattering
SMEC	Scanning microscope of electrochemistry
TBAP	Tetrabutylammonium perchlorate
Tchl	Total chlorophyll
TEM	Transmission electron microscopy
VK1	Vitamin K1
WAXD	Wide angle X-ray scattering

LIST OF SYMBOLS

1. ROMANS SYMBOLS

Symbol	Meaning
Å	Angström (10^{-10} metre)
C	Concentration
$\mathbf{C_{dl}}$	Interfacial (double layer) capacitance
D	Diffusion coefficient ($m^2\ s^{-1}$)
$\boldsymbol{d_s}$	The thickness of a surfactant layer (Å)
E	Equilibrium potential (V)
$\mathbf{E^o}$	Standard potential
F	Faraday's Constant (96485 C mol^{-1})
I	Total current (A)
i	Current (A)
$\mathbf{i_a}$	Anodic current(A)
$\mathbf{i_c}$	Cathodic current(A)
$\boldsymbol{i_{mp}}$	The current at the power point
$\mathbf{i_o}$	Exchange current(A)
$\mathbf{i_p}$	Peak current (A)

i_{sc}	The short circuit current
$\mathbf{j_m}$	The flux due to migration
k	Rate constant
$\mathbf{k_a}$	Anodic rate constant
k_b	Homogeneous rate constant for backward (cm sec)
$\mathbf{k_c}$	Cathodic rate constant
k_D	Rate constant of redox reaction
k_f	Homogeneous rate constant for forwarding (cm sec)
$\mathbf{k_J}$	Kilojoules
$\mathbf{k^o}$	Standard rate constant
n	Number of electrons transferred per mole
N	Number of moles of molecule reacted (mol)
O	Oxidized species
P_{max}	The maximum power of the photogalvanic cell
Q	Charge (C)
$\mathbf{q_m}$	Charge on the electrode surface (C)
$\mathbf{q_o}$	Initial charge
$\mathbf{q_s}$	Charge in the solution (C)

R	Reduced species
R	Gas constant (8.314 J mol^{-1} K^{-1})
$\mathbf{R_{ext}}$	Load resistance
$\mathbf{R_i}$	Resistance (Ω)
$\mathbf{R_s}$	Internal resistance
$\boldsymbol{R_{ext}^{mp}}$	The optimum load in the external circuit
T	Absolute temperature (K)
t	Time (s)
V	Rate of reaction (V)
$\boldsymbol{V_{mp}}$	The terminal potential
$\mathbf{V_o}$	The Faradaic charging of the battery redox chemistry
υ	Scan rate (Vs^{-1})

2. GREEK SYMBOLS

Symbol	Meaning
μ	Ionic mobility ($cm^2\ V^{-1}\ s^{-1}$)
α	Transfer coefficient
β	1- α
δ	Diffusion layer thickness (cm)
η	Overpotential (V)
π	Constant composition
Γ	Surface coverage (mol cm^{-2})
Φ_M	Metal electrode potential (V)
Φ_S	Solution potential (V)
Ω	Resistance
ω	Angular rotation rate (rad sec^{-1})
ψ	Dimensionless rate parameter in CV
λ_f	The kinetic parameter
ξ	The electromotive force of photogalvanic cell

Chapter 1

Photosynthesis system (Natural and Artificial)

This thesis is concerned with the development of electron transfer cascades for light-to-electrical energy harvesting.

Accordingly, this chapter provides an overview of research within this field. It is divided into three sections:

The first section deals with the basics of the photosynthesis process, definition, structure, electron transfer and Z-scheme system.

The second section covers photosynthetic processes, both natural and artificial. The types of artificial photosynthetic process are covered here such as carbon compounds and water splitting.

The last section illustrates light-energy harvesting.

1.1 The natural Photosynthesis Process

In Photosystem, there is a vital phenomenon, which takes place in the chloroplast of the green plants called: Natural Photosynthesis process. Food (carbohydrates) by this process is synthesised for plants using water (H_2O) and carbon dioxide (CO_2) in the presence of solar light. In general, oxygenic photosynthesis has been summarised by the following equation:

$$CO_{2+} + 12H_2O \xrightarrow[Green\ pigment]{Light} 6O_2 + \underset{carbohydrates}{C_6H_{12}O_6}$$

Equation1.1: Photosynthesis process in the green plants

Photosynthesis sometimes is termed "carbon assimilation", which means uptake of carbon into a system. This process produces chemical energy from the light energy, which is stored as carbohydrate (glucose; organic substance). During the photosynthesis process, oxygen and glucose are formed from the raw materials (carbon dioxide and water) in the presence of light. Each molecule of glucose comprises about 686 kcal energy.

In 1727, Stephen Hales was the first scientist to identify the relationship between sunlight and leaves[1,2] and later in 1887 Sachs established that the visible product of photosynthesis process was glucose.[3] The scientists between (1930-1960) discovered from their experiments by measuring the activity of photosynthetic upon lighting with various wavelengths of light (*i.e*. green to far-red light) that there are two photosynthetic processes working together sequentially,[4-6] there are given as follows.

- The first process is photosynthesis I or light reactions, which converts excited energy into chemical energy (NADPH and ATP).
- The second one is photosynthesis II or dark reactions or Calvin-Benson cycle[7], which produces glucose by using the product of the first photosynthetic process. Figure 1.1 shows the electromagnetic spectrum of the visible light.

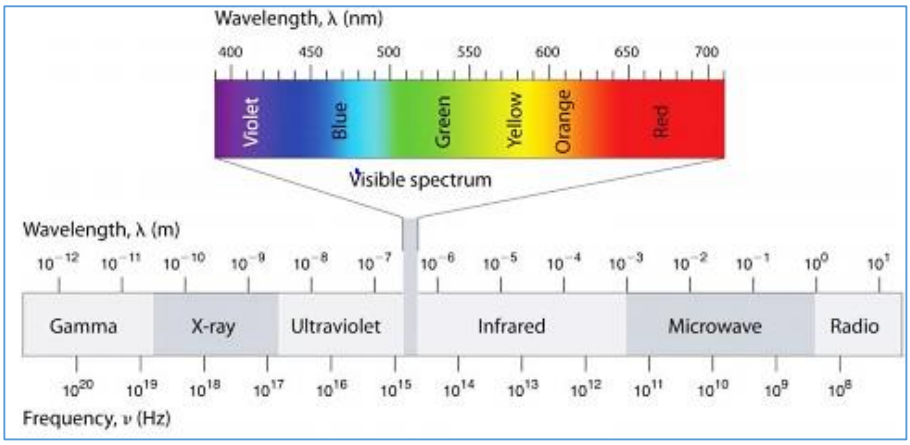

Figure 1.1: The electromagnetic spectrum, highlighting the wavelengths of the visible light adapted from reference[8]

1.1.1 The Photosystem I and II structure and electron transfer

Photosynthesis occurs in organelles known as chloroplasts. The structure of a chloroplast is shown in figure 1.2. There are two-bilayer membranes (outer and inner) covering the chloroplast. Inside the chloroplast region, there are thylakoid membranes, which are covered by the inner membrane (stroma) and served for light reaction. Grana is one of the thylakoids. Inside of the stroma of the chloroplast, there are enzymes that catalyse CO_2 fixation and three other biosynthetic pathways. The stroma consists of protein-pigment complexes such as Photosystem I (PSI), Photosystem II (PSII), cytochrome b_6f (cyt b_6f) light-harvesting complex II (LHCII) and F- adenine nucleotide bound to three phosphates synthase (F-ATPase).[9,10]

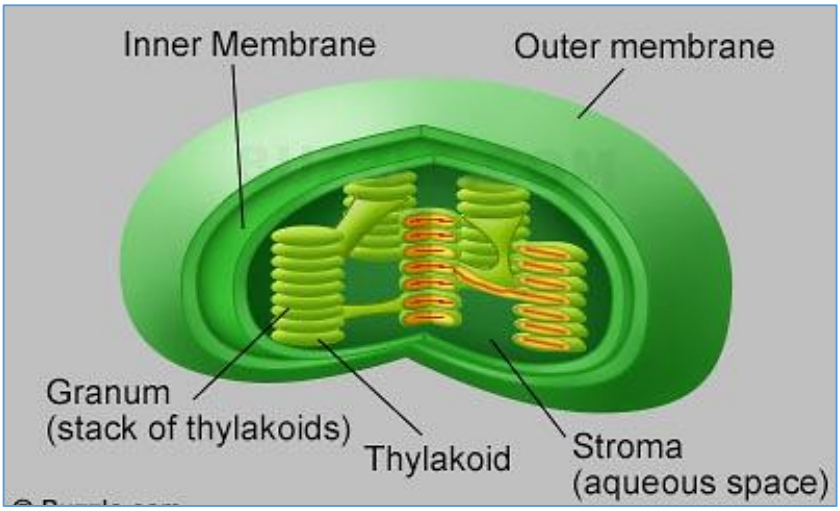

Figure 1.2: The chloroplast function structure, adapted from reference[11]

In both oxygenic Photosystems PSI and PSII, solar light is trapped and used to elicit a series of oxidation-reduction reactions resulting in electrons transfer across the thylakoid membrane *via* a chain of electron carriers.[10,12,13]

The first step of the photosynthesis process produces O_2 by oxidation of two H_2O molecules. Also, it is enabled by the excited state of the primary electron donor of PSII (the P680). Furthermore, the electrons are passed from PSII to the cytochrome b_6f complex by a mobile plastoquinone pool and then to PSI by the soluble electron carrier proteins plastocyanin (plants and algae) or cytochrome c_6 (cyanobacteria).

In the final step, ferredoxin is reduced by PSI to provide the essential electrons for the reduction of $NADP^+$ to NADPH by the ferredoxin-$NADP^+$ oxidoreductase.

An electrochemical potential is formed across the thylakoid membrane by coupling all the electron transfer process. It is this proton motive force that is used to drive ATP synthesis later. In the stroma, NADPH and ATP cooperate in consequent dark reactions to reduce CO_2 to carbohydrates.[10,12,13] Figure 1.3 elucidates the photosynthetic reactions.

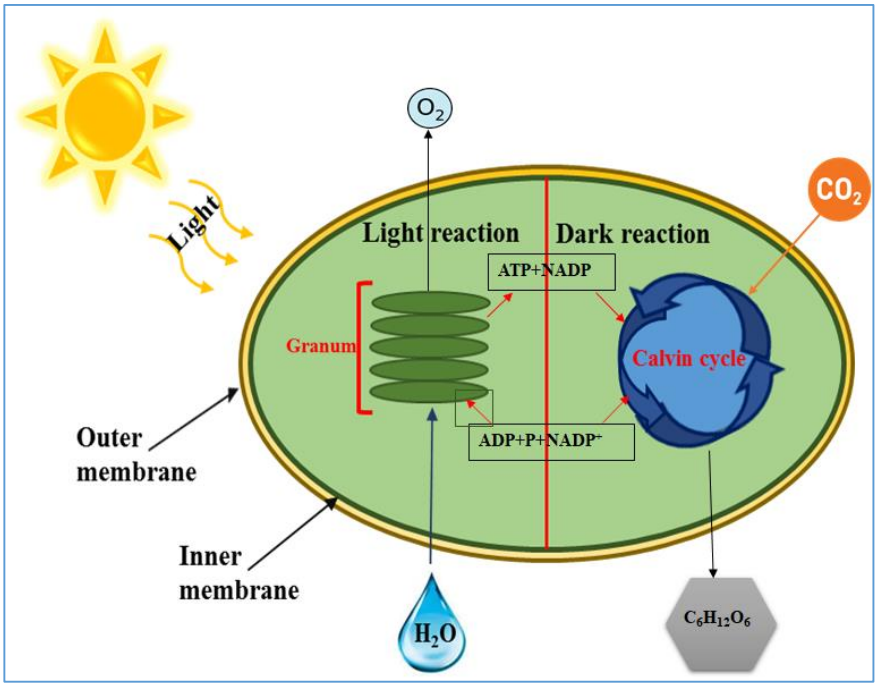

Figure 1.3: A diagram of the Photosynthesis I and II reactions, adapted from reference[14]

1.1.2 The required steps of converting light energy into chemical energy

In natural photosynthesis, the conversion process of sunlight to chemical energy in plants involves four main steps.[15,16]

1. Light absorption: the electromagnetic radiation (photon) is absorbed and concentrated in antenna molecules, so as to capture energy that will be used later in reaction centres.
2. Charge separation: this step happens in the reaction centre of Photosystem II, which uses the sunlight energy to a separate positive charge of a chlorophyll holes from negative charge of the chlorophyll molecules (electron) from each other.
3. Water splitting: the positive charges from the second step are collected, and then used in the splitting step of H_2O molecule into H^+ and O_2 with releasing four electrons.
4. Fuel production: these electrons with photons from sunlight are utilised in a chemical reaction of Photosystem I to produce food for plants (carbohydrates). The following equations are the chemical reactions of water splitting to produce fuel:

$$2H_2O \xrightarrow{4hv} O_2 + 4H^+ + 4e^-$$

Equation1.2

$$CO_2 + 4H^+ + 4e^- \xrightarrow{4hv} (H_2CO) + H_2O$$

Equation1.3

The total photosynthesis reaction, equation 1.4, is combined with both chemical reactions:

$$CO_2 + H_2O \xrightarrow{8hv} (H_2CO) + O_2$$

Equation1.4

The effect of all these steps is important for achieving significant efficiencies of converting solar energy to chemical energy. Until now, no material meets the requirements of converting solar energy, *i.e.*, electronic properties, band gap and band edge position.[17]

1.2 Artificial Photosynthetic Systems

Artificial photosynthesis (AP) is technology that researchers develop in order to try to understand the natural processes of photosynthesis. It mimics natural photosynthesis through applying the similar principles of converting the solar energy into chemical fuels using human-made devices. Artificial Photosynthesis is an efficient and a direct way to convert abundant and natural materials to fuels such as CO_2 and steam produce CO, H_2 and hydrocarbons.[17,18] It is considered as an alternative, sustainable and renewable energy sources for the future.[17] In general, such systems meet some requirements such as efficient, durable and cost-effective for the more sustainable source of renewable energy. Photovoltaic (PV) solar panels are one aspect of AP, which produces electrical energy by using the solar energy.

1.2.1 Z-Scheme Photocatalytic Systems and the Comparison between Natural and Artificial Photosynthesis Systems

Solar conversion, which occurs in the natural photosynthesis systems (NPS), is achieved through a series of step-wise electron transfer processes, which is called the 'Z-scheme' that is demonstrated in figure 1.4. The 'Z-scheme' occurs as the light energy is collected by two Photosystems, *i.e*. Photosystem I (PSI) and Photosystem II (PSII).

First, inside a reaction centre, chlorophyll electrons are excited to higher electronic states through light-harvesting methods. The electrons progress over the two Photosystems involving a number of electron transfer chains. The water splitting happens at a $CaMn_2O_4 \cdot x\ H_2O$ complex at the donor side of PSII. In this process, the charge separation quantum efficiency is close to 100% under (optimal conditions).

For Artificial Photosynthesis Systems (APS), there are two different types of materials. A single light-excitation site, which is placed between an electron donor and an electron acceptor on the other. An excitation site (chromophore) could be either visible-light-

absorbing semiconductor or a dye molecule. Wavelengths of absorption light are adjusted by modifying the structure of dye molecule, *i.e.*, the energy gap between the lowest unoccupied molecular orbital (LUMO) or band and the highest occupied molecular orbital (HOMO) or band. The structure of dye molecule could be modified by designing the semiconductors or molecules with certain electronic structure.

There are a number of requirements for a potential material to be either an electron donor or an electron acceptor. The potential of energy level has to be more negative than the excited state reduction potential of the chromophore and more positive than the water oxidation potential for the electron donor. In addition, the donor must be linked to the chromophore to support a rapid electron transfer reaction prior to the decay of the chromophore-excited state. For the electron acceptor, the potential of energy level must be between the water reduction potential and the chromophore excited state oxidation potential. Water splitting, co-catalysts are usually introduced to induce the reaction.[18]

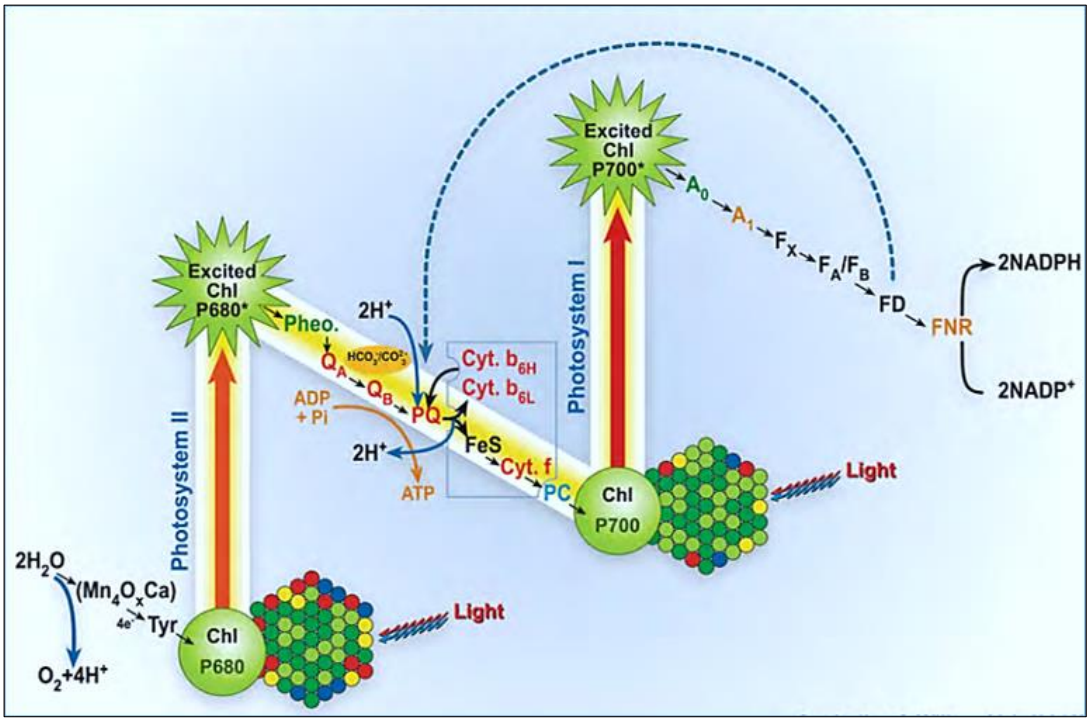

Figure 1.4: Z-Scheme of Electron Transport, adapted from reference [19]

1.2.2 Types of artificial photosynthesis systems

This section focuses on the kinds of artificial photosynthesis such as carbon dioxide and water splitting and the comparison between them.

1.2.2.1 Artificial Photosynthesis with Carbon Compound Production

A high-density fuel is a preferable material for power generation and transportation, such as carbon compounds fuel. Carbon compounds are considered an alternative fuel to petrochemicals. It is a carbon source for renewable polymers, plastics and solvent. Carbon dioxide is an excellent source of carbon compounds fuel.

Reduction of CO_2 in the presence of sunlight is an example of converting the solar energy into chemical energy. The photoreduction of CO_2 involves reduction of the C=O bonds into C–H bonds and forms carbon compounds, such as methane, methanol, CO and other higher hydrocarbons.[20,21]

Despite various attempts, using numerous reaction conditions and achieving different products, this process is still challenging.[22-24] Halmann, in 1978, first reported CO_2 reduction by using photocatalysis. When CO_2 was bubbled over a p-type GaP cathode illuminated with Hg lamp and single crystal through an electrochemical cell, formic acid, formaldehyde and methanol were formed as products.[17]

Mimicking this procedure would require the production of fuel feedstock that is far from depending on oil, coal and natural gas. In other words, the utilising of CO_2 would reduce its emissions on the environmental. Figure 1.5 shows the utilisation of CO_2 that emissions from factory to solar fuels and renewable alkanes during the photocatalytic reduction process. [25]

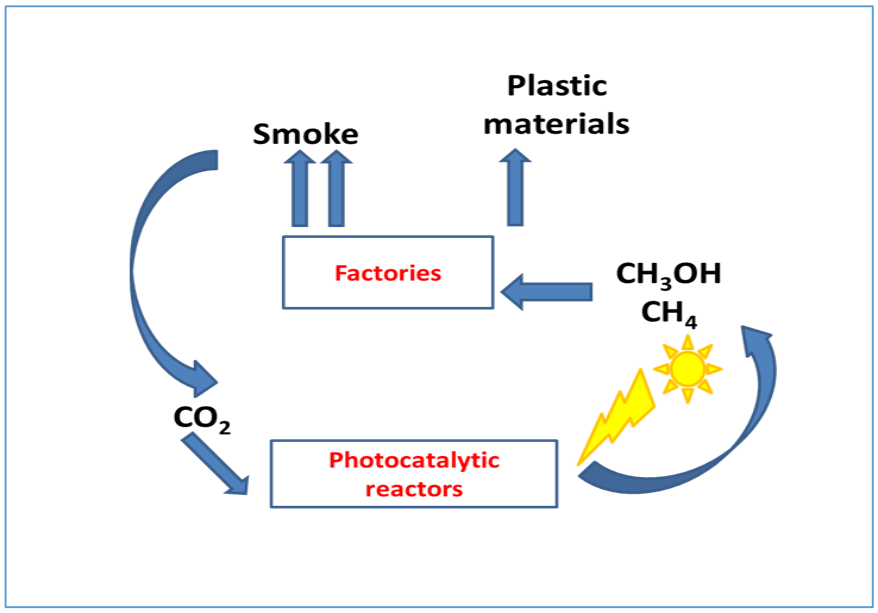

Figure 1.5: The route of CO_2 through the photocatalytic reduction of CO_2, adapted from reference[25]

Some materials have been investigated for over 40 years. Currently, there is much work on nanotechnological materials. These new materials include the modification of the physicochemical properties of various semiconductor materials such as TiO_2, g-C_3N_4, TaON, $BiVO_4$, Ta_3N_5, $SrTiO_3$, Ag_3PO_4, CdS. It is reported that for different oxidation-reduction reactions, the photocatalysts process harnesses solar energy directly.[26]

Considerable attention has been directed to TiO_2, for it has been considered as "golden" photocatalyst. The most published work dedicated to heterogeneous photocatalysis TiO_2 due to its chemical stability, high inertness chemically, low-cost and limited toxicity. Nevertheless, Anatase TiO_2 has a large bandgap, *i.e.*, 3.2 eV that limits the exploitation of broad spectrum of solar light. This spectrum is ultraviolet, which incomes 4% of the solar spectrum. In other words, the solar spectra were utilised in much lower quantum efficiencies. There were two approaches to overcome used limitation and enrich the photocatalytic efficiency of titanium dioxide under the visible light that is equal 43% of the solar light. Regarding titania materials: the band gap, band structure, optical properties and available surface area for photo-induced reactions need to control. The other approach

has modified the strategies of utilising TiO_2 involving surface sensitisation, doping, a hybrid with carbon and other semiconductors, nanostructuring and introducing defects or amorphous disorder layers.[26] Nevertheless, no available material meets all requirements of the Artificial Photosynthesis, *i.e.*, stability, high visible-light quantum efficiency, stability, cost-effective and safety[26]. Consequently, it is essential to drive semiconductor materials under the visible light as well as build efficient systems with architectures for energy source and eco-friendly solution.

In 2009, Wang and his assistants exposed the photocatalytic oxygen and hydrogen progression over graphite-carbon nitride (g-C_3N_4) firstly. The later material has seven different phases, *i.e.*, pseudo-cubic C_3N_4, cubic C_3N_4, α-C_3N_4, β-C_3N_4 and g-C_3N_4.

g-C_3N_4, *i.e.*, graphite is the most stable form of C_3N_4 under ambient conditions. G-C_3N_4 is classified as a metal-free polymer n-type semiconductor, a 2-D π-conjugated polymeric and mild bandgap 2.7 eV. Due to these possessions with promising physicochemical properties, for instance, unique optical, electric and structural properties, g-C_3N_4-based materials became a new caste of multi- practical nano-platforms for catalytic, electronic and energy applications. Thus, the photocatalysts of g-C_3N_4 became more interested universal.

Moreover, g-C_3N_4-based nanostructures are perfect applicants through different energy and photocatalytic environmental purposes, for example, carbon dioxide reduction, degradation of contaminants and photocatalytic water (oxidation and reduction).[26,27]

g-C_3N_4 has been synthesised by using some approaches to different structure and physicochemical properties, for example, chemical vapour deposition (CVD), physical vapour deposition (PVD), solvothermal, isothermal synthesis, solid state, sonochemical, single step nitridation and thermal condensation. Thermal condensation method is a preferable for preparation, for it is a simple procedure, cost-effective and abundant starter

materials. Moreover, nitrogen-rich compounds have been used as starter materials in thermal condensation method, for example, cyanamide, urea, dicyanamide, thiourea and trit isocyanuric acid.[27]

Pure g-C_3N_4 has lower photocatalytic efficiency and low conductivity. Through modifying g-C_3N_4 by using polymers, dyes and surface complexes, thus the photoactivity of g-C_3N_4, visible light utilisation and charge separation will be enhanced. Regarding improving photocatalytic activity of g-C_3N_4, heterostructures (non-metal and metal doping) have been introduced into this material. The examples of this improvement were hybridising with carbon nanomaterials, metal deposition and coupling with other semiconductors.[27-29]

M. Li *et al.*, in 2017 reported the novel core/shell structured of the $LaPO_4$/g-C_3N_4 nanocomposite was synthesised by the facile hydrothermal method. The photocatalytic activity of this nanocomposite was enhanced without the presence of noble metal co-catalyst. It is supposed that the attribution due to a synergic project effect between $LaPO_4$ and g-C_3N_4 origination from their well-matched band structures. In this approach, it is enhancement the light sensitivity and effectively accelerates of the charge transfer or separation through the interfacing bond tCN/$LaPO_4$. $LaPO_4$/g-C_3N_4 nanocomposite has potential in solar fuel production and CO_2 photocatalytic reduction.[30]

F. Raziq *et al.* studied the heterogeneous photocatalysts activities of tin oxide (SO)/ Boron and phosphorus Co-doped CN nanosheets (B-P-CN). The CN-based photocatalysts involved co-doping B and P, and then coupling SO. This novel work showed that using SO/B-P-CN nanocomposite was enhanced visible-light activities efficiently through converting CO_2 compound contained approximately nine times water molecule to CH_4 compound, as well as for phenol and acetaldehyde degradation~7 times when it was compared with the bare of CN nano-sheets. Additionally, a highly produced of OH

radicals on that nanocomposite was responsible for the significantly improved photocatalysis activity. This was interpreted by visible-light absorption, which was extended from 460 nm to 550 nm as a result of co-doping B-P, charge separation via the dopant-induced surface states promoted and coupled SO. SO/B-P-CN is a promising in the utilisation of solar energy in environmental applications.[31]

B. Zhu *et al.* synthesised g-C_3N_4/Ag_2WO_4 composite photocatalysts using *in situ* precipitation of β-Ag_2WO_4 nanoparticles (NPs) on the surface of g-C_3N_4 nanosheets. g-C_3N_4/Ag_2WO_4 composite has excellent photocatalysts activity for methyl orange (MO) degradation. The study showed that the degradation rates were 95%, 71% and 42% in the presence of g-C_3N_4/Ag_2WO_4, Ag_2WO_4 and g-C_3N_4, respectively. The existence of β-Ag_2WO_4 improved the light absorption as well as an efficient decrease in the rearrangement of photoinduced electron-hole pairs.[32]

1.2.2.2 Studying Artificial Photosynthesis with Water-Splitting Approach.

The second approach of Artificial Photosynthesis is the water-splitting approach. Water molecules can be split into oxygen O_2 and hydrogen H_2 as seen in equation 1.5. This method could be referred to hydrogen and oxygen evolution reactions (HER and OER), respectively. Water-splitting approach is a more attractive approach to generate energy from solar energy than the reduction of CO_2.

There is a limited CO_2 reduction yield for mainly systems. In solar energy application, even though there was an extensive usage of CO_2 atmosphere to generate fuels, hydrogen feedstock met the artificial photosynthesis requirement, for its availability was more than CO_2 in the air. Therefore, the best raw materials are signified a synthetic, sustainable, and pure fuel. Conversely, hydrogen gas generated from water splitting could be stocked (see equation 1.5). Hydrogen could be oxidised into create energy, *i.e*. carbon-neutral fuel and regenerate water.[17,33]

$$2H_2O \rightarrow O_2 + 2H_2$$

Equation1.5

Another reason for preferring the water-splitting approach is that seawater is nontoxic and most resource on earth. It is sustainable and a clean supply of energy for future. A number of methodologies and materials have been reported in the development of artificial photosynthesis using water-splitting approach. Semiconducting catalysts that are photocatalytic have shown the potential for water splitting into O_2 and H_2. Those photocatalytic have attracted interest from both environmental concerns and economy as it is renewable power.

In 1972, Fujishima and Honda reported the potential of semiconductor materials; *i.e.*, TiO_2 in the electrochemical photolysis of water.[34,35] Their investigation initiated the advanced application of the semiconducting photocatalysts in energy and environmental applications.[36] Water splitting is a thermodynamically uphill process. It is not a spontaneous process and requires input energy about 286 kJ mol^{-1}at room temperature and pressure.[37,33] The water splitting over semiconductor photocatalysts is achieved through three main steps:

1. Photons absorption: only those photons with energies exceeding the semiconductor band gap will be observed by the semiconductors, resulting in the electron (e^-) and hole (h^+) pairs being formed.
2. Charge separation: this step involved the passing of the photogenerated carriers that resulted in the first step in the particles of the semiconductor.
3. Chemical reactions on the surface: these steps are followed by chemical reactions between these photons and different compounds such as H_2O. It might recombine holes with electrons without any contribution of chemical reactions.[36]

Water splitting into O_2 and H_2 using photocatalysts materials have efficacies that depend on both crystal structure and the particle size of semiconductor materials. Therefore, the preparation conditions for the elements requires significant consideration.[36,38,39]There are other requirements for photocatalytic water regarding band levels and band gaps. Water reduction reaction, the potential of the conduction band gap should be less than 0.0 V *vs* NHE (H^+/H_2), and the potential of the valence band should be more than 1.23 V that corresponds to light of 1008 nm. Visible light has much lower photonic energy than ultraviolet light. Therefore, hydrogen production *via* solar water splitting is preferable for ultraviolet-based photocatalysts than visible light-based ones.

Studies have been conducted for photocatalysts material under ultraviolet light irradiation. However, the total solar irradiation consists of 4% of ultraviolet light (<400 nm), 53% of visible light (400–800 nm) and 43% of infrared light (>800 nm). Due to the fact that ultraviolet light has a small portion of solar energy, it is indispensable to manufacture active photocatalysts to get the visible/infrared light to improve the efficiency of their low solar-to-hydrogen conversion over a broad spectral range.[37]

1.2.2.2.1 Photoelectrochemical (PEC) water splitting

The photoelectrochemical (PEC), water splitting approach, is a preferable approach to solar energy conversion for some reasons, *i.e.*, a direct conversion, a single-step process for generating hydrogen, cost-effective, long-lasting and environmentally friendly.[40]

In the photoelectrochemical (PEC), water splitting requires electrical charges, *i.e.*, electron-hole pairs of catalysts under the solar light.[41] The PEC water splitting has three electrodes, which is a build-up of four critical components: a photoelectrode (with one semiconductor), a counter electrode, a reference electrode and an electrolyte.[41]

A large number of materials have been reported in the development of photoelectrochemical water splitting such as Fe_2O_3, $BiVO_4$ and WO_3. The modification to these chemical structures includes one of the following methods: doping, the formation of heterojunctions, swift heavy ion irradiation and co-catalyst deposition.[37]

Banerjee *et al*. reported the surface modification of Fe_2O_3 to enhance the oxygen evolution reaction during PEC water splitting. Co-Ac/Ti–Fe_2O_3 photo-anode systems were fabricated. The Fe_2O_3 was doping *via* Ti then Co-Ac co-catalyst was deposited on the base semiconductor. The figures showed that the catalyst-modified photo-anode systems at two different pHs are more efficient than the unmodified systems.[41] Fang *et al*. demonstrated the novel dodecahedron $Bi_xY_{1-x}VO_4$ solid solution, which has a new dodecahedron shape with two exposed facets. The results display a highly efficient photocatalytic activity in response to the crystal system.[42]

Sun *et al*. developed an uncompleted procedure to fabricate TiO_2 NTs/WO_3 composite electrode. 3D hierarchical structure of WO_3 was grown into the TiO_2 nanotube arrays. This composite showed the highest photocurrent density under visible light and the high photocurrent density under simulated solar irradiation.[43]

1.2.2.3 Photovoltaic-photoelectrochemical (PV-PEC) hybrid systems

The conversion of solar light to electrical energy is achieved *via* a photovoltaic system. Solar light can be converted to energy through hydrogen production, *i.e*., solar-to-hydrogen (STH). The new generation of the conversion of solar light into energy is the combination of the photovoltaic system and the electrolytic water splitting. The efficiency of hybrid systems has been investigated with three different approaches.

The first system is photovoltaic with integrated PEC devices; the second is photovoltaic with partially integrated PEC devices. The last system is photovoltaic with non-integrated PEC devices. The photovoltaic system with integrated PEC devices has the highest

efficiency of solar hydrogen production. Khaselev *et al*. were the pioneers in reporting the first monolithic PV-PEC device; the $GaInP_2$/GaAs tandem cell was used. The effectiveness of solar-to-hydrogen was more than 10%. In recent years, Bonke *et al*. reported a high efficiency of the solar-to-hydrogen system. A multi-junction GaInP/GaAs/Ge solar cell and Ni electrodes were fabricated; more than 20% efficiency of the system. The effectiveness of the photovoltaic solar cell and electro-catalyst was used to measure the efficiency of PV-PEC hybrid system.[37,44]

1.3 Energy system

This section presents the types of energy that were used in daily life and how they were developed to achieve sustainable and clean energy in the ecosystem.

1.3.1 Conventional and non-conventional (renewable energy)

Energy plays a crucial role in improving and driving man's life in various forms: conventional and non-conventional energy (renewable energy). Conventional energy sources are based on fossil fuel hydraulic and nuclear energy. Although it provides around 60% of the current total the world energy request, it causes a severe damaging to our planet natural resources and human health. Evidently, the future growth in the energy sector needs sustainability in the new system of renewables and the increase in electricity generating.

Renewable energy resources are one of the possible solutions, which refer to energy sources: (hydro, wind, and tidal power) or solar cell technologies offer many opportunities to supplement world energy demands.[45] These energies currently supply between 15 and 20 percent of world's total energy demand. All forms of renewable energy come either directly from the sun or indirectly from its impacts on the earth. As a result of creating long-term sustainable energy these human-made energy name renewable.[46] In

addition, solar cells address the long-term power concerns with minimal environmental degradation.[47]

1.3.2 The history of solar technologies

Solar technologies refer to the use of light or the direct heat of the sun to generate energy for industrial processes, transportation, and buildings.[48] Using solar energy offers a clean, climate-friendly and infinite energy resource to human life, which will spread over the universe.[49] The technologies of sun energy are classified into passive and active. The first form collects the energy without converting the heat or light to other types such as the system of heating or lighting, which is used in building design. The second form of solar energy stores or converts energy for other applications, which is classified into two groups[48,50]:

1. Photovoltaic cells (PV): the photovoltaic (PV) cell or related devices are the most valuable method for direct conversion of the sunlight energy into electrical energy. The device, which is used for this process is called solar cells. The first attempt to generate electric energy was in 1954 at the Bell Telephone Laboratories in the United States of America using a p- junction type solar cell with ~ 6% efficiency.

It was later followed by utilising semiconductor as PV cells in the space programme. The principle of a conventional process in PV cell depends on excited electrons through the absorption of photons and energy, which consequently lose this energy as heat.[51,52] There are two types of PV generation technologies:

- The first generation of PV cell is crystalline-silicon (c-Si) either single crystalline (sc-Si) or multi-crystalline (mc-Si).
- The second generation of PV cell is thin film technologies, which involve a variety of different semiconductor materials such as cadmium telluride (CdTe), unstructured silicon [amorphous (a-Si) and micro-morph silicon (μ-Si)], copper indium selenide

(CIS) and copper indium gallium diselenidz (CIGS). There is another generation under development and still not widely marketing such as organic and concentrating PV cells.

2. Solar thermal energy: solar thermal technologies collect the incoming solar heat, converts it into heat energy for useful heating application or electricity generation. Thus, thermal is divided into two categories:

- Solar thermal non-electric: the applications for this type of agricultural drying, solar (water and air) heaters, solar cookers, and solar cooling systems.[53]
- Solar thermal: it uses solar heat to produce steam for electricity generation.

The history of solar energy technologies goes far back. It is noticed that upon the steam revolution between 1860 and the First World War series of machinery were developed these making use of the solar' s heat and through that engines and irrigation pumps were run.[54] In 1954 solar PV cells were invented at Bell Labs, which had been used to generate electricity in space satellites since the 1950s.[55]

In the 1970s, PV cell witnessed an interest in the development and marketable of solar energy technologies through the oil-shock. The 1970s and early 1980s experienced a decrease in the oil prices and a shortage of a sustained policy collaboration, which was reflected in the collapse of the solar manufacturing.[48] According to investment analysts, photovoltaic witnessed significant increasing after 2000 because of increasing the cell efficiency, beneficial policy and reducing the capital costs.[56] In the coming year, it is predicted that solar energy will gain a high level in a particular the future of PV system.[57]

1.4 Objectives of this study

There are two critical questions that this thesis aims to study.

1. Is it possible to exploit liquid nanotechnology to develop an electron-transfer chain that may mimic the first stages of photosynthesis, using natural materials, such as chlorophyll (or its derivatives)?
2. Is it possible to use self-assembled systems for light-to-electrical energy harvesting *via* photogalvanic cell?

The approach is taken to answering thesis questions:

The first study was the electrochemical behaviour of active materials and their electron transfer cascade on a working electrode as well as in the bulk solution.

The second study was the conditions of forming LCs, which can be used in a photogalvanic cell under appropriate light. The thesis is organised as follows.

- Chapter one presents the photosynthesis system and solar energy.
- Chapter two provides an outline of the fundamental and experimental principles underpinning the electrochemical processes.
- Chapter three describes the electrochemical cell and techniques.
- Chapter four investigates the electrochemical attitude of chlorpromazine hydrochloride and the influence of some electroactive species on it.
- Chapter five and six discuss the electron transfer cascade in homogeneous and heterogeneous processes of chlorophyll and its derivative.
- Chapter seven describes the liquid crystals system of chlorpromazine hydrochloride shows the using of chlorpromazine gel in the photogalvanic cell.
- Chapter eight outlines a summary of this work.
- Chapter nine is an appendix.

1.5 References

(1) Rabinowitch, E. An unfolding discovery. *Proceedings of the National Academy of Sciences of the United States of America* **1971**, *68*, pp 2875.

(2) Bard, A. J.; Faulkner, L. R.; Leddy, J.; Zoski, C. G.: *Electrochemical methods: fundamentals and applications*; Wiley New York, **1980**; Vol. 2.

(3) Hangarter, R. P.; Gest, H. Pictorial demonstrations of photosynthesis. *Photosynth. Res.*, **2004**, *80*, pp 421-425.

(4) Emerson, R., Chalmers, R., and Cederstrand, C. Some factors influencing the longwave limit of photosynthesis. 1957.

(5) Hill, R., and Bendall, F. Function of two cytochrome components in chloroplasts: A working hypothesis. *Nature.*, **1960**, *186*, pp 136-137.

(6) Duysens, L. M. N. Two photochemical systems in photosynthesis. *Nature.*, **1961**, *190*, pp 510-511.

(7) Ke, B.: *Photosynthesis photobiochemistry and photobiophysics*; Springer Science & Business Media, **2001**; Vol. 10.

(8) Averill, B.; Eldredge, P.: *General Chemistry: Principles, Patterns, and Applications*; The Saylor Foundation, **2011**.

(9) Hoerner, L. J. Photosynthetic Solar Cells Using Chlorophyll and the Applications Towards Energy Sustainability. Doctoral dissertation. University of South Florida St. Petersburg, 2013.

(10) Nelson, N.-S., Adam. The complex architecture of oxygenic photosynthesis. *Nat. Rev. Mol. Cel.l Bio.*, **2004**, *5*, pp 971-982.

(11) Chloroplast: Structure and Function. http://www.buzzle.com/articles/chloroplast-structure-and-function.html (accessed **12/03/ 2015**).

(12) Fromme, P.; Jordan, P.; Krauß, N. Structure of photosystem I. *Biochim. Biophys. Acta, Bioenerg.*, **2001**, *1507*, pp 5-31.

(13) Saenger, W., Jordan, P. and Krauss, N. The assembly of protein subunits and cofactors in photosystem I. *Curr. Opin. Struct. Biol.*, **2002**, *12*, pp 244-254.

(14) Light Emitting Diodes for Indoor Growing Operations: A comparison of traditional lighting and LEDs. https://smartgrowtechnologies.com/wp-content (accessed **11/11 /2015**).

(15) Cogdell, R. J.; Brotosudarmo, T. H.; Gardiner, A. T.; Sanchez, P. M.; Cronin, L. Artificial photosynthesis–solar fuels: current status and future prospects. *Biofuels.*, **2010**, *1*, pp 861-876.

(16) Purchase, R.; Vriend, H.; de Groot, H.; Harmsen, P.; Bos, H.: *Artificial photosynthesis: for the conversion of sunlight to fuel*; Leiden University, **2015**.

(17) Su, J.; Vayssieres, L. A Place in the Sun for Artificial Photosynthesis? *ACS Energy Lett.*, **2016**, *1*, pp 121-135.

(18) Tachibana, Y.; Vayssieres, L.; Durrant, J. R. Artificial photosynthesis for solar water-splitting. *Nat. Photonics.,* **2012**, *6*, pp 511-518.

(19) Jaiswal, S.; Bansal, M.; Roy, S.; Bharati, A.; Padhi, B. Electron flow from water to $NADP^+$ with students acting as molecules in the chain: a Z-scheme drama in a classroom. *Photosynth. Res.,* **2016**, pp 1-9.

(20) Liu, G.; Hoivik, N.; Wang, K.; Jakobsen, H. Engineering TiO_2 nanomaterials for CO_2 conversion/solar fuels. *Sol. Engy. Mat. Solar Cells.,* **2012**, *105*, pp 53-68.

(21) Inoue, T.; Fujishima, A.; Konishi, S.; Honda, K. Photoelectrocatalytic reduction of carbon dioxide in aqueous suspensions of semiconductor powders. *Nature.,* **1979**, *277*, pp 637-638.

(22) Zhang, Q.-H.; Han, W.-D.; Hong, Y.-J.; Yu, J.-G. Photocatalytic reduction of CO_2 with H_2O on Pt-loaded TiO_2 catalyst. *Catal. Today.,* **2009**, *148*, pp 335-340.

(23) Varghese, O. K.; Paulose, M.; LaTempa, T. J.; Grimes, C. A. High-rate solar photocatalytic conversion of CO_2 and water vapour to hydrocarbon fuels. *Nano letters.,* **2009**, *9*, pp 731-737.

(24) Centi, G.; Perathoner, S. Towards solar fuels from water and CO_2. *ChemSusChem.,* **2010**, *3*, pp 195-208.

(25) Chen, D.; Zhang, X.; Lee, A. F. Synthetic strategies to nanostructured photocatalysts for CO_2 reduction to solar fuels and chemicals. *J. Mater. Chem. A.,* **2015**, *3*, pp 14487-14516.

(26) Wen, J.; Xie, J.; Chen, X.; Li, X. A review on g-C_3N_4-based photocatalysts. *Appl. Surf. Sci.,* **2017**, *391, Part B*, pp 72-123.

(27) Mamba, G.; Mishra, A. Graphitic carbon nitride(g-C_3N_4) nanocomposites: A new and exciting generation of visible light driven photocatalysts for environmental pollution remediation. *Appl Catal B-Environ.,* **2016**, *198*, pp 347-377.

(28) Lu, C.; Chen, R.; Wu, X.; Fan, M.; Liu, Y.; Le, Z.; Jiang, S.; Song, S. Boron doped g-C_3N_4 with enhanced photocatalytic UO_2^{2+} reduction performance. *Appl. Surf. Sci.,* **2016**, *360*, pp 1016-1022.

(29) Shi, H.; Chen, G.; Zhang, C.; Zou, Z. Polymeric g-C_3N_4 coupled with $NaNbO_3$ nanowires toward enhanced photocatalytic reduction of CO_2 into renewable fuel. *ACS Catal.,* **2014**, *4*, pp 3637-3643.

(30) Li, M.; Zhang, L.; Fan, X.; Wu, M.; Wang, M.; Cheng, R.; Zhang, L.; Yao, H.; Shi, J. Core-shell $LaPO_4$/g-C_3N_4 nanowires for highly active and selective CO_2 reduction. *Appl. Catal. B-Environ.,* **2017**, *201*, pp 629-635.

(31) Raziq, F.; Qu, Y.; Humayun, M.; Zada, A.; Yu, H.; Jing, L. Synthesis of SnO_2/B-P codoped g-C_3N_4 nanocomposites as efficient cocatalyst-free visible-light photocatalysts for CO_2 conversion and pollutant degradation. *Appl. Catal. B-Environ.,* **2017**, *201*, pp 486-494.

(32) Zhu, B.; Xia, P.; Li, Y.; Ho, W.; Yu, J. Fabrication and photocatalytic activity enhanced mechanism of direct Z-scheme g-C_3N_4/Ag_2WO_4 photocatalyst. *Appl. Surf. Sci.,* **2017**, *391, Part B*, pp 175-183.

(33) Roger, I.; Shipman, M. A.; Symes, M. D. Earth-abundant catalysts for electrochemical and photoelectrochemical water splitting. *Nat. Rev. Chem.*, **2017**, *1*, pp 1-13.

(34) Fujishima, A.; Honda, K. Electrochemical Photolysis of Water at a Semiconductor Electrode. *Nature.*, **1972**, *238*, pp 37-38.

(35) Fujishima, A.; Honda, K. Electrochemical Evidence for the Mechanism of the Primary Stage of Photosynthesis. *Bull. Chem. Soc. Jpn.*, **1971**, *44*, pp 1148-1150.

(36) Ismail, A. A.; Bahnemann, D. W. Photochemical splitting of water for hydrogen production by photocatalysis: A review. *A review. Sol. Energy Mater. Sol. Cells.*, **2014**, *128*, pp 85-101.

(37) Tee, S. Y.; Win, K. Y.; Teo, W. S.; Koh, L.-D.; Liu, S.; Teng, C. P.; Han, M.-Y. Recent Progress in Energy-Driven Water Splitting. *Adv. Sci.*, **2017**, *4*, pp 1600337.

(38) Tong, H.; Ouyang, S.; Bi, Y.; Umezawa, N.; Oshikiri, M.; Ye, J. Nano-photocatalytic Materials: Possibilities and Challenges. *Adv. Mater.*, **2012**, *24*, pp 229-251.

(39) Méndez-Ramos, J.; Ruiz-Morales, J. C.; Acosta-Mora, P.; del-Castillo, J.; Yanes, A. C. Rare-earth doped nano-glass-ceramics for extending spectral response of water-splitting semiconductor electrodes by high intense UV-blue up-conversion: Turning the sun into blue. *Power Sour.*, **2013**, *238*, pp 313-317.

(40) Yang, X.; Liu, R.; He, Y.; Thorne, J.; Zheng, Z.; Wang, D. Enabling practical electrocatalyst-assisted photoelectron-chemical water splitting with earth abundant materials. *Nano Res.*, **2015**, *8*, pp 56-81.

(41) Banerjee, A.; Mondal, B.; Verma, A.; Satsangi, V. R.; Shrivastav, R.; Dey, A.; Dass, S. Enhancing efficiency of Fe_2O_3 for robust and proficient solar water splitting using a highly dispersed bioinspired catalyst. *J. Catal.*, **2017**, *352*, pp 83-92.

(42) Fang, W.; Jiang, Z.; Yu, L.; Liu, H.; Shangguan, W.; Terashima, C.; Fujishima, A. Novel dodecahedron $BiVO_4$:YVO_4 solid solution with enhanced charge separation on adjacent exposed facets for highly efficient overall water splitting. *J. Catal.*, **2017**, *352*, pp 155-159.

(43) Sun, W.; Wang, D.; Rahman, Z. U.; Wei, N.; Chen, S. 3D hierarchical WO_3 grown on TiO_2 nanotube arrays and their photoelectrochemical performance for water splitting. *J. Alloys Compd.*, **2017**, *695*, pp 2154-2159.

(44) Li, R. Latest progress in hydrogen production from solar water splitting via photocatalysis, photoelectrochemical, and photovoltaic-photoelectrochemical solutions. *Chin. J. Catal.*, **2017**, *38*, pp 5-12.

(45) Martinot, E.; Chaurey, A.; Lew, D.; Moreira, J. R.; Wamukonya, N. Renewable energy markets in developing countries*. *Annu. Rev. Energy Environ.*, **2002**, *27*, pp 309-348.

(46) Dincer, I. Renewable energy and sustainable development: a crucial review. *Renew Sust Energ Rev.*, **2000**, *4*, pp 157-175.

(47) Connors, S. R. *Issues in energy and sustainable development*: Energy Laboratory, Massachusetts Institute of Technology

1998.

(48) Bradford, T. Solar revolution: the economic transformation of the global energy industry. *Mit Press.*, **2006**, *1*.

(49) Armaroli, N.; Balzani, V. The future of energy supply: challenges and opportunities. *Angew. Chem. Int. Ed.*, **2007**, *46*, pp 52-66.

(50) van Helden, W. G. J.; van Zolingen, R. J. C.; Zondag, H. A. PV thermal systems: PV panels supplying renewable electricity and heat. *rog. Photovolt: Res. Appl.*, **2004**, *12*, pp 415-426.

(51) Chapin, D. M.; Fuller, C.; Pearson, G. A new silicon p‐n junction photocell for converting solar radiation into electrical power. *J. Appl. Phys.*, **1954**, *25*, pp 676-677.

(52) Sørensen, A.; Sutheeshna, B. S. Tourism and the Informal Sector. *Tourism Development Revisited.*, **2008**, pp 88.

(53) Timilsina, G. R.; Kurdgelashvili, L.; Narbel, P. A. A review of solar energy: markets, economics and policies. **2011**.

(54) Tomlinson, L. O.; Smith, R. W.: Steam cycle for combined cycle with steam cooled gas turbine. Google Patents, **1995**.

(55) Hoogwijk, M. M. On the global and regional potential of renewable energy sources. " PhD diss", **2004**.

(56) Pinkse, J.; Van den Buuse, D. The development and commercialization of solar PV technology in the oil industry. *Energy Policy.*, **2012**, *40*, pp 11-20.

(57) Arnulf, A.-W. *PV Status Report 2016*; EUR - Scientific and Technical Research Reports for Union, P. O. o. t. E.**2016**.

Chapter 2

Electrochemistry (EC)

This introductory chapter furnishes an outline of the fundamental principles and theoretical aspects of electrochemistry and the techniques used in this work. Specifically, provide an overview of the basic concepts of electrochemistry including the Nernst equation, Faradaic law and the setup of an electrochemical cell. The chapter discusses electrode kinetics and experimental techniques, such as linear sweep voltammetry, cyclic voltammetry, hydrodynamic method and chronoamperometry.

2.1 Basic Concepts of Electrochemistry

Electrochemistry is a branch of chemistry that studies chemical reactions which occur in a solution across an interface between an electric conductor (the electrode: a metal or a semiconductor)[1] and an ionic conductor (the electrolyte). Both of these reactions involve charge transfer across the electrode and the electrolyte interface.

If the chemical reaction is driven by an externally applied voltage or, if a redox reaction produces electrical energy from chemical species, as in a battery. In contrast, chemical reactions where electrons are transferred between molecules in homogeneous solution are called redox (oxidation-reduction) reactions.[2] In general, electrochemistry deals with redox reactions when connected to an external electric circuit. There are three essential advantages of using electrochemical methods over other procedures.

1. Electrochemical methods make it possible to determine the concentration of a particular oxidation state of an element, whereas as most other analytical techniques can reveal only the total element concentration.
2. Inexpensive instrumentation.
3. These methods provide information for about the activities of chemical species rather than their concentration.[3]

2.1.1 Nernst equation and Faradaic law

Dynamic electrochemistry is concerned with the reactions between electrodes and electroactive species during electrolytic processes when electrons are exchanged across a solid/liquid interface resulting in a redox reaction that is driven by the size of the applied potential (E) imposed across the electrode/electrolyte interface. It is the exchange of charge over the interface that gives rise to current flow. For simplicity, a single electron transfer reaction is considered, see equation 2.1:

$$O + ne^{-} \underset{k_a}{\overset{k_c}{\rightleftarrows}} R$$

Equation2.1

Where O corresponds to the oxidised species, R corresponds to the reduced species and n is the number of electrons which are transferred. At equilibrium, when k_a and k_c are equal, the Nernst equation gives the relationship between E of an electrode and the concentration of O and R, equation 2.2:

$$E = E^{o} + \frac{RT}{nF} \ln\left(\frac{C_O}{C_R}\right)$$

Equation2.2

Where E^o is the redox potential for the reaction when all species have unit concentration, R is the gas constant (8.314 JK^{-1} mol^{-1}), T is the absolute temperature, while n is the number of electrons transferred, F is the Faraday constant (96484.6 $C.mol^{-1}$), and C_O/ C_R are the concentrations of the O and R species. The Nernst equation is used to study the thermodynamic concept of the redox reaction; therefore, electron transfer is easy to understand.[4]

2.1.2 Faradaic and non-Faradaic currents

At an electrode surface, two fundamental electrochemical processes can be distinguished (Faradaic and non-Faradaic processes) that can transfer currents across the electrodes/analytes phase boundary. The process that includes electron transfer directly by way of the oxidation-reduction reaction, thus changing the oxidation state of the analyte, is called a "Faradic current" due to being governed by Faraday's Law[3], equation 2.3.

$$Q = nFN$$

Equation2.3

Here Q is the charge, F is Faraday's constant (96484.6 C mol^{-1}), *n* is the number of electrons transferred per mole of product, and N is the number of moles of molecule reacted. Electrochemical cells will only enable the Faradaic processes to occur provided the applied potential exceeds a certain threshold. At lower potentials, however, a variety of non-Faradaic processes will occur. Such processes include adsorption and desorption processes that may take place on the electrode.[5]

Non-Faradaic currents are also called capacitive currents or double-layer currents. They occur whenever the electrical charges from both the electrode-side and the electrolyte-side without any chemical reactions. They can only happen whenever the applied potential changes in time.

2.1.3 The Interfacial Region and Electrolyte Double Layer

The region, which contains the electrode/electrolyte interface, is called an interfacial region. It plays a vital role regarding electron transfer reactions and the electric potential that occurs in the electrical circuit.

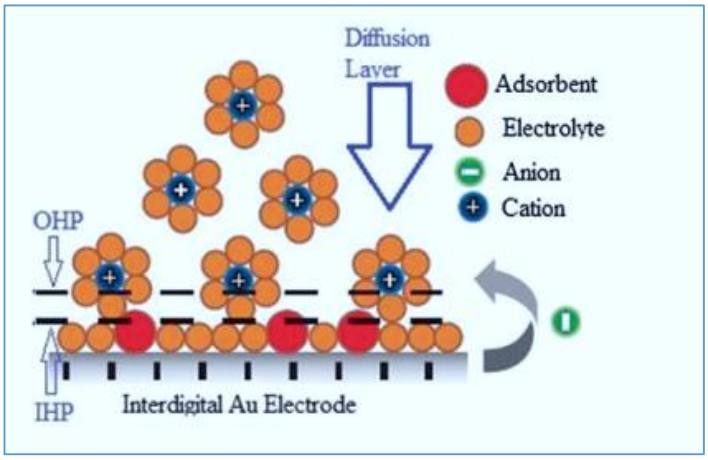

Figure 2.1: The electrical double layer adapted from reference[6]

Figure 2.1 shows the model of double layer elucidated by Helmholtz, Gouy and Chapman, and Stern. The electric double layer occurs at the electrode/solution interface. The concept of this phenomenon is that two charges exist, one at the electrode surface, q_m: this is equal

to that of the solution, but with opposite charge, q_s, equation 2.4. This phenomenon occurs when applying potential to the cells.[4]

$$q_{m=-}q_s$$

Equation2.4

This charged layer of the solvent molecules involves two planes. The inner Helmholtz plane (IHP) is formed from dissolved molecules/ions adsorbed to the metal surface, the outer Helmholtz plane (OHP), which consists of solvated ions, is ~1nm along the surface and closer to the first plane. Promoting of these two layers and extending from the OHP to the bulk solution, the so-called diffuse layer is located. The concentration of ions in the solution determines the thickness of the diffuse layer: for more than 0.1 M concentration, the thickness will be less than ~ 10 nm.[5] Figure 2.2 is a schematic representation of a typical electric double layer according to Newman and Thomas-Alyea.[7]

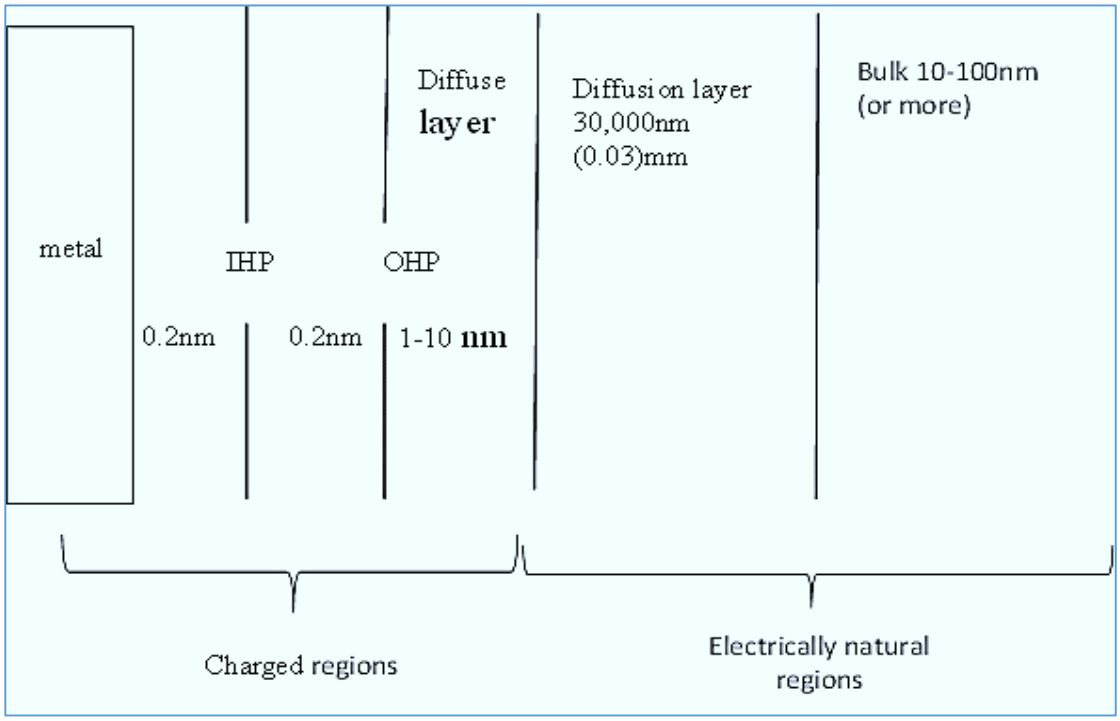

Figure 2.2: Typical schematic of an electric double layer adapted from reference[7]

2.2 Electrochemical cells and electrodes

Electrochemical cells are devices that are used for either generating electrical energy from chemical reactions (Galvanic cells), as mentioned in chapter one; or providing an external potential into a system which induces a chemical reaction (electrolytic cell) figure 2.3.

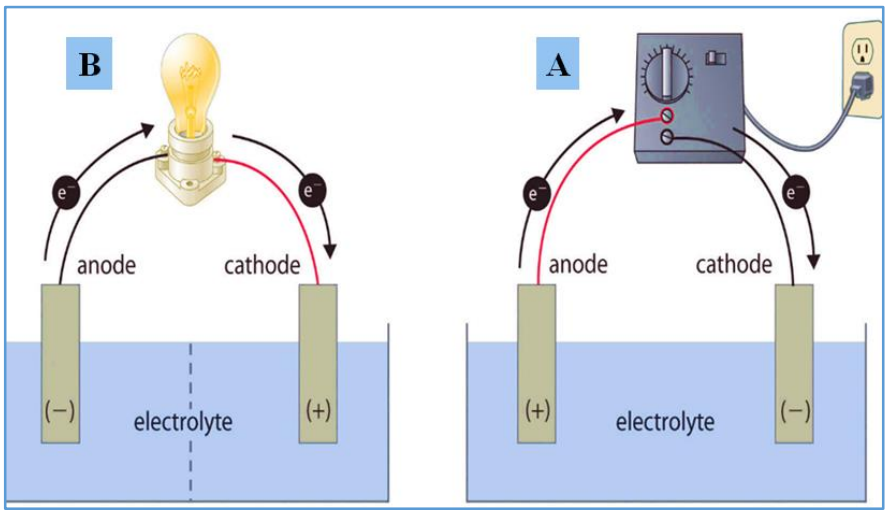

Figure 2.3: (A) An electrolytic electrochemical cell, (B) A galvanic electrochemical cell adapted from reference[2]

Although the latter system requires at least two electrodes, a system with a three-electrodes is the most commonly used.[5,8] A three-electrode system, comprising of working, reference and counter electrodes were used in this thesis and is represented in figure 2.4.

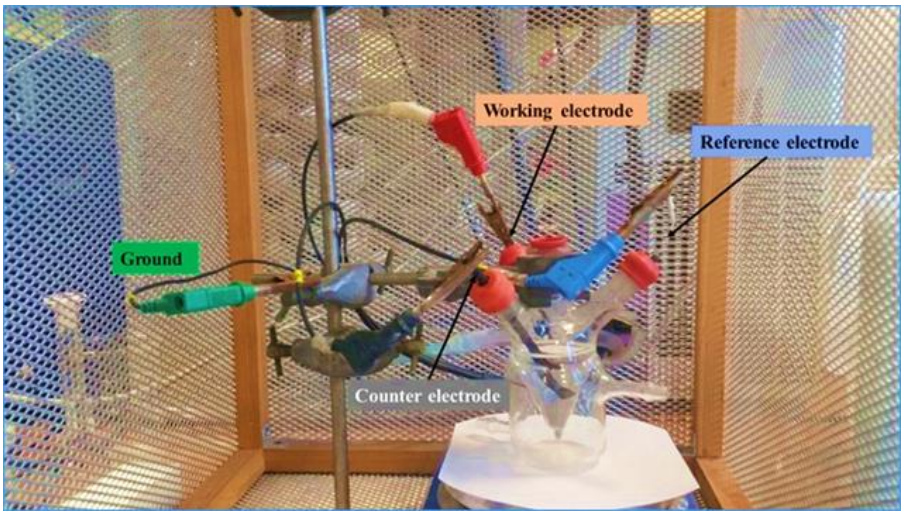

Figure 2.4: Photographic diagram of an electrochemical three-electrode system

2.2.1 Working electrode (WE)

A working electrode plays a vital role in electroanalysis, concerning the source of electrons that are transferred to its surface and electroactive species in the solution. Thus, the properties of materials that are used for the electrode can affect the heterogeneous kinetics of the electrochemical reaction (see chapter 5).

Furthermore, there are some essential factors reflected in the successful reaction: the potential window, the stability of electrode substrates, reproducible surface, reliability, cost, and toxicity. Commonly, a range of materials can be used for working electrodes, from inert metals such as silver, gold, and platinum to inactive form of carbon such as glassy (and pyrolytic) carbon, and mercury drop electrodes.[8,9]

2.2.2 Reference electrode (RE)

A reference electrode is an electrode whose potential is known and constant under applied external potential in the electrochemical cell. A proper electrode needs to be reversible, reproducible, and capable of regaining the original potential.[10,11] The common types used for studying electrochemical reactions are silver-silver chloride electrode and saturated calomel electrode: these electrodes will be discussed in more detail in chapter 3.

2.2.3 Counter Electrode (CE)

A counter electrode is an inert conductor that is used to complete an electrical circuit and let flow a current connection with a working electrode.[8,12] Thus, the surface area of one of these is either equal to or larger than that of a working electrode. Platinum and nickel are common materials used for an auxiliary electrode; they do not need any special care, such as polishing.

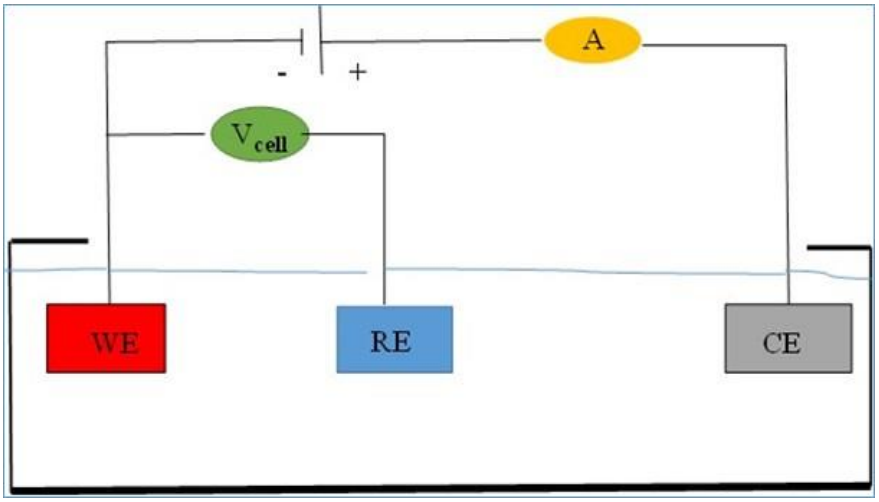

Figure 2.5: A schematic diagram of a three-electrode cell and notation for the different electrode adapted from reference[13]

From figure 2.5, we can see that the working electrode (WE) must be connected to the counter electrode (CE) to ensure that no current will be passed through the second electrode (RE). The potential E that applies to the electrical circuit with different potential at an electrode surface ($\emptyset_M$) and a solution ($\emptyset_S$) is given by:

$$E = (\emptyset_M - \emptyset_S)_{working} - (\emptyset_M - \emptyset_S)_{refernce}$$

Equation2.5

As mentioned previously, the potential of the reference electrode is constant, so potential E depends on $(\emptyset_M - \emptyset_S)$ at the working electrode only. When a potential, E, is applied to the working electrode it will induce current flow between two electrodes (working and reference) electrodes. The bulk solution gives an ohmic (resistive) voltage drop, which is accounted in equation (2.6).

$$E = (\emptyset_M - \emptyset_S)_{working} - (\emptyset_M - \emptyset_S)_{refernce} - IR$$

Equation2.6

In which I is the total current flowing and R is the solution resistance. The IR voltage drop can be minimised or neglected by increasing the conductivity of electrolyte (e.g.0.1M KCl).[14]

2.2.4 Solvents and Supporting Electrolytes

Electrochemical measurements are carried out in a solvent containing a supporting electrolyte. The choice of solvent depends on a number of factors such as the solubility and redox behaviour of the analyte, as well as the properties of the solvent (*i.e.*, electrical conductivity, electrochemical activity and chemical reactivity). The chosen solvent should not react with the analyte or any products and should be electrochemically inert over a wide potential window for the study of the redox reaction.

Supporting electrolytes are necessary for potential controlled experiments to disregard electro-migration effects, decrease resistance and sustain a constant ionic strength. Thus, possible electrolytes are inorganic salts, mineral acids or buffers (Table 2.1).[8,15]

Table 2.1: The common standard solvents and supporting electrolytes utilised in electrochemical methods

Standard Solvent		Standard Supporting electrolytes		Buffer solution
Aqueous	Double distilled H_2O	**Aqueous**	KCl, HCl, NH_4Cl, NaOH, KNO_3	Acetate, citrate and phosphate
Non-Aqueous	DMSO, DMF, CH_3CN	**Non-Aqueous**	Tetra-alkyl ammonium salts	

2.2.5 Removal of Oxygen

The electrochemical reduction of oxygen proceeds *via* a two-step mechanism as outlined below (Reactions 2.1 and 2.2).

$$O_2 + 2H^+ + 2e^- \rightarrow H_2O_2 \text{.....Reaction 2.1}$$

$$H_2O_2 + 2H^+ + 2e^- \rightarrow 2H_2O \text{.....Reaction 2.2}$$

Hydrogen peroxide is formed in the first reaction, while peroxide reacts to form water in the second reaction. The $E_{1/2}$ of these two reactions against a saturated calomel electrode is approximately (-0.1 V and -0.9 V) respectively. A significant current can arise from

these processes, which is likely to interfere with the measurement of analytical cathodic currents. Furthermore, chemical products may affect the chemical processes under investigation. It is, therefore, prudent to remove dissolved oxygen from the electrochemical cell. The most common method has been purging the cell with an inert gas such as N_2 or Ar.[15]

2.3 Mass transfer

Generally, in electroanalytical reactions, if electroactive species in solution are transported to the surface of an electrode, for electrochemical reaction, the process is called mass transfer. It plays a critical role in the concept of the dynamic reactions. Mass transport at the electrode-electrolyte phase boundary is classified into three different processes: diffusion, migration, and convection.

2.3.1 Diffusion

Diffusion takes place by transport of an active species due to the effect of a concentration gradient. So an unequal concentration distribution in the boundary region between electrode and electrolyte will diminish.[12] In other words, the electrode is oxidised as a result of reducing the analyte; therefore the concentration of the analyte in the interface area of the electrode will be reduced. Fick's first Law (equation 2.7) has described the relationship between the rate of diffusion (flux) of chemical species and the concentration gradient:

$$\boldsymbol{j = -D\frac{\partial C}{\partial X}}$$

Equation2.7

where j is a flux of material by diffusion in the X direction, D is the diffusion coefficient ($cm^{-2}\ s^{-1}$) for the transported species, and $\frac{\partial C}{\partial X}$ is the concentration gradient (mol ml^{-3}) at

distance X (m). Fick's second Law, (equation 2.8), describes how the concentration of material at point X changes with time:

$$\frac{\partial C}{\partial t} = D\frac{\partial^2 C}{\partial X^2}$$

Equation2.8

When the movement of the species is considered in three dimensions, the last equation becomes:

$$\frac{\partial C}{\partial t} = D_c\frac{\partial^2 C}{\partial X^2} + D_c\frac{\partial^2 C}{\partial Y^2} + D_c\frac{\partial^2 C}{\partial Z^2}$$

Equation2.9

2.3.2 Migration

Migration occurs when an electrostatic force is used. As a result, charged particles are moved. The migration flux (j_m) is described by:

$$j_m\alpha = \mu(c)\frac{\partial \emptyset}{\partial X}$$

Equation2.10

It can be seen that j_m is proportional to the concentration of the charged particles, the ionic mobility (μ), and the electric field $\frac{\partial \emptyset}{\partial x}$, although, the charge transfer process can occur at the electrode by a change in concentration of electroactive particles, ohmic resistance in solution and/or electric field.[5] Thus, the experimental data will be difficult to interpret. In this case, the experimental conditions can be modified by using an inert supporting electrolyte.

2.3.3 Convection

Convection is the name for the process of transportation by currents through the bulk fluid. It may be classified into two types. Natural convection is caused by density or thermal variations within the solution: electrolysis to form products near the electrode

with a different density to those in the bulk solution will give rise to natural convection. The other type is forced convection, which occurs by pumping, stirring or bubbling gas through the solution. Natural convection is observed in some voltammetric experiments using conventional electrodes with longs time scales (10-20 s)[16,17]. Thus, convection can be eliminated by stopping the use of mechanical forces or doing an experiment over shorter time-scales. In contrast, it may be necessary to introduce this force into a solution, so that the mass transport pattern to the electrode can be dictated. The changing in concentrations as a result of moving solution with a velocity (V_x) is given by:

$$\frac{\partial C}{\partial t} = -v_X \frac{\partial c}{\partial X}$$

Equation2.11

Figure 2.6 signifies all of the mass transfer processes that have been discussed.

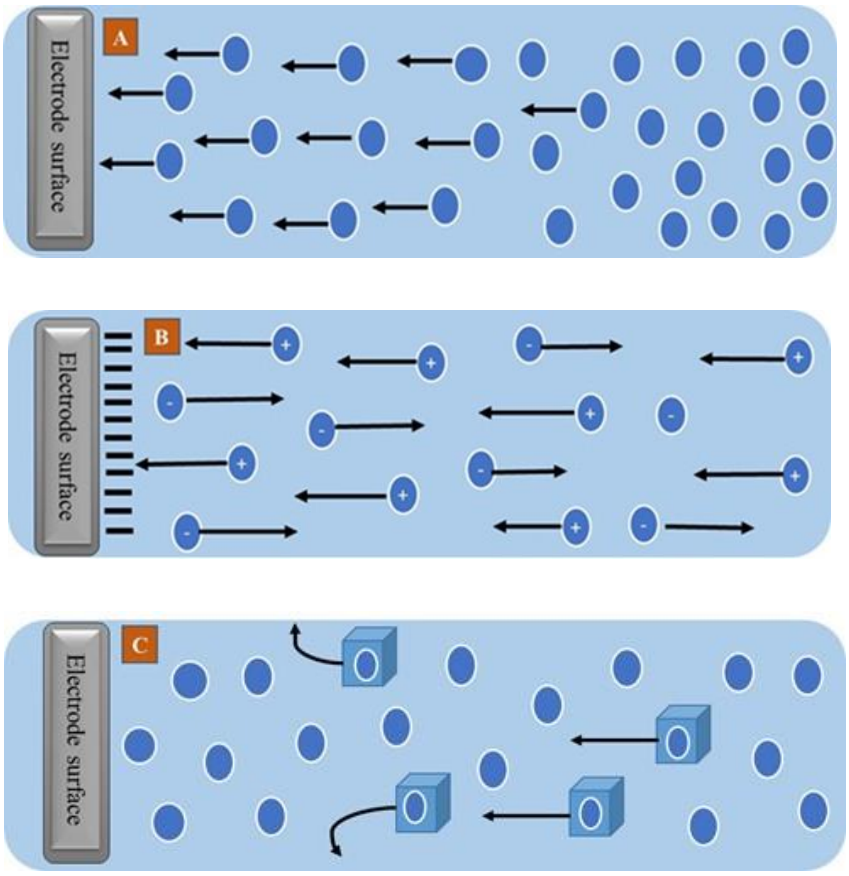

Figure 2.6: Schematic carton representation of three types processes of mass transfer in the electrode/electrolyte interface, which are: A. diffusion, B. migration and C. convection, adapted from reference[15]

2.4 Electrochemical Kinetic Theories

This section gives an overview of essential theories such as the Butler-Volmer and Tafel equations. Through these theories, the kinetic behaviour at the electrode concerning potential and concentration will be understood, beginning with a practical potential of the electrochemical system and going on to details of these theories.[5,17-19]

2.4.1 Overpotential

To stimulate the flow of current into the electrochemical cell, it is necessary to apply overpotential (η), which can be given by:

$$\boldsymbol{\eta = E - E^{o}}$$

Equation2.12

where E is applied potential and E^{o} is the standard potential. The flowing current (i) can be given by:

$$\boldsymbol{i = \oint nFjdA}$$

Equation 2.13

where n is the number of electrons transferred per mole of reaction, F is Faraday's constant, A is the electrode area and j is the flow of electroactive materials.

To describe the electrode kinetics, the general reaction is considered with a rate constant.

$$\boldsymbol{O + ne^{-} \underset{ka}{\overset{kc}{\rightleftarrows}} R}$$

Equation 2.14

The following theories have elucidated the kinetics of electrons in the interfacial region.

2.4.2 Butler–Volmer Kinetics

The Butler–Volmer model can be used to interpret the current of electrode kinetics that results from applying an overpotential and an elimination of mass-transfer limitations:

n= 1 is assumed. From equation 2.14, it can be seen that the heterogeneous rate constants k_c and k_a describe the forward reduction and backward oxidation electrode reactions, respectively. The following law can be viewed as net current (i) which refers to the difference between the cathodic current [(i_c) reduction] and the anodic current [(ia) oxidation]:

$$\boldsymbol{i = i_c - i_a}$$

Equation 2.15

In applying Equation 2.13, each current can be presented by:

$$\boldsymbol{i_c = FAk_cC_O}$$

$$\boldsymbol{i_a = FAk_aC_R}$$

Equation 2.16

In addition, the net current (i) is given by:

$$\boldsymbol{i = FA(k_cC_R - k_aC_O)}$$

Equation 2.17

The rate of forwarding and backward reactions at the (cathode and anode) surfaces can be described as a function of the standard rate constant, k^o:

$$\boldsymbol{k_c = k^o e^{-\alpha f(E-E^o)}}$$

$$\boldsymbol{k_a = k^o e^{(1-\alpha)f(E-E^o)}}$$

Equation 2.18

When the transfer coefficient ($0<\alpha<1$), and is often suggested to be 0.5 [4], and the coefficient $f = F/(RT)$. By substituting equation 2.18 into equation 2.17, the Butler–Volmer equation[20] is formed:

$$\boldsymbol{i = FAk^o\left[C_o e^{-\alpha f(E-E^o)} - C_R e^{(1-\alpha)f(E-E^o)}\right]}$$

Equation 2.19

At equilibrium, net current will be equal to zero, because a cathodic current is equal and opposite to an anodic current, thus:

$$\boldsymbol{i_o = i_c = i_a}$$

The exchange current, i_o, can be used to calculate K°, when $e^{-\alpha\, nf(E_{eq} - E^o)} = \left(\frac{C_O}{C_R}\right)^{-\alpha}$ then it can be written as:

$$\boldsymbol{i_o = FAk^o {C_O}^{(1-\alpha)} {C_R}^{\alpha}}$$

Equation 2.20

When the mass transfer is efficient, the bulk concentrations of the solution being equal to the concentrations at the electrode surface, the apply overpotential equation 2.12 is substituted. Thus, the Butler–Volmer equation is simplified to:

$$\boldsymbol{i = i_o\left[e^{-\alpha f\eta} - e^{(1-\alpha) f\eta}\right]}$$

Equation 2.21

2.4.3 Tafel equation

The Tafel equation links the applied overpotential to the current, i (A) that passes through the circuit. The flux for a reduction process of O to R (Equation 2.17) is calculated according to the equation below:

$$\boldsymbol{j = k^o exp\left[\frac{-\alpha F(E - E^o)}{RT}\right] C_O}$$

Equation 2.22

and for an oxidation process:

$$\boldsymbol{j = k^o exp\left[\frac{(1-\alpha) F(E - E^o)}{RT}\right] C_R}$$

Equation 2.23

Therefore, the net flux for the redox process is described in equation 2.27:

$$j = k^o exp\left[\frac{-\alpha F(E - E^o)}{RT}\right] C_O - k^o exp\left[\frac{+\beta F(E - E^o)}{RT}\right] C_R$$

Equation 2.24

Where $k^o=k_a=k_c$, $\beta=1-\alpha$. When the redox process is under overpotential, it becomes possible to neglect the reductive current in the oxidation process, and the Butler–Volmer equation 2.24 is simplified:

$$\ln i = \ln i_o + \beta f$$

Equation 2.25

Similarly, the Butler–Volmer equation for the reductive process is simplified:

$$\ln -i = \ln i_o - \alpha f \eta$$

Equation 2.26

The transfer coefficient α and β can be calculated by plotting of *ln /i/ vs* E. This plot is known as a Tafel plot: see figure 2.6. The factors α and β can be calculated by using $slope = \frac{-\alpha F}{2.3RT}$ $and\ slope = \frac{\beta F}{2.3RT}$ for redox process.[17]

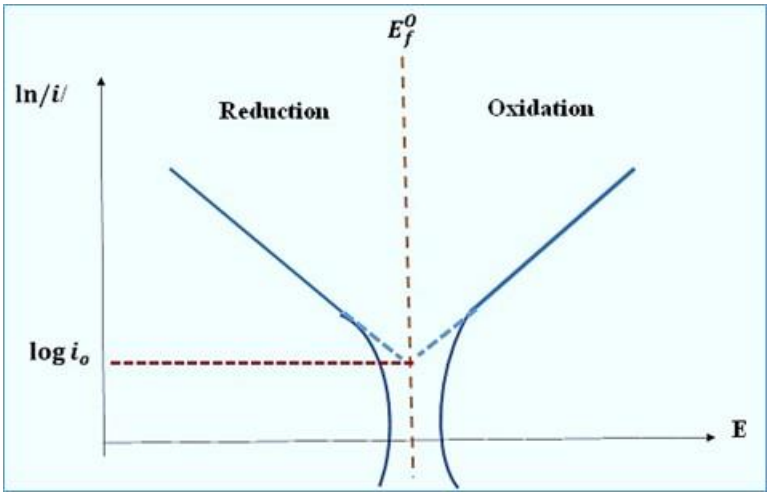

Figure 2.6: The Tafel plot, adapted from reference[5]

2.5 Electrochemical Techniques and Their Theoretical Backgrounds

Electrochemical techniques are analytical techniques that are applied to determine a wide variety of both organic and inorganic species and offer high sensitivity, accuracy and large linear concentration range. These methods are based on applying a potential to an electrode (the working electrode): then the current is measured as a function of the applied potential over a period. Thus, electroactive species in solution will be electrolysed; reduced or oxidised, at the electrode surface. The plot results (current/voltage) are known as a voltammogram. During the last decades, electrochemical analysis has witnessed an extraordinary progression in discovery, synthesis, and sensitivity.[21-26] Several techniques of voltammetry such as cyclic voltammetry, linear sweep, and hydrodynamic voltammetry have been investigated. These methods have been used in this study and are described here. Their theoretical background is given below.

2.5.1 Linear Sweep Techniques

Linear Sweep Voltammetry (LSV) is the simplest and earliest electrochemical methods: this technique and cyclic voltammetry (CV) are widely used for studying thermodynamic or kinetic mechanisms of electrode reactions mostly in an unstirred solution. Thus, a gradient in concentration governs the transfer of electroactive species.

Initially, in LSV, the applied potential is too low compared with a formal potential, so that the analyte remains at its initial redox state. As the potential gets close to the formal potential, the electrode kinetics for redox transformation of the analyte increase. As more significant quantities of analyte are consumed through redox transformation at the electrode surface, while the potential inverses beyond the formal potential. Thus, the results depletion in active material near the electrode surface gives rise to a concentration

gradient, so that the voltammogram is dominated by the diffusion transfer of the analyte from the bulk solution to the electrode surface.[27] This dual effect of electrode kinetics and mass transfer give rise to the peak in the current-voltage curve in figure 2.7.

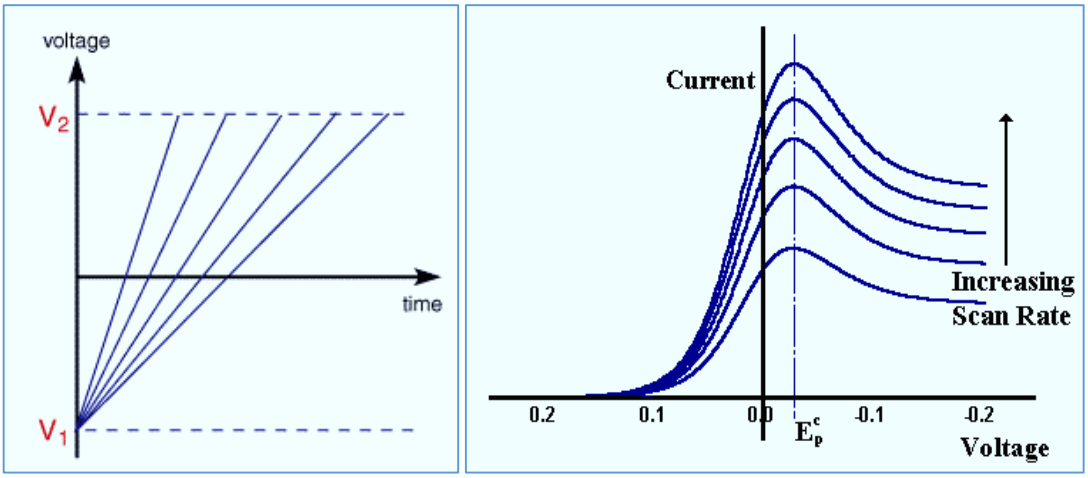

Figure 2.7: linear sweep waveform (left side), current vs voltage for linear sweep voltammograms (right side), adapted from reference[28]

The current as a function of potential is given by the Randles-Sevick equation (2.27):

$$i_P = (2.69 \times 10^5) n^{3/2} A C D^{1/2} \nu^{1/2}$$

Equation 2.27

where n is the number of electrons, A is the electrode area in cm^2, C is the concentration of the bulk solution in mole m^{-3}, D is the diffusion coefficient of the electroactive species ($m^2\ s^{-1}$), and ν is the sweep rate of potential in Vs^{-1}. Therefore, the relationship between current and concentration is directly proportional. Using various sweep rates, a plot of peak current against square rate should be linear, and the diffusion coefficient of species can be determined from the slope by using the following information, equation 2.28:

$$\text{Slope} = (i_p/\nu^{1/2}) = 2.69 \times 10^5\ n^{3/2}\ A C D^{1/2}$$

Equation 2.28

2.5.2 Cyclic Voltammetry

Cyclic voltammetry (CV) is widely used in different areas of electrochemistry due to its simplicity, and its high information gathering[29,30], although it is also used for studying

thermodynamics observed in the system and the potentials at which they occur. At the same time, this technique is seldom used for determining the specified quantity.[31]

This method was first described in 1948 and defined theoretically by Randles, it is considered as an extension of LSV. Therefore, the theory and equations, which explained in the previous section, also apply with more detail in this part. Briefly, this technique can be presented as a reversal process, which is based on sweeping different potential at an electrode surface in two directions (forward and backward): thus, the current will be recorded. Consequently, cyclic voltammetry and linear sweep voltammetry are similar in sweeping potential but they are different in reversible cases. Figure 2.8 b shows a typical cyclic voltammogram for a reversible single electron transfer reaction.

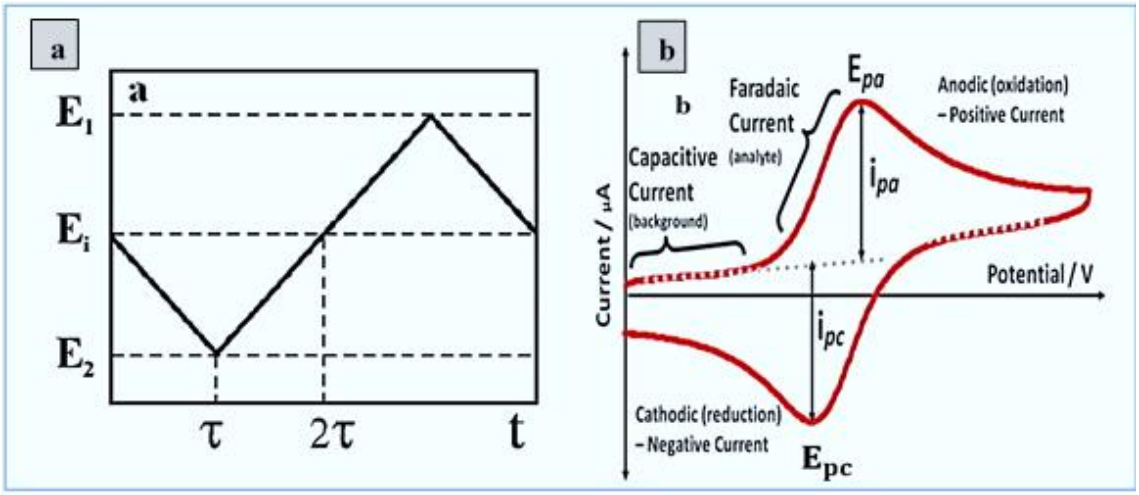

Figure 2.8: (a). A typical plot of the potential sweep during cyclic voltammetry; E_i is the initial value; E_1 and E_2 are two limiting values. (b). Cyclic voltammogram for reversible electron transfer reaction adapted from reference[32]

In the previous figure (a) introduces reversible CV technique when a potential is applied to the working electrode and changes with time. In the beginning, no electrode reactions occur and some potential, E_i, is held at the working electrode. During an experiment, there is a linear sweep of the potential at a rate ν between two limiting potentials E_1 and E_2. Usually the same sweep rate is chosen for the forward and reverse sweep when the corresponding current is recorded as a function of different rates of the potential.

In figure (b), the current had a negative sign (peak i_{pc}) for the cathodic scan and applied a potential (E_{pc}) is decreasing, while the current had a positive sign (peak i_{pa}) for the anodic scan and applied a potential (E_{pa}) is increasing. The mechanisms of electron transmission in this technique can be categorised as the following process.

1. Reversible process

When a redox reaction is completely reversible, the peak i_{pc} and the peak i_{pa} are equivalent and present in a cyclic voltammogram. Thus, it is easy to identify this reversibility from a CV figure. The peak current is given by the Randles-Sevčík equation[27,33] :

$$\boldsymbol{i_p = \left(2.69 \times 10^5\right) n^{3/2} A C D^{1/2} v^{1/2}}$$

Equation2.29

where n is the number of electrons, A is the electrode area in cm^2, C is the concentration of the bulk solution in mol ml^{-3}, D is the diffusion coefficient of the species (m^2 s^{-1}), and ν is the sweep rate in Vs^{-1}. Thus, from equation (2-31), the peak current (i_{pa}) is directly proportional to the concentration of electroactive species.

In the case of variable scan rates, a linear plot of i_{pa} *vis* $\nu^{1/2}$ should be shown: in other words, if the scan rate is increased, both cathodic and anodic peak potentials are proportionally increased. This indicates that the redox process is under diffusion control, which means that the reaction is reversible. The value of the diffusion coefficient is determined from the linear slope of the electroactive species.

2. Irreversible process

An irreversible process can be described by using a modification of the Randles-Sevčik equation[31]:

$$\boldsymbol{i_p = \left(2.99 \times 10^5\right) n(\alpha n_a)^{1/2} A C D^{1/2} v^{1/2}}$$

Equation2.30

Again, from equation 2.32, the increase in the concentration and scan rate will reflect on increasing the peak current (i_{pa}) or (i_{pc}), and only one of these peaks is present in a cyclic voltammogram. Figure 2.9 shows cyclic voltammograms for reversible, quasi-reversible and irreversible voltammetry redox process.

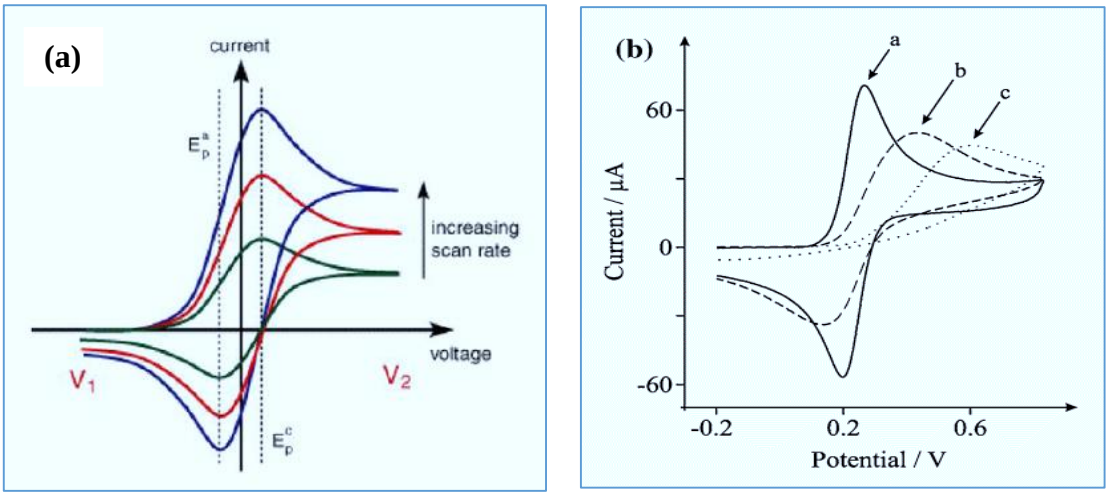

Figure 2.9: (a).Typical voltammograms for depicting the increasing of scan rate. (b). Cyclic voltammograms for reversible (a), quasi-reversible (b) and irreversible (c). Adapted from reference[28,34]

3. Quasi-reversible process

In this system, charge transfer and mass transport are controlled at peak current. From the above figure (right-hand side), a quasi-reversible voltammogram can be located between both reversible and irreversible processes. Also from this figure, in the quasi-reversible process, the separation in peak potential is larger than in the reversible.

2.5.3 Hydrodynamic Methods and rotating disk electrode (RDE)

In all the methods described previously, the electrolyte solution is not stirred. Thus, the diffusion is controlled by getting electroactive species to an electrode surface. The techniques that introduce forced convection (that is, stirring) into the electrochemical regime, thereby very quickly bring the analyte to the electrode. Such methods are called hydrodynamic.

Hydrodynamic methods can be performed in different ways. One method includes stirring the solution forcefully. Here there is no contact with a precise microelectrode. On the other hand, using a high-speed rotating microelectrode or macro electrode in the bulk solution will provide the stirring action.

A typical rotating electrode is the disk electrode (RDE), which is a solid electrode inserted in the middle of a plane surface without driving any liquid into it (see Figure 4.2 in chapter 4), and rotated around its vertical axis at a constant speed: hence a convective flow will be stimulated. In this case, the bulk solution is spun out by rotation of the electrode surface (see Figure 2.10), thereby drawing fresh solution up towards the electrode surface. As a result of the stirring action of the electrode, a constant flow of electroactive species will be supplied at the electrode surface.[5]

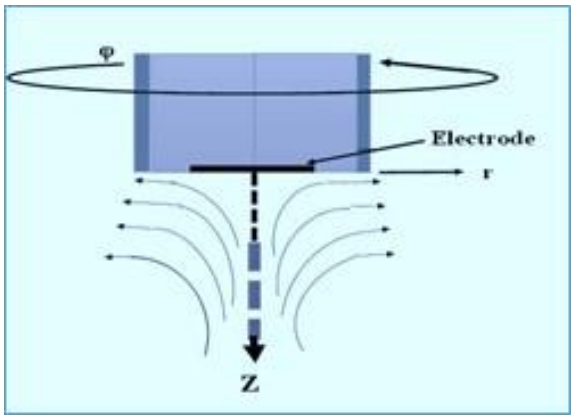

Figure 2.10: A model of the rotating disk electrode around z-axis, adapted from reference[35]

Consequently, a voltammogram of current versus potential is obtained, and a sigmoid shape is observed. The limiting current obtained from a voltammogram can be predicted by using the Levich equation[36]:

$$i_{lim} = 0.621nFA(C)_o {D_o}^{2/3} \upsilon^{-1/6} \omega^{1/2}$$

Equation2.31

Where ω is the angular rotation rate of the electrode in rad s^{-1}, and *v* is the kinematic viscosity of the bulk solution in cm^2 s^{-1}, which is determined using the ratio of the solution Kinematic viscosity to its density. From this equation, a plot of i_{lim} *vis* $\omega^{1/2}$ should obtain a straight line, and any fluctuation is referred to limitation in k_i.

2.5.4 Potential Step Chronoamperometry

In Chronoamperometry method, there is a corresponding to a current with a time under potential control. It also used a small working electrode compared with a bulk solution in the stationary system. In this method, the potential of WE is stepped from an initial value where no redox process takes place (E_1) to a value at which the reduction or oxidation reaction of electro species is taken (E_2), see figure 2.11.[37]

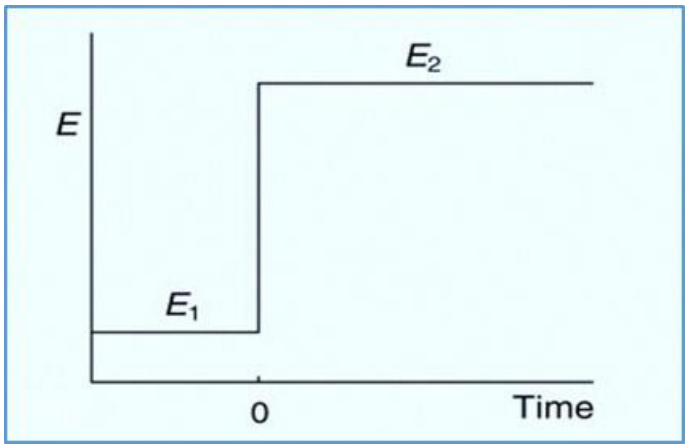

Figure 2.11: Atypical diagram of chronoamperometry

Thus, a current flowing as a result of this potential step is monitored as a function of time. Immediately following the step in potential, large current flows due to the reduction of O to form R. As O is continually converted to R, the concentration gradient increases, causing a flux of O to the electrode surface and hence a large current to flow. However, with a continuous flux of O to the surface, the thickness of the diffusion layer increases, decreasing the concentration gradient and therefore the current decreases steadily with

time to a limiting point. The response of current as a function of time was reported by Cottrell equation[38]:

$$\boldsymbol{i = \frac{nFAC_O\, D^{1/2}}{(\pi t)^{1/2}}}$$

Equation2.32

From this equation, the value of the diffusion coefficients (D) can be determined by using the potential steps of an experiment. In addition, the equation shows at which decrease in concentration of electroactive species (C_O) at the electrode surface; the $t^{1/2}$ becomes an inverse function, which suggests that the redox process occurs under diffusion control.[39]

2.6 Electrochemical Reaction Mechanisms

A molecule which receives or which has lost an electron does not have to be chemically stable: it may react with solvent or with other species added into the electrolyte. This gives rise to the notion of an electrochemically-induced chemical reaction.[40-42] Three general types of mechanism are considered in this thesis, in which the chemical reaction takes place in homogeneous solution with electron exchange at the electrode surface. Testa and Reinmuth developed the notation for ET mechanisms: they introduced E for a reversible heterogeneous electron transfer step and C as an irreversible homogeneous chemical reaction step.[43] In the following, EC, CE and EC' reactions are detailed.

2.6.1 EC Reactions

This reaction occurs when, under applied potential, a product is formed such as y, which is unstable, and non-electroactive and this is followed by some form of homogeneous chemical reaction, equation 2.12:

$$\boldsymbol{x + ne^- \underset{k_a}{\overset{k_c}{\rightleftarrows}} y} \qquad \boldsymbol{(E)}$$

$$y \rightarrow z \qquad (C)$$

Equation2.33

In an EC reaction, the rate of production of y at the E step and the rate of conversion of it to z at the C step influence the voltammetry process. If k_c is very fast when y is formed and converted to x, there is not enough time to reverse the process an irreversible voltammogram is obtained. On the other hand, if the k_c is slow this means that there is enough time for reducing y to form x, which case a reversible voltammogram to be obtained. One example is the oxidation of 1, 4-amino phenol (PAP) in acidic aqueous solution.[5]

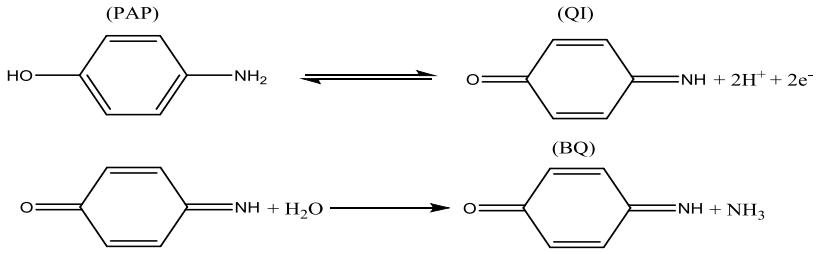

2.6.2 CE Reactions

The mechanism of this chemical reaction in the solution (homogeneous process) followed by the electrolysis of an electroactive species at the electrode surface. See equation 2.13:

$$y \Leftrightarrow z \quad (C)$$

$$x + e^{-} \Leftrightarrow y \quad (E)$$

Equation2.34

Although the characteristics of CE and EC reactions are similar, at higher scan rates there is a decrease in the reverse peak, while more reversible reaction can be observed at lower scan rates, for example, the reduction of an aqueous solution of formaldehyde.[5]

2.6.3 EC' Reactions

The general equation for this reaction is given by:

$$\mathbf{x} + e^{-} \Leftrightarrow y \quad (E) \quad \ldots\ldots\ldots (1)$$

$$\mathbf{y} + \mathbf{b} \Leftrightarrow \mathbf{x} + \mathbf{z} \quad (\mathbf{C}) \quad \ldots\ldots\ldots (2)$$

Equation2.35

Step (2) introduces the idea that the electroactive species x is regenerated through a homogeneous chemical reaction with an active material b. In addition, equation 2-14 shows that the relationship between x concentration on the electrode surface and b concentration in the bulk solution is proportional. Thus, an increase can be observed in the current response of electron transfer, and the voltammogram shape will be sigmoidal. An example of this type of reaction is the oxidation of cysteine by ferricyanide in aqueous solution.[44]

2.7 Adsorbed Electroactive Species on the electrode surface

The electroactive species has essential interaction with the electrode surface. Therefore, it is probable that adsorbed-desorption species exist, which arise during the electron transfer process. There is a similar behaviour between the rate of adsorption onto an electrode surface of adsorbed species and general electrode reaction.

If the adsorbed species are oxidised or reduced on the electrode surface in the case of a fast kinetic reaction, the shape of the cyclic voltammogram will be symmetrical, see figure 2.12. However, in slow kinetic reactions, some peak separation is observed. Note, that for the diffusion-controlled response the peak current is proportional to the square root of the potential. Equation 2.35 represents the reversible process of the adsorbed species onto the electrode surface[19,45,46]:

$$I_p = \frac{n^2 F^2}{4RT} \upsilon A \Gamma_{ox}$$

Equation2.36

In which Γ is the surface coverage mol cm^{-2}, and A is the surface area. The effects of adsorption species in cyclic voltammetry can be removed or reduced by changing electrodes or the solvent material. In addition, the adsorb reactants not directly involved in the mass transfer process are used to modify electrode reactions, change the product of reactions and to decelerate electron transfer reactions.[18]

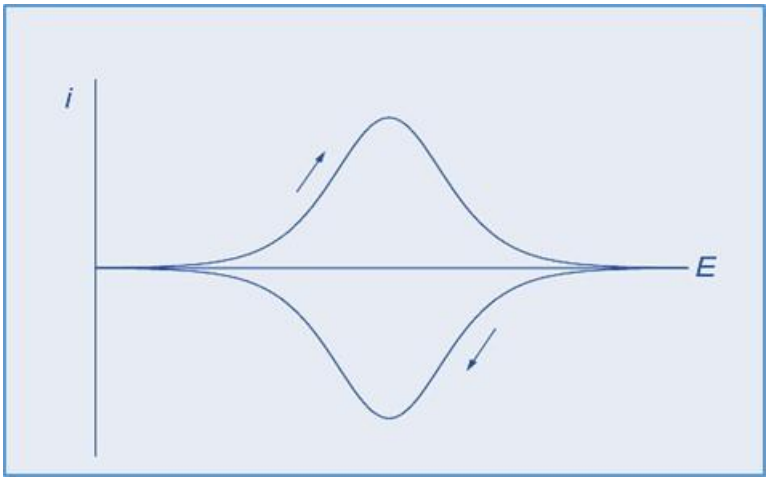

Figure 2.12: Cyclic voltammogram of a reversible redox couple adsorbed on an electrode surface, reproduced from [8]

2.8 Reference

(1) Crow, D. R.: *Principles and Applications of Electrochemistry*; 4th ed.; Blackie Academic and Professional: Glasgow, **1994**. pp. 4th1-2.

(2) Averill, B. A.: *Principles of General Chemistry*; Andy Schmitz, **2012**; Vol. 1.0.

(3) D.A.Skoog, J. J. L.: *Principles of Instrumental Analysis*; 4th ed.; A Harcourt Brace Jovanovich College: the United States of America, **1992**. pp. 462-495.

(4) A.C.Fisher: *Electrode Dynamics*; illustrated, reprint ed.; Oxford University Press, **1996**.

(5) Bard, A. J.; Faulkner, L. R.; Leddy, J.; Zoski, C. G.: *Electrochemical methods: fundamentals and applications*; Wiley New York, **1980**; Vol. 2.

(6) Chang, B.-Y.; Park, S.-M. Electrochemical impedance spectroscopy. *Annu. Rev. Anal. Chem.*, **2010**, *3*, pp 207-229.

(7) J. Newman, K. E. T.-A.: *Electrochemical Systems*; 3rd ed.; JohnWiley& Sons: Hoboken, **2004**.

(8) Zoski, C. G.: *Handbook of electrochemistry*; Elsevier Science: The Netherlands, **2007**.

(9) Scholz, F.: *Electroanalytical methods*; Springer, **2010**; Vol. 1.

(10) de Bethune, A. J.: Reference electrodes: Theory and practice (Ives, David JG; Janz, George J.; eds.). ACS Publications, **1962**.

(11) Brett, C.; Brett, A. M. O.: *Electrochemistry: Principles, Methods, and Applications*; Oxford University Press, **1993**.

(12) Kissinger, P. H., William.R.: *Laboratory Techniques in Electroanalytical Chemistry, revised and expanded*; CRC press, **1996**.

(13) Tighineanu, I. L., S; Föll, H; Ursachi, V.: *Porous III-V Semiconductors*; Ştiinţa, **2005**.

(14) Sarkar, S.; Lai, S.; Lemay, S. G. Unconventional Electrochemistry in Micro-/Nanofluidic Systems. *Micromachines.*, **2016**, *7*, pp 81.

(15) Wang, J.: *Analytical electrochemistry*; John Wiley & Sons, **2006**.

(16) A.C. Michael, L. B.: *Electrochemical Methods for Neuroscience*; CRC Press Taylor & Francis Group: Florida, **2010**.

(17) Compton, R. G.; Banks, C. E.: *Understanding voltammetry*; World Scientific, **2011**.

(18) Pletcher, D.; Greff, R.; Peat, R.; Peter, L.; Robinson, J.: *Instrumental methods in electrochemistry*; Elsevier, **2001**.

(19) H.Philip.Rieger: *Electrochemistry*; Second Edition ed.; Champman & Hall: the United States of America, **1994**.

(20) Butler, J. A. V. Studies in heterogeneous equilibria. Part II.-The kinetic interpretation of the Nernst theory of electromotive force. *J. Chem. Soc. Faraday Trans* **1924**, *19*, pp 729-733.

(21) Farghaly, O. A.; Ghandour, M. Square-wave stripping voltammetry for direct determination of eight heavy metals in soil and indoor-airborne particulate matter. *Environ. Res.*, **2005**, *97*, pp 229-235.

(22) Wang, Y.; Shao, Y.; Matson, D. W.; Li, J.; Lin, Y. Nitrogen-doped graphene and its application in electrochemical biosensing. *ACS nano.*, **2010**, *4*, pp 1790-1798.

(23) Shahrokhian, S.; Karimi, M.; Khajehsharifi, H. Carbon-paste electrode modified with cobalt-5-nitrolsalophen as a sensitive voltammetric sensor for detection of captopril. *Sens. Actuator B-Chem.*, **2005**, *109*, pp 278-284.

(24) Ren, Y.; Deng, H.; Shen, W.; Gao, Z. A highly sensitive and selective electrochemical biosensor for direct detection of microRNAs in serum. *Anal. Chem.*, **2013**, *85*, pp 4784-4789.

(25) Belharouak, I.; Johnson, C.; Amine, K. Synthesis and electrochemical analysis of vapor-deposited carbon-coated $LiFePO_4$. *Electrochem. Commun.*, **2005**, *7*, pp 983-988.

(26) Hallman, H.; Farnebo, L.-O.; Hamberger, B.; Jonsson, G. A sensitive method for the determination of plasma catecholamines using liquid chromatography with electrochemical detection. *Life Sci.*, **1978**, *23*, pp 1049-1052.

(27) Faulkner, A. J. B. a. L. R.: *Electrochemical Methods: Fundamentals and Applications*; 2nd ed.; John Wiley & Sons, Inc: New York, **2001**.

(28) Fisher, A. C.: Linear Sweep and Cyclic Voltametry: The Principles. University of Cambridge, Department of Chemical Engineering and Biotechnology, **2010**.

(29) Kissinger, P. T. H., W. R. Cyclic voltammetry. *Chem. Educ.*, **1983**, *60*, pp 702-706.

(30) Lu, X. Q. Z., L.; Sun, P.; Yao, D. Thin-layer cyclic voltammetric studies electron transfer across liquid/liquid interface. *Eur. J. Chem* **2011**, *2*, pp 120-124.

(31) Wang, J.: *Analytical Electrochemistry*; Wiley-VCH Publishers, **2000**.

(32) cyclic voltammetry.http://urrjaa.blogspot.co.uk/2013/08/cyclic-voltammetry-urrjaa-p0110-2013.html (accessed **20/09/2014**).

(33) Randles, J. E. A., Trans; Soc, F., Ed., **1948**; Vol. 44; pp 322-327.

(34) Brownson, D. A. C.; Banks, C. E.: *The Handbook of Graphene Electrochemistry*; Springer London, **2014**.

(35) A Brief History of Pine. www.pineinst.com/echem (accessed **08/11/ 2014**.

(36) Levich, V. G.: *Physicochemical Hydrodynamics*; Prentice-Hall:Englewood Cliffs: New Jersey, **1962**.

(37) Michael, A. C.; Borland, L. M.: An introduction to electrochemical methods in neuroscience. In *Electrochemical methods for neuroscience*; CRC Press, **2006**; pp 1-16.

(38) Wadhawan, J. D.; Wain, A. J.; Compton, R. G. Electrochemical probing of photochemical reactions inside femtolitre droplets confined to electrodes. *Chem.Phys.Chem.*, **2003**, *4*, pp 1211-1215.

(39) Brett, C.; Brett, M. O.; Brett, A. M. C. M.; Brett, A. M. O.: *Electrochemistry: principles, methods, and applications*, **1993**.

(40) Rudolph, M.; Reddy, D. P.; Feldberg, S. W. A simulator for cyclic voltammetric responses. *Anal. Chem.*, **1994**, *66*, pp 589A-600A.

(41) Diao, G.; Zhang, Z. Theory and application of cyclic voltammetry at a hemispherical microelectrode for a quasi-reversible reaction. *J. Electroanal. Chem.*, **1996**, *410*, pp 155-162.

(42) Saito, Y. A theoretical study on the diffusion current at the stationary electrodes of circular and narrow band types. *Rev. Polarogr* **1968**, *15*, pp 177-187.

(43) Testa, A.; Reinmuth, W. Stepwise reactions in chronopotentiometry. *Anal. Chem.*, **1961**, *33*, pp 1320-1324.

(44) Nekrassova, O.; Allen, G. D.; Lawrence, N. S.; Jiang, L.; Jones, T. G.; Compton, R. G. The oxidation of cysteine by aqueous ferricyanide: a kinetic study using boron-doped diamond electrode voltammetry. *Electroanalysis.*, **2002**, *14*, pp 1464-1469.

(45) David K. Gosser, J.: *Cyclic Voltammetry Simulation and Analysis of Reaction Mechanisms*; illustrated ed.; Wiley: United States, New York, **1993**.

(46) Brett, C. B., A.M: *Electroanalysis-Oxford Chemistry Primers.*; Oxford University Press Inc., New York.: the United States, **1998**.

Chapter 3

Experimental methods

Chapter configuration

Many different experimental procedures and techniques have been used throughout this thesis, more details of which will be presented during relevant chapters. This chapter aims to describe the general equipment and experimental instrumentation, which were used in this work.

3.1 Chemical reagents and Electrochemical cells

Analytical grade chemicals were used to prepare all reagents and metal salts without further purification. All aqueous solutions were made up by using deionised water from an Elgstat water system (Vivendi, UK) with resistivity greater than18 MΩ cm.

All experiments were performed at room temperature except the liquid crystal study in chapter 7. The most common electrochemical cell consists of three electrodes, which are immersed in a solvent containing supporting electrolyte with high conductivity and the sample under investigation.

In all cases of this research, unless mentioned otherwise, all electrochemical experiments were carried out using the three-electrode system. These are the working electrode (WE), on the surface of which the redox reaction takes place; the reference electrode (RE), where the applied potential is measured; and the counter or auxiliary electrode (CE), where the electrical circuit is closed to enable the current to flow.[1-3]

3.2 Voltammetry Instrumentation

3.2.1 Potentiostat

A potentiostat is an electronic device used to control potential and measure the current through the three-electrode system for most electroanalytical experiments[4], the potentiostat arrangement and the electrodes cell is shown in figure 3.1.

Electrochemical measurements were undertaken by using an AutoLab PGSTAT30 potentiostat (Eco-Chemie, The Netherlands), which was controlled by an Intel® Core ™ 2 Quad processor computer using window® Vista ™ as an operating system. General Purpose Electrochemical System (GPES) was used as the software to control the Auto Lab system and to record and analyse data.

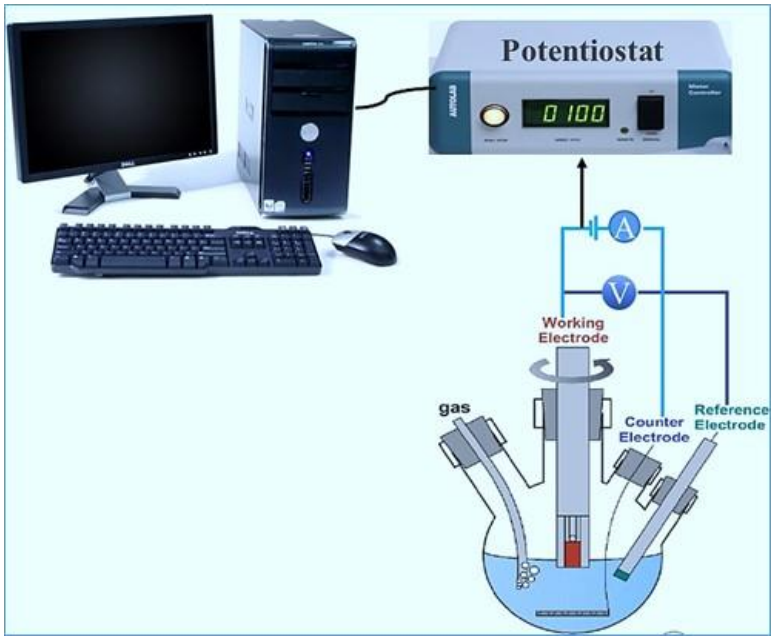

Figure 3.1: Typical diagram of CV experimental setup and notations

3.2.2 Electrodes

An electrode is a conductor or semiconductor, which accepts or receives electrons during electrolysis. It is in direct contact with an electrolyte solution.[5] The next sections explain the significant electrodes, which were utilised in this work.

3.2.2.1 Working electrode, glassy carbon electrode

Working electrodes, (WE) are typically made from substrate materials, which are electrochemically inert over a wide range of potentials. Therefore, noble metals, such as gold, platinum and silver, and carbon are widely used as WE.[6-8] A chemically inert covering made of glass, Teflon or epoxy is used to expose only a fraction of this electrode to the solution.[9]

Two commonly used forms of carbon electrode are glassy carbon (GC) and carbon paste. However, the former is expensive and difficult to machine whereas the latter is not resistant to mechanical stresses and can easily be damaged.[10,11] A glassy carbon disc (BASI, UK) was used as a working electrode in almost all the electrochemical experiments of this research unless otherwise mentioned in the specific chapters. The

exposed area of GCE was 3 mm in diameter and mounted on a 7.4 cm length Delrin tube. A copper wire was used to reach the electrical contact, which was sealed and protected by using Araldite resin at the top of this electrode. A sample of this electrode and its description are shown in figure 3.2.

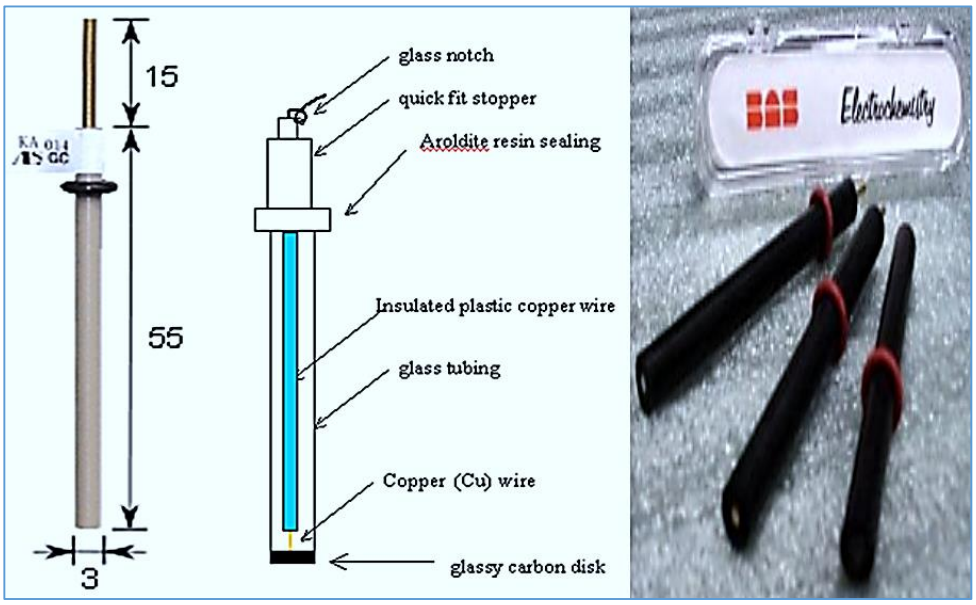

Figure 3.2: Schematic diagrams of working electrodes adapted from the Bioanalytical system Inc. Product catalogue, © BASI

Prior to use or modification, the working electrode was mechanically polished on a napped polish cloth (Presi, France) wetted with 0.3µm alumina slurry (Presi, France). This was followed by rinsing the working electrode with deionised water. In this way, any adsorbed substance was removed from the electrode surface.

3.2.2.2 Reference electrode

Two types of reference electrodes (RE) were used in this work. The first group of experiments in chapter 4 used a Saturated Calomel electrode (SCE), which was purchased from (Radiometer). This electrode contains mercury and mercury chloride paste (Hg^{o}/Hg_2Cl_2) immersed in a saturated aqueous solution of potassium chloride: see figure 3.3. At 25^{o}C, the potential of the SCE *via* standard hydrogen electrode (SHE) is + 0.2415 V.

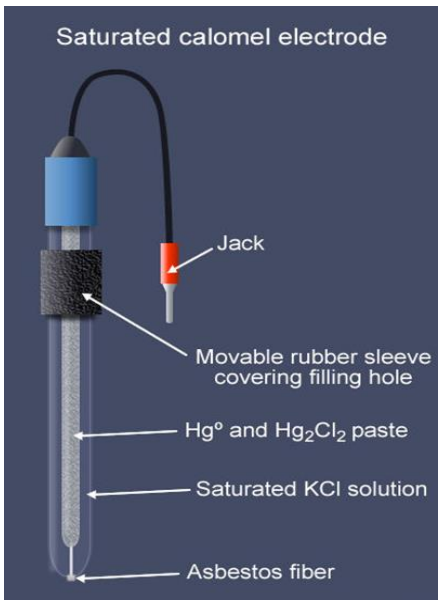

Figure 3.3: A schematic diagram of Hg/Hg_2Cl_2 the reference electrode (Obtained from BASI)

Almost all experiments in this work used a silver /silver chloride electrode. A diagram of this electrode is shown in figure 3.4. This electrode included a silver wire coated with a layer of silver chloride (AgCl) immersed in the saturated salt of 3 M KCl, surrounded by a glass tube with a porous polymer tip (*Vycor* frit). The potential of this electrode against SHE was + 0.222V at 25°C. This electrode should be stored in 3M KCl salt for long life use.

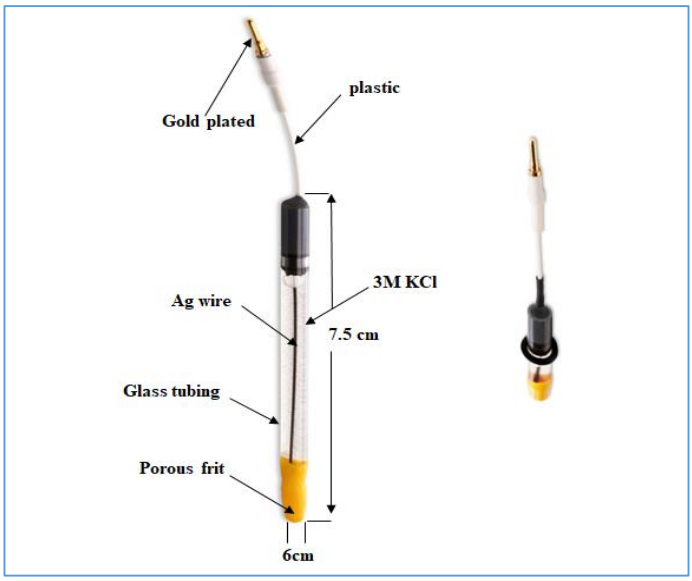

Figure 3.4: A schematic diagram of an Ag / AgCl reference electrode (Adapted from BASI sales literature)

3.2.2.3 Counter electrode CE

Counter electrodes are usually made of an inert material, with a large surface area. In this research, a carbon material (graphite) was used as an auxiliary electrode in almost all experiments unless mentioned in the relevant chapters. The surface area of graphite was often larger than a working electrode with a wide potential window in both negative and positive ranges. This allows the electroanalytical measurements to be limited by the processes occurring at the working electrode, and not the counter-reaction. Figure 3.5 shows a sample of this electrode

Figure 3.5: A schematic diagram of auxiliary electrode

3.3 Techniques

There are numerous methods used to identify liquid crystals phases to characterise their positions and orientations. Below are the common techniques used for identifying liquid crystals phases, which is studied in chapter 7.

3.3.1 Polarized microscopy (POM)

The polarising microscope is an observing birefringence (double refracting) technique for varying materials such as liquid crystal; it is the most widely used for determination and identification the different phases of LCs. This method can be used for heating and

cooling LCs when it is combined with a temperature controller. When this technique is coupled with X-ray investigation and differential scanning calorimetry, the combined instrument can be utilised to determine the temperature of a phase transition and its structure.

The polarisation phenomenon refers to the vibration of the electric field. Thus, polarised is light with one direction and particular vibration such as linear, circular and elliptical polarisation.[12,13] This microscope contains a light source halogen and a pair of polarising filters: A polariser, which is usually placed below the stage in a horizontal align, and an analyser, which is mounted above the stage in a vertical align with other accessories, figure 3.6 shows an image of POM.

By using a polariser, light with an east-west position is allowed to move through a sample, while the analyser is permitted a north-south position light to cross a sample. Thus, the observer can see darkness. At the end of this process images with high quality and slide and films are achieved.[14] An Olympus BX-51 optical polarising microscope with a digital camera was used to exam all samples of LCs. Figure 3.6 shows the POM and its components.

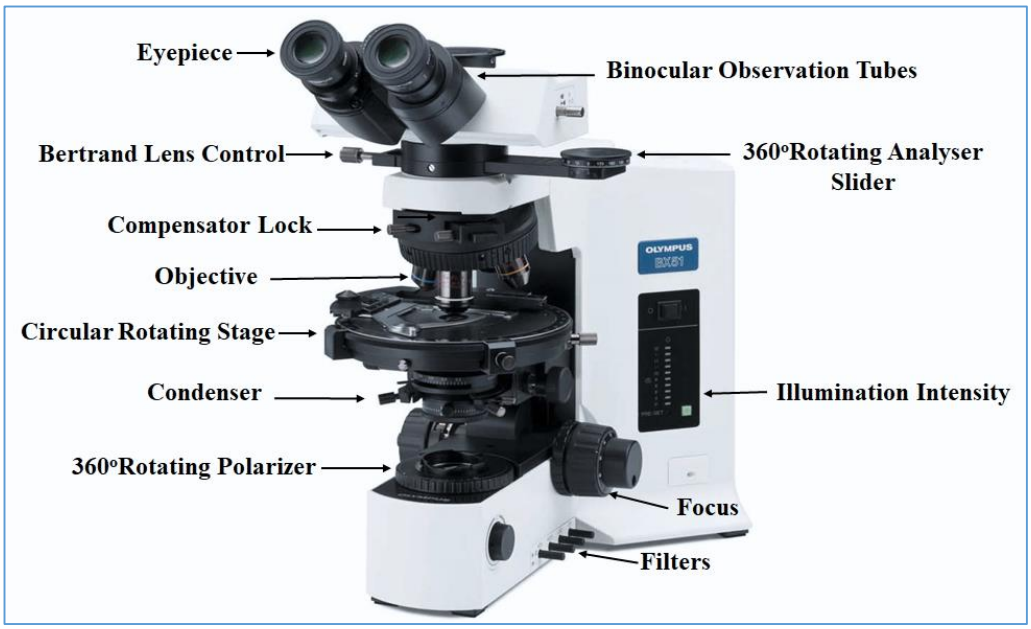

Figure 3.6: A schematic diagram of a polarising microscope BX51

3.3.2 Ray Diffraction (XRD)

X-Ray diffraction is the most precise method for identifying and measuring LCs phases with molecules arrangements. It provides the exact information of the phase structure, the atom position, the chemical bond and to which particular phase it belongs.

In 1895, X-rays were discovered by W. Rontgen, and its characteristics were unclear at that time. However, it is a powerful method for identifying LCs due to its properties: a deep penetration into all materials and has a small investigative structure. The electromagnetic radiation with a wavelength range of 10^{-3} nm to 10 nm was used in this technique. In addition, it is widely used for imaging objects and analysing materials.[15]

The principle of this method is related to hit a crystal sample with a monochromatic X-ray beam, which distributes the beam in space that spreads into particular directions and transmits the beam through crystal materials. As a result of this process, a pattern of intensities will be produced, which maps out the precise molecular position in the structure at each given temperature; see figure 3.7. Consequently, the type of LCs phase at each temperature is identified.[16,17]

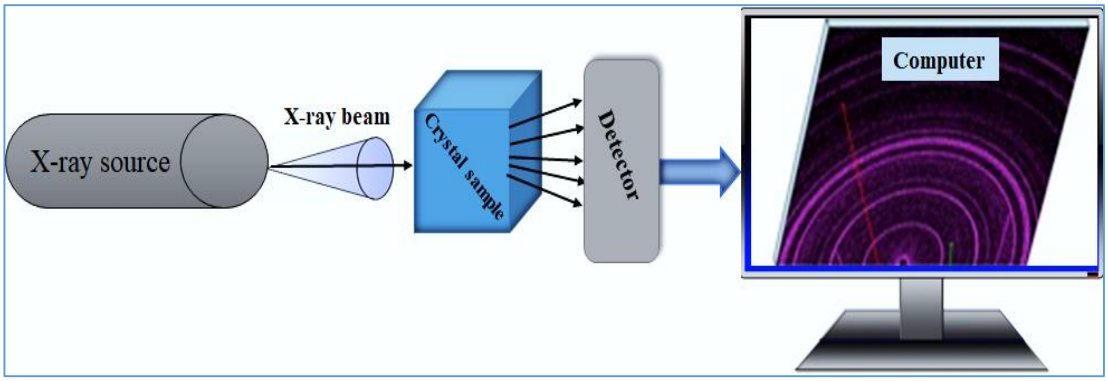

Figure 3.7: Schematic diagram of the components in XRD system

The part of X-ray diffraction was measured by filling capillary tubes with the viscous samples of LCs. These samples were placed into a MAR 345 diffractometer with diameter 345mm, which was detected by a two-dimensional image plate.

The copper tube used to generate X-rays with these properties: Cu Kα radiation, graphite monochromator, λ = 1.54 Å, 130–300 mm detector-sample distance and 30 min exposure time. These samples were heated between 297 and 355 K; a magnetic field was presented by using a home-built capillary furnace. Data squeeze software was utilised to analyse the data.[18]

3.3.3 UV-Vis Spectroscopy

The UV-Visible spectrometry was undertaken using a Perkin-Elmer (USA) UV-Vis spectrophotometer, (model Bio Lambda 10), with a clear quartz cuvette of path length 1 cm. The spectrometer was controlled using UV-Vis Chemstation software. Figure 6.1 shows the general instruments employed in this study.

Figure 3.8: UV-Visible spectrometer

3.4 References

(1) Kissinger, P. H., William.R.: *Laboratory Techniques in Electroanalytical Chemistry, revised and expanded*; CRC press, **1996**.

(2) Zoski, C. G.: *Handbook of electrochemistry*; Elsevier, **2006**.

(3) Bard, A. J., Faulkner, L. R.: *Electrochemical Methods, Fundamentals and Applications*; John Wiley and Sons: New York, **1980**; Vol. 2.

(4) EC08, A. Basic overview of the working principle of a potentiostat/galvanostat (PGSTAT)–Electrochemical cell setup. *Metrohm Autolab. BV.*, **2011**, pp 1-3.

(5) Scholz, F.: *Electroanalytical methods*; Springer, **2010**; Vol. 1.

(6) Bonfil, Y.; Brand, M.; Kirowa-Eisner, E. Trace determination of mercury by anodic stripping voltammetry at the rotating gold electrode. *Anal. Chim. Acta.,* **2000**, *424*, pp 65-76.

(7) Arévalo, M. C.; Luna, A. M. C.; Arévalo, A.; Arvia, A. J. Voltammetric approach to multicomponent electrochemical systems at platinum electrode surfaces. *J. Electroanal. Chem.,* **1992**, *330*, pp 595-614.

(8) Wang, J.; Cai, X.; Fernandes, J. R.; Ozsoz, M.; Grant, D. H. Adsorptive potentiometric stripping analysis of trace tamoxifen at a glassy carbon electrode. *Talanta.,* **1997**, *45*, pp 273-278.

(9) Skoog, D.; West, D.; Holler, F.; Crouch, S.: *Fundamentals of analytical chemistry*; Nelson Education, **2013**.

(10) Bommer, J.; Ruiter, M. Adsorption of redox-active molecules on platinum and boron-doped diamond electrodes in nanofluidic electrochemical sensors. BS, The University of Twente, **2012**.

(11) Wang, J.: *Analytical electrochemistry*; John Wiley & Sons, **2006**.

(12) Kliger, D. S.; Lewis, J. W.: *Polarized light in optics and spectroscopy*; Elsevier, **2012**.

(13) Konnen, G.: *Polarized light in nature*; CUP Archive, **1985**.

(14) Dierking, I.: *Textures of liquid crystals*; John Wiley & Sons, **2003**.

(15) Lee, M.: *X-ray Diffraction for Materials Research: From Fundamentals to Applications*; CRC Press, **2016**.

(16) Warren, B. E.: *X-ray Diffraction*; Courier Corporation, **1969**.

(17) He, B. B.; Preckwinkel, U.; Smith, K. L. Fundamentals of two-dimensional X-ray diffraction (XRD2). *Adv. X-Ray Anal.*, **2000**, *43*, pp 273-280.

(18) Halls, J. E.; Bourne, R. W.; Wright, K. J.; Partington, L. I.; Tamba, M. G.; Zhou, Y.; Ramakrishnappa, T.; Mehl, G. H.; Kelly, S. M.; Wadhawan, J. D. Electrochemistry of organometallic lyotropic chromonic liquid crystals. *Electrochem Commun.*, **2012**, *19*, pp 50-54.

Chapter 4

Electroanalysis and redox reactions of Electroactive species

This chapter is concerned with the study of electrochemical redox processes for chlorpromazine (CPZ.HCl) in a weakly acidic solution, using compounds such as L- cysteine (L-Cys.H) and potassium iodide (KI), to encourage further electron transfer processes in homogeneous solution, thereby setting-up an electron transfer cascade in a catalysis.

4.1 Basic Concepts

Electroanalytical methods are regarded as the study of chemical reactions that are induced by interfacial charge transfer processes. They allow for quantitative measurement of the extent of the electron transfer, through measurement of current-voltage curves. There are a wide range of applications, involving the determination of toxic metals in aqueous solution[1-4], environmental monitoring[5-7], and pharmaceutical analysis.[8-13] A series of excellent books and monographs have described electroanalytical methods, principal polarography, cyclic, square wave and differential pulse voltammetry, coulometry together with electron spin resonance (ESR)[14-16]and redox chemistry and biological compounds.[17-22]

In various areas of chemistry, cyclic voltammetry (CV) is an essential technique. It is extensively used to study electroactive species to interpret the intermediates of reactions, supply information about the thermodynamics of oxidation-reduction reactions and elucidate the kinetics of electron transfer reactions.[23-26]

4.1.1 Chlorpromazine: Characterization and Determination

Chlorpromazine-hydrochloride(CPZ.HCl)[2-chloro-10-(3-dimethylaminopropyl) phenothiazine mono hydrochloride] is one of the most important derivatives of the phenothiazine drug groups.[27]All phenothiazine compounds are used as neuroleptic, anti-allergic, psychotropic, local anaesthetic and anti-vomiting drugs. Scheme (4.1) shows the chemical structure of (CPZ.HCl).

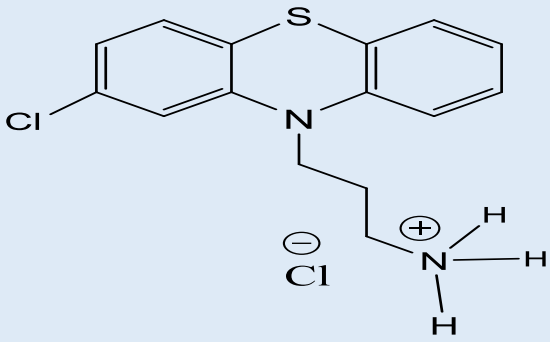

Scheme 4.1: Chemical structure of (CPZ.HCl)

Phenothiazine compounds have been analysed using methods and techniques involving thin-layer chromatography[28], UV-visible spectrophotometric[29-32], capillary electrophoresis[33-35], High-performance liquid chromatography HPLC with coulometric electrochemical detection[36] and electrochemical techniques.[37-39]Electrochemical methods are widely used to analyse a variety of biologically significant molecules.[40,41] However, there are a number of limitations inherent in using these methods directly, for instance, lack of selectivity and sensitivity, slow electron transfer kinetic and high overpotentials. To determine these compounds and other drugs in real samples, such as biological fluids, there is a need to pre-treat samples properly.[42,43]

An elegant alternative route exploits electroactive materials such as CPZ.HCl as homogeneous electron-transfer mediator[44-46] for the biological compound, or alternatives, the use of a more active electrode (electrocatalysts), for example, graphite paste[47,48], pencil graphite fibre[49], and carbon nanotubes-ionic liquid electrode, may assist in the quantitative determination of the analyte. The oxidation of chlorpromazine has been studied by choosing oxidants such as [Ce(IV), Br_2, Fe(III), and Co(III)].[50] The reduction of $[CPZ]^{+\cdot}$ to CPZ by ascorbic acid[51,52], cysteine, reduced glutathione and Fe(III)[46,50,53] has been exhibited. In this study, chlorpromazine was used as a suitable homogeneous catalyst to oxidise (L-Cys.H and KI) electrochemically.

4.1.2 Electrochemical oxidation of L-Cysteine and its properties

L-Cysteine (L-Cys.H) [2-amino-3-mercaptopropanoic acid] is a sulphur-containing α-amino acid, see scheme 4.2.The compound contains one sulphur atom, with a single group (-SH) in its molecule. Due to this fact, L-Cys.H plays a vital role in the biochemical and biomedical fields[54,55]. Furthermore, it has been utilised in the food and the pharmaceutical industries as a biomarker[56,57].

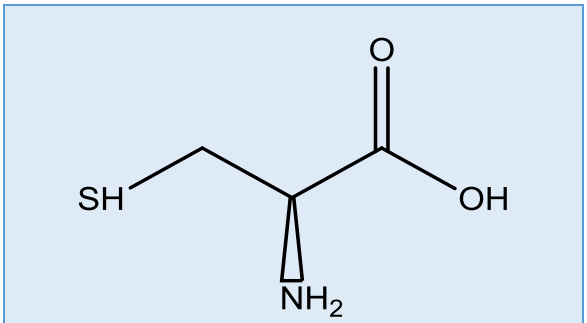

Scheme 4.2: Chemical structure of L-Cys.H

L-Cys.H and its oxidised form cystine (CSSC) [L-Cystiene3-3-di thio bis (2-amino propanoic acid) occupy a unique place among the amino acids because they contain sulphur in their molecules.[58]These distinctive features of the species attracted the interest of analytical scientists and led them to suggest numerous methods for detecting these compounds in biological and protein samples.

Moreover, various methods have been proposed for their determination, involving high-performance liquid chromatography[59,60], spectrophotometric[61,62] and flow injection amperometric.[63-65] However, most of these methods suffer from the complicated nature of the preparation needed for the samples. The detection of thiol groups has received attention for decades.The use of solid classical electrodes such as (Ag, Pt, Au, carbon and graphite) [66-70] has proved inefficient because of their high over-potential and slow heterogeneous electron transfer at the electrode. Consequently, it is necessary to

overcome these problems by modifying the surface of conventional electrodes and applying a variety of mediators.[44,71-75] Recently, the use of nanoparticles immobilised on electrodes has witnessed broad applications for determination of thiol groups.[76,77] The transferring electrons between electroactive molecules and electrodes has been enhanced by using catalysts. This chapter demonstrates how some electrochemical techniques produced redox reactions. CPZ.HCl was utilised as a mediator in EC' reactions to investigate electro-oxidations of some active species such as L-Cys.H and KI in aqueous solution.

4.2 Experimental

This section describes the general equipment used, the electrodes prepared and the experimental set-up.

4.2.1 Chemicals and Reagents

Analytical grade chemicals were used to prepare all reagents. CPZ.HCl (chlorpromazine hydrochloride), L-cysteine, and potassium iodide were purchased from Sigma-Aldrich. Potassium chloride (Laboratory reagent grade) and acetic acid glacial (Analytical reagent grade) were purchased from Fisher Scientific. Sodium acetate-3-hydrate was obtained from (BDH Laboratory Supplies). Aqueous solutions were all made using deionised water with resistivity approximately 18 MΩ cm, which was obtained from Milli-Q Advantage Al0 Water Purification System (Millipore, UK). The aqueous buffer solution was acetate buffer at pH 4.5, made using 0.1 M glacial acetic acid and 0.1M sodium acetate.

4.2.2 pH meter

The pH of the buffer solution was adjusted each time using a 210-microprocessor pH meter (HANNA Instruments), see figure 4.1.

Figure 4.1: pH Meter

4.2.3 Rotating Disc Electrode RDE

The Autolab (Metrohm 628-10) is a high-end rotating disc electrode with high rotation speeds between 500 and 3000 rpm and low noise. The RDE was used to perform electrochemical measurements under controlled hydrodynamic conditions and was designed to identify reaction intermediates *in situ* through collection experiments. Further, the RDE is suitable for a wide range of working electrodes and available in platinum, gold and glassy carbon.[78-80] The rotation speed of this electrode is controlled manually with a button at the front of the motor control unit. The operating temperature for RDE and tip is 40 °C at the maximum. The three-electrode system was outlined earlier, in section 3.2.2, (glassy WE, silver RE and graphite CE). Figure (4.2) shows this equipment.

Figure 4.2: The Autolab Rotating Disc Electrode (RDE)

4.2.4 Electrochemically induced catalytic processes

The EC' mechanism was studied as an analytical detection method. L-Cysteine and other active species may be detected by the EC' process with a mediator such as chlorpromazine hydrochloride (CPZ.HCl). The oxidation of active compounds (L-cysteine and potassium iodide) was carried out by dissolving different concentrations of CPZ.HCl in acetate buffer solution (pH 4.5). Varying concentrations of L-Cyst.H and KI were added to the solution. The buffer solution (pH 4.5) was prepared by mixing 153 mL of 0.1 M sodium acetate and 847 mL of 0.1 M acetic acid with 0.1 M potassium chloride as an electrolyte.

4.3 Results and discussion

4.3.1 The oxidation of Chlorpromazine by using cyclic voltammetry (CV)

The oxidation behaviour of 1.0 mM CPZ.HCl was examined initially by using cyclic voltammetry in a 0.1M aqueous solution of potassium chloride and 0.1 M acetate buffer solution at pH 4.5, a 3.0 mm diameter glassy carbon electrode at different scan rates 20, 50, 75, 100, 200, 400, and 500 mV s^{-1} for four consecutive cyclic voltammetry experiments. Figure 4.3 shows a pair of poor redox peaks were observed at (GCE) of 20 mV s^{-1} CPZ.HCl. The repetition of scanning caused a slight decrease in the peak current for all scan rates in figure 4.3 A. Further, It can be seen that upon increasing, the scan rates both anodic and cathodic peak currents were increased in [Figure 4.3: (B-E)] and was a slight decrease in the peak current of each scan rate.

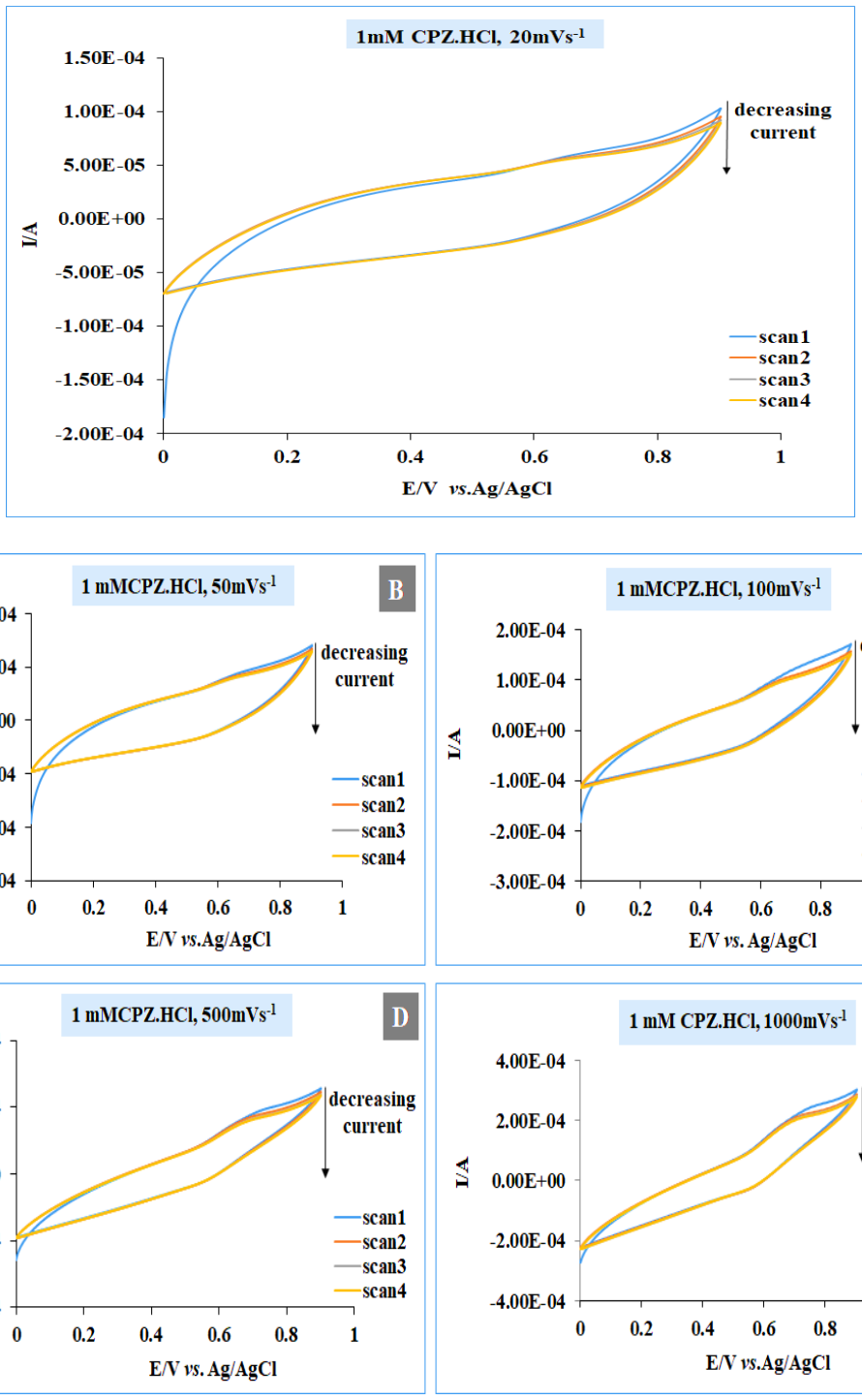

Figure 4.3: CVs for 1 mM CPZ.HCl on a GCE and in 0.1 M KCl as a supporting electrolyte. 0.1 M acetate buffer solution at pH 4.5, Ag/AgCl as a reference electrode and graphite rod as the counter electrode. Scan rates: A. 20, B. 50, C. 100, D. 500 and E. 1000 mV s^{-1}

To increase the current signal due to CPZ.HCl concentration, the previous experiment was repeated using 30 mM at the same conditions. The results obtained showed that both oxidative and reductive peak current increase along with the increase in scan rate as illustrated in figure 4.4 A-E.

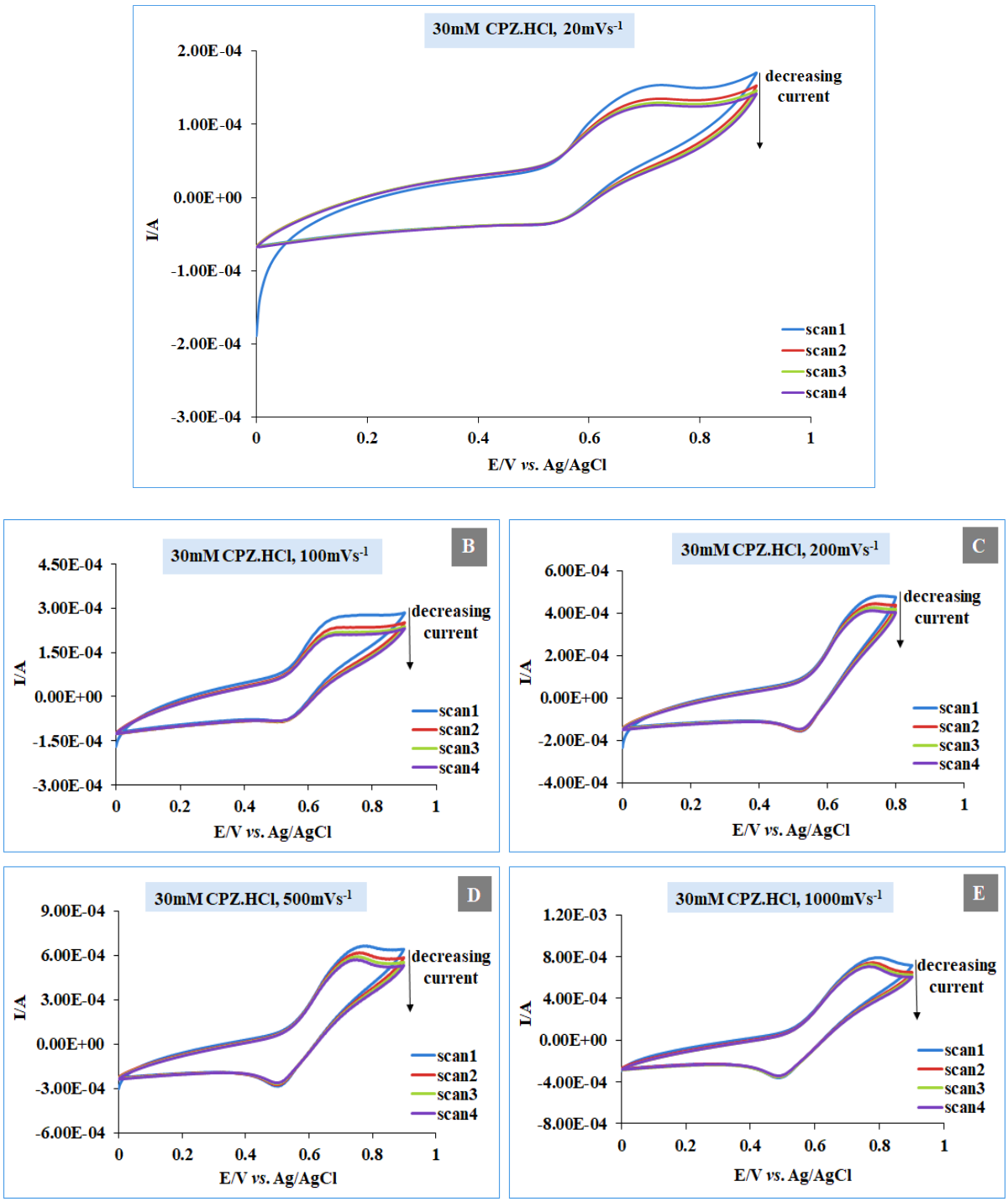

Figure 4.4: CVs for redox process of 30 mM CPZ.HCl on a GCE in 0.1 M KCl as a supporting electrolyte and 0.1M acetate as a buffer solution (pH 4.5), Ag/AgCl as a reference electrode and carbon as the counter electrode. Scan rates: A. 20, B. 100, C. 200, D. 500 and E. 1000 mV s^{-1}

Figure 4.4 A shows a well-defined and reproducible oxidative peak current at + 0.72 V *vs* Ag/AgCl with a reverse reductive peak current at + 0.52V; that resulted in a single electron oxidation that formed a stable radical of$(CPZ)^{\cdot+}$, with a cation radical back to *CPZ.HCl* (scheme 4.3).

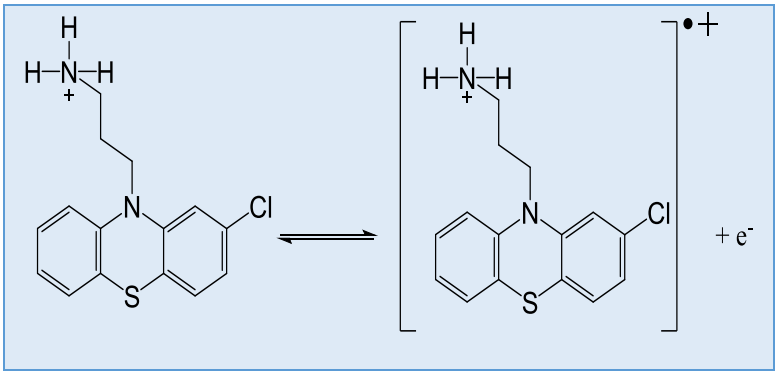

Scheme 4.3: A redox behaviour of CPZ.HCl

Through repetitive scanning in all charts in the figure 4.4 A-E, a decrease in both the oxidation and reduction peak currents were presented in each chart, and that concomitant decrease slightly shifted towards more positive potentials. Due to a complex series of chemical steps[81], see schematic 4.4:

$$CPZ.HCl - e^{\cdot} \rightleftharpoons CPZ.HCl^{\dot{+}}$$

$$CPZ.HCl^{\dot{+}} + H_2O \xrightarrow{slow} CPZ.HCl(OH)^{\cdot} + H^{+}$$

$$CPZ.HCl(OH)^{\cdot} + CPZ.HCl^{\dot{+}} \xrightarrow{fast} CPZ.HCl + CPZ.HCl(OH^{+})$$

Scheme 4.4: The rate proton mechanism of CPZ.HCl in an aqueous solution

In this process, the chlorpromazine radical cation is slowly hydrated to form an intermediate that is rapidly oxidised by a second chlorpromazine radical cation. This complex first-order disproportionation mechanism is not the subject of study in this thesis; instead, we are interested in exploring the radical cation in faster electron transfer processes in homogeneous solution. Since the latter are expected to occur more rapidly than the rate of radical cation hydration, we will ignore this complex hydrolysis mechanism.

4.3.2 Eletro-oxidation attitude of Chlorpromazine by using linear sweep voltammetry (LSV) at Rotating disc electrodes (RDE)

The oxidation process dependence of LSV of CPZ.HCl (1mM) was studied at the GCE surface by using a rotating disk electrode at a scan rate of 0.54 Vs^{-1}, with Hg/Hg_2Cl_2 as a reference electrode, see figure 4.5 **a**. It showed that there was an increase in the anodic peak currents for the oxidation of CPZ.HCl upon increasing speeds, whereas the anodic peak potentials were the same (+0.64). Figure 4.5 **b** shows the plot of oxidation peak current (I_{lim}) against the square root of speeds ($\omega^{1/2}$). The linearity of the plot indicated that the oxidation process of CPZ.HCl was diffusion controlled with R^2= 0.9832, and the value of diffusion coefficient obtained (D) was ($1.28x10^{-6}$) $m^2\ s^{-1}$. The next experiment considered the electrochemical behaviour of CPZ.HCl as a mediator upon introducing various concentrations of L-Cys.H.

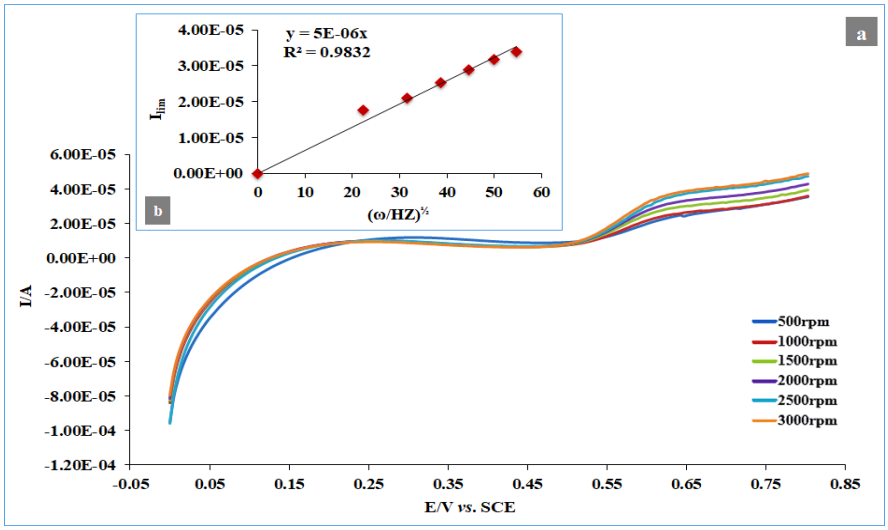

Figure 4.5: a. LSV for different speeds of 1mM CPZ.HCl (500, 1000, 1500, 2000, 2500 and 3000 rpm), pH=4.5. b. The plot of I_{lim} vs $\omega^{1/2}$ for the oxidation of chlorpromazine at the GCE with a reference electrode (SCE)

4.3.3 The electrocatalytic oxidation of L-Cys.H in the presence of CPZ.HCl as a mediator

The influence of CPZ.HCl concentrations 1, 2 and 5 mM on the peak currents were studied. The ranges involved were 0.0, 0.5, 1.0, 2.0, 5.0 and 10.0 mM of L-Cys.HCl at

various rotational speeds of the electrode, ranging from 500 to 3000 rpm. The bulk solution contained 0.1M KCl with pH (4.5) of acetate buffer solution. Accordingly, the mass transport in the bulk solution and the time of the equilibrium reaction were enhanced by using the stirring method at the constant scan rate, which gives more sensitivity.

Figure 4.6 A (**a)** presents the LSV investigation of the variation of peak currents against the potential of 1.0 mM CPZ.HCl with 1.0 mM L-Cys.H. It shows that there was an increase in oxidation peak currents with an increase in the electrode rotation speeds (ω), which meant that there was an increase in sensitivity as expected, due to high mass transport rates at the high rotation speeds. Figure 4.6 A (**b**)demonstrates the plot of peak current *versus* $\omega^{1/2}$ which is linear, with coefficient value R^2 0.968, this indicates that the reaction is transport-controlled. While, figure 4.6 A (**c)** plots half-potential for the oxidation peak *versus* log ω, where it is evident that a fluctuation in the oxidative peak potential exits. This is consistent with that expected for a following homogeneous processes, as expected that the peaks observed in the current at the higher rotation speeds correspond to the case of the classical EC' split wave that occurs when these materials and analytes concentrates are comparable.

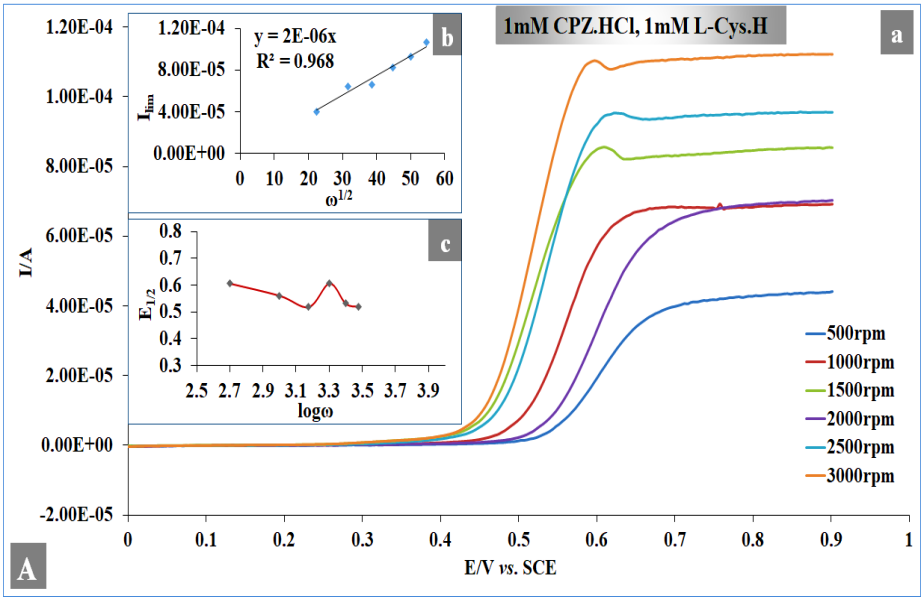

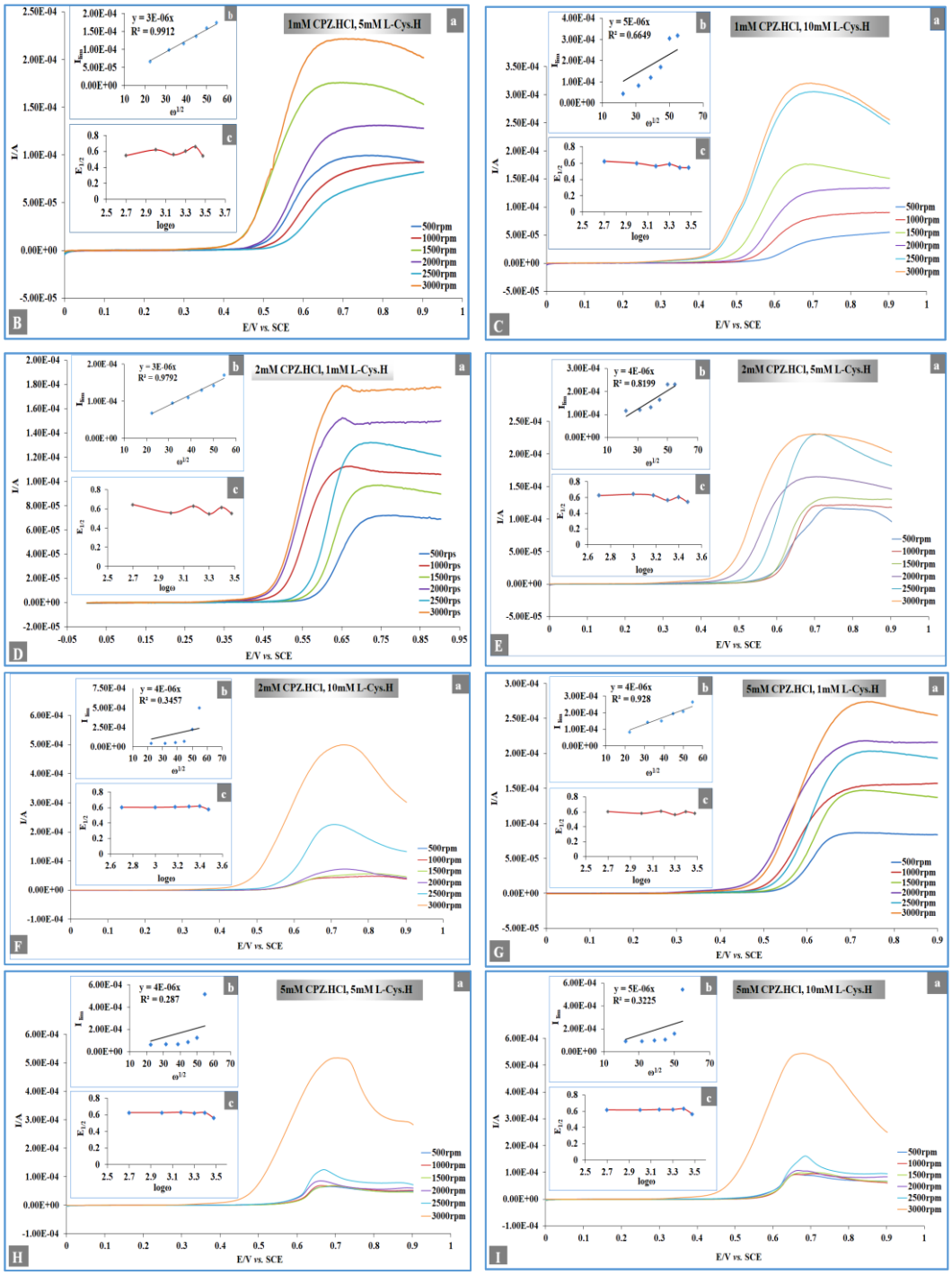

Figure 4.6 A: a. LSV of the oxidation (1.0) mM CPZ.HCl and (1.0) mM L-Cys.H at GCE in rotating the disk. SCE as a reference electrode and various ranges of rotational speeds (500-3000 rpm); b. The plot of I_{lim} vs $\omega^{1/2}$and c. A corresponding of $E_{1/2}$ vs logω. B, C, D, E, F, G, H and I were nominated inside their charts

Once more, the similarities in the trends were found upon introducing higher concentration in the range 5-10 mM of L-CysH with an increase in the mediator concentrations in the range 1-2 mM. Figures 4.6 **a** from (B) to (I) showed that the

oxidation currents increase with an increase in rotation speeds in all figures. The occurrence of split waves again is only apparent when the mediator concentrations exceed that of the analyte. The plots of maxim currents (I_p) for CPZ.HCl oxidation was linear *versus* square roots of rotational speeds in the range of 500-3000 rpm, which proposed that the process was under transport controlled, see figures 4.6 **b** from (B) to (I). The relationship of the half potentials ($E_{1/2}$) for CPZ.HCl against the logarithm of rotational speeds was fluctuating in low concentrations of CPZ.HCl for all concentrations of L-Cys.H, figure 4.6 **c** from (B) to (I), but shifts generally to less positive values (becomes easier) on increasing the transport to the surface, as expected for an EC' reaction. To understand the redox reaction electrochemically, the CVs for CPZ.HCl with L-Cys.H in different concentrations was next investigated.

4.3.4 The electrocatalytic reduction of CPZ.HCl induced by electroactive species L-Cys.H

The electrochemical reduction of various concentrations CPZ.HCl (0.1, 0.2, 0.3, 0.5, 1.0, 5.0 and 10.0 mM) in the absence and presence of different concentrations of L-Cys.H (0.0, 0.1, 0.5, 1.0, 2.0, 5.0 and 10.0 mM) were carried out using CV under the same conditions as in the previous experiments, different scan rates (20, 50, 100, 200 and 500 mV s^{-1}). A typical figure 4.7 A (**a**) shows the response of the oxidation peak current, which was increased by introducing higher concentrations of L-Cys.H with a slight shift towards less potential for all scan rates. The corresponding reduction in peak current disappeared on the backward scan of the potential from 2 mM L-Cys.H for all scan rates, which indicated that the process was chemically irreversible in these concentrations, figures 4.7 B, and C are examples of this study. The oxidation peak currents (I_p) of CPZ.HCl increases linearly with increasing the concentration of L-Cys.H within different scan rates between 20 to 500 mV s^{-1}, implying that the redox process of CPZ.HCl in the

presence of L-Cys.H was reproducible as in figures 4.7 (**b**) for A, B, and C. To obtain further information about the nature of the reaction the plots of peak potential *versus* the logarithm of scan rates were drawn, figure 4.7 (**c**) for A, B, and C.

According to the below figures, there was mainly constant in the oxidative peaks, but there is an outline for all concentrations of CPZ.HCl through introducing higher concentrations L-Cys.H to the solution, which means that the oxidation process was electrochemically reversible. Scheme 4.4 shows the mechanistic reaction of CPZ.HCl by oxidation of L-Cys.H at the GCE:

$$(CPZHCl)_{red} \rightleftharpoons (CPZHCl)^{\dagger}_{(ox)} + e^{\cdot} \qquad E$$

$$(CPZHCl)^{\dagger} + (CysH)_{(red)} \rightarrow (CPZ)_{(red)} + (CysH)_{(ox)} \qquad C'$$

Scheme 4.5: the redox reaction of CPZ.HCl

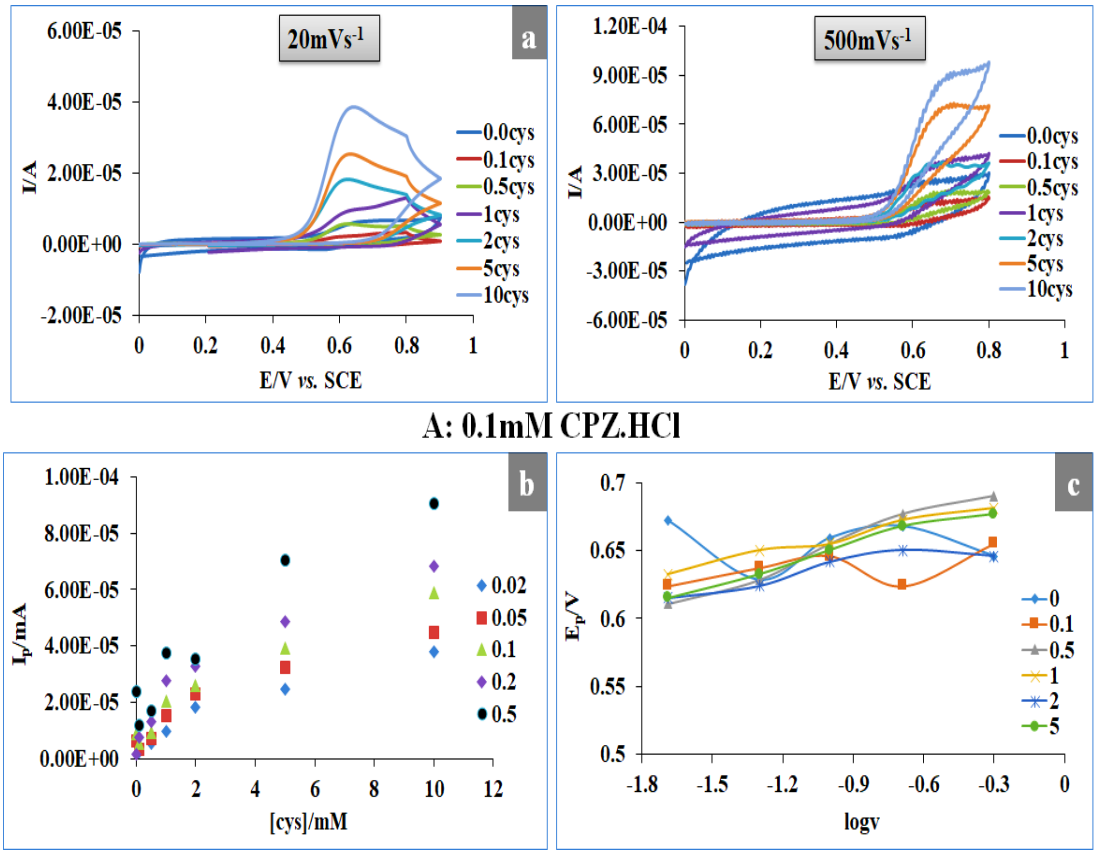

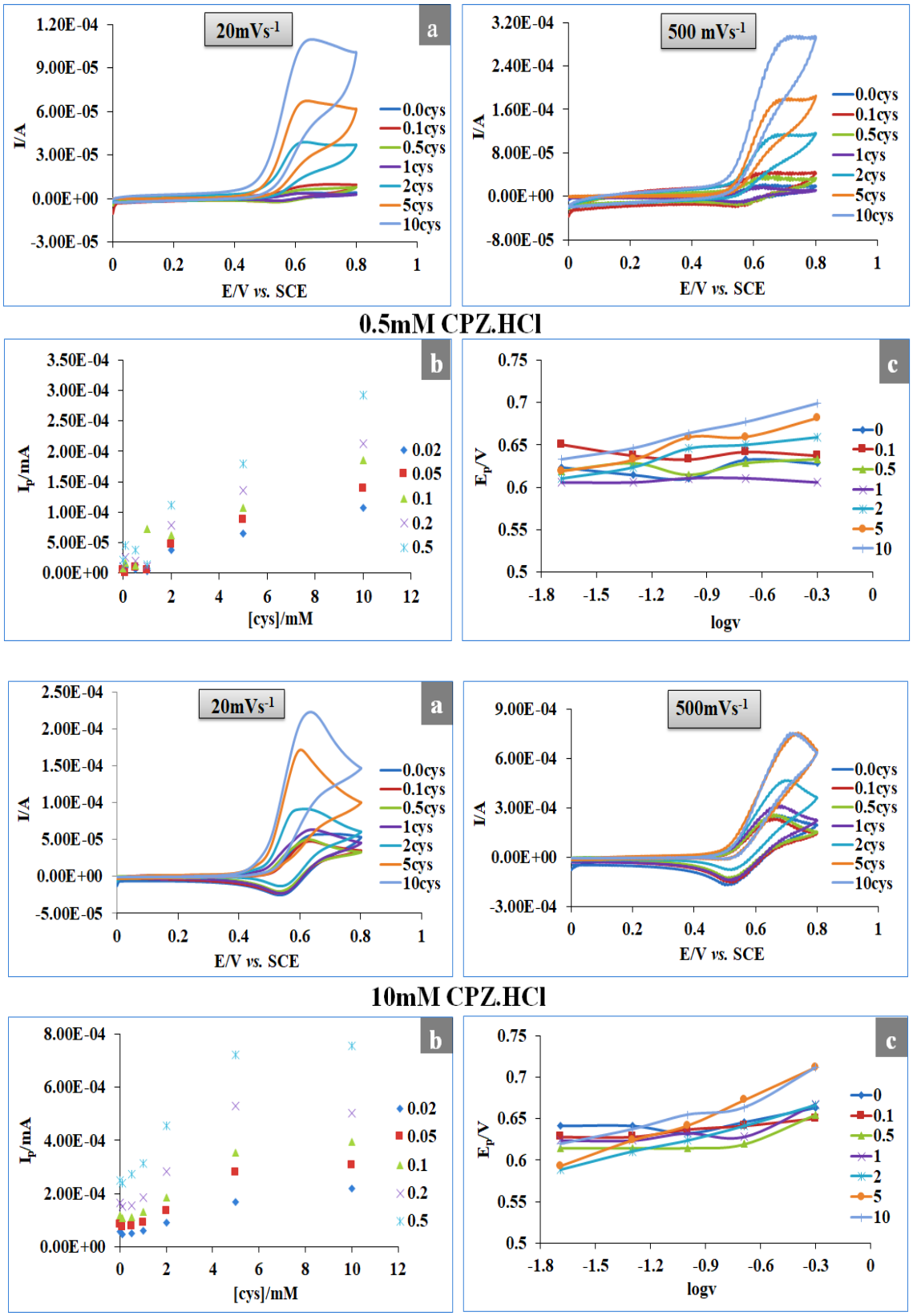

Figure 4.7A: 0.1 mM CPZ.HCl. (a): CVs for different concentrations of L-Cys.H (0.0-10.0) mM in the same conditions of the previous experiments with 20mVs^{-1} scan rate. (b): the effect of L-Cys.H concentrations on the oxidative peak currents of CPZ.HCl in various scan rates. (c): the plots of oxidative peak potentials vs log scan rates for all concentrations of L-Cys.H

4.3.5 Electroactive species KI induced catalytic reduction of CPZ.HCl by cyclic voltammetry

It is known the I_2/I^- or I_3^-/I^- redox couple may catalyse or be catalysed in homogeneous solution. Dye- sensitised solar cells (Grätzel cells) exploit this to transfer electrons from an illuminated electrode to the dark electrode. Accordingly, the investigation into whether there may be an interaction between I_3^- and CPZ.HCl or I^- and $CPZ.HCl^+$ was next undertake using various concentrations of CPZ.HCl (0.1, 0.2, 0.3, 0.5, 1.0, 5.0 and 10.0 mM) and KI at different concentrations (0.0, 0.1, 0.5, 1.0, 2.0, 5.0 and 10.0 mM) at a glassy carbon electrode. This electrode was rotated at speeds between 500 to 3000 rpm. A SCE was used as a reference electrode, while a graphite rod was used as a counter electrode. Experiments were undertaken in the buffer solution (pH 4.5), and 0.1 mM KCl as a supporting electrolyte. Three concentrations of CPZ.HCl were selected as examples to study the catalytic reaction induced by KI. The below figures 4.8 **a**: (A, B, and C) show that the anodic peak currents increase with an increase in scan rate, as expected. The plots **b**: (A, B, and C) demonstrated that the oxidative peak currents increase with an increase in the concentrations of KI for all scan rates and concentrations of CPZ.HCl. The 10 mM case is slight special owing to aggregation of CPZ.HCl at those concentrations.

In order to investigate the electrochemical reactions, the plots of oxidative peaks potential *versus* the logarithm of scan rates were found to be essentially independent of the scan rate, suggesting fast electrode kinetics, see figures 4.8 **c**: (A, B, and C).

The turnover number for various concentrations of CPZ.HCl and all concentrations of KI at the rotating disc electrode were found to be at a maximum value which was is 9 in 5.0 mM KI and 1.0 mM CPZ.HCl at the lowest scan rate (20 mV s^{-1}). The last results suggested that there was enough time for electrocatalytic reaction between

$(CPZ.HCl)^{+}$ and KI at a lower rotating rate, whereas the concentrations of CPZ.HCl up to 1.0 mM recorded lowest values in the highest rotating rates for all concentrations of KI.

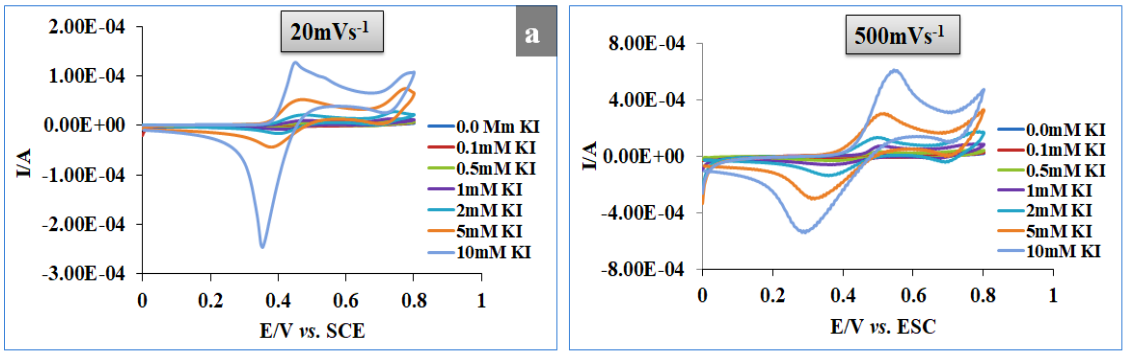

A: 0.1mM CPZ.H

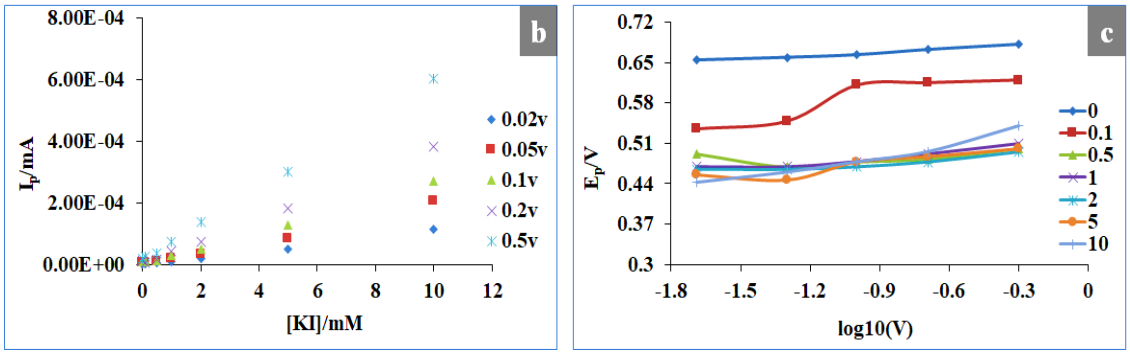

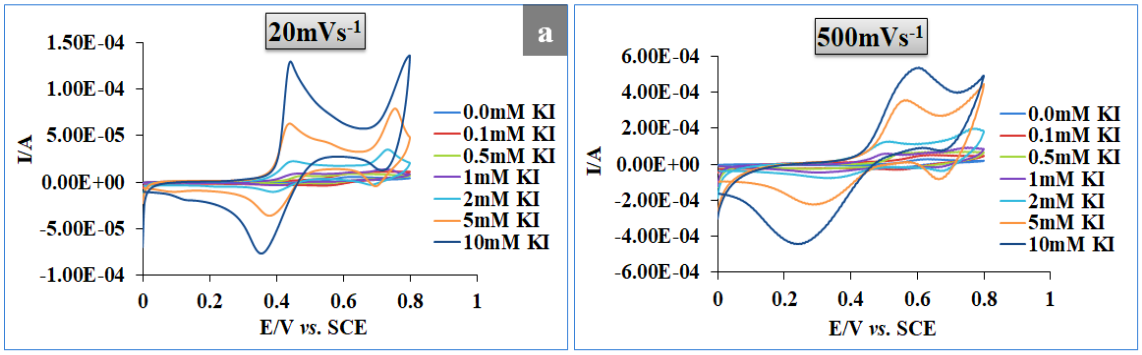

B: 1.0mM CPZ.HCl

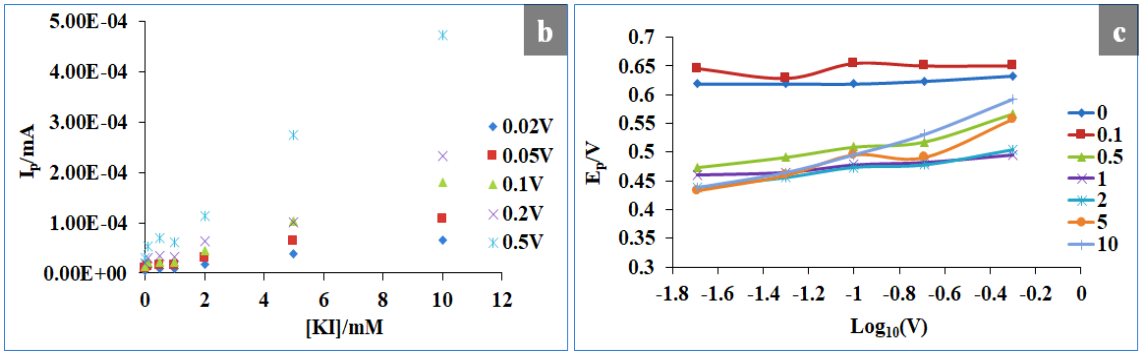

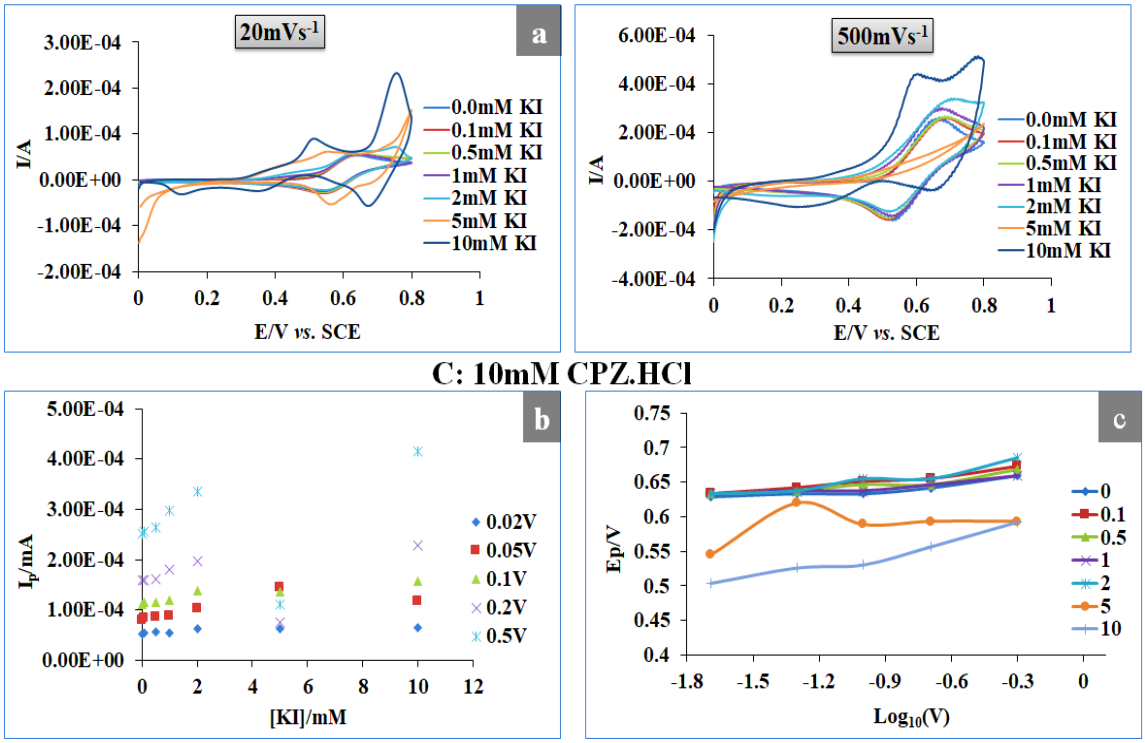

Figure 4.8: (a). CVs for different concentrations of KI (0.0-10.0 mM) in the same conditions as the previous experiments, 20 and 500 mV s^{-1} scan rates, (b). The effect of KI concentrations on the oxidative peak currents of CPZ.HCl, (c). The plots of oxidative peak potentials vs log scan rates for all concentrations of KI. A, B and C were nominated inside these figures

4.4 Conclusion

In this chapter, the fundamentals of charge transfer processes that occurred across an interface between an electrode and electrolyte were studied. A dynamic reaction was presented at a chemically reversible electrode. The work in this study was reviewing electrochemical characteristics and oxidation process of CPZ.HCl in a buffer solution (pH 4.5) at the glassy carbon electrode with and without stripping. Electroactive species such as L-cysteine and potassium iodide were used to investigate the electrocatalytic reduction of CPZ.HCl in bulk solution.

By using glassy carbon as a working electrode, it was found that that process provided a well-defined peak current upon the introduction of higher concentrations of these active species. Moreover, the electrochemical techniques that were used, notably, CVs, LSV and rotating disc electrode, voltammetry were shown to be successful in the study of

CPZ.HCl electrochemistry. The reaction between the oxidised form of CPZ.HCl and L-L-Cys.H was determined to follow the classical redox catalytic EC'.

All the electrochemistry experiments demonstrated that the oxidative peak currents of CPZ.HCl at GCE were linear to the concentration of species undertaking and that such electrode reactions occur under diffusion control.

4.5 References

(1) Mojica, E.; Gomez, S. P.; Micor, J. R. L.; Deocaris, C. C. Lead detection using a pineapple bioelectrode. *Philipp. Agric. Sci.,* **2006**, *89*, pp 134.

(2) Shao, Y. Electrochemical Cells-New Advances in Fundamental Researches and Applications. **2012**, pp 204-218.

(3) Zhao, H.; Chang, J.; Boika, A.; Bard, A. J. Electrochemistry of High Concentration Copper Chloride Complexes. *Anal. Chem.,* **2013**, *85*, pp 7696-7703.

(4) Yu, C.; Guo, J.; Gu, H. Electrocatalytical oxidation of nitrite and its determination based on Au@ Fe_3O_4 nanoparticles. *Electroanal.,* **2010**, *22*, pp 1005-1011.

(5) Zhu, G.; Yi, Y.; Han, Z.; Wang, K.; Wu, X. Sensitive electrochemical sensing for polycyclic aromatic amines based on a novel core–shell multiwalled carbon nanotubes@ graphene oxide nanoribbons heterostructure. *Anal. Chim. Acta.,* **2014**, *845*, pp 30-37.

(6) Halls, J. E.; Johnson, T.; Altalhi, A. A.; Wadhawan, J. D. Wastewater as a photoelectrochemical fuel source: Light-to-electrical energy conversion with organochloride remediation. *Electrochem. Commun.,* **2012**, *22*, pp 4-7.

(7) Yue, L.; Wang, L.; Shi, F.; Guo, J.; Yang, J.; Lian, J.; Luo, X. Application of response surface methodology to the decolorization by the electrochemical process using $FePMo_{12}O_{40}$ catalyst. *J. Ind. Eng. Chem.,* **2015**, *21*, pp 971-979.

(8) Yi, Q.; Liu, Q.; Gao, F.; Chen, Q.; Wang, G. Application of an Electrochemical Immunosensor with a MWCNT/PDAA Modified Electrode for Detection of Serum Trypsin. *Sensors,* **2014**, *14*, pp 10203-10212.

(9) Hussein, W.; Bishop, E.; Waqar, D. Electro-analysis of the drugs in solid dosage form at platinum and gold electrodes. *Pak. J. Pharm. Sci.,* **2013**, *26*, pp 977-984.

(10) Mazloum-Ardakani, M.; Beitollahi, H.; Ganjipour, B.; Naeimi, H.; Nejati, M. Electrochemical and catalytic investigations of dopamine and uric acid by modified carbon nanotube paste electrode. *Bioelectrochemistry.* **2009**, *75*, pp 1-8.

(11) Naik, K. M.; Nandibewoor, S. T. Development of Electrochemical Methods for the Determination of 6-Mercaptopurine Drug and its Analytical Applications. *India.,* **2014**.

(12) Bilibio, U.; de Oliveira, L. H.; Ferreira, V. S.; Trindade, M. A. G. Enhanced simultaneous electroanalytical determination of two fluoroquinolones by using

surfactant media and a peak deconvolution procedure. *Microchem. J.,* **2014**, *116*, pp 47-54.

(13) Dryhurst, G. Applications of electrochemistry in studies of the oxidation chemistry of central nervous system indoles. *Chem. Rev.,* **1990**, *90*, pp 795-811.

(14) Bard, A. J., Faulkner, L. R.: *Electrochemical Methods, Fundamentals and Applications*; John Wiley and Sons: New York, **1980**; Vol. 2.

(15) Lunte, S. M. L., C.E.; Kissinger, P.T.; Heineman, W.R.; (Eds.): *In Laboratory Techniques in Electroanalytical Chemistry*; 2 ed.; Marcel Dekker: New York, **1996**.

(16) Mandler, D. Fritz Scholz (Ed.): Electroanalytical methods. Guide to experiments and applications. *Analytical and Bioanalytical Chemistry* **2010**, *398*, pp 2771-2772.

(17) Sawyer, D. T. Electrochemical Studies of Biological Systems: ACS Symposium Series 38. *J. Am. Chem. Soc.,* **1977**.

(18) Dryhurst, G., Niki, K., Eds: *Redox Chemistry and Interfacial Behaviour of Biological Molecules*: New York, **1988**.

(19) Dryhurst, G. K., K. M.; Scheller, F.; Renneberg, R: In *Biological*

Electrochemistry New York, **1982**.

(20) Dryhurst, G., S., Chizmadzhev, Yu, A., Bockris, J. O.'M.,; Conway, B. E., Yaeger, E., Eds: *In Comprehensive Treatise on Electrochemistry*: New York, **1985**.

(21) Kadish, K. M., Ed. Electrochemical and Spectrochemical Studies of Biological Redox Components; Advances in Chemistry Series 201. *J. Am. Chem. Soc.*, **1982**.

(22) Dryhurst, G.: *Electrochemistry of Biological Molecules*: New York, **1977**.

(23) Kounaves, S. P. Voltammetric techniques. *Handbook of instrumental techniques for analytical chemistry* **1997**, pp 709-726.

(24) Christopher M. A. Brett, A. M. O. B.: *Electrochemistry Principles, Methods, and Applications*; 2nd ed.; Oxford University press: Oxford New York Tokyo, **1994**.

(25) Wang, J.: *Analytical Electrochemistry*; Wiley-VCH Publishers, **2000**.

(26) Bott, A. W.; Jackson, B. Study of ferricyanide by cyclic voltammetry using the CV-50W. *Curr. Sep.* **1996**, *15*, pp 25-30.

(27) Kane, J. M.; Correll, C. U. Past and Present Progress in the Pharmacologic Treatment of Schizophrenia. *J. Clin Psychiat.,* **2010**, *71*, pp 1115-1124.

(28) Chan, T.; Gershon, S. Chlorpromazine metabolism in humans. Part I. *Microchim. Acta.,* **1973**, *61*, pp 435-452.

(29) Ni, Y.; Lin, D.; Kokot, S. Synchronous fluorescence and UV–vis spectrometric study of the competitive interaction of chlorpromazine hydrochloride and Neutral Red with DNA using chemometrics approaches. *Talanta.,* **2005**, *65*, pp 1295-1302.

(30) Basavaiah, K.; Nagegowda, P.; Prameela, H.; Somashekar, B. Sensitive titrimetric and spectrophotometric assay methods for chlorpromazine with bromate-bromide mixture and two dyes. *Indian J. Chem. Technol.*, **2005**, *12*, pp 25-29.

(31) Daniel, D.; Gutz, I. G. R. Spectroelectrochemical determination of chlorpromazine hydrochloride by flow-injection analysis. *J. Pharmaceut. Biomed.*, **2005**, *37*, pp 281-286.

(32) Ni, Y. N. Q., Z.B. [Differential kinetic spectrophotometric determination of chlorpromazine hydrochloride and promethazine hydrochloride by chemometric method]. *Guang pu xue yu guang pu fen xi= Guang pu.*, **2006**, *26*, pp 1364-1367.

(33) Lin, C. E.; Liao, W. S.; Chen, K. H. Enantioseparation of phenothiazines in cyclodextrin- modified capillary zone electrophoresis: Reversal of migration order. *Electrophoresis.*, **2003**, *24*, pp 3139-3146.

(34) Chen, K.-H.; Lin, C.-E.; Liao, W.-S.; Lin, W.-Y.; Hsiao, Y.-Y. Separation and migration behavior of structurally related phenothiazines in cyclodextrin-modified capillary zone electrophoresis. *J. Chromatogr. A.*, **2002**, *979*, pp 399-408.

(35) Muijselaar, P.; Claessens, H.; Cramers, C. Determination of structurally related phenothiazines by capillary zone electrophoresis and micellar electrokinetic chromatography. *J. Chromatogr. A.*, **1996**, *735*, pp 395-402.

(36) Svendsen, C. N.; Bird, E. D. HPLC with electrochemical detection to measure chlorpromazine, thioridazine and metabolites in human brain. *J. Psychopharmacol.*, **1986**, *90*, pp 316-321.

(37) Ni, Y.; Wang, L.; Kokot, S. Voltammetric determination of chlorpromazine hydrochloride and promethazine hydrochloride with the use of multivariate calibration. *Anal. Chim. Acta.*, **2001**, *439*, pp 159-168.

(38) Belal, F.; El-Ashry, S. M.; Shehata, I. M.; El-Sherbeny, M. A.; El-Sherbeny, D. T. Differential-pulse polarographic determination of some N-substituted phenothiazine derivatives in dosage forms and urine through treatment with nitrous acid. *Microchim. Acta.*, **2000**, *135*, pp 147-154.

(39) Zhang, Z.-Q.; Chen, Z.-G.; Yang, Z.-G.; Zhang, H. Adsorptive voltammetric determination of chlorpromazine in the presence of Triton X-100. *Microchem. J.*, **1996**, *53*, pp 282-289.

(40) Fei, H.; Quan-ping, Y.; Bai-Zhao, Z. Electrochemical behaviour and determination of trifluoperazine at decanethiol self-assembled monolayer modified gold electrodes. *Wuhan Univ. J. Nat. Sci.*, **2005**, *10*, pp 435-440.

(41) Sanghavi, B. J.; Wolfbeis, O. S.; Hirsch, T.; Swami, N. S. Nanomaterial-based electrochemical sensing of neurological drugs and neurotransmitters. *Microchim. Acta.*, **2015**, *182*, pp 1-41.

(42) Biryol, I.; Sentuerk, Z.; Özkan, S.; Dermis, S.; Uslu, B. Voltammetric determination of some phenothiazines using glassy carbon electrode. *Portugaliae Microchim. Acta.*, **1997**, *15*, pp 5-16.

(43) Yang, Z.; Kauffmann, J.-M.; Valenzuela, M.-I. A.; Özkan, S. Electroanalytical behaviour of a nanoarray self-assembled thiocholesterol gold electrode. *Microchim. Acta.*, **1999**, *131*, pp 85-90.

(44) Gholami-Orimi, F.; Taleshi, F.; Biparva, P.; Karimi-Maleh, H.; Beitollahi, H.; Ebrahimi, H. R.; Shamshiri, M.; Bagheri, H.; Fouladgar, M.; Taherkhani, A. Voltammetric determination of homocysteine using multiwall carbon nanotube paste electrode in the presence of chlorpromazine as a mediator. *J. Anal. Methods. Chem.,* **2012**, *2012*.

(45) Bahramipur, H.; Jalali, F. Voltammetric determination of captopril using chlorpromazine as a homogeneous mediator. *Int. J. Electrochem.,* **2011**, *2011*.

(46) Ensafi, A. A.; Taei, M.; Khayamian, T.; Karimi-Maleh, H.; Hasanpour, F. Voltammetric measurement of trace amount of glutathione using multiwall carbon nanotubes as a sensor and chlorpromazine as a mediator. *J. Solid State. Chem.,* **2010**, *14*, pp 1415-1423.

(47) Frag, E. Y.; Zayed, M.; Omar, M.; Elashery, S. E.; Mohamed, G. G. Potentiometric determination of chlorpromazine HCl using carbon paste electrode in pure and pharmaceutical preparations. *Int. J. Electrochem. Sci.,* **2012**, *7*, pp 650-662.

(48) Parvin, M. H. Graphene paste electrode for detection of chlorpromazine. *Electrochem Commun.,* **2011**, *13*, pp 366-369.

(49) Saraji, M.; Hajialiakbari Bidgoli, A. A.; Ensafi, A. A.; Heydari-Bafrooei, E.; Farajmand, B. Highly sensitive determination of chlorpromazine by electrochemically treated pencil graphite fiber as both solid-phase microextraction fiber and working electrode for use in voltammetry method. *Anal Methods-UK.,* **2013**, *5*, pp 5024-5030.

(50) D. C. Borg and G. C. Cotzias. "Interaction of trace metals with phenothiazine drug derivatives, II. Formation of free radicals." Proceedings of the National Academy of Sciences. *Proc. Natl. Acad. Sci U.S.A* **1962**, *48*, pp 623-642.

(51) Klein, N. A.; Toppen, D. L. Kinetics and mechanism of the reduction of chlorpromazine radical by ascorbic acid. *J. Am. Chem. Soc.,* **1978**, *100*, pp 4541-4543.

(52) Huang, Y.; Chen, Z. Chemiluminescence of chlorpromazine hydrochloride based on cerium(IV) oxidation sensitized by rhodamine 6G. *Talanta* **2002**, *57*, pp 953-959.

(53) Zhou, Y. Molecular Electrochemistry. The University of Hull. PhD thesis, **2012**.

(54) Zhang, M.; Yu, M.; Li, F.; Zhu, M.; Li, M.; Gao, Y.; Li, L.; Liu, Z.; Zhang, J.; Zhang, D. A highly selective fluorescence turn-on sensor for cysteine/homocysteine and its application in bioimaging. *J. Am. Chem. Soc.,* **2007**, *129*, pp 10322-10323.

(55) Álvarez, C.; Calo, L.; Romero, L. C.; García, I.; Gotor, C. An O-acetylserine (thiol)lyase homolog with L-cysteine desulfhydrase activity regulates cysteine homeostasis in Arabidopsis. *Plant Physiol.,* **2010**, *152*, pp 656-669.

(56) Ismail, N. I.; Hashim, Y. Z. H.-Y.; Jamal, P.; Othman, R.; Salleh, H. M. Production of Cysteine: Approaches, Challenges and Potential Solution. *Int. J. Biotech. Well. Indus.,* **2014**, *3*, pp 95-101.

(57) Piste, P. Cysteine–master antioxidant. *Inter J Pharm Chem Biol Sci.,* **2013**, *3*, pp 143-149.

(58) Spãtaru, N.; Sarada, B. V.; Popa, E.; Tryk, D. A.; Fujishima, A. Voltammetric determination of L-cysteine at conductive diamond electrodes. *Anal. Chem.,* **2001**, *73*, pp 514-519.

(59) Persichilli, S.; Gervasoni, J.; Castagnola, M.; Zuppi, C.; Zappacosta, B. A Reversed-Phase HPLC Fluorimetric Method for Simultaneous Determination of Homocysteine-Related Thiols in Different Body Fluids. *Lab Med.,* **2011**, *42*, pp 657-662.

(60) Katrusiak, A. E.; Paterson, P. G.; Kamencic, H.; Shoker, A.; Lyon, A. W. Pre-column derivatization high-performance liquid chromatographic method for determination of cysteine, cysteinyl–glycine, homocysteine and glutathione in plasma and cell extracts. *J. Chromatogr. B Biomed. Sci. Appl.* **2001**, *758*, pp 207-212.

(61) Bulatov, A. V.; Petrova, A. V.; Vishnikin, A. B.; Moskvin, L. N. Stepwise injection spectrophotometric determination of cysteine in biologically active supplements and fodders. *Microchem J.,* **2013**, *110*, pp 369-373.

(62) Warad, I.; Al-Nuri, M.; Abu Eid, M.; Al-Othman, Z.; Al-Resayes, S.; Diab, N. Kinetics and Mechanism of Oxidation of L-Cysteine by Bis-3-di-2-pyridylketone-2-thiophenylhydrazone-iron (III) Complex in Acidic Medium. *J. Chem-Ny.,* **2010**, *7*, pp S527-S535.

(63) Cao, Q.-E.; Zhao, Y.; Hu, Z.; Xu, Q. Study on the flow injection method for the determination of L-cysteine with a Cu (II) complex by fluorescence quenching. *Indian J. Chem. Sect A.,* **2001**, *40*, pp 1344-1347.

(64) Martinović, A.; Cerjan-Stefenović, Š.; Radić, N. Flow Injection Analysis with Two Parallel Detectors: Potentiometric and Spectrophotometric Determination of Thiols and Ascorbic Acid in Mixture. *J. Chem. Metrol.,* **2008**, *2*.

(65) Dursun, Z.; ŞAHBAZ, İ.; Ertaş, F. N.; NİŞLİ, G. Voltammetric and flow injection amperometric determination of cysteine at a glassy carbon electrode in the presence of Copper (II) ions. *Turk J Chem.,* **2003**, *27*, pp 513-520.

(66) Maleki, N.; Safavi, A.; Sedaghati, F.; Tajabadi, F. Efficient electrocatalysis of L-cysteine oxidation at carbon ionic liquid electrode. *Anal. Biochem.,* **2007**, *369*, pp 149-153.

(67) Arrigan, D. M. A study of L-cysteine adsorption on gold via electrochemical desorption and copper (II) ion complexation. *Analyst.,* **1999**, *124*, pp 1645-1649.

(68) Hager, G.; Brolo, A. G. Adsorption/desorption behaviour of cysteine and cystine in neutral and basic media: electrochemical evidence for differing thiol and disulfide adsorption to a Au (111) single crystal electrode. *J. Electroanal. Chem.,* **2003**, *550*, pp 291-301.

(69) Drożdż, R.; Naskalski, J.; Ząbek-Adamska, A. Potentiometric determination of cysteine with thiol sensitive silver-mercury electrode. *Acta Biochim. Pol.,* **2007**.

(70) Barus, C.; Gros, P.; Comtat, M.; Daunes-Marion, S.; Tarroux, R. Electrochemical behaviour of N-acetyl-l-cysteine on gold electrode—A tentative reaction mechanism. *Electrochim.Acta.,* **2007**, *52*, pp 7978-7985.

(71) Fei, S.; Chen, J.; Yao, S.; Deng, G.; He, D.; Kuang, Y. Electrochemical behavior of L-cysteine and its detection at carbon nanotube electrode modified with platinum *Anal. Biochem.,* **2005**, *339*, pp 29-35.

(72) Lu, L.; Zi, Y.; Wang, H. Microdetermination of human serum albumin by differential pulse voltammetry at a L-cysteine modified silver electrode. *J. Chem Sci.,* **2008**, *120*, pp 419-424.

(73) Benvidi, A.; Jahanbani, S.; Mazloum-Ardakani, M.; Mirjalili, B. F. Electrocatalytic determination of cysteine on the multi-wall carbon nanotubes glassy carbon electrode using a homogenous mediator. *J .Appl. Chem.,* **2013**, *8*, pp 49-54.

(74) Mazloum-Ardakani, M.; Rajabi, H.; Bietollahi, H. Electrocatalytic oxidation of cysteine by indigo carmine modified glassy carbon electrode. *J. Argentine Chem. Soc.,* **2009**, *97*, pp 106-115.

(75) Yang Song , Y.-Z. S., An-Feng Zhu&Hui Zhong Jingliang. L-cysteine - nano-gold modified glassy carbon electrode and its application for determenation of dopamine hydrochloride *Indian J. Chem.,* **2011**, *50A*, pp 1006-1009.

(76) Zhang, L.; Yuan, R.; Chai, Y.; Li, X. Investigation of the electrochemical and electrocatalytic behavior of positively charged gold nanoparticle and l-cysteine film on an Au electrode. *Anal. Chim. Acta.,* **2007**, *596*, pp 99-105.

(77) Jasimuddin, K. B. S. Elecyrocatalytic oxidation of ascorbic acid by immobilized silver nanoparticals on self-assembled L-cysteine monolayer modified gold electrode *Indian. J. Chem.,* **2014**, *33A*, pp 57-61.

(78) Bonfil, Y.; Brand, M.; Kirowa-Eisner, E. Trace determination of mercury by anodic stripping voltammetry at the rotating gold electrode. *Anal. Chim. Acta.,* **2000**, *424*, pp 65-76.

(79) Paulus, U. A.; Schmidt, T. J.; Gasteiger, H. A.; Behm, R. J. Oxygen reduction on a high-surface area Pt/Vulcan carbon catalyst: a thin-film rotating ring-disk electrode study. *J. Electroanal. Chem.,* **2001**, *495*, pp 134-145.

(80) Štulíková, M. The deposition and stripping of mercury on a glassy carbon rotating disk electrode. *J. Electroanal. Chem. Interfac.,* **1973**, *48*, pp 33-45.

(81) Cheng, H. Y.; Sackett, P. H.; McCreery, R. L. Kinetics of chlorpromazine cation radical decomposition in aqueous buffers. *J.Am.Chem.Soc.,* **1978**, *100*, pp 962-967.

Chapter 5

Heterogeneous Electron Transfer of Chlorophyllin

This chapter presents a short overview of the definition and the structure of chlorophyll. It will scrutinise some of the derivatives of chlorophyll; the chapter will also review the structure and the practical use of chlorophyllin derivative of chlorophyll. The topics above will be presented in the first section. The second section will deal with the details of the experimental method. The analysis of data gathered through the experiments and a discussion form the third section. The chapter ends with a summary and concluding remark.

5.1 Light-harvesting pigments (LHP) chlorophyll and its derivatives

Natural pigments play a crucial role in harvesting solar energy and converting visible light into electrical energy.[1-4] The light conversion process is supported with sensitisation of numerous semiconductors by appropriate dyes.[5,6]

Several organic dyes and metal complexes have been synthesised and used as sensitisers. Although the most effective sensitisers are ruthenium-based complexes, due to their properties, charge transfer between metal/ligand and absorption over wide visible range[6,7], they are costly to manufacture and environmental pollution. Therefore, an alternative method is suggested such as natural dyes from plants and fruits with low cost, high light-harvesting efficiency and eco-friendliness. [8-10] In this regard, several dyes have been used as sensitisers such as anthocyanins, carotenoids and chlorophyll which are easily extracted from natural sources.[11,12]

5.1.1 Background information and basic structure of chlorophyll

Chlorophyll is a green pigment in the chloroplast of almost all plant cells. It is mostly present in green plant tissues, algae and cyanobacteria. The leaves of a plant have approximately 70 million cells and 5 billion chloroplasts, which contains about 600 million molecules of chlorophyll. Chlorophyll derives its name from the Greek words "chloros" meaning green and "phyllon" meaning leaf[13]. Chlorophyll plays a crucial role in the photosynthesis process for plants by harvesting solar energy, which is converted into food and oxygen; see equation 1.1 in chapter one.[14-17]

Chlorophylls (chls) are planar molecules composed of chlorin pigments that are derived from the original compound porphyrin[18] a cyclic tetrapyrrole (figure 5.1). Porphyrin (and its parent porphin) plays a vital role in nature; it is considered the basic unit of the red

pigment of blood (heme) and the green pigment of the plant (chlorophyll). Moreover, porphyrin and metalloporphyrin compounds involve particular structure and larger molecular surface. They have been used in theoretical research on the foundation of life and its processes, such as respiration, photosynthesis and energy conversion especially electron transfer and photoelectrochemical conversions.[19,20]

In 1817, chlorophyll was isolated by Pierre Joseph and Joseph Bienamine´ for the first time.[17] Stokes in (1864) was the first scientist to conclude spectroscopically that two types of chlorophyll existed. Sorby isolated these in 1873. The structures of chlorophyll a and b were shown in 1940 by Hans Fischer.[21] In the order of their discovery, the four types of chlorophyll can be classified as a, b, c and d.[14,22] These have four tetrapyrrole rings (figure 5.1), and four nitrogen atoms, which are strongly bound to a magnesium ion (Mg^{2+}) at the centre of the porphyrin ring: they are different only in the side of the carbon chain (phytol).[23]

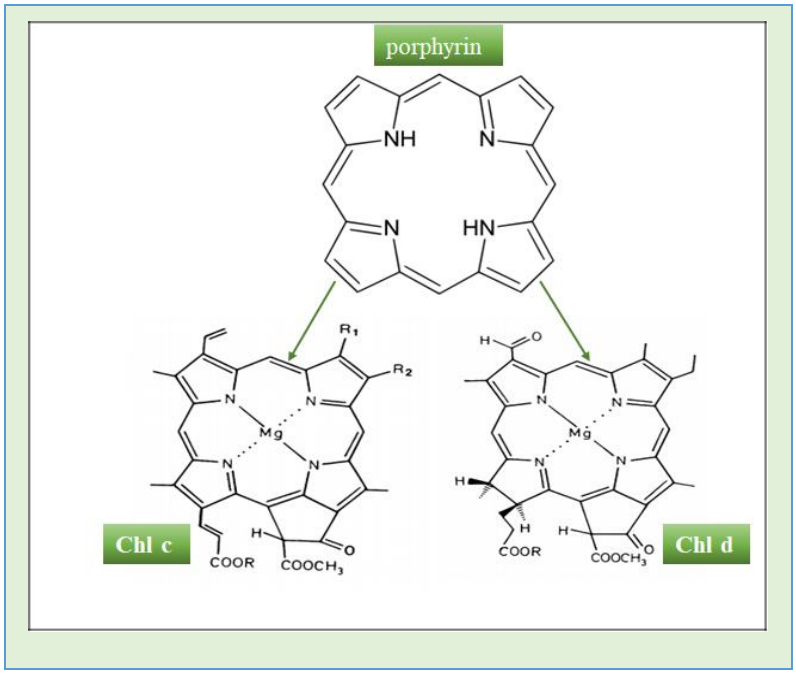

Figure 5.1: Porphyrin structure and chlorophyll (c and d) adapted from online web source [15]

Chl a, and b (figure 5.2) are the most common for their essential roles in operating light-harvesting and performing electron transfer reactions.[14,24]

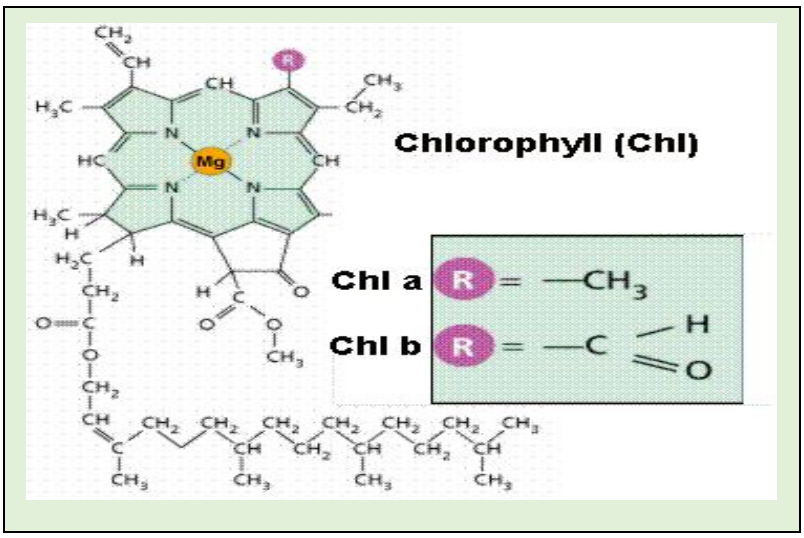

Figure 5.2: Structure of chlorophyll a and b adapted From the online web source[25]

A mixture of chlorophyll a and b is responsible for the green pigment in plants, which are present in the ratio 3 (for a): 1 (for b).[15,21,26] Traditionally, chlorophyll has been classified into two types: soluble in oil and soluble in water. The former is used as a pigment in paints, foods, waxes, ointments and pharmaceuticals.[27] The latter is used in the preparation of soaps, shampoos, candies, toothpaste, mouthwashes and medical products.[28] Figure 5.3 displays the range of the visible light spectrum from violet to red in which plants possess pigments that can absorb light in particular regions of the spectrum.

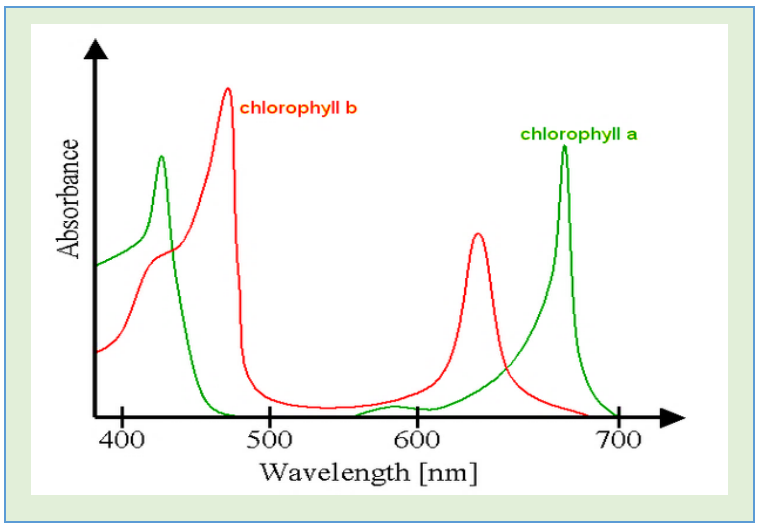

Figure 5.3: The absorption spectrum for chlorophyll (a and b) adapted from an online source[29]

Chlorophyll a absorbs light for photosynthesis in the spectrum regions violet, blue and red. Conversely, chlorophyll b absorbs more in the blue and orange-red ranges. From the figure 5.3, the strong absorption peaks for chlorophyll a are located in the visible region 420 nm and 660 nm wavelengths. Chlorophyll absorption in the visible region can be utilised as a natural sensitiser.[30,31] Accordingly, the colour of chlorophyll pigment is green as it absorbs light in all of the other colour ranges; thus, only green is transmitted to the human eye.

5.1.2 Use of chlorophyll in photovoltaic cells

Chlorophyll is a light harvesting pigment, which absorbs light in the visible spectrum of sunlight and promotes electron transfer. Nowadays, chlorophyll pigment and its derivatives are utilised in organic photosynthetic solar cells for their desirable photovoltaic properties.[32,33] Chlorophyll alpha (α) or a, and chlorophyll beta (β) or b are necessary for proper absorption of different parts of the visible solar spectrum. Photosynthesis takes place because of light energy absorption; a process which gives rise to an electron transfer cascade. Therefore, the energy will flow through the photovoltaic system with electron transference. Further, these pigments and their derivatives are used as donor molecules in the process of energy transfer in plants.

There is an abundance of research investigating the replacement of the central atom of magnesium with other transition metal ions such as copper, zinc or iron. By doing so, the electron transfer process is significantly increased.[34-37] Due to their semiconducting properties, the common dyes attracted the attention of researchers who began to use them in the photovoltaic cell.[38-40] The effects of several important biological molecules, such as chlorophyll, carotenes and other porphyrins, on photovoltaic cells have been observed. In 1970 Meilinov *et al*., calculated the photoconductivity quantum of a film sandwich system of Al/chla/Al.[41] Since research on chlorophyll a and other organic dyes with

varying electrodes and systems used in photovoltaic cells, researchers have concluded that the use of organic than inorganic dyes in solar cells is still limited in the marketplace.[42-45]

5.1.3 Chlorophyllin, characteristics and usages

One of the most essential derivative molecules of natural green pigment chlorophyll is chlorophyllin (CHL). It is a semi-synthetic water-soluble salt, which is obtained by hydrolysis of the phytol tail in a chlorophyll molecule with the replacement of the magnesium in the centre of the porphyrin ring by copper atom while methyl and phytyl ester group by sodium.[46] The replacement process is considered a way of increasing electron transfer in chlorophyll.

Chlorophyllin, as a hydrophilic molecule, is more soluble in water than chlorophyll and is more stable in moderate light, heat, oxygenated conditions, extreme absorption in the visible light and low pH. [15,47-49] Figure (5.4) shows the molecular structure of copper trisodium chlorophyllin.

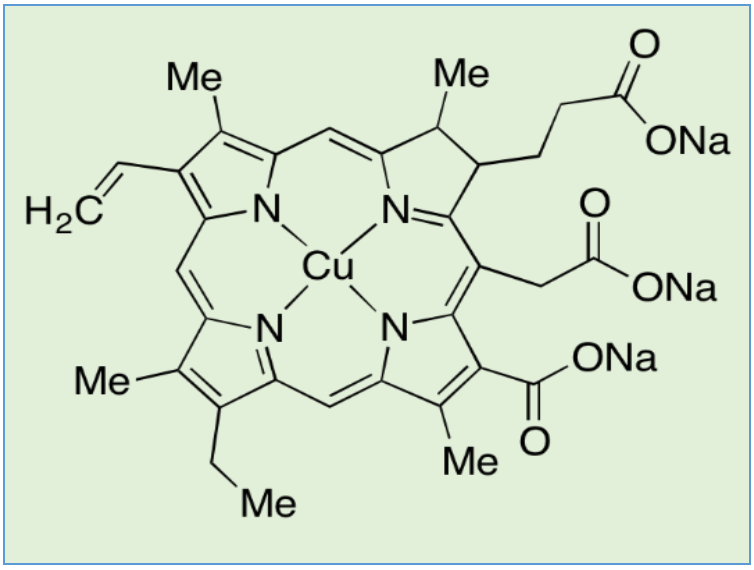

Figure 5.4: The diagram of chlorophyllin, copper trisodium salt

Regarding antioxidant activity, chlorophyllin has been shown to be higher than chlorophylls including a and b. Despite research related to the biological activities of

chlorophyllin, the full mechanism of its action is still not understood. That being the case, it is very significant to get insight into the reductive-oxidative behaviour of chlorophyllin, using voltammetry. There are many steps to produce a commercial compound of CHL from raw material, which is almost always alfalfa or grass.[21,47]

There are numerous applications of chlorophyll and its derivatives such as chlorophyllin in our daily lives due to their particular structure. The structure confers the ability of this pigment to act as an antioxidant, serve in the treatment of anaemia, control of offensive body odour, and act as anti-carcinogenic agent.[50-54] Despite using chlorophyllin in solar cell applications[55] through a broad range potential, using objective chlorophyllin is difficult in such applications as thin films due to its extreme mechanical strength.[56] There are no toxic effects of using chlorophyll or its derivatives for treatment.[47,57]

5.1.4 Chlorophyll derivatives: radiation and photosynthesis

Recently, sodium copper chlorophyllin (CHL) has become an area of interest of several studies in vivo and in vitro such as radiation and photosensitization, which produced lipid peroxidation in subcellular fractions and biological tissues, such as lysosomes, mitochondria, microsomes and rat liver mitochondria.[58-60] Recently, a group of scholars researching into cancer have discovered that chlorophyll can accumulate in growing tissues and tissues undergoing regeneration.[61] Chlorophyll and their derivatives are common light-sensitive compounds of photosensitizers and are selectively retained by tumour cells.[61,62]The therapeutic potential lies in the ability of the porphyrin structure to undergo photosensitization upon exposure to light. Illumination of the molecule converts it to a short-lived triplet excited state. Typically, sensitiser molecules in the triplet state can abstract an electron (or hydrogen atom) from, or donate an electron (or hydrogen atom) to, a substrate molecule. The anionic or cationic radicals of the sensitiser can then react with oxygen and form reactive oxygen species. These species rapidly react with

some electron-rich molecules such as unsaturated lipids, amino acids, DNA-bases and so forth, thereby the interference with the normal activities of subcellular structures resulted in the injury and death of cells in proximity to the sensitiser molecule. Moreover, the chlorophyll and chlorophyllin photosynthetic process have been studied in light of the electrochemical oxidation of chlorophyll and metal ion/b-substitution, which affects the redox properties of chlorine/bacteriochlorins in aqueous and non-aqueous solutions. These studies summarise that chlorophyll a, b and d in non-aqueous media undergo four reversible redox reactions, while in the aqueous media chlorophyll a shows irreversible reactions corresponding to one-electron oxidation.[63-66]

5.2 Experiment setup

5.2.1 Reagents

All chemical reagents were used in this research without further purification. Deionised water with 18 MΩ cm resistivity was used to prepare all aqueous solutions; the temperature was 20 ± 3 ˚C. The electrolyte solutions were purged for 10-30 minutes with nitrogen. Table 5.1 shows the list of those reagents.

Table 5.1: The list of Chemical reagents

Chemical name	Chemical Formula	Common name	Supplier and percentage
Aluminum oxide	Al_2O_3	alumina	Electron Microscopy Sciences, 0.3µm, metal polishing compound
Argon gas	Ar	-	BOC Gases, UK, Energas LTD, 99.9%

Chlorophyllin, coppered trisodium salt	$C_{34}H_{31}CuN_4Na_3O_6$	Chlorophyllin	Alfa Aesar
Hydrochloric acid	HCl	Muriatic acid	Sigma-Aldrich>99.99%
Methyl cyanide	CH_3CN	acetonitrile	Fisher Chemical >99.9%
Nitrogen gas	N_2	-	BOC Gases, UK, Energas LTD 99.99%
potassium chloride	KCl	Salt substitute	Fisher Scientific>99.99%

5.2.2 Instrumentation and Experimental Setup

The experimental equipment used in this section were potentiostats manufactured by Metrohm® µAutolab Type III and equipped with GPES 10.1 software for all voltammetric measurements, written by Metrohm®. The temperature was maintained at 296 ± 0.5 K in the dark for all electrochemical experiments. In all cases, unless otherwise stated, a conventional three-electrode system was employed in all experiments. Graphite as a counter electrode, and silver/silver chloride (3mol L^{-1}) as a reference electrode while two different working electrodes, a Metrohm® gold disk electrode, Figure 5.5 (2mm diameter, 80mm length) and a Metrohm® glassy carbon disk electrode (3mm diameter, 0.07cm^2 area), were used.

Figure 5.5: A gold Disc Electrode

In all experiments, the redox reactions were undertaken at the surface of a working electrode. Therefore, the working electrode required frequent polishing by the appropriate size of carborundum paper (400, 1200 2400 grade, Presi, France) with 3μm alumina paste (Presi, France). Thus, reproducible results were obtained, and the absorbed species was removed from the surface of this electrode.

5.2.3 Preparation of working electrode

The working electrode was polished mechanically to a mirror finish before each run and then rinsed with deionised water (DI). The working electrode was modified by immersing a gold or glassy carbon disk in the chlorophyllin copper salt solution for a period ranging from two hours to three days.

After that, the modified electrode surface was rinsed with distilled water, which was coated successfully with chlorophyllin before immersing in the appropriate solution. Electrochemically, during this procedure, General Purpose Electrochemical System (GPES) measured acceptable ranges of potentials (20-2000 mV s^{-1}). The solutions were degassed with high-purity nitrogen before the electrochemical measurements.

5.3 Results and Discussion

Electrochemical behaviour of adsorbed Chlorophyllin on Gold electrode immersed in different electrolytes

A range of oxidation-reduction (redox) processes was studied at the gold electrode.[67-72] It has been reported that at such gold electrodes those inorganic redox couples that are oxidised and reduced *via* an outer sphere electron transfer mechanism show reversible electrochemical behaviour. The redox electrochemistry at gold electrodes has been investigated in a range of active species in aqueous solution.[73-75]

This chapter scrutinises electrochemical adsorption of one of the semi-synthetic derivatives of chlorophyll such as chlorophyllin at the gold electrode in a range of adsorption times, various electrolytes, concentrations and electroactive species. Specifically, a gold electrode is employed in a study of the cyclic voltammetry of chlorophyllin as a mediator in redox reactions. The importance of gold electrode surface preparation in determining the mechanism of redox is described, and the environment of the adsorption process of the different concentrations of chlorophyllin on the surface of the gold electrode has been elucidated in this section.

5.3.1 The influence of electrochemical parameters on chlorophyllin (CHL) adsorption at the electrode surface

Adsorption of the substance on the electrode surface is a phenomenon, which affects electrochemical signals. Conversely, on the electric field at an electrode surface may enlarge adsorption, with current signals that may trigger binding and unbinding of the analyte to the electrode. The binding is either a chemical bond (chemisorption) or a physical bond (physisorption). Chemisorption is stronger than physisorption, because it consists of ionic or covalent bonding of the molecules, whereas physisorption consists of

weak intermolecular forces such as van der Waals forces and dipole-dipole interactions.[76,77]

There are various conditions for the amount of active species which are adsorbed on the working electrode, such as the material of the surface, the nature of the molecules, the applied potential, temperature and so forth.[78,79] In the following section, some of these parameters are examined.

5.3.1.1 The substantial electrode surface used of glassy carbon electrode (GCE)

The initial study was to examine the redox process of different adsorption concentrations of chlorophyllin on the glassy carbon (GC) electrode using inorganic electrolytes such as KCl and HCl. It was followed by investigating a working electrode of another substance such as gold (Au) in both inorganic and organic electrolytes by using cyclic voltammetry.

Prior to the electrochemical study, the working (GCE) and (AuE) electrodes surfaces were prepared by immersing them in the various concentrations of chlorophyllin (1, 2 and 5 mM) for three days. The electrolyte was degassed by using N_2 or Ar for approximately 30 minutes inside a Faraday cage before any electrochemical experiment was performed. Also, the gas was passed over the electrolyte during the experiments.

A three electrode system was used with Ag/AgCl as a reference electrode, graphite as a counter and the working electrode. The electrochemical response, of (1, 2 and 5 mM) CHL for the glassy carbon disk was immersed firstly in 0.1M KCl, and secondly in 0.1M HCl by using various scan rates (20, 50, 100, 200 and 500 mVs^{-1}). Figures (5.6 and 5.7) show the voltammograms of some scan rates.

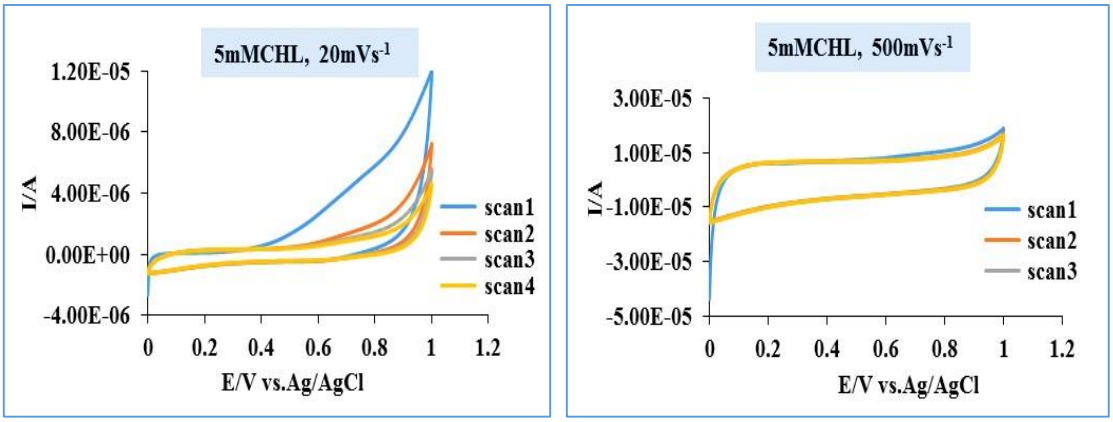

Figure 5.6: Cyclic voltammograms 20 and 500 mV s^{-1} are detailing the response of the CHL 5mM in 0.1 KCl, which was adsorbed on the GCE

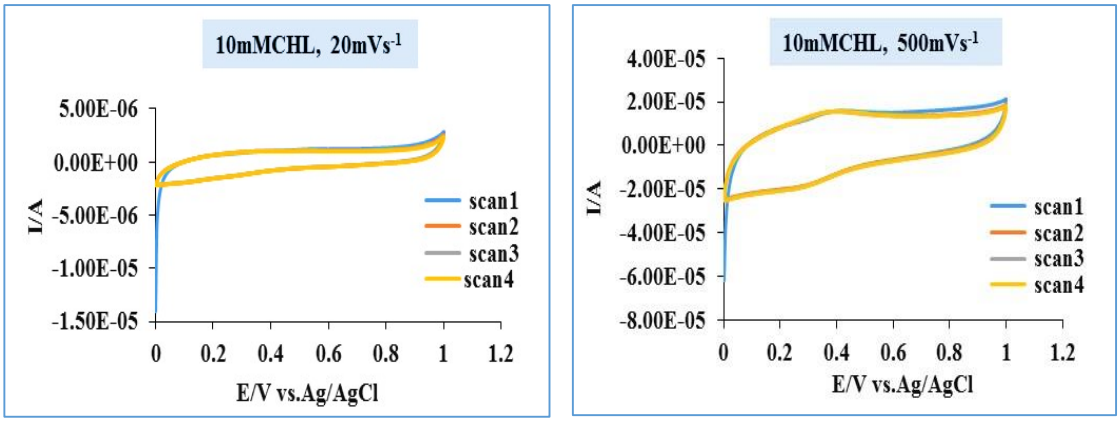

Figure 5.7: Cyclic voltammograms for 10 mM of CHL recorded at GCE immersed in 0.1 M HCl, selected scan rates 20 and 500 mV s^{-1}

As seen in the figures above, the correspondence of the oxidation and reduction peaks are not observed well at the electrode/electrolyte interface for all scan rates, potentials and concentrations of chlorophyllin, indicating that only weak adsorption of CHL occurs on carbon. Accordingly, experiments were undertaken on a gold surface.

5.3.1.2 The influence of the gold electrode (AuE) surface

Cyclic voltammograms were recorded for the electrochemical redox reactions of 10 mM CHL on the gold electrode in 0.1 M for both inorganic (HCl) and organic (acetonitrile) electrolytes. Figure 5.8 illustrates the responses at the gold electrode, which was immersed in a CHL solution for two hours, followed by using an inorganic electrolyte (HCl) in an electrochemical cell.

The voltammograms show a well-defined oxidation peak at +0.68 V due to the single-electron oxidation of CHL to form the chemically stable radical cation, which is shown in the Scheme (5.1). There was an increase in peak current with increasing scan rates. In contrast, the corresponding peaks current in the reverse scan rates were not clear. Moreover, the background will not deal with integrating impact and the area integrate will not go back. Thus, the gold electrode was sufficient for adsorbing CHL pigment on its surface.

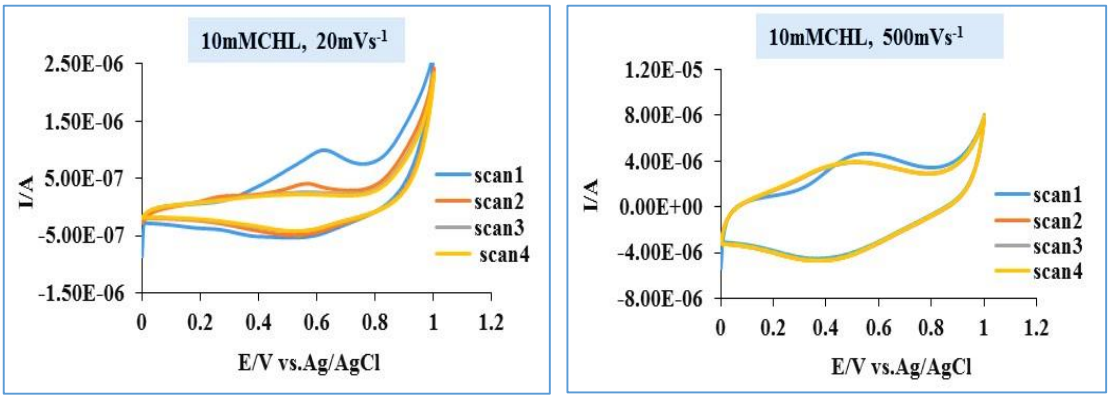

Figure 5.8: Cyclic voltammograms 20 and 500 mV s^{-1} are detailing the response of 10 mM CHL in 0.1 M HCl, which was adsorbed on the gold electrode for two hours

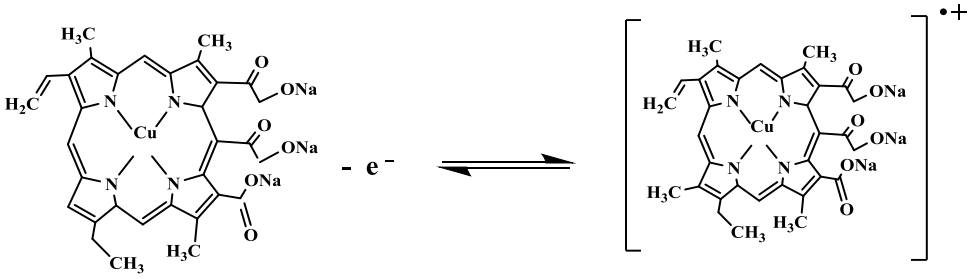

Scheme 5.1: one electron oxidation of CHL to obtain the cation radical.

The redox catalysis of 10 mM CHL was carried out again in 0.1 M organic solution of acetonitrile (MeCN), as shown in figure 5.9.

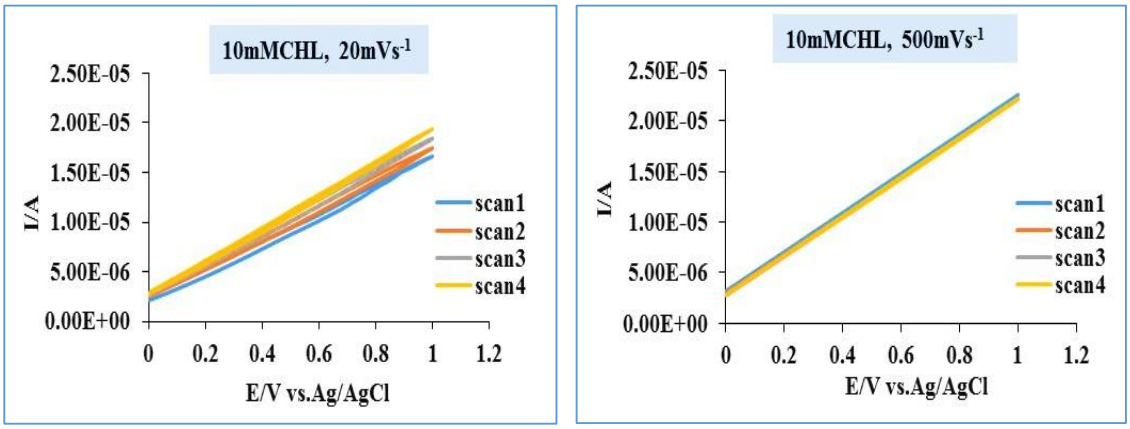

Figure 5.9: Cyclic voltammograms 20, and 500 mV s^{-1} detailing the response of 10mM CHL in 0.1M acetonitrile, which was adsorbed on the gold electrode for two hours

Figure 5.9 reveals that there were no analogous peak currents at all scan rates the response is pure resistance indicating that the solution lacks sufficient electrical conductivity.

5.3.2 The nature of electrolytes

Once the procedure was repeated, and voltammetry carried out to examine the redox reaction which took place on the glassy carbon electrode after soaking for two hours in the solution of 10 M CHL, three electrodes were immersed in different environments of the electrolytes 0.1 M HCl and 0.1 M acetonitrile.

The varying scan rate (20-500 mV s^{-1}) was monitored. The results are illustrated in figure 5.10 (A and B). Neither oxidation nor reduction peaks were observed. Similar to the case of the previous study in the organic electrolyte, it can be seen that both organic and inorganic electrolytes are not electrochemically sufficient for the observation of adsorption of CHL pigment on the glassy carbon surface for all scan rates.

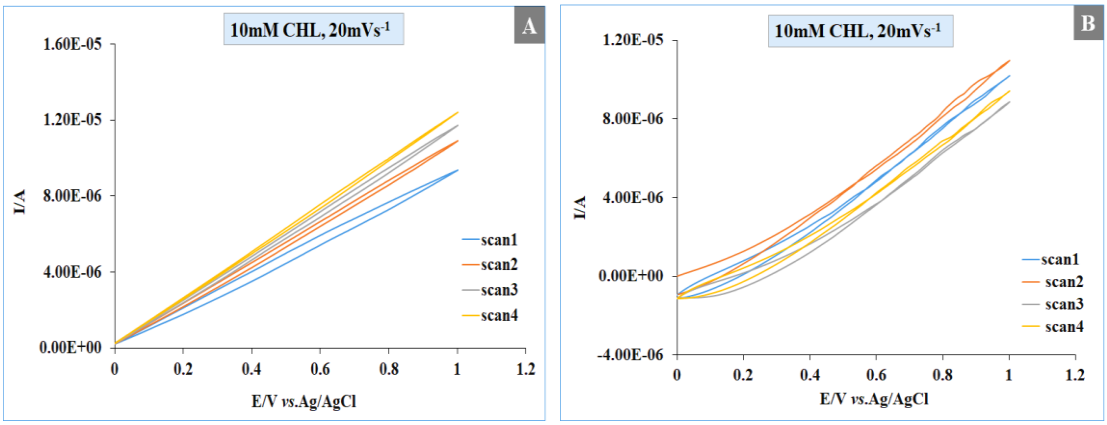

Figure 5.10: Cyclic voltammograms of 10 M CHL recorded at GCE soaking in A: 0.1 M HCl and B: 0.1 M MeCN in scan rates 20 mV s^{-1} using Ag/AgCl as a reference electrode and graphite as counter electrode

5.3.3 Voltammetry of CHL pigment on the gold electrode

Firstly, the voltammetry of adsorbed CHL was achieved by soaking the gold electrode in 10 mM CHL for two hours, and consecutively three times of ten minutes. After which it was rinsed with deionised water prior to undertaking voltammetry in 0.1M HCl using the same reference and counter electrodes as in the previous experiment, with scan rates 20 to 2000 mV s^{-1}. Figure 5.11 shows four consecutive voltammetry sweeps for the pigment above.

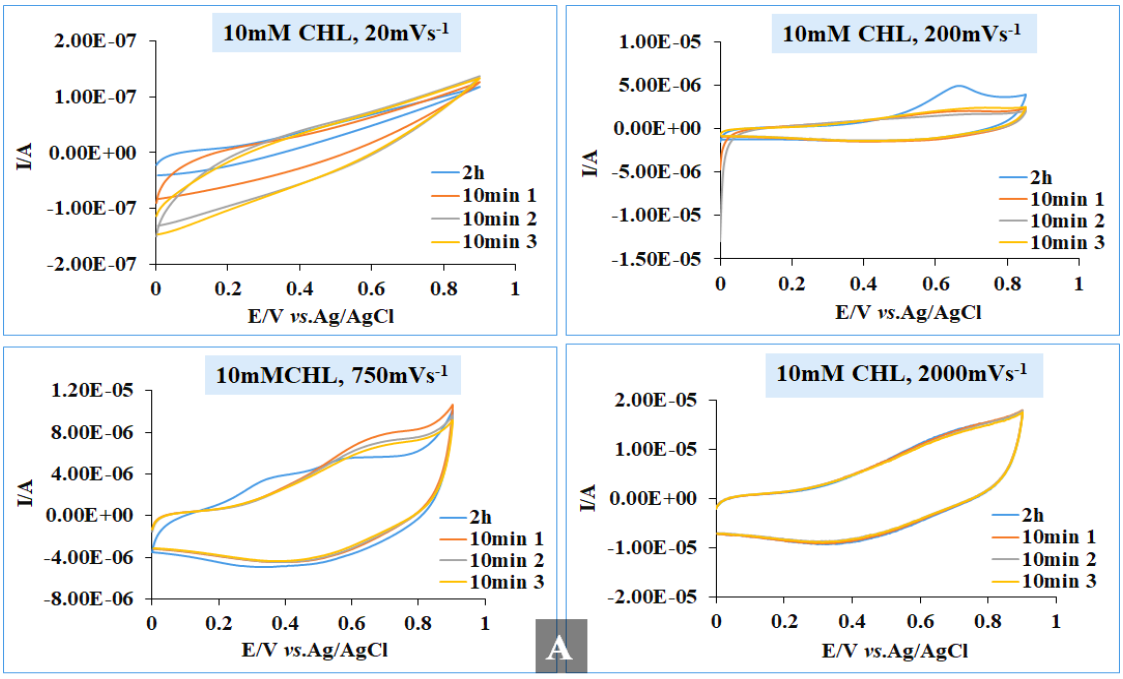

Figure 5.11: A. Scan rate dependence CVs of 10 mM CHL in 0.1 M HCl on AuE at 20-2000 mV s^{-1}in different times

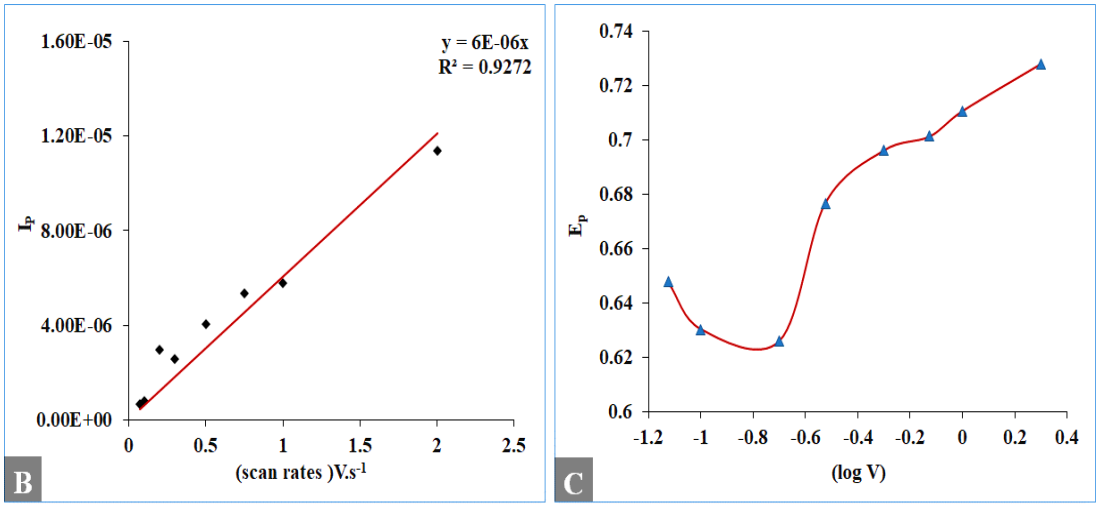

Figure 5.12: B. anodic current as a function of the scan rates (V) and (C). Potential as a function of the scan rates logarithms 20-2000 mV s^{-1} for 2 hours

Figure 5.11 (A) demonstrates the oxidation peaks *via* scan rates of the system. There was an increase in the peak current, which was coupled with a slight positive shift in peak potentials with an increase in scan rates from 20 to 2000 mV s^{-1} and adsorption incubation time. A plot of oxidation peak current (I_{lim}) against scan rates, figure 5.12 (B), shows a linear trend with coefficient value R^2 (0.9272), which is suggestive of adsorbed voltammetry. While plot 5.12 (C) performs a fluctuation in the oxidative peaks of potential *via* logarithm of scan rates, this means that the electron transfer process is complicated.

Furthermore, the slight shift in potential with an increase in time adsorption for all scan rates highlights the one-electron oxidation of CHL is becoming more difficult, which indicates that there was no pigment adsorption on the electrode surface. It is necessary to evaluate the environment of electroactive species by using CHL as a mediator, which will be the next step of the present thesis.

5.4 Conclusion

This chapter has dealt with one of the common derivatives of chlorophyll, chlorophyllin. Adsorption reaction into the surface of modifying working electrodes that were coated prior with chlorophyllin in specified times was examined.

The electrochemical study showed that the cyclic voltammetry responses of the studied organic dye, chlorophyllin, was depended on the inert material of the working electrode. From the cyclic voltammetry experiments, the glassy carbon electrode/dye interface presented no corresponding in peak currents compared with the gold surface for both organic and inorganic electrolytes for all scan rates and adsorption times. In the case of the gold electrode, there were well-defined peak currents in the inorganic rather than organic, electrolyte, for all scan rates and adsorption times.

Overall, the first CV response of the environment of the gold electrode/ chlorophyllin dye interface was considered to be a quasi-reversible process and corresponds to one-electron formation radical cations in HCl solution.

5.5 References

(1) Polo, A. S.; Murakami Iha, N. Y. Blue sensitizers for solar cells: Natural dyes from Calafate and Jaboticaba. *Sol. Energy Mater. Sol. Cells.,* **2006**, *90*, pp 1936-1944.

(2) Sinha, K.; Saha, P. D.; Datta, S. Extraction of natural dye from petals of Flame of forest (Butea monosperma) flower: Process optimization using response surface methodology (RSM). *Dyes Pigments.,* **2012**, *94*, pp 212-216.

(3) Al-Bat'hi, S. A.; Alaei, I.; Sopyan, I. Natural photosensitizers for dye sensitized solar cells. *International Journal of Renewable Energy Research* **2013**, *3*, pp 138-143.

(4) Abdel-Latif, M. S.; El-Agez, T. M.; Taya, S. A.; Batniji, A. Y.; El-Ghamri, H. S. Plant seeds-based dye-sensitized solar cells. *Mater. Sci. Appl.,* **2013**, *4*, pp 516.

(5) Grätzel, M. Dye-sensitized solar cells. *J. Photochem. Photobiol. C: Photochem. Rev.,* **2003**, *4*, pp 145-153.

(6) Wongcharee, K.; Meeyoo, V.; Chavadej, S. Dye-sensitized solar cell using natural dyes extracted from rosella and blue pea flowers. *Sol. Energy.,* **2007**, *91*, pp 566-571.

(7) Hao, S.; Wu, J.; Huang, Y.; Lin, J. Natural dyes as photosensitizers for the dye-sensitized solar cell. *Solar Energy* **2006**, *80*, pp 209-214.

(8) Luque, A.; Hegedus, S.: *Handbook of photovoltaic science and engineering*; John Wiley & Sons, **2011**.

(9) Yazie, N.; Worku, D.; Reda, A. Natural dye as light-harvesting pigments for quasi-solid-state dye-sensitised solar cells. *Mater Renew.Sustain Energy.,* **2016**, *5*, pp 13.

(10) Cherepy, N. J.; Smestad, G. P.; Grätzel, M.; Zhang, J. Z. Ultrafast Electron Injection: Implications for a Photoelectrochemical Cell Utilizing an Anthocyanin Dye-Sensitized TiO_2 Nanocrystalline Electrode Nerine. *J. Phys. Chem.,* **1997**, *101*, pp 9342-9351.

(11) Nwanya, A.; Ugwuoke, P.; Ejikeme, P.; Oparaku, O.; Ezema, F. Jathropha curcas and citrus Aurantium leaves dye extract for use in a dye-sensitised solar cell with TiO2films. *Int. J. Electrochem. Sci.,* **2012**, *7*, pp 11219-11235.

(12) Li, Y.; Ku, S.-H.; Chen, S.-M.; Ali, M. A.; AlHemaid, F. M. Photoelectrochemistry for red cabbage extract as a natural dye to develop a dye-sensitised solar cells. *Int. J. Electrochem. Sci.*, **2013**, *8*, pp 1237-1245.

(13) Grimm, B.: Chlorophyll: Structure and Function. In *eLS*; Wiley Online Library, **2001**.

(14) Scheer, H.: An Overview of Chlorophylls and Bacteriochlorophylls: Biochemistry, Biophysics, Functions and Applications. In *Chlorophylls and Bacteriochlorophylls: Biochemistry, Biophysics, Functions and Applications*; Grimm, B., Porra, R. J., Rüdiger, W., Scheer, H., Eds.; Springer Netherlands: Dordrecht, **2006**; pp 1-26.

(15) Scheer, H. Structure and occurrence of chlorophylls. **1991**.

(16) Tang, C.; Albrecht, A. Transient photovoltaic effects in metal‐chlorophyll‐a‐metal sandwich cells. *J. Chem. Phys.,* **1975**, *63*, pp 953-961.

(17) Sur, U. K. A near-infrared light photosynthetic pigment. *Curr. Sci.,* **2011**, *100*, pp 286.

(18) Senge, M. O.; Smith, K. M.: Biosynthesis and structures of the bacteriochlorophylls. *In Anoxygenic photosynthetic bacteria*; Springer, **1995**; pp 137-151.

(19) Furukawa, Y.; Ishimori, K.; Morishima, I. Electron Transfer Reactions in Zn-Substituted Cytochrome P450cam. *Biochemistry.,* **2000**, *39*, pp 10996-11004.

(20) Sakai, H.; Onuma, H.; Umeyama, M.; Takeoka, S.; Tsuchida, E. Photoreduction of Methemoglobin by Irradiation in the Near-Ultraviolet Region. *Biochem.,* **2000**, *39*, pp 14595-14602.

(21) Humphrey, A. M. Chlorophyll. *Food Chem.,* **1980**, *5*, pp 57-67.

(22) Chen, M.; Schliep, M.; Willows, R. D.; Cai, Z.-L.; Neilan, B. A.; Scheer, H. A red-shifted chlorophyll. *Sci.,* **2010**, *329*, pp 1318-1319.

(23) Schwartz, S. J.; Lorenzo, T. V. Chlorophylls in foods. *Crit. Rev. Food Sci. Nutr.*, **1990**, *29*, pp 1-17.

(24) LR, M.: *In The Colours of Life: An Introduction to the Chemistry of Porphyrins and Related Compounds*; Oxford University Press: New York, **1997**.

(25) Photosynthesis. http://www.egbeck.de/skripten/12/bs12-12.htm (accessed **12/04 /2015**).

(26) Chen, B.; Chen, Y. Stability of chlorophylls and carotenoids in sweet potato leaves during microwave cooking. *J. Agric. Food Chem.*, **1993**, *41*, pp 1315-1320.

(27) Edwards, B. Treatment of chronic leg ulcers with ointment containing soluble chlorophyll. *J. Physiother.*, **1954**, *40*, pp 177-179.

(28) Suslick, K. Kirk-Othmer encyclopedia of chemical technology. *J. Wiley&Sons: New York* **1998**, *26*, pp 517-541.

(29) Chlorophyll ab spectra2.PNG. https://en.wikipedia.org/wiki/File:Chlorophyll_ab_spectra2.PNG **2015**).

(30) Al-Alwani, M. A. M.; Mohamad, A. B.; Kadhum, A. A. H.; Ludin, N. A. Effect of solvents on the extraction of natural pigments and adsorption onto TiO_2 for dye-sensitized solar cell applications. *Acta Mol. Biomol. Spectrosc.*, **2015**, *138*, pp 130-137.

(31) Syafinar, R.; Gomesh, N.; Irwanto, M.; Fareq, M.; Irwan, Y. M. Chlorophyll Pigments as Nature Based Dye for Dye-Sensitized Solar Cell (DSSC). *Energy Procedia.*, **2015**, *79*, pp 896-902.

(32) Antohe, S.; Tugulea, L.; Gheorghe, V.; Ruxandra, V.; Caplanus, I.; Ion, L. Electrical and photovoltaic properties of ITO/chlorophyll a/TPyP/Al p–n junction cells. *Status Solidi(a).*, **1996**, *153*, pp 581-588.

(33) Diarra, A.; Hotchandani, S.; Max, J. J.; Leblanc, R. M. Photovoltaic properties of mixed monolayers of chlorophyll a and carotenoid canthaxanthin. *J. Chem.Soc.Faraday Trans.2.*, **1986**, *82*, pp 2217-2231.

(34) Del Giovine, L.; Fabietti, F. Copper chlorophyll in olive oils: identification and determination by LIF capillary electrophoresis. *Food Control.*, **2005**, *16*, pp 267-272.

(35) Zvezdanović, J.; Marković, D. Copper, iron, and zinc interactions with chlorophyll in extracts of photosynthetic pigments studied by VIS spectroscopy. *Russ.J. Phys.Chem.A.*, **2009**, *83*, pp 1542-1546.

(36) Tamiaki, H.; Yagai, S.; Miyatake, T. Synthetic zinc tetrapyrroles complexing with pyridine as a single axial ligand. *Bioorg. Med. Chem.* **1998**, *6*, pp 2171-2178.

(37) Li, F.; Gentemann, S.; Kalsbeck, W. A.; Seth, J.; Lindsey, J. S.; Holten, D.; Bocian, D. F. Effects of central metal ion (Mg, Zn) and solvent on singlet excited-state energy flow in porphyrin-based nanostructures. *J. Mater. Chem.*, **1997**, *7*, pp 1245-1262.

(38) Bube, R. H. Photoconductivity. *Wiley Encyclopedia of Electrical and Electronics Engineering* **1960**.

(39) Anthoe, S. Organic photovoltaic cells: a review. *Rom. Rep. Phys.*, **2002**, *53*, pp 427-449.

(40) Chamberlain, G. Organic solar cells: A review. *Sol. Cells.*, **1983**, *8*, pp 47-83.

(41) Tang, C. W.; Albrecht, A. C. Photovoltaic effects of metal‐chlorophyll‐a‐metal sandwich cells. *J. Chem. Phys.*, **1975**, *62*, pp 2139-2149.

(42) Mabrouki, M.; Oueriagli, A.; Outzourhit, A.; Ameziane, E.; Hotchandani, S.; LeBlanc, R. Dark signals and photovoltaic properties of Al/chlorophyll a/Ag cells. *Phys. Status Solidi (a).*, **2002**, *191*, pp 345-354.

(43) Kay, A.; Graetzel, M. Artificial photosynthesis.1.Photosensitization of TiO [sub 2] solar cells with chlorophyll derivatives and related natural porphyrins. *J. Phys.Chem.(United States).*, **1993**, *97*.

(44) Brabec, C. J. Organic photovoltaics: technology and market. *Sol. Energy Mater. Sol. Cells.*, **2004**, *83*, pp 273-292.

(45) Kalowekamo, J.; Baker, E. Estimating the manufacturing cost of purely organic solar cells. *Sol. Energy.*, **2009**, *83*, pp 1224-1231.

(46) Tumolo, T.; Lanfer-Marquez, U. M. Copper chlorophyllin: A food colorant with bioactive properties? *Food Res. Int.*, **2012**, *46*, pp 451-459.

(47) Kephart, J. C. Chlorophyll derivatives—Their chemistry? commercial preparation and uses. *Economic Botany.*, **1955**, *9*, pp 3-38.

(48) Robinson, D. S.: *Food-biochemistry and nutritional value*; Longman Scientific & Technical, **1987**.

(49) Mortensen, A.; Geppel, A. HPLC–MS analysis of the green food colorant sodium copper chlorophyllin. *Innov. food sci. & emerg. Technol.*, **2007**, *8*, pp 419-425.

(50) Aoki, S. Experimental studies on effect of chlorophyll upon formation of haemoglobin. *Sci-I-Kwai Med. Jour.*, **1931**, *50*, pp 1.

(51) Patek, A. J. Chlorophyll and regeneration of the blood: Effect of administration of chlorophyll derivatives to patients with chronic hypochromic anemia. *Arch Intern Med (Chic).*, **1936**, *57*, pp 73-84.

(52) Young, R. W.; Beregi, J. S. Use of chlorophyllin in the care of geriatric patients. *J Am Geriatr Soc.*, **1980**, *28*, pp 46-47.

(53) Nahata, M. C.; Slencsak, C. A.; Kamp, J. Effect of chlorophyllin on urinary odor in incontinent geriatric patients. *Drug Intell Clin Pharm.*, **1983**, *17*, pp 732-734.

(54) Lanfer-Marquez, U. M.; Barros, R. M. C.; Sinnecker, P. Antioxidant activity of chlorophylls and their derivatives. *Food Res. Int.*, **2005**, *38*, pp 885-891.

(55) Amao, Y.; Yamada, Y.; Aoki, K. Preparation and properties of dye-sensitized solar cell using chlorophyll derivative immobilized TiO_2 film electrode. *J. Photochem. Photobiol A: Chemistry.*, **2004**, *164*, pp 47-51.

(56) Thanpitcha, T.; Sirivat, A.; Jamieson, A. M.; Rujiravanit, R. Physical and Electrical Properties of Chlorophyllin/Carboxymethyl Chitin and Chlorophyllin/Carboxymethyl Chitosan Blend Films. *Macromol Symp.*, **2008**, *264*, pp 168-175.

(57) Bowers, W. Chlorophyll in Wound Healing and Suppurative Disease. *Plast. Reconstr. Surg.*, **1949**, *4*, pp 121.

(58) SATO, M.; IMAI, K.; KIMURA, R.; MURATA, T. Effect of sodium copper chlorophyllin on lipid peroxidation. VI. Effect of its administration on mitochondrial and microsomal lipid peroxidation in rat liver. *Chem. Pharm. Bull.,* **1984**, *32*, pp 716-722.

(59) Kumar, S. S.; Shankar, B.; Sainis, K. B. Effect of chlorophyllin against oxidative stress in splenic lymphocytes in vitro and in vivo. *Biochim. Biophys. Acta.,* **2004**, *1672*, pp 100-111.

(60) Boloor, K. K.; Kamat, J. P.; Devasagayam, T. P. A. Chlorophyllin as a protector of mitochondrial membranes against γ-radiation and photosensitization. *Toxicology.,* **2000**, *155*, pp 63-71.

(61) Spikes, J. D.; Bommer, J. C. Chlorophyll and related pigments as photosensitizers in biology and medicine. *Chlorophylls.,* **1991**, pp 1181-1204.

(62) Packer, M.; Carver, J. R.; Rodeheffer, R. J.; Ivanhoe, R. J.; DiBianco, R.; Zeldis, S. M.; Hendrix, G. H.; Bommer, W. J.; Elkayam, U.; Kukin, M. L. Effect of oral milrinone on mortality in severe chronic heart failure. *N. Engl. J. Med.,* **1991**, *325*, pp 1468-1475.

(63) Pemberton, R.; Amine, A.; Hart, J. P. Voltammetric behavior of chlorophyll a at a screen‐printed carbon electrode and its potential role as a biomarker for monitoring fecal contamination. *Anal. Lett.,* **2004**, *37*, pp 1625-1643.

(64) Fajer, J.; Borg, D.; Forman, A.; Felton, R.; Dolphin, D.; Vegh, L. The cation radicals of free base and zinc bacteriochlorin, bacteriochlorophyll, and bacteriopheophytin. *Proc. Natl. Acad. Sci.,* **1974**, *71*, pp 994-998.

(65) Kobayashi, M.; Ohashi, S.; Iwamoto, K.; Shiraiwa, Y.; Kato, Y.; Watanabe, T. Redox potential of chlorophyll d in vitro. *Biochim. Biophys. Acta, Bioenerg.,* **2007**, *1767*, pp 596-602.

(66) Geskes, C.; Meyer, M.; Fischer, M.; Scheer, H.; Heinze, J. Electrochemical investigation of modified photosynthetic pigments. *J. Phys. Chem.,* **1995**, *99*, pp 17669-17672.

(67) Oesch, U.; Janata, J. Electrochemical study of gold electrodes with anodic oxide films—II. Inhibition of electrochemical redox reactions by monolayers of surface oxides. *Electrochim. Acta.,* **1983**, *28*, pp 1247-1253.

(68) Bonewitz, R.; Schmid, G. Oxygen adsorption on gold and the Ce (III)/Ce (IV) reaction. *J.Chem.Sci.,* **1970**, *117*, pp 1367-1372.

(69) Pasta, M.; La Mantia, F.; Cui, Y. Mechanism of glucose electrochemical oxidation on gold surface. *Electrochim. Acta.,* **2010**, *55*, pp 5561-5568.

(70) Ureta-Zañartu, M. S.; Berríos, C.; González, T.; Fernández, F.; Báez, D.; Salazar, R.; Gutiérrez, C. Electrocatalytic oxidation of alcohols at gold electrodes in alkaline media. *Int.J Electrochem.Sci.,* **2012**, *7*, pp 8905-8928.

(71) Ferapontova, E. E. Electrochemistry of guanine and 8-oxoguanine at gold electrodes. *Electrochim. Acta.,* **2004**, *49*, pp 1751-1759.

(72) Iotov, P. I.; Kalcheva, S. V. Mechanistic approach to the oxidation of phenol at a platinum/gold electrode in an acid medium. *J. Electroanal. Chem.,* **1998**, *442*, pp 19-26.

(73) Maskus, M.; Abruña, H. D. Synthesis and Characterization of Redox-Active Metal Complexes Sequentially Self-Assembled onto Gold Electrodes via a New Thiol−Terpyridine Ligand. *Langmuir.,* **1996**, *12*, pp 4455-4462.

(74) Ozoemena, K. I.; Nyokong, T.; Nkosi, D.; Chambrier, I.; Cook, M. J. Insights into the surface and redox properties of single-walled carbon nanotube—cobalt(II) tetra-aminophthalocyanine self-assembled on gold electrode. *Electrochim. Acta.,* **2007**, *52*, pp 4132-4143.

(75) Zhang, S.; Wang, N.; Yu, H.; Niu, Y.; Sun, C. Covalent attachment of glucose oxidase to an Au electrode modified with gold nanoparticles for use as glucose biosensor. *Bioelectrochemistry.,* **2005**, *67*, pp 15-22.

(76) Housecroft, C. E.; Constable, E. C.: *Chemistry: An introduction to organic, inorganic and physical chemistry*; Pearson education, **2010**.

(77) Wu, Z.; Li, M.; Mullins, D. R.; Overbury, S. H. Probing the surface sites of CeO_2 nanocrystals with well-defined surface planes via methanol adsorption and desorption. *ACS Catal.,* **2012**, *2*, pp 2224-2234.

(78) Housecroft, C. E.: Chemistry an introduction to organic, inorganic and physical chemistry. 4th ed. ed.; Constable, E. C., Ed.; Prentice Hall: Harlow, **2010**.

(79) Bard, A. J.; Faulkner, L. R. Fundamentals and applications. *Electrochemical Methods, 2nd ed.; Wiley: New York* **2001**.

Chapter 6

Homogeneous ET of Chlorophyll and its Derivative Chlorophyllin

In chapter 5, the effectiveness of different parameters in transferring electrons between chlorophyllin (CHL) pigment and the working electrode surface was illustrated. It was suggested that electrons reduce chlorophyll pigment by adding active species in the bulk solution homogeneous transfer.

This chapter presents an outline of chlorophyll (chl) extraction and isolation techniques. It covers some methods of chl determination, active materials influence and working electrode modification. Detections of chl on spinach leaves using various methods are reported. Given the importance of the homogenous ET process in the presence of active species, section three performs this method.

6.1 Introduction

6.1.1 Chlorophyll: extraction and determination methods

Several approaches have been developed to extract and determine chlorophyll and its derivatives from different plants and photosynthetic organisms since Pelletier and Caventou discovered it in 1818. The complete dissolution of chloroplasts into an extractive solvent is an indicative of a good extraction procedure.[1,2] Methods of determining chlorophyll are based on three steps: extraction and purification methods using appropriate solvents, followed by quantification using either spectrophotometry or fluorometry and recently by high-performance liquid chromatography (HPLC).

The most common solvents used to extract chlorophyll and its derivatives are acetone, methanol, and ethanol, while chloroform, dimethyl sulfoxide and petroleum ether are rarely utilized .[3-5] Table 6.1 shows some methods of extraction and determination of chlorophyll.

Table 6.1: Chlorophylls: extraction and determination methods

Chlorophyll: types and sources	Extraction Solvents	Methods of Determination	Ref.
chl a & b from moso bamboo culms (40 mg)	Acetone, DMF, or DMSO/ 3.23 mg for chl a and 1.56 mg for chl b	Ultraviolet-visible spectrometry	6
chl a from cultured and natural phytoplankton cells	Acetone and DMF	Fluorometer	7
chl a and b, pheophytin and chlorophyllide from spinach leaves	methanol and petroleum ether (2:1 ratio) and petroleum ether and diethyl ether (1:1 ratio)	Visible spectrometry, HPLC chromatography and Electrospray Ionisation-Mass Spectrometry	8

chl$_s$ and carotenoids from tea leaves	50 ml of cold water (-20°C) and 80% aqueous acetone.	high-performance liquid chromatography (HPLC)	9
Chls, carotenes and xanthophyll from spinach leaves	Methanol and 40–75°C petroleum ether in 2:1 ratio, and with 40–75°C petroleum ether and diethyl ether in 1:1 ratio.	Ultraviolet-visible irradiation and fluorescence spectroscopy	10
Chl a from freshwater green algae	90% acetone or methanol	HPLC	11
chl a and pheophytin a in marine and freshwater algae	90% acetone	fluorescence	12
chl a in seawater	90 % acetone or 96 % ethanol	Visible spectrometry and Fluorometry	13

6.1.2 Donor-acceptor systems containing chlorophyll and active species

Green plant chlorophyll is considered to be the electronic centre of the photosynthesis process. This pigment captures solar energy and converts it into chemical energy through many steps.[14-16] In addition, during this process chlorophyll acts as both a reductant and an oxidant due to its molecular structure (the central magnesium ion and a phytol chain): see mechanisms 6-1 and 6-2[17]:

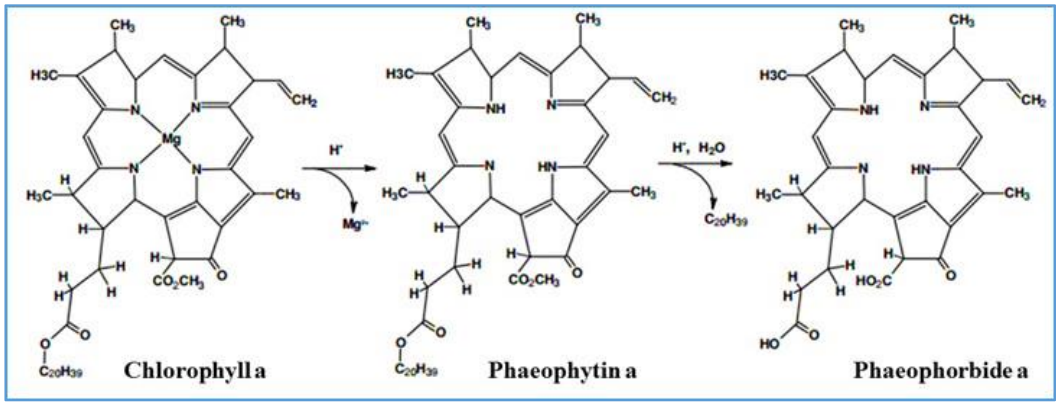

Mechanism 6-1: Chlorophyll a with acid

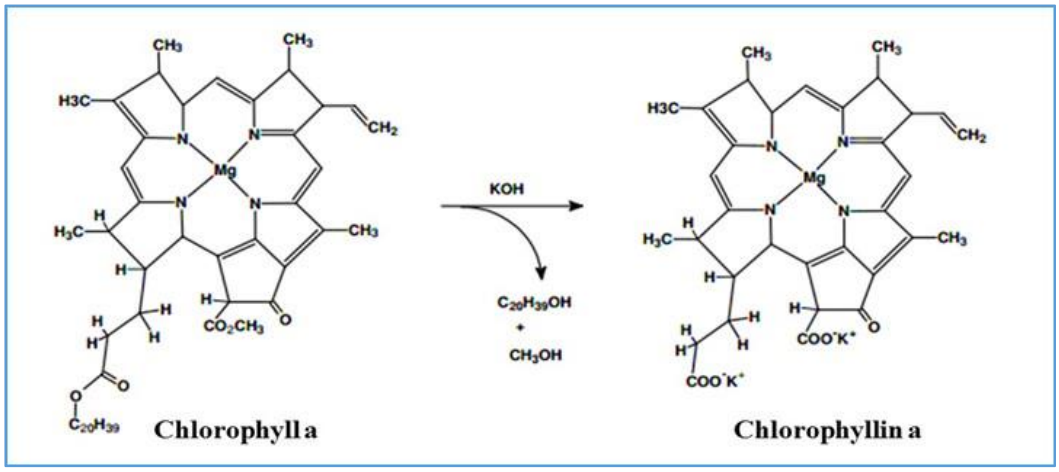

Mechanism 6-2: Chlorophyll a with base

The donor-acceptor systems containing chlorophyll have, thus, been widely explored by various methods. These methods including self-assembled tetra pyrrole-carbon nanotubes for light-induced electron transfer applications, photo-induced ET between chl a and Au nanoparticles by fluorescence, polarisation transient grating technique on several chlorophylls as donor molecules and the redox potentials of chlorophylls using cyclic voltammetry (CV) and square wave voltammetry (SWV).[18-21]

The redox reactions of chlorophyll or its analogues (CHL) in an aqueous solution containing some active species such as CPZ.HCl, L-Cyst.H and KI in the presence and absence of Triton X100 and Vitamin K_1 will be discussed later.

6.1.3 Modified working electrodes (MWEs)

In the past two decades, modifications of working electrodes have seen many widely differing applications in the electrochemical field. Through modification, the surface properties of the selected electrode, such as stability and sensitivity will improve. Therefore it can be applied in particular areas such as electrochemical sensors and photoelectrochemical devices.[22-25]

The idea underpinning modified electrodes is to localise chemical reagents on the WE surface so as to keep a locally high concentration of reactant. This can be achieved by covering the electrode surface with a mediator solution and then allowing the mediator to evaporate.[26,27] Different compounds have been used to modify WEs in this way; some reaction requirements have been achieved such as electrocatalytic, electrochemical and photochemical properties.[28-31]

Metallic electrodes such as gold (AuE), silver and platinum have usually been used while materials of graphite and its derivatives such as carbon are employed as supports.[32-34] In spite of numerous reports of oxides on gold electrodes, they are useful in electrochemical applications especially sensors constrictions due to their properties such as chemical inertness, high electrical conductivity, flexibility for electrode manufacture and large potential.[35-37]

Here, the direct electron transfer of chlorophyllin and the extraction of chl on modified electrodes have been reported. In addition, CHL or chl on modified AuE have been utilised to study the catalytic activity of the oxidation of the active species in presence and absence of surfactant.

6.2 Extraction and identification of chlorophyll and its derivative

This section of the chapter gives an account of the extraction of chlorophyll pigment from fresh spinach. The chl pigment and its derivative CHL were identified using methods such as UV-Vis spectroscopy and thin layer chromatography. Cyclic voltammetry was used to investigate the homogeneous electron transfer process for both chl and CHL.

6.2.1 Experimental Materials

Chemical materials were purchased as follows:

Table 6.2: Information about chemical substances

Chemical name	Chemical Formula	Common name	Chemical supplier and percentage
Acetone	C_3H_6O	Acetone	VWR chemicals(BDH)
Ethanol	C_2H_6O	Ethyl Alcohol	VWR chemicals(BDH)
Hexane	C_6H_{14}	n-Hexane	VWR chemicals(BDH)
Hydrogen peroxide	H_2O_2	peroxide	Fisher Scientific>30%
Methanol	CH_4O	Methyl Alcohol	VWR chemicals(BDH)

Nitrogen gas	N_2	Nitrogen	BOC Gases, UK, Energas Ltd, 99.99%
Octyl phenolethoxylate	$C_{14}H_{22}O(C_2H_4O)_n$	TritonX100	Sigma-Aldrich
Potassium iodide	KI	Radiation Pills	Aldrich Chemical>99%
Phylloquinone	$C_{31}H_{46}O_2$	Vitamin K_1	Sigma-Aldrich
Sulphuric acid	H_2SO_4	vitriol	Fisher Scientific>95%

All supporting electrolytes used for the investigations were of laboratory grade. All the chemical materials were used as received without further purification. Deionised water obtained from Millipore Milli-Q purification system was used for dilution with a resistivity approximately 18 MΩ cm. Standard solutions such as chl and CHL were prepared daily and protected from light by using aluminium foil.

6.2.2 Electrochemical Instrumentation

The potential was measured by using a commercial electrochemical system, the μAutolab Type III, which is controlled by a Pentium IV processor computer. All voltammetry data were recorded utilising a three-electrode cell. The three-electrode cell used the electrodes described in section 3.2.2 of chapter 3 and 5.2.2 of chapter 5 in all cases unless otherwise mentioned. The working electrode was immersed in piranha solution for 10 minutes prior to every change of the experimental parameter. After that, carborundum paper (200, 400 and 2400 grade, Presi, France) was used to remove active adsorbed species from the WE surface which had been used in a previous experiment, and then it was polished using aqueous 3 μm alumina slurry (Presi, France).

6.2.3 Experimental Methods

6.2.3.1 Pigment extraction

The crude chlorophyll (a mixture of a and b) was extracted from fresh spinach leaves as described previously in protocols.[38-42] The spinach was purchased from a local market. Spinach leaves (*Spinacia oleracea*) were separated from the stems, and then about 20 grammes were weighed and mixed with an aqueous acetone solution [4:1(v/v) acetone/water], stirred for approximately two hours at room temperature. Following filtration, the solvent was removed using a rotary evaporator, and the resulting solid examined *via* UV/visible spectroscopy in methanol and TLC method, which are described below.

6.2.3.2 Detection of pigments

The plant pigments extracted were identified using chromatographic analysis and spectral properties. The following techniques are used to identify and qualify the dyes.

6.2.3.2.1 UV-Vis spectroscopy

Ultraviolet-visible spectroscopy is commonly used to determine the quantity and quality of materials. The pigment extracted was dissolved in ethanol solvent to obtain a finely detailed spectrum and accurate measurement of the concentration of the pigment. Chlorophyll, both a and b, absorbs light between wavelengths 300 and 800 nm.

6.2.3.2.2 Thin layer chromatography

Thin-layer chromatography (TLC) is the most commonly used method for analysing pigments. A small amount of the pigment sample was placed in a spot near the bottom of the plate, which was then put into the mobile phase by dissolving it in 70:30 hexane:

acetone solvent. The components were separated relative to the physical and chemical compositions.[43-45]

6.2.3.3 Preparation of Electrode

All electrochemical measurements were undertaken using the three-electrode system. The working electrode of gold (AuE) was immersed initially in chlorophyllin in aqueous solution for two hours in all experiments described in this chapter.

Prior to each experiment, the gold disk substrate electrode was immersed for 10 minutes in piranha solution (3:1 proportion of sulfuric acid: hydrogen peroxide 30%). To form a smooth surface on the working electrode, it was polished with wetting cloth using 0.3µm alumina slurry for at least 60 seconds. It was then rinsed with distilled water and dried at room temperature before use in each experiment. Prior to voltammetry, all solutions were purged with free N_2 or Ar gas for 30 minutes, while the experiments themselves were conducted under the stem of these gases atmosphere on the solution surface.

6.2.3.4 Preparation of Mediator Electrolyte

A mediator electrolyte plays a crucial role in reducing the resistivity of the solution and overcomes the charged migration of electroactive species. Therefore, the mediator electrolyte must be inert and ionic for electrochemical work. In this study, a 50/50% ratio of aqueous/surfactant (hydrochloric acid-TritonX100) was used as supporting electrolyte. The mixture was heated, with vigorous stirring under nitrogen to 70^{o}C for at least two hours, and then the mixture was allowed to cool slowly to room temperature 25^{o}C, before further experiments that examined chlorophyllin, plant pigment and vitamin K_1.

6.3 Results and Discussion

6.3.1 The oxidative Voltammetry of CHL using some electroactive species

The charge transfer between electrode and material (chlorophyllin) initiated in chapter 5 of this thesis. This chapter, we focus on the thermodynamics of the CHL pigment in bulk solution using cyclic voltammetry. Measurements were carried out in 0.1M HCl with the presence of some electroactive species such as L-Cyst.H, KCl, and CPZ.H.

These solutions were purged with a constant flow of N_2 at varying scan rates of 20-2000 mV s^{-1}, and the following explains this in detail.

6.3.1.1 CHL adsorption on AuE in the presence of L-Cyst.H

CHL adsorption on AuE was tested with varying concentrations of L-Cyst.H 0.5, 1.0, 2.0, 5.0, and 10.0 mM. The responses of the voltammograms are shown in figure 6.1 a.

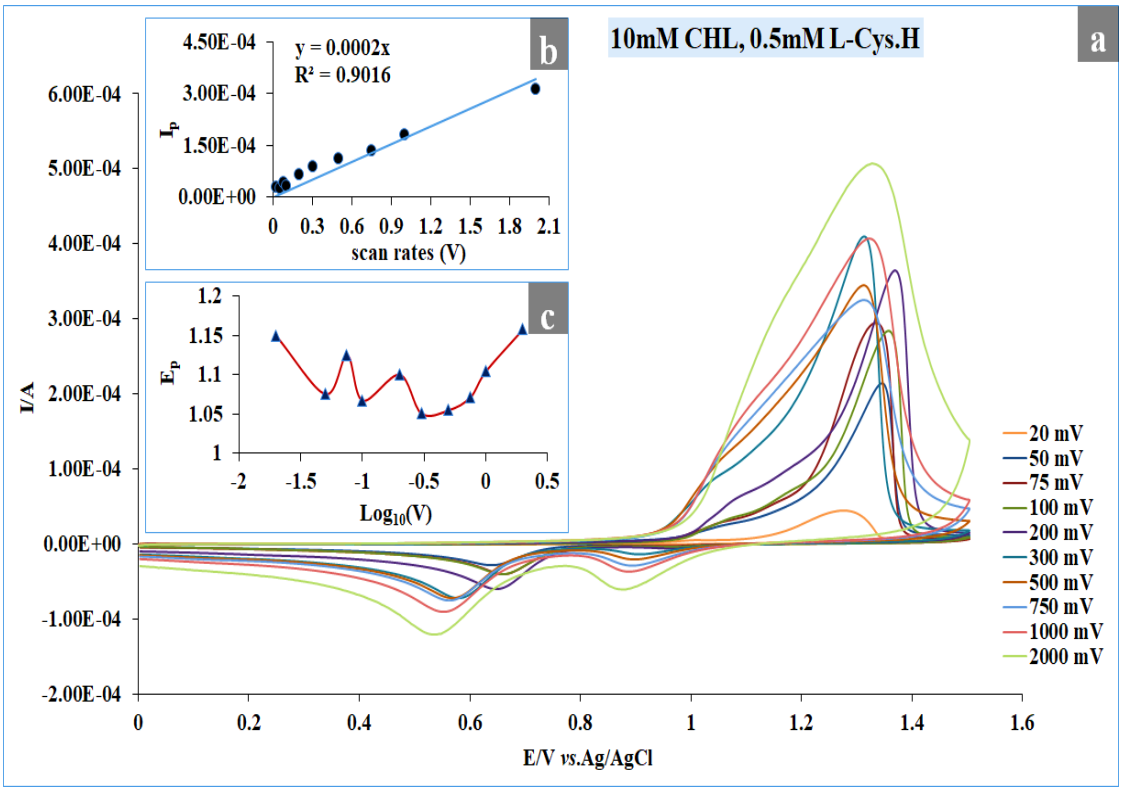

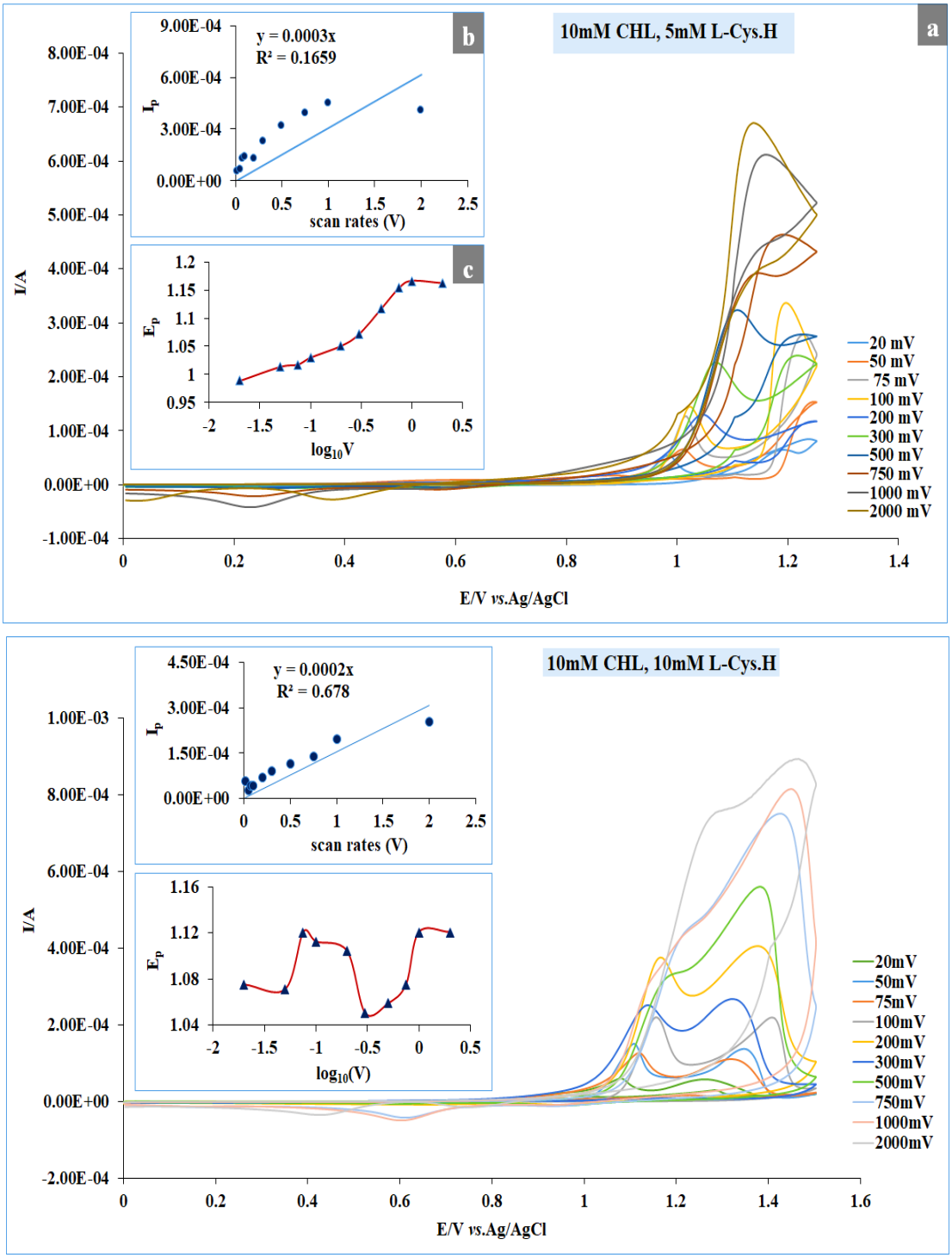

Figure 6.1: (a) cyclic voltammograms for the oxidation of 10 mM CHL, two hours adsorption on the gold electrode with 0.5, 5.0 and 10.0 mM L-Cyst.H in 0.1 M HCl. Scan rate 20-2000 mV s^{-1}. Ag/AgCl electrode served as the reference electrode, and graphite served as a counter electrode. (b) The corresponding plot of peak currents against scan rates for all concentrations of L-Cyst.H. (c) Corresponding plot of peak potentials against logarithms of scan rates for all concentrations of L-Cyst.H

The curves at (**a**) show the dependence of net peak currents of the adsorption of CHL at the AuE surface on the concentration of L-Cst.H. In low (0.5 mM) and high (5, and 10

mM) concentrations of L-Cys.H there are two anodic and cathodic peaks observed for all scan rates. The net peak potentials of the adsorption CV response shifted toward lower values by increasing the concentration of L-Cyst.H, indicating more facile electron transfer. Figure 6.1 (**b**) shows the relationship between peak currents and scan rates for oxidative waves. The maximum current holds on approximate proportionally with scan rates as expected for surface-attached species.

The plot of peak potentials *via* logarithms of scan rates for the oxidation peaks for all concentrations of L-Cyst.H as in figure 6.1 **(c)** generally, move to higher potential with increasing scan rate, suggesting a complex interplay between heterogeneous and homogeneous kinetics. Thus, further information on the oxidation process of CHL using L-Cyst.H at concentrations higher than 10 mM and lower than 0.5 mM was obtained. Here, the same procedure was undertaken as in the previous experiment, using 0.5 mM CHL and 20 mM L-Cyst.H, see figure 6.2 (**a**).

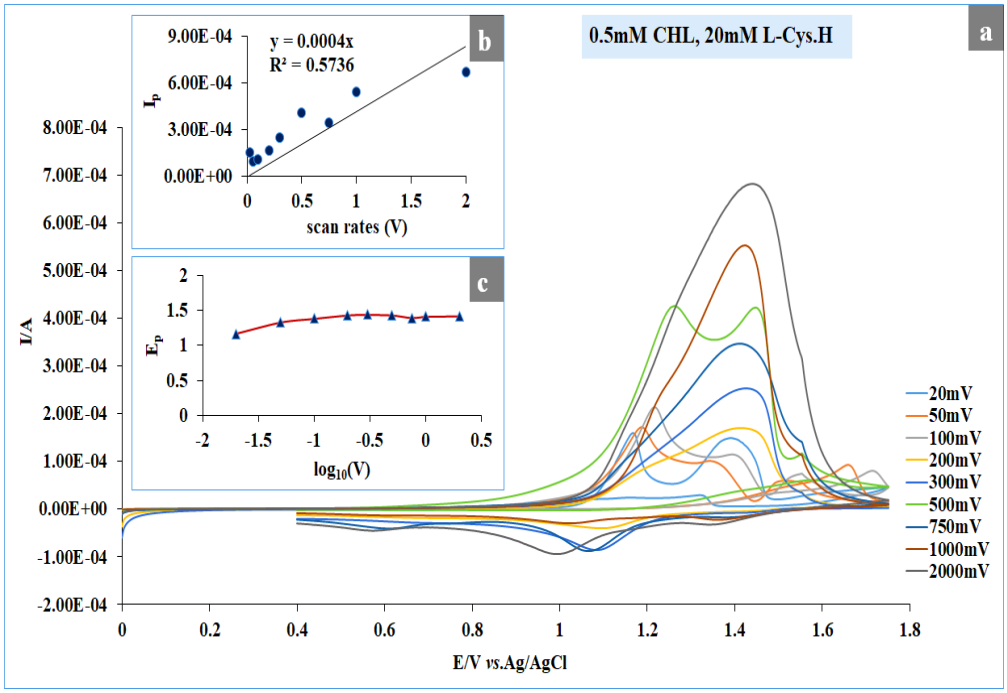

Figure 6.2: (a) CVs of the oxidation 0.5 mM CHL with 20 mM L-Cyst.H, two hours adsorption on the AuE in 0.1 M HCl at variable scan rates (20-2000 mV s^{-1}). (b): The plot of peak currents vs scan rates. (c): The plot of peak potentials vs log scan rates for the oxidation process

In figure 6.2 **a**, there is the same trend as that of the oxidation of 0.5 mM L-Cyst.H. However, the peak potential (fig. **b**) gives a different trend from that of 0.5mM L-Cyst.H, which confirms that the oxidation process of CHL on AuE is reversible with an increase in the concentration of L-Cyst.H.

6.3.1.2 CHL adsorption on AuE in the presence of potassium iodide KI

Again, cyclic voltammetry for another active species was examined. Figure 6.3 (**a)** illustrates four curves of different concentrations of KI (0.01, 0.05, 0.1, and1.0 mM) with 10 mM CHL in an aqueous solution of 0.1 M HCl.

The peaks in the oxidative- reductive currents were observed for all concentrations of KI, which suggests that the redox process is reversible. Moreover, the linear voltammograms for concentrations 0.01 and 0.05 mM of KI in the plot **(b)** mean that the reactions are under diffusion control. The fluctuations in the peak potentials *vs* log scan rates plot in **(c)** confirm the reversibility of the redox process, albeit with a much experimental error in potential measurement. This likely stems from the difficulty in reproducing the surface coverage.

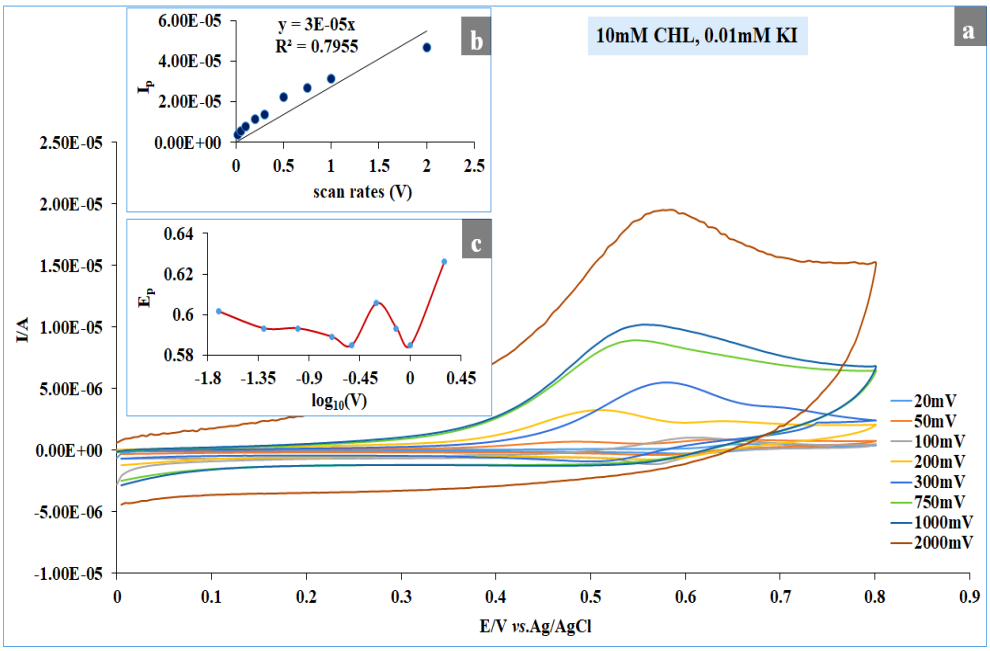

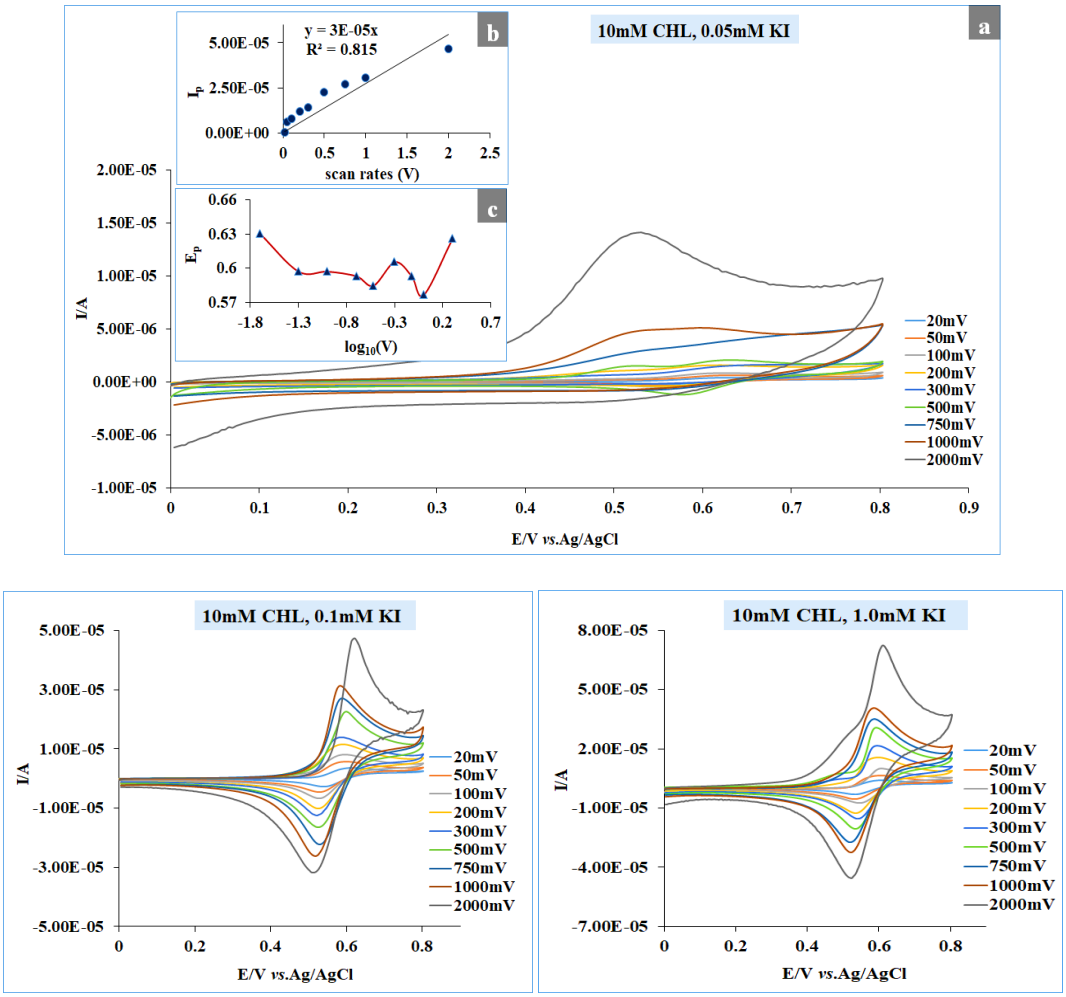

Figure 6.3: (a): Typical CVs observed for 10 mM CHL with varying concentrations (0.01, 0.05, 0.1 and 1.0 mM) of KI at different scan rates 20-2000 mV s^{-1}. (b): The plot of peaks current against scan rates and (c): The plot of peaks potential against logarithms of scan rates for the oxidation process

6.3.1.3 CHL adsorption on AuE in the presence of CPZ.HCl

Finally, previous electrochemical work with CPZ.HCl was undertaken in 0.1 M HCl at AuE after soaking for two hours in 10 mM CHL pigment. This work shows a similar trend to that of the previous electroactive species, L-Cyst.H in the cases of peak currents and potential responses, see Figure 6.4 (**a**, **b** and **c**). As a result of using different electroactive species, it is clear that the best one is KI due to the correspondence in both current and potential peaks. The reactions on the electrode surface were taking place between adsorbed CHL and active molecules. Thus, the reaction in the bulk solution will be the next section.

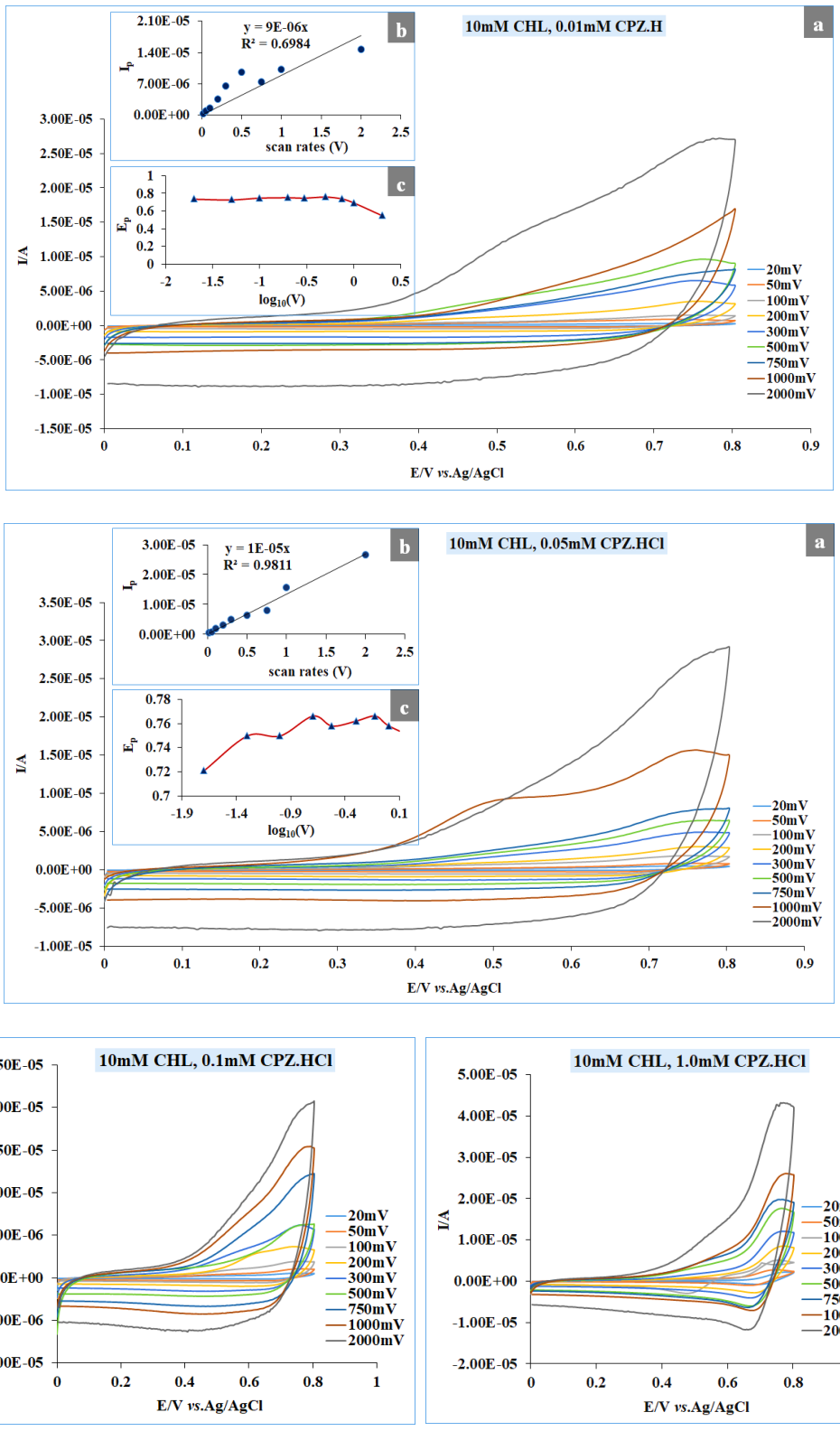

Figure 6.4: (a). CVs of 10 mM CHL with varying concentrations of CPZ.H at different scan rates 20-2000 mV s^{-1}, (b). The plot of peak current against scan rates and (c). The plot of peak potential against logarithms of scan rates for the oxidation process

6.3.2 Electrochemical studies of CHL in the bulk solution

Electrochemical reactions between electroactive species can take place on an electrode surface or in a bulk solution, as mentioned in chapter 2. In the first section of the results, the electrochemistry of CHL on the electrode surface was examined.

In this part, we will first elucidate the electron transfer in the bulk solution between CHL and a more easily oxidised substance such as KI in the presence and absence of anionic surfactant such as Triton X 100. Secondly, we will extract chlorophyll pigment from fresh spinach and then study its characteristics in the presence of vitamin K_1 and Triton X 100. The latter material will enhance the electrochemical reaction by reducing the surface tension at the electrode surface or the electrode/electrolyte interface, thus making molecules spread more easily.

6.3.2.1 Voltammetry of CHL with the introduction of surfactant

To study electron transfer between electroactive species in bulk solution, the effects of surfactant and concentration of the materials using an aqueous solution were investigated. The initial examination was the effect of Triton X 100 on the electron transfer of CHL solution in 0.1 M HCl by using cyclic voltammetry. Figure 6.5 (**C**) shows the response of CHL pigment in an aqueous solution only; there is a well-defined oxidation peak at +0.65 due to the single oxidation on the gold electrode itself to form the stable chemical cation, shown in the below mechanism:

$$6Cl^{-} + Au - 3e^{-} \rightarrow Au_2\ O_2(s) \rightarrow Au^{+3}\ (aq)$$

Mechanism 6-3: One-electron oxidation on the gold electrode surface.

The voltammetry behaviour of CHL at various concentrations (0.05, 0.1, 0.2, and 0.5 mM) was also investigated in the presence of TX 100 on AuE, see Figure 6.5 A.

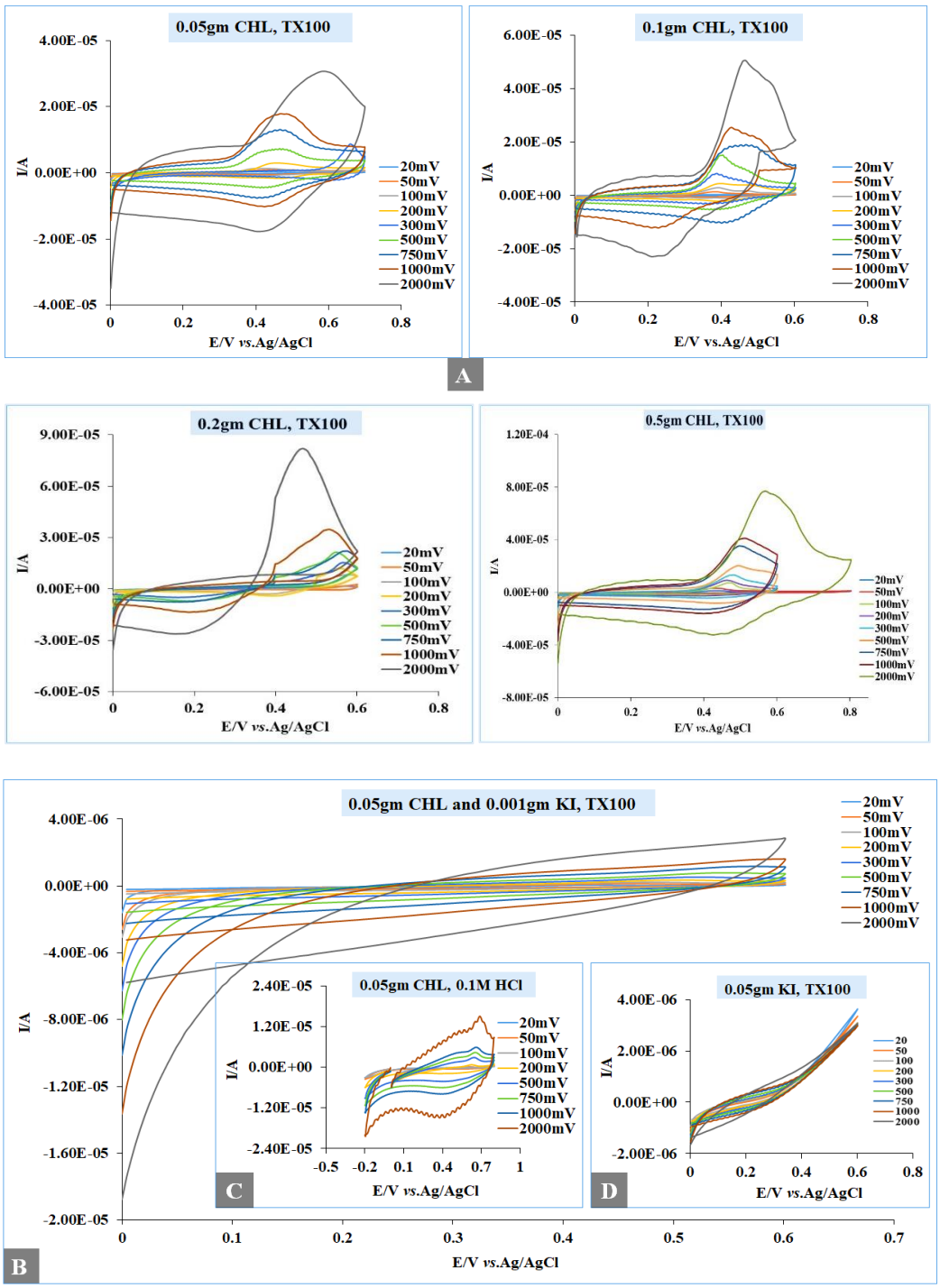

Figure 6.5: (A): CVs of varying concentrations of CHL in aqueous solution with T X100 presence at different scan rates (20-2000 mV s^{-1}), (B): CVs are detailing 0.05 gm CHL in an aqueous solution containing 0.001 gm KI and 50% T X100. Inset, (C): CVs of 0.05gm CHL in 0.1M HCl and (D): CVs of T X 100 in solution involving 0.05 gm KI

The forward and reverse peak currents of the response of CHL were increased in the presence of T X100 in all concentrations figure 6.5 (**A**). These peaks are positioned with a slight negative shift in potentials with increasing scan rate as compared with figure 6.5 (**C**), suggesting that some materials were absorbed on the electrode surface.

To understand the process in more detail, the scan rate dependent experiment of CHL oxidation was undertaken in the presence of TX 100 and an active species such as KI, see Figure 6.5 (**B**). It can be seen that the oxidative and reductive peaks current are not clear, which means that the electron transfer process in bulk solution is not readily apparent. Single-electron-oxidation between active species in the bulk solution can be assumed following this mechanism:

$$CHL - e^- \leftrightarrows CHL^{\dagger}$$
$$I^- - e^- \rightleftharpoons \frac{1}{2} I_2$$
$$CHL^{\dagger} + I^- \rightleftharpoons CHL + \frac{1}{2} I_2$$

Mechanism 6-4: Single-electron transferring in bulk solution

To determine whether the same effects are observed using TX 100 to enhance the electrochemical process, the voltammetry of hydrophobic molecules such as chlorophyll and vitamin K_1 in the acidic electrolyte will be examined next.

6.3.2.2 Chlorophyll, extraction, absorption spectra, and electrochemical reaction

Chlorophyll was extracted from fresh spinach leaves using the procedure described in (6.2.4.1); the TLC technique identified the pigment. Figure 6.6 (**a**) shows the standard sample of chlorophyll and (**b**) the pigment extracted from fresh spinach. It will be seen that the spectrum bands of chlorophyll are observed in both of them.

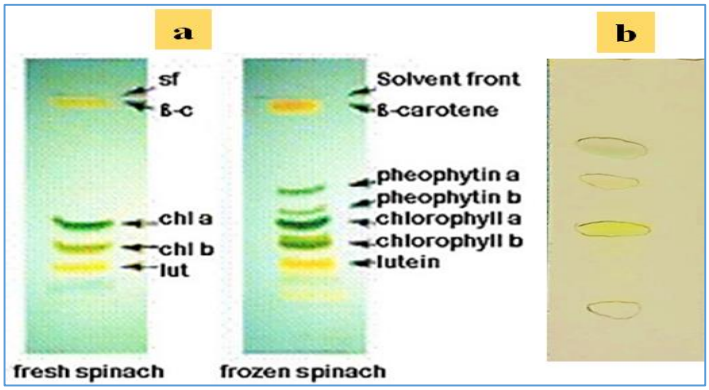

Figure 6.6: (a): TLCs of fresh and frozen chlorophyll in spinach leaves. (b): TLC of chlorophyll extracted from spinach in this work

Figure 6.7 (A and B) show the wavelengths of a standard sample of chlorophyll and its structure, while (C) shows the recording of the absorption spectrum of chlorophyll in spinach leaves made with a UV-Visible spectrophotometer.

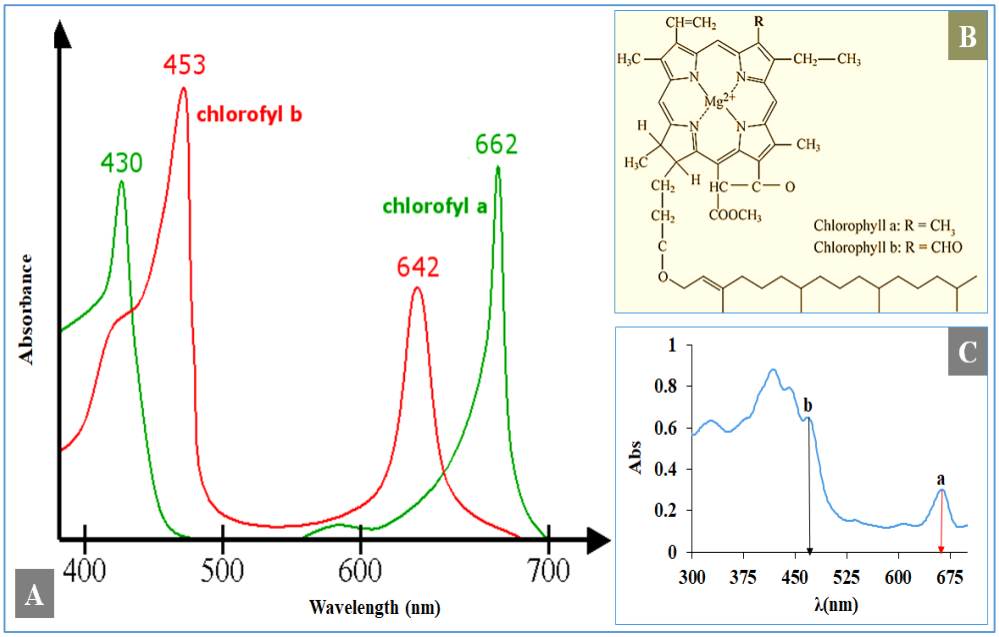

Figure 6.7: A: Typical wavelength of chlorophyll, B: Chlorophyll structure and C: wavelength of chlorophyll in the fresh spinach leaves

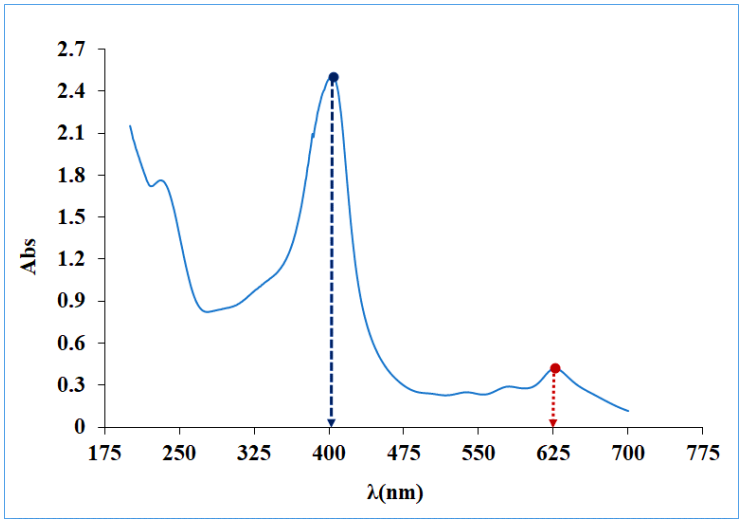

Figure 6.8: Absorption spectrum of chlorophyll derivative (chlorophyllin)

It is clear that the principal bands of chlorophyll a and b in the typical sample are in a similar position in the extracted pigment, while Figure 6.8 presents the shifting to low wavelength in both of these bands for chlorophyllin due to the changing in the CHL structure as mentioned in chapter 5 section (5.1.3).

6.3.2.3 Elucidation CVs in the system of (extraction pigment, TX100 and vitamin K_1)

The cyclic voltammetry of the extracted pigment (chl) in the presence of TX 100 and vitamin K_1 was examined. Figure 6.9 (**A**) illustrates voltammograms in varying scan rates (20-1000 mV s^{-1}) corresponding to the redox reaction on the surface of the AuE with 50% by weight of TX 100 in 0.1 M HCl. As shown in the same figure (insets **B** and **C**), both oxidative and reductive peak currents increased with the increase in scan rates. Both forward and backward peak potentials remained in the same position, indicating that the product in the surfactant phase is stable, although vitamin K_1 is expected to reside within T X 100 due to its hydrophobic property. In addition, single-electron transfer between chl and vitamin K_1 becomes easier. The mechanism of this reaction is shown below:

$$chl - e^- \rightarrow chl^{\dotplus}$$
$$chl^{\dotplus} + VK_1 \rightarrow chl + VK_1^{\dotplus}$$

Mechanism 6-5: Chlorophyll with vitamin K_1

The photosensitised reactions between total chlorophyll and donor-acceptor molecule will be studied in the next chapter.

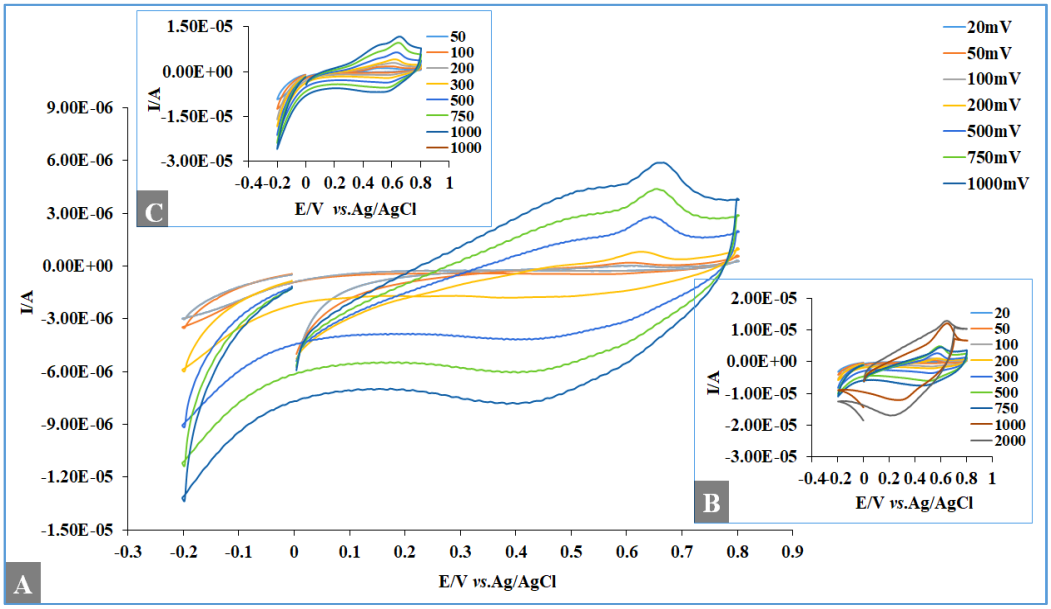

Figure 6.9: (A): CVs of TX100 in aqueous 0.1 M HCl at different scan rates 20-1000 mV s^{-1}. Inset (B): CVs of (A) detailing of 0.0075 gm chl and (C): CVs of (B) in the presence of vitamin K_1

6.4 Conclusion

The objective of the present study was to see if electro-induced, electron transfer process occurred between extracted chlorophyll or chlorophyllin and some active species. It has been shown that, although the oxidation behaviour of the electroactive species potassium iodide is easy to see regarding the responses of current and potential peaks, it was electrochemically sufficient. In addition, the identification of chlorophyll pigment was achieved in this study using various techniques (TLC, and UV-Visible). Moreover, for the case of the redox reaction of the chlorophyll pigment in an aqueous solution of HCl in the presence of Triton X 100 and vitamin K_1, it was observed that both peaks current and potential increased with increase in the scan rates of potential due to the role of the surfactant in the bulk solution. The last part of this chapter has described the behaviour of extracted chl and CHL in KI solution with and without Triton X 100 and vitamin K_1.The results established that TritonX100 enhanced electron transfer in bulk solution due to the correspondence of the peak current and peak potential, while potassium iodide inhibits it in the previous solution. Finally, the mechanism of the reaction was suggested to be one-electron transfer; it is EC' reaction.

6.5 References

(1) Svec, W. A.: *The distribution and extraction of the chlorophylls, in: chlorophylls*; CRC Press,Boca Raton, **FL 1991**. pp. 89-114.

(2) Green, B. R.; Anderson, J. M.; Parson, W. W.: *Photosynthetic membranes and their light-harvesting antennas*; Springer, **2003**.

(3) Mantoura, R.; Llewellyn, C. The rapid determination of algal chlorophyll and carotenoid pigments and their breakdown products in natural waters by reverse-phase high-performance liquid chromatography. *Anal. Chim. Acta.,* **1983**, *151*, pp 297-314.

(4) Sartory, D.; Grobbelaar, J. Extraction of chlorophyll a from freshwater phytoplankton for spectrophotometric analysis. *Hydrobiologia.,* **1984**, *114*, pp 177-187.

(5) Strain, H. H.; Svec, W. A. Extraction, separation, estimation and isolation of the chlorophylls. *The chlorophylls.,* **1966**, *1*, pp 22-66.

(6) Wu, J.-H.; Wang, S.-Y.; Chang, S.-T. Extraction and determination of chlorophylls from moso bamboo (Phyllostachys pubescens) culm. *J. Bamboo and Rattan.,* **2002**, *1*, pp 171-180.

(7) Yentsch, C. S. M., David W. A method for the determination of phytoplankton chlorophyll and phaeophytin by fluorescence. In *Tilte***1963**; Elsevier.

(8) Milenković, S. M.; Zvezdanović, J. B.; Anđelković, T. D.; Marković, D. Z. The identification of chlorophyll and its derivatives in the pigment mixtures: HPLC-chromatography, visible and mass spectroscopy studies. *Adv. Tech.,* **2012**, *1*, pp 16-24.

(9) Suzuki, Y.; Shioi, Y. Identification of chlorophylls and carotenoids in major teas by high-performance liquid chromatography with photodiode array detection. *J. Agric. Food Chem.,* **2003**, *51*, pp 5307-5314.

(10) Zvezdanović, J.; Cvetić, T.; Veljović-Jovanović, S.; Marković, D. Chlorophyll bleaching by UV-irradiation in vitro and in situ: Absorption and fluorescence studies. *Radiat. Phys. Chem.*, **2009**, *78*, pp 25-32.

(11) Simon, D.; Helliwell, S. Extraction and quantification of chlorophyll a from freshwater green algae. *Water Res.,* **1998**, *32*, pp 2220-2223.

(12) Holm-Hansen, O.; Lorenzen, C. J.; Holmes, R. W.; Strickland, J. D. Fluorometric determination of chlorophyll. *ICES J. Mar. Sci.,* **1965**, *30*, pp 3-15.

(13) Aminot, A.; Rey, F. Standard procedure for the determination of chlorophyll a by spectroscopic methods. *ICES J. Mar. Sci.,* **2000**, *112*.

(14) Vernon, L. P.; Seely, G. R.: *The chlorophylls*; Academic press, **2014**.

(15) Zuber, H.; Cogdell, R. J.: Structure and organization of purple bacterial antenna complexes. In *Anoxygenic photosynthetic bacteria*; Springer, **1995**; pp 315-348.

(16) Parusel, A. B.; Grimme, S. A theoretical study of the excited states of chlorophyll a and pheophytin a. *J. Phys. Chem. B.,* **2000**, *104*, pp 5395-5398.

(17) İnanç, A. L. Chlorophyll: Structural Properties, Health Benefits and Its Occurrence in Virgin Olive Oils. *Academic Food Journal/Akademik GIDA.,* **2011**.

(18) Chitta, R.; D'Souza, F. Self-assembled tetrapyrrole–fullerene and tetrapyrrole–carbon nanotube donor–acceptor hybrids for light induced electron transfer applications. *J. Mater. Chem.,* **2008**, *18*, pp 1440-1471.

(19) Barazzouk, S.; Kamat, P. V.; Hotchandani, S. Photoinduced Electron Transfer between Chlorophyll a and Gold Nanoparticles. *J. Phys. Chem. B.,* **2005**, *109*, pp 716-723.

(20) Wiederrecht, G. P.; Svec, W. A.; Niemczyk, M. P.; Wasielewski, M. R. Femtosecond transient grating studies of chlorophylls and a chlorophyll-based electron donor-acceptor molecule. *J. Phys. Chem.,* **1995**, *99*, pp 8918-8926.

(21) Kobayashi, M.; Ohashi, S.; Iwamoto, K.; Shiraiwa, Y.; Kato, Y.; Watanabe, T. Redox potential of chlorophyll d in vitro. *Biochim. Biophys. Acta, Bioenerg.,* **2007**, *1767*, pp 596-602.

(22) Zhao, G.-C.; Zhang, L.; Wei, X.-W.; Yang, Z.-S. Myoglobin on multi-walled carbon nanotubes modified electrode: direct electrochemistry and electrocatalysis. *Electrochem Commun* **2003**, *5*, pp 825-829.

(23) Cheng, G.; Zhao, J.; Tu, Y.; He, P.; Fang, Y. A sensitive DNA electrochemical biosensor based on magnetite with a glassy carbon electrode modified by muti-walled carbon nanotubes in polypyrrole. *Anal. Chim. Acta.,* **2005**, *533*, pp 11-16.

(24) Goyal, R. N.; Gupta, V. K.; Bachheti, N.; Sharma, R. A. Electrochemical Sensor for the Determination of Dopamine in Presence of High Concentration of Ascorbic Acid Using a Fullerene‐C60 Coated Gold Electrode. *Electroanal.,* **2008**, *20*, pp 757-764.

(25) Bard, A. J. Photoelectrochemistry and heterogeneous photo-catalysis at semiconductors. *J. Photochem.,* **1979**, *10*, pp 59-75.

(26) Wang, J.: *Analytical electrochemistry*; John Wiley & Sons, **2006**.

(27) Guadalupe, A. R.; Abruna, H. D. Electroanalysis with chemically modified electrodes. *Anal. Chem.,* **1985**, *57*, pp 142-149.

(28) Wring, S. A.; Hart, J. P. Chemically modified, carbon-based electrodes and their application as electrochemical sensors for the analysis of biologically important compounds. A review. *Analyst.,* **1992**, *117*, pp 1215-1229.

(29) Inoue, T.; Kirchhoff, J. R. Electrochemical Detection of Thiols with a Coenzyme Pyrroloquinoline Quinone Modified Electrode. *Anal. Chem.,* **2000**, *72*, pp 5755-5760.

(30) Goyal, R. N.; Gupta, V. K.; Oyama, M.; Bachheti, N. Differential pulse voltammetric determination of paracetamol at nanogold modified indium tin oxide electrode. *Electrochem. Commun.,* **2005**, *7*, pp 803-807.

(31) Yang, W.; Justin Gooding, J.; Brynn Hibbert, D. Characterisation of gold electrodes modified with self-assembled monolayers of l-cysteine for the adsorptive stripping analysis of copper. *J. Electroanal. Chem.,* **2001**, *516*, pp 10-16.

(32) Wrzosek, B.; Bukowska, J. Molecular structure of 3-amino-5-mercapto-1, 2, 4-triazole self-assembled monolayers on Ag and Au surfaces. *J. Phys. Chem. C.,* **2007**, *111*, pp 17397-17403.

(33) Lee, S.; Park, J.; Ragan, R.; Kim, S.; Lee, Z.; Lim, D. K.; Ohlberg, D. A.; Williams, R. S. Self-assembled monolayers on Pt (111): molecular packing structure and strain effects observed by scanning tunneling microscopy. *J. Am. Chem. Soc.,* **2006**, *128*, pp 5745-5750.

(34) Seger, B.; Kamat, P. V. Electrocatalytically active graphene-platinum nanocomposites. Role of 2-D carbon support in PEM fuel cells. *J. Phys. Chem. C.,* **2009**, *113*, pp 7990-7995.

(35) Nicol, M. J. The anodic behaviour of gold. *Gold Bull.,* **1980**, *13*, pp 46-55.

(36) Tremiliosi-Filho, G.; Dall'Antonia, L. H.; Jerkiewicz, G. Growth of surface oxides on gold electrodes under well-defined potential, time and temperature conditions. *J. Electroanal. Chem.,* **2005**, *578*, pp 1-8.

(37) Montilla, F.; Morallon, E.; Vázquez, J. Electrochemical behaviour of benzoic acid on platinum and gold electrodes. *Langmuir.,* **2003**, *19*, pp 10241-10246.

(38) Sandiningtyas, R. D. a. S., V.: Isolation of chlorophyll a from spinach and its modification using Fe^{2+} in photostability study: In *Proceedings of the Third International Conference on Mathematics and Natural Sciences*, **2010**; pp 859-873.

(39) Ciesielski, P. N.; Faulkner, C. J.; Irwin, M. T.; Gregory, J. M.; Tolk, N. H.; Cliffel, D. E.; Jennings, G. K. Enhanced photocurrent production by photosystem I multilayer assemblies. *Adv. Funct. Mater.*, **2010**, *20*, pp 4048-4054.

(40) Rozkiewicz, D. I.; Ravoo, B. J.; Reinhoudt, D. N. Reversible covalent patterning of self-assembled monolayers on gold and silicon oxide surfaces. *Langmuir.*, **2005**, *21*, pp 6337-6343.

(41) Reeves, S. G. H., D.O. Higher plant chloroplasts and grana: General preparative procedures (excluding high carbon dioxide fixation ability chloroplasts). *Methods Enzymol, 69* **1980**, pp 85-94.

(42) Baba, K.; Itoh, S.; Hastings, G.; Hoshina, S. Photoinhibition of photosystem I electron transfer activity in isolated photosystem I preparations with different chlorophyll contents. *Photosynth. Res.*, **1996**, *47*, pp 121-130.

(43) Scheer, H. Structure and occurence of chlorophylls. **1991**.

(44) Milenković, S. M.; Zvezdanović, J. B.; Anđelković, T. D.; Marković, D. Z. The identification of chlorophyll and its derivatives in the pigment mixtures: HPLC-chromatography, visible and mass spectroscopy studies. *Advanced technologies* **2012**, *1*, pp 16-24.

(45) Zapata, M.; Garrido, J. L.; Jeffrey, S. W.: Chlorophyll c pigments: current status. In *Chlorophylls and Bacteriochlorophylls*; Springer, **2006**; pp 39-53.

Chapter 7

Chlorpromazine.HCl as Lamellar (L_α) liquid crystal system

The work in this chapter splits into three sections.

The first section briefly covers the history and literature review of the liquid crystal. It defines the liquid crystalline phase and the diversity of types of these systems. The last part of this section discusses the structures and the varied applications of the liquid crystal.

Section two explains the chemical materials, electrochemical cells and instruments used in this study. It further discusses the general procedure for preparing liquid crystal and its utilisation in the electrochemical application.

The last section deals with the experiments data analysis and experimental results of inferences.

7.1 Liquid crystals system LCs

Liquid crystals may form from large molecules such as potassium or sodium salts of higher fatty acids in a fitted amount of solvent like water; the organic molecules that compose these species are mesogens.[1] The consequence times of it has discovered, the meaning, the structures and applications will be discussed in the next sections.

7.1.1 Historical Introduction and Literature Review

The history of liquid crystals dates back to early 1888; Friedrich Reinitzer discovered an intermediate state of matter between liquid and sold. In the process of finding a precise formula and molecular weight of cholesterol in the experimental preparation of cholesteryl ester, he realised that there were two melting points with different properties.[2,3]

The German physicist Otto Lehmanna, Friedrich's friend, identified the order as being between solid and liquid, which he termed as liquid crystal. He published his first work on liquid crystals, subsequently.[4,5] Later, Merck, the industry company, started to commercialise LCs. Since 1904, this company has pioneered the applications of these materials.[6,7] Between 1969 and 1972 the effect of photovoltaic in smectic-LC and the effect of ionic photovoltaic in nematic-LC were illustrated.[8,9]

In 1973 at Hull University, Gary, George W discovered the stable nematic phases at room temperature.[10] After a hundred years of exploring the first LCs, scholars discovered calamitic phase (CLCs) or rod-like molecule. In 1977 Chandrasekhar *et al.,* observed another phase of LCs, which was a disk-like molecule or discotic LCs (DLCs).[11]

The study of mass transport in LCs system received increasing attention for researchers in photovoltaic devices applications.[12-14] Thus, the year of 1994 witnessed the first use of discotic LCs in a photovoltaic device.[15] These discoveries were followed by another

exploration in 2006 as Miguel C-Orozco and *et al*. discovered nematic-LCs gel, which was first used in solar cells application.[16] Nowadays, LCs materials have wide applications in electronic devices and exhibition machinery.[17] To present various phases of LCs and techniques that use to characterise LCs, the table below is a brief literature review studied since 2014.

Table 7.1: The overview of studying Liquid crystals system

Type of liquid crystals	Analysis methods	Characterised study	Ref
lamellar microphase contains discotic liquid crystalline	Transmission electron microscopy (TEM), X-ray and polarising microscopy (POM)	The effect of slit-like nano confinements on columnar discotic	18
Polymethacrylate (PPHM) with LCs	Differential scanning calorimetry (DSC), Wide-angle X-ray diffraction (WAXD) and Polarized microscopic	Aggregation states of PPHM	19
liner liquid crystal polymers (LLCPs)	Differential scanning calorimetry (DSC) and POM	Visible light induced of LLCPs	20
Chiral liquid crystals(CLCs)	POM and WAXD	Reviewing the structures, phases and effects of CLCs on liquid crystals	21
Nematic LC	DSC and POM	Designing and synthesising four new LC-thiophene compounds	22

LC honeycombs	Small-angle X-ray scattering (SAXS) and atomic force microscopy (AFM)	Studying arranging patterns of two LC on anodic aluminium oxide (AAO) template	23
Benzenammonium columnar LCs	DSC, POM and XRD	Designing new columnar ionic liquid crystals-ammonium salt	24
Photonic crystals (PhCs)	TEM and XRD	Reviewing the chemical and biochemical parameters and application of PhCs	25
Lyotropic liquid crystalline	Macroscopic fluid assembly, POM, TEM and SAXS	Investigating graphene liquid crystals	26
Lyotropic chromonic Nematic LCs	Dynamic light scattering	Studying orientation and some physical properties in the nematic phase	27
Lyotropic chromonic LCs	Cryo-transmission electron microscopy (cryo-TEM)	Determination micro and nanostructures of disclination cores in chromonic nematics phases	28
Chiral nematic liquid crystals (CLCs)	POM and UV light	Studying the three dimensions of the helical axis of CLCs phase inducing by UV light	29
Ionic liquid crystals (ILCs)	POM and SAXS	The reviewing of the design, synthesis, characterisation and application of ILCs phase	30

Twist-bend liquid crystal (N_{TB})	Resonant x-ray scattering	Studying the behaviour of N_{TB} phase in bent molecular dimers(CB7CB)	31
Thermotropic LC	Mass, Infrared, ^{1}H NMR, IR spectra and POM	Evaluation and comparison the thermotropic LC properties of derivatives chalconyl ester with similar homologous series	32

In this chapter, we develop novel the first LCs- photogalvanic cells using CPZ.HCl gel.

7.1.2 Definition, Properties and Classifications

Liquid crystals or mesophases, are an intermediate state of matter between two classic states (liquid and solid or crystal), and its form is combined with these two states; its schematic form is shown in figure 7.1. Thus, liquid crystals are considered as the fourth state of the material.

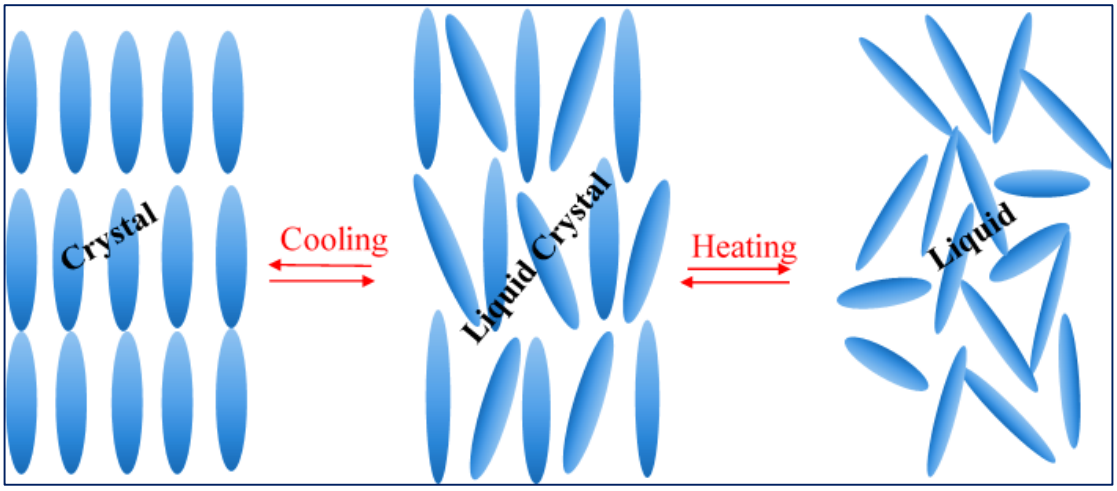

Figure 7.1: The molecular orders of crystal, liquid crystal and liquid adapted from reference [33]

Liquid crystals are often organic compounds with disk or rod-shaped molecules. Their properties are similar to organic compounds such as solubility, melting point, phase,

conductivity, absorbing and reflecting light.[34,35] Further, LCs involves many small regions with molecules that all are easily aligned with each other by surface forces. Furthermore, they have different optical properties with large aligned areas, for these reasons and besides their low-cost productions with large areas, they are widely used in electronic displays[36] as well as semiconductors in photovoltaic cells.[37,38]

LCs are grouped from the chemical viewpoint into lyotropic (LLC), thermotropic (TLC) and metallotropic (MLC). All of these groups involve various types of phases with different properties and structures. The first phase (LLC) consists of organic molecules in aqueous solution often is water, and the transition of these molecules into LC phase is dominated by various temperature range and solvent concentration.

The second phase (TLC) involves pure organic substance, which reached this phase in a certain temperature range. However, the third one is composed of organic and inorganic molecules. Thus, the transition molecules to LCs depends not only on temperature and concentration but also on the composition ratio of organic/inorganic.[39] The table below performs the most common types of LCs phases:

Table 7.2: The types of liquid crystal phases

Liquid Crystal Phases LCs					
Lyotropic LLC			Thermotropic TLC		
Lamellar **L*α***	Hexagonal H1	Cubic I1	Nematic	Cholestric	Sematic

The focus of this study is on LLC. LLC involves amphiphilic molecules with hydrophobic and hydrophilic parts, which are solved in a suitable solvent. Some of the living systems are LLCs such as cell membrane, biological membranes and many proteins. In an aqueous

solution with a low concentration of molecule such as a surfactant, (soap is LLC) with a certain temperature, soap molecules form micelles without order as shown in figure 7.2.

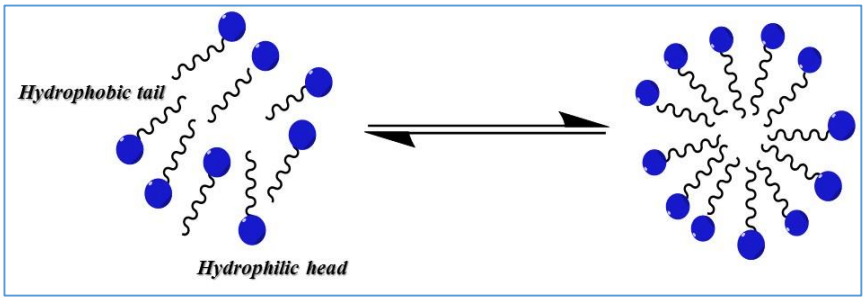

Figure 7.2: The typical form of Micelle

As increasing concentrations of surfactants, the micelles became rod-shaped and arranged in an ordered with specific structures that include lamellar (bilayer structure), hexagonal (cylinder form) and cubic phases[40]; they are sketched in figure 7.3.

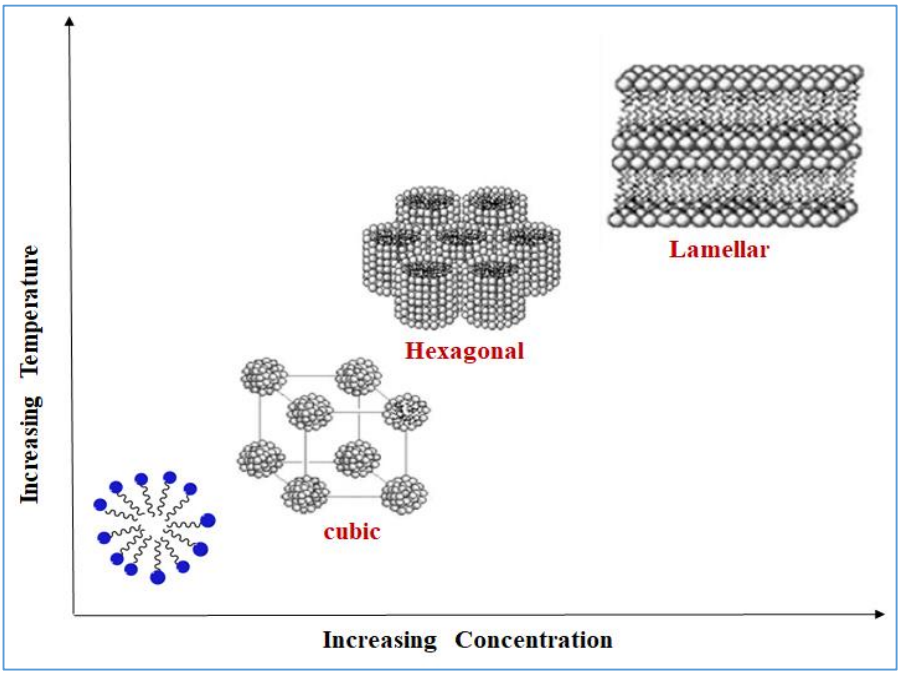

Figure 7.3: Typical lyotropic liquid crystal phases, adapted from referenc[41]

The above structures of LLC are investigated by various techniques such as X-ray diffraction, polarised light microscopy, fluorescence quenching and Transmission Electron Microscope. LCs structures play a crucial role in biology and living systems as well as in substances science. In appropriate conditions, several biological compounds have existed in different phases of liquid crystals in *vivo* and in *vitro* such as proteins,

carbohydrates, lipids and nucleic acids.[42] Therefore, LCs meet the interest of many researchers in biochemistry, biophysics and bionic fields.

7.1.3 Application of liquid crystals

Liquid crystals are universal in our daily life, particularly in the electronic display devices, optoelectronics devices and sensor devices.[43] Thereby, these soft materials molecules were rapidly increased in the commercial applications during the last thirty years for their appropriate properties such as order and mobility at molecular, supramolecular and macroscopic level. The type of LCs (thermotropic) is useful in materials science. The lyotropic LCs is invaluable in materials as well as the biological area. The applications of these elements are described below.

- **Nanoscience and nanotechnology fields**

Liquid crystals-nanoscience deals with the relationship between LCs and nanomaterials. This field of study has interested many researchers recently in industrial and academic areas. Different materials have been used in high-technology devices and medical investigations. The recent global research concentrates on design nanoparticles with the ability of self-assembly in ordered and larger structures.[44-46]

The applications of LCs in nanoscience and nanotechnology have drawn the attention of chemists, engineers, physicists and recently physicians and biologists.[47,48] The incredible breakthrough in the nanoscience and nanotechnology fields was distinctive after the discovery of novel mechanisms and fascinating phenomena that occurred in micro and nano-scale materials.[49]

- **Biomedical materials**

LCs were valuably used in biomedical fields due to the similarity between the self-organised structure of LLCs and living organisms.[50-52] There were enormous applications

of LCs in the biomedical fields such as drug delivery control, phospholipid category, microbe finding and protein binding. There were various applications of LC devices in biomedical optical imaging systems such as polarimetry imaging, phase shift interferometric imaging, fluorescence imaging and hyperspectral imaging.[53]

Lyotropic liquid crystals have been used as a nanoreactor for the synthesis of nanomaterials with a uniform size and shape.[54]Also, LLCs have been employed as a pattern for the synthesis mesoporous nanostructures in uniform pore size and shape combined with many various metals. Recently, the condensed of thermotropic LCs has been used in spherical nanoparticles self-assembly. Therefore, there will be several challenges in future research of using TLCs phase for nanoparticles (assembly and synthesis) through spreading shape and size at the same time.[55]

- **Electronic liquid crystal display(LCD)**

The development of electronic displays using LCs started in 1964 when dynamic scattering mode (DSM) was exposed for the first in 1968 by Wysocki *et al.*[56] After few decades, namely in 1990, the manufacturers of LCDs technology witnessed a significant development in the electronic industry that witnessed the manufacturing of the wall hanging television.[6] Due to the elastic, magnetic and optoelectronic properties of the liquid crystals, they are wide range used in displays devices such as smartphones, laptop computers, cameras, digital watches, stereos, calculators and flat-screen televisions.[57,58]

Regarding continuing research in liquid crystals and developing new applications, LCs will play a vital role in modern technology especially in electronic devices. It is expected that the next twenty years of LCDs production will witness an enormous improvement, particularly TV screen and personal computers. Other applications use different types of LCs such as cholesteric, nematic, smectic in field sensors[17,59,60], laser[61,62] and optical

computing[63,64] and so forth. In addition, it is a highlight that LCs were utilised in visual art field by many researchers.[65-67] Moreover, cholesteric LCs are widely used in cosmetic industry such as lipsticks, makeup removers and lip glosses.[68,69]

Subsequently, liquid crystal polymers such as polyester gained a lot of industrial applications after the development of its properties (surface and resistance) as it was used in multi-fibre coating, optical cables and fire resistant.[70] Recently, the applications of LCs by using a special kind of materials are continuing to improve the efficiency of these materials that can be used in different fields of science and device machinery.

7.2 Methodology

This section reports the details about general reagents and different electrodes diameters such as macro and micro; a method for the analysis of liquid crystal system will be described.

7.2.1 Chemical Reagents

The reagents and materials used in this chapter experiments were all analytical grade, which were explained in sections 4.2.1, 5.2.1 and 6.2.1 of chapters (4, 5 and 6) without further purification.

7.2.2 Electrochemical Cells

The electrolysis cell and the potentiostat with computerised apparatus were used as the same of previous experiments in the chapters 4, 5 and 6. The potentials were measured against a silver/silver chloride electrode with carbon rod or a nickel wire coiled into a spiral wire as the counter electrode. Working electrodes with different diameters and materials were explained in the next parts.

7.2.2.1 Macro Electrode

Electrochemical measurements were undertaken as a sketch in section 3.2.1 chapter three for all macro electrode experiments including the investigation of CPZ.HCl system in this chapter, a 3.0 mm diameter Au and glassy carbon electrodes were employed as the working electrodes. These electrodes were polished before each experiment as labelled in section 3.2.2.1 of chapter three and the followed chapters. All experiments were carried out at room temperature (20 ± 3 ℃) excluding those with the liquid crystal process.

7.2.2.2 Micro Electrode

Microelectrode (ME) is an electrode in which transport process controls diffusion, and its radius is less or equal 20µm.[71] It is categorised into single and composite; the types of former ME are a cylinder, band, sphere, disc and so forth. Moreover, there are two types of later ME: ensemble and array. Figure 7.1 shows the image of these electrodes that were used in this section.

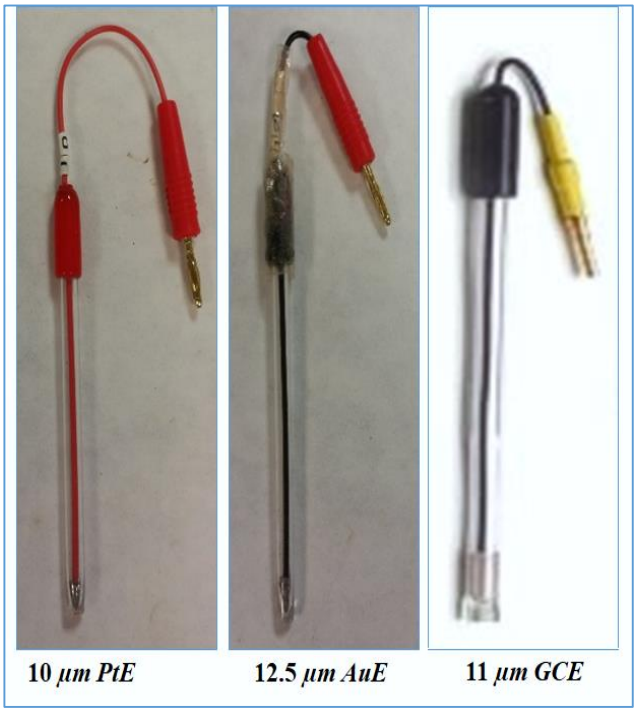

Figure 7.4: Microelectrodes; Platinum (Pt), gold (Au) and glassy carbon (GC)

Microelectrodes, including single and composite microelectrodes, can be produced in diverse geometries with different electrode materials by using various fabrication techniques.

Microelectrodes have the following advantages over the normal macro electrode.

- It has a small size, which allows measurement of smaller volumes in comparison with the conventional electrodes.
- Microelectrode allows a tiny amount of total current passing through the cell. Thus, its diffusion layer is larger than the electrode size. Consequently, it has higher mass transport than the macro electrode.
- It possesses a good signal resolution as well as producing low detection limits due to high current density.
- This electrode can produce currents at a steady state on shorter time scale through reducing the current.

The steady-state current at micro disc electrodes can be calculated by using the following equation:

$$I = 4nF\Gamma Dc_{\infty}$$

Equation7.1

When n is the number of electrons, F is the Faraday constant, Γ is the electrode radius, D is the diffusion coefficient, and c is the concentration of the material under examination. The applications of the microelectrodes and their methods are shown in the below table 7.3.

Table 7.3: Some applications of microelectrodes

Applications	Methods	Ref.
Electrochemical analysis of trace elements	The determination of trace heavy metals in aquatic systems	71
Electrochemical sensors	Electrochemical sensor based on carbon nano tubes (CNT)	72
The mechanisms and kinetics of electrochemical reactions	The study of homogeneous chemical reactions coupled to electrode reactions at platinum microelectrodes	73
The scanning Electrochemical microscopy of (SECM)	SECM was used to characterise the surface of addressable microelectrode arrays (10µm platinum micro discs)	74
Electrochemical reaction in high resistance solutions	Used of a platinum microelectrode in high-resistance organic solvents.	75
Measurements of biological application	Used microelectrode arrays technology in the field drug discovery.	76

In this area of study, we used two types of microelectrodes, which were gold and platinum with different diameters 12.5, 25, 33 and 50 µm for gold, while 10 µm for platinum.

Preliminary microelectrodes were polished in each scan rates using the same polishing steps that presented in chapter three section 3.2.2; this takes place with changing the position of a used electrode.

7.2.3 Procedure

CPZ.HCl liquid crystals solution was prepared by mixing the required amount of solid (CPZ.HCl) with 1mL of deionised water in screw-capped vials. Then, solubility was induced through heating with stirring to approximately 70 ^{o}C for less than one hour, accomplishing homogenisation of the sample. The heating step was followed by cooling the sample to ambient room temperature.

These steps were preceding to further electrochemical experimentations at that temperature and were required for LCs formation.[77] Before every electrochemical experiment, the working electrode was cleaned and polished by using the same procedure that was mentioned in section 2 in the previous chapter. Thus, a clean surface of this electrode was revealed to various positions of LCs sample for every change in experimental parameters.

7.3 Results and Discussions

In the previous chapter, we explored the electron transfer using various materials, electrodes, electrolytes and methods. This work, besides other studies[78,79], identified that CPZ.HCl can be used as a good mediator for redox catalysis.

The overall aim of this study in this chapter is to develop liquid crystal for the electrochemical study of photoinduced electron transfer. This section covers the following studies: investigating the inducing chlorophyll a and total chlorophyll by using laser light and examining the lyotropic liquid crystal system of these compounds, the description of the laminar liquid crystals system by using CPZ.HCl material and the application of photosynthesis system.

To achieve this aim, CPZ.HCl with different diameters of WE and materials was investigated. Liquid crystals system was characterised by polarised microscopy (POM) and X-ray diffraction (XRD), cyclic voltammetry was employed for the studies. The performance of the macro and microelectrodes concerning sensitivity, linear range and selectivity towards LCs was evaluated and discussed. The LCs applicability of CPZ.HCl was demonstrated for the photosynthesis system.

7.3.1 Studying CVs of droplet T-chlorophyll and LLCs system

In this part, two pigments Tchl and chlorophyll a were investigated in droplets immobilised onto different sizes and materials of working electrodes surfaces. Many parameters were studied here such as concentrations of Tchl, solvents and electrolytes, these studies were considered under red light (on/off) atmosphere. In the last part, the LLCs of total chlorophyll was studied.

7.3.1.1 The effect of pH on a pigment in dark and light on

Preliminary effect of pH on the electrochemical behaviour of both droplet 2.3 mM chlorophyll a and 6% total chlorophyll on the glassy carbon electrode surface was studied. The cyclic voltammograms of that electrode were recorded in aqueous solutions. It was applied by using two pH medium 2 and 7 under red light with wavelength approximately 650 nm and in dark atmosphere. Figures 7.5 and 7.6 show the response of these compounds at scan rate 100 mV s^{-1}.

The general reaction for the pH sensitivity of chl a was mentioned in section 6.1.2 of chapter six. CVs responses of dissolved chl a and Tchl, as illustrated in the figure below, showed no corresponding oxidation peaks regardless of pH in dark and light environment. It had been reported that there were no effects of electrolyte pH from 7 to 11, which means the electrode reaction does not involvement protons.[80]

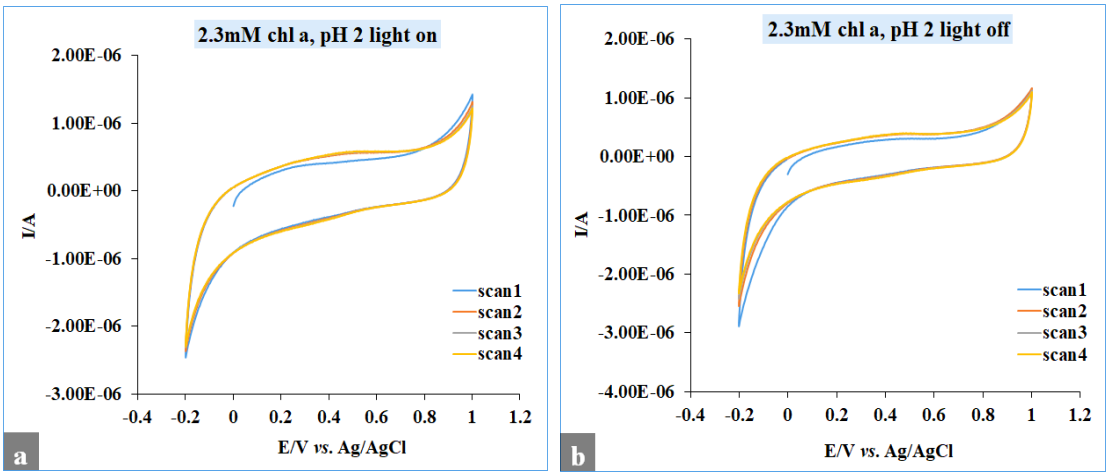

Figure 7.5: CVs of the filtrated chlorophyll a in the presence of buffer solution (Britton-Robinson) pH 2 under red light effect. a: Light on and b: Light off, the scan rate is 100mV s^{-1}

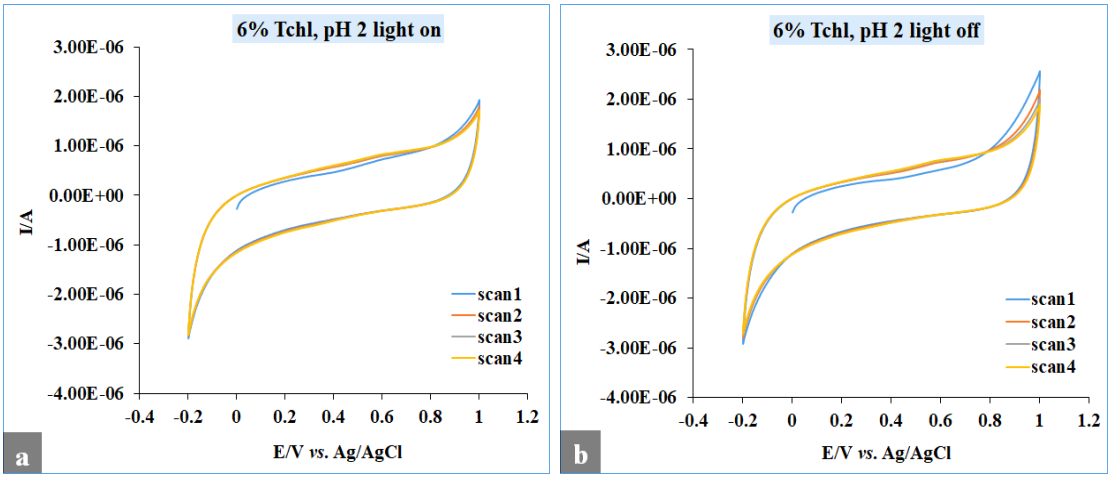

Figure 7.6: CVs of the filtrated T-chlorophyll in the presence of buffer solution (Britton-Robinson) pH 2 under red light effect. a: Light on and b: Light off, the scan rate is 100mV s^{-1}

Once more, the electrochemical behaviour of these pigments in pH 7 showed a similar trend of pH 2, see figure 7.7.

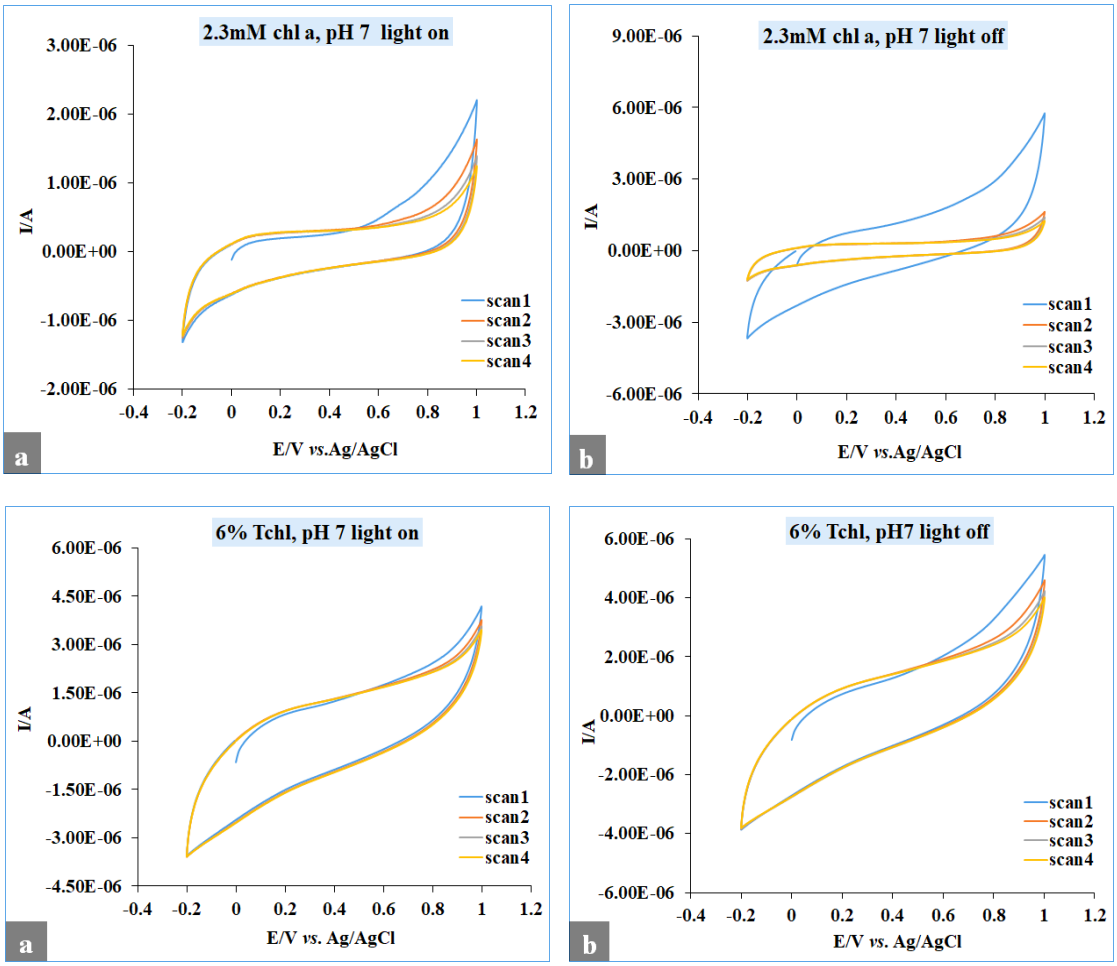

Figure 7.7: CVs of the filtrated chlorophyll a and Tchl in the presence of buffer solution (Britton-Robinson) pH 7 under red light effect. a: Light on and b: Light off, the scan rate is 100mVs^{-1}

7.3.1.2 The examination of the solubility of Tchl in different solvents and supporting electrolytes

Another topic of investigation was the solubility of 1% (w/v) Tchl pigment in various organic solvents such as ethanol, dichloromethane, diethyl ether, toluene and hexane. Figure 7.10 displays CVs diagrams of 1% Tchl in these solvents with their insert images. According to the solubility, it is shown that dichloromethane the best solvent for soluble Tchl pigment, thus it was selected as the solvent of this pigment in the next experiments.

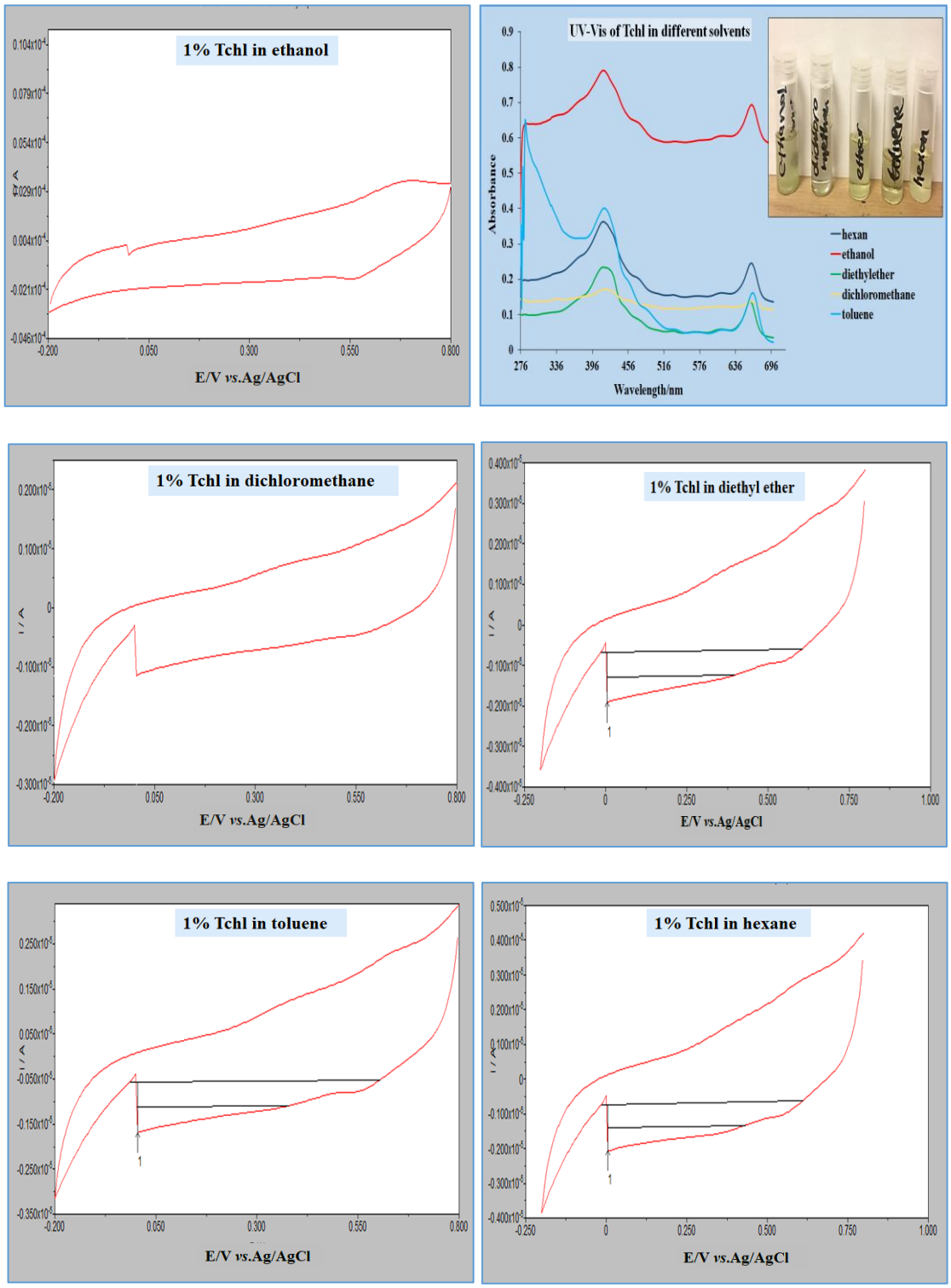

Figure 7.8: CVs diagrams for 1% Tchl soluble in various solvents were mentioned inset each chart, 100 mV s^{-1} scan rate. The first image on the right side was UV-Vis absorption spectra of Tchl pigment in different solvents with the inset image for this pigment that was dissolved in these solvents

In the case of using supporting electrolyte HCl and tetrabutylammonium perchlorate ($Bu_4N.ClO_4$ or TBAP) were used for the aqueous and organic phases. CVs results; figure

7.9, showed a clear oxidation peak in TBAP electrolyte for both dichloromethane and acetonitrile, and there was a feeble anodic peak in HCl electrolyte.

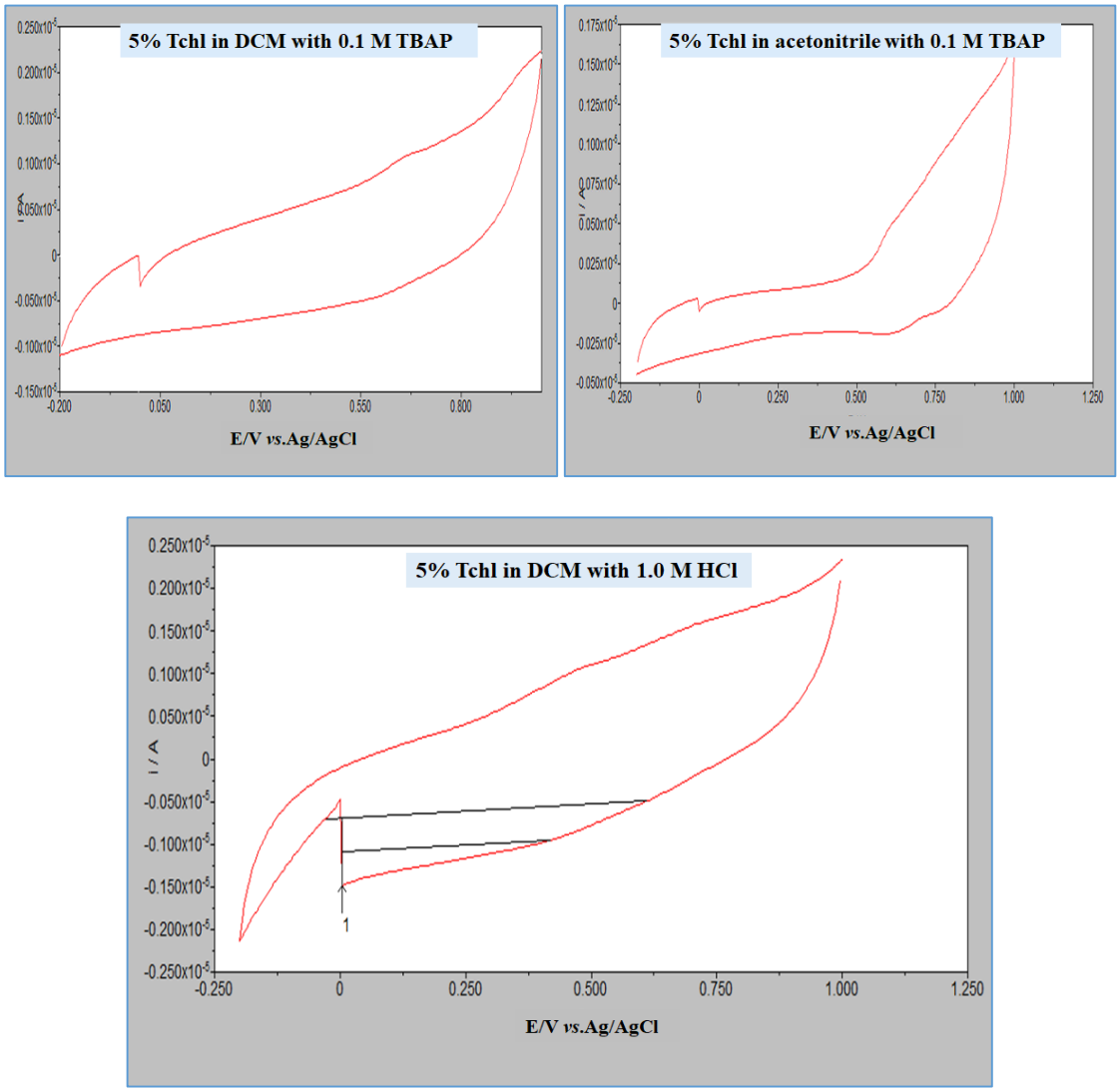

Figure 7.9: CVs of 5%Tchl in nonaqueous solvents (DCM and ACN) using supporting electrolyte. (a): TBAP and (b): HCl in both cases, a scan rate of 100 mV s^{-1} was used

7.3.1.3 Studying the effect of Tchl concentration

As mentioned in the previous chapters, the peak current and potential window of electrochemical reaction are influenced by the concentration of materials under examining. Thus, this study is presented here for two concentrations of Tchl (10 and 20%) dissolved in DCM in the presence of TBAP, which were deposited as a droplet on either macroscopic or microscopic carbon electrode. Figure 7.10 shows the responding of peak current for droplet Tchl pigment on the macro glassy carbon electrode was increased with

increase in its concentration, while there was no single on the micro glassy carbon electrode for this pigment. Regarding of the measuring absorbance of this pigment by using UV-Visible spectrometry, there was a similar trend of increasing its absorbing with increasing concentration; see the right-bottom image.

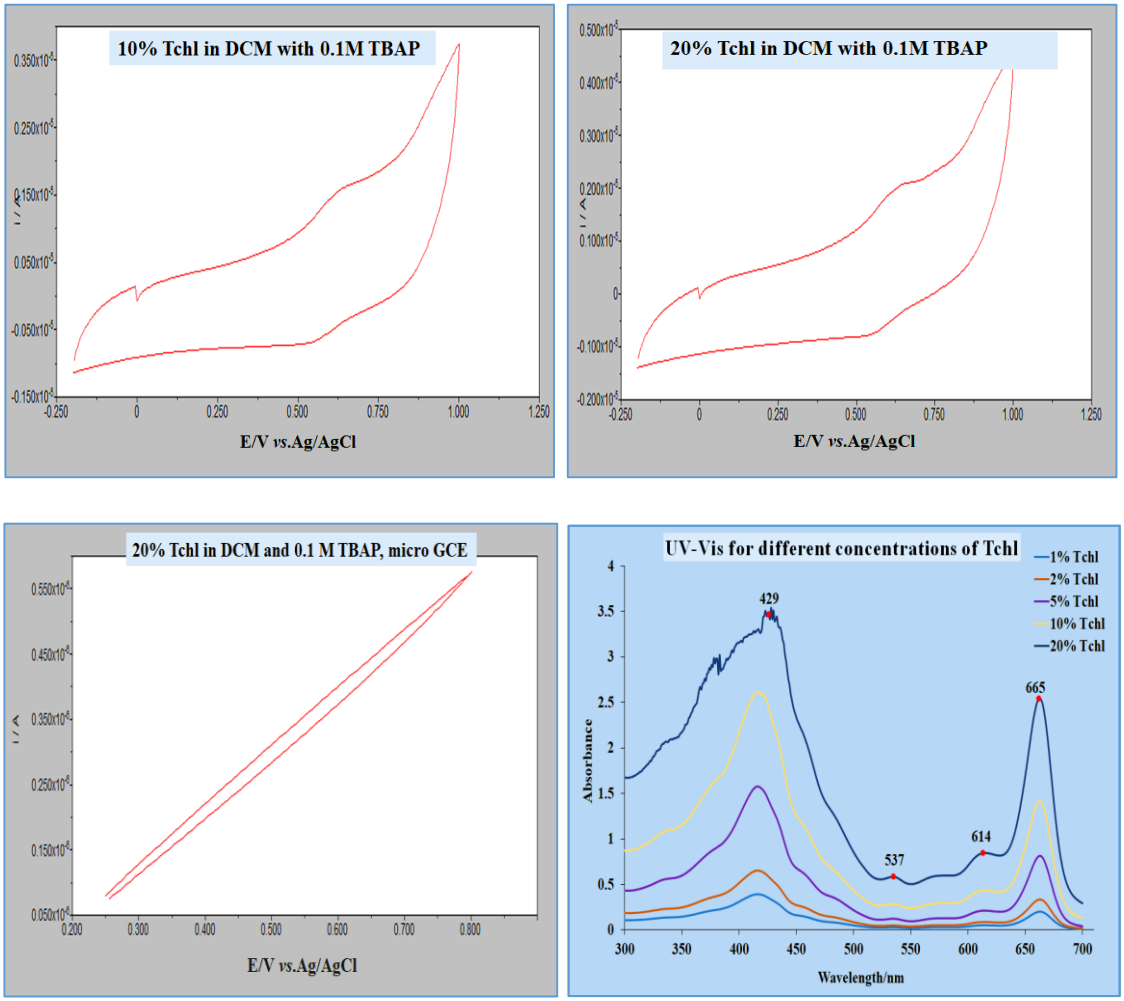

Figure 7.10: CVs of 10 and 20%Tchl in 0.1M TBAP. In scan rate, 100 mV s^{-1}, using macro GCE for the two charts on the top and micro GCE for the left chart at the bottom. The right chart at the bottom is UV-Vis diagram for various concentrations of Tchl

To gain further insight into the oxidation of Tchl droplet onto the surface of macro GCE under the same conditions of previous experiments, we studied the effect of the red light (on and off) on this pigment before and after filtration. The cyclic voltammetry of these studies; figure 7.11 shows that the oxidative peak currents are slightly bigger when the light on and the filtered pigment solution does not give as well-defined signals as unfiltered pigment solution.

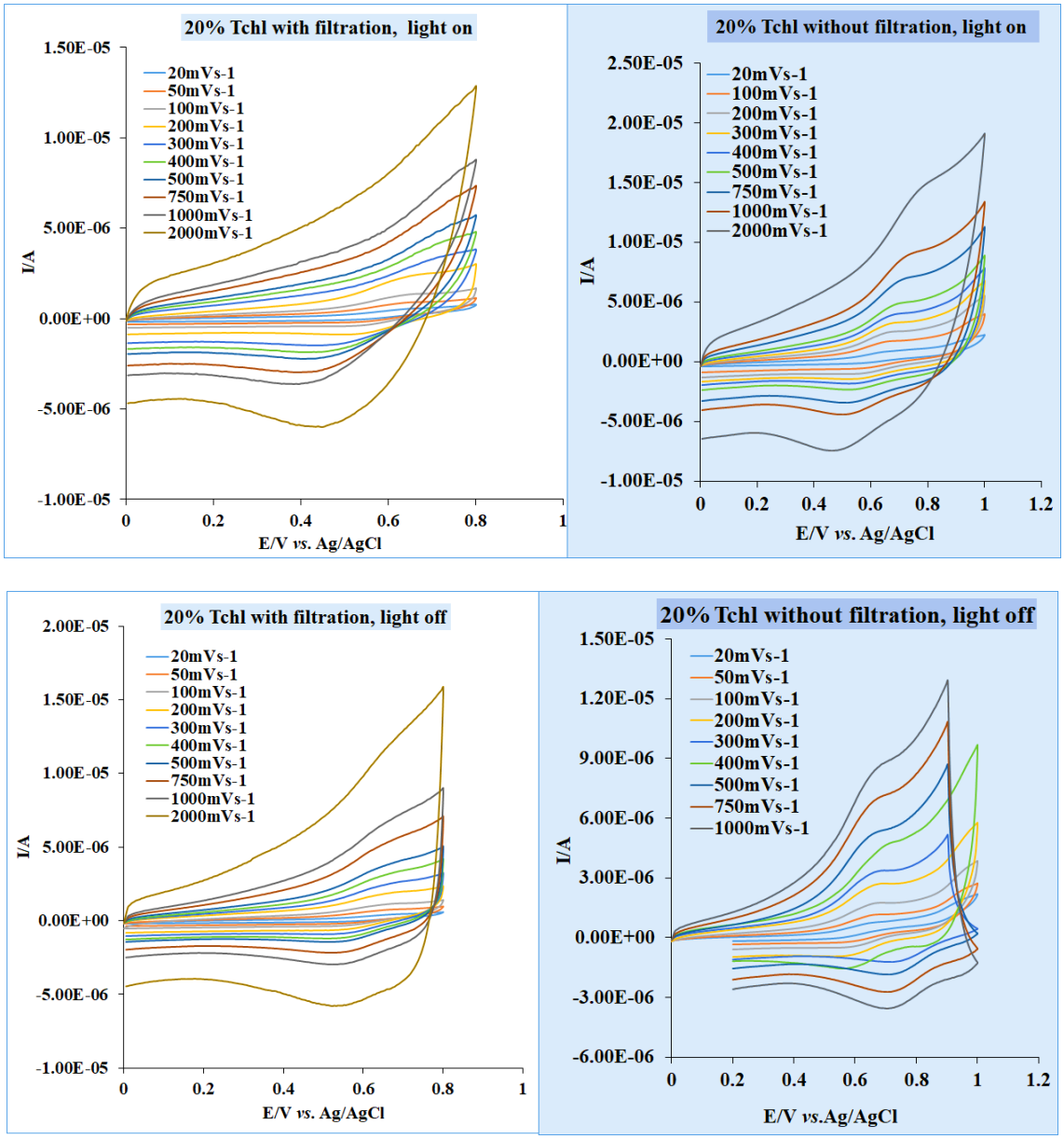

Figure 7.11: CVs of 20%Tchl dissolved in 25ml DCM and presence of 0.1M TBAP after and before filtration, droplet onto macro GCE suing light on/off for scan rates 20- 2000 mV s^{-1}

7.3.1.4 The effect of the presence of various concentrations of Vitamin K_1 on the Redox reaction of Tchl

The oxidation behaviour of Tchl on macro GCE was investigated, which was dissolved in 25 ml DCM solvent and filtrated before experimenting, that took place in presence and absence of various concentrations of vitamin K_1 using the light on/off in this system. The cyclic voltammograms corresponding to dissolved pigment recorded on macro GCE showed a single oxidation peak, regardless of VK_1 concentrations, see figure 7.12.

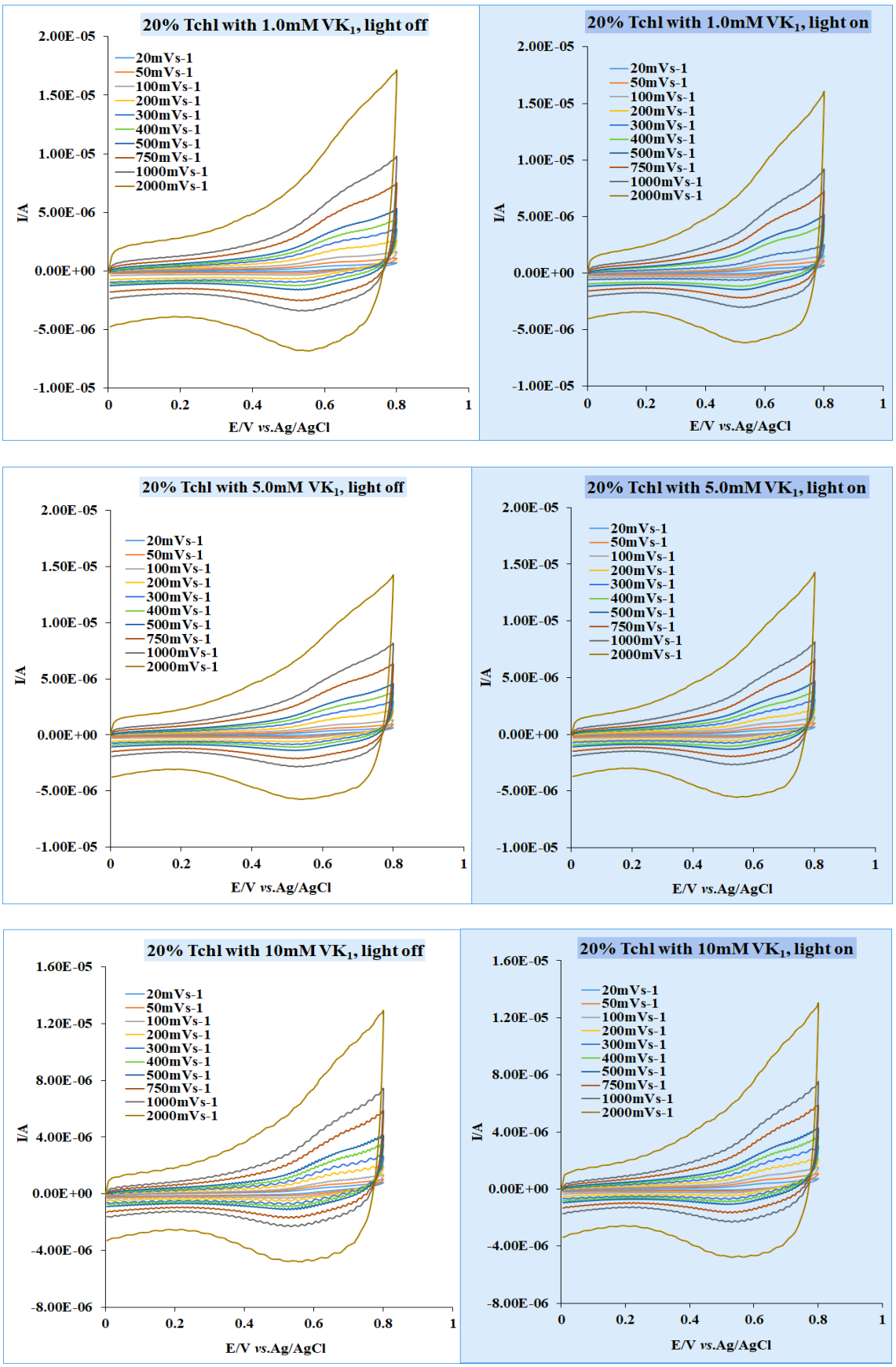

Figure 7.12: Cyclic voltammograms of the current peaks I/A against E/V recorded in the light and dark on Tchl pigment immersed in 0.1M DCM for (1.0, 5.0 and 10.0 mM) VK_1. Stepping the scan rates from 20 to 2000 mV s^{-1}

As seen in above figures, there are steady state cyclic voltammograms of Tchl pigment in the presence of VK_1 in light on and off for all concentrations. Also, there are slightly declined in oxidative peak currents through increasing VK_1 concentrations, which means VK_1 does not enhance the electrochemical reaction of this pigment.

7.3.1.5 Coulometric and Amperometric measurements of total chlorophyll

The coulometry and amperometry methods were used to gain additional knowledge about oxidation process of 20% Tchl soaking in the same atmosphere of the previous experiments. The results of these methods showed that there were no corresponding charges in the peak charges and the peak currents over potential ranges (0.0, 0.2, 0.4, 0.6 and 0.8 V) in the presence or absence of light, which means need to find more reliable 3-D formation for photoreduction processes.

7.3.2 Studying LLCs system of CPZ.HCl and its photosynthesis application

According to many reports in the literature that CPZ.HCl can be surface active and form micelles in aqueous solution.[81,82] Thus, this study focuses and confirms this fact through forming liquid crystals from this compound. We first examine the formation and physical characteristics of the liquid crystalline phase formed through mixing chlorpromazine hydrochloride and water, before investigating its electrochemical properties. Polarised Optical Microscopy (POM) along with X-ray diffraction (XRD) were employed to identify and determine the liquid crystals phases, orientations phase and transition phase. The LLCs phase of CPZ.HCl depends on many factors including the effect of CPZ.HCl concentration, working electrode material, working electrode diameter and scan rate were presented. UV-Vis spectroscopy was used to investigate obtaining CPZ.HCl-LCs through a changing in the band spectrum of CPZ.HCl system. Finally, the system of CPZ.HCl-LLCs was examined to be applied as a photogalvanic cell.

7.3.2.1 Formulation of chlorpromazine/water lyotropic liquid crystals and their structural and stability characterisation

The observations of micelle formation of chlorpromazine hydrochloride (CPZHCl) in water encourages the notation that these micelles may, under conditions of sufficiently high monomer concentration compared with the critical micelle concentration, self-assemble into aggregates that form a lyotropic liquid crystalline phase. Accordingly, experiments were undertaken in which CPZHCl was mixed with water under conditions of high shear, thermostatted at 90 ^{o}C, so as to ensure melting of any resulting phase for approximately 2 h, and then cooled to room temperature, for afford mixtures in the range $1 < m/mol\ kg^{-1} < 12$. At molalities of 5 mol kg^{-1} and higher, the resulting gel-type material appeared yellow, and furnished a maximum absorption band over a large range: 250-460 nm (figureFigure 7.13); in contrast, solid CPZ.HCl is white, while the free base CPZ is, in fact yellow.[83]

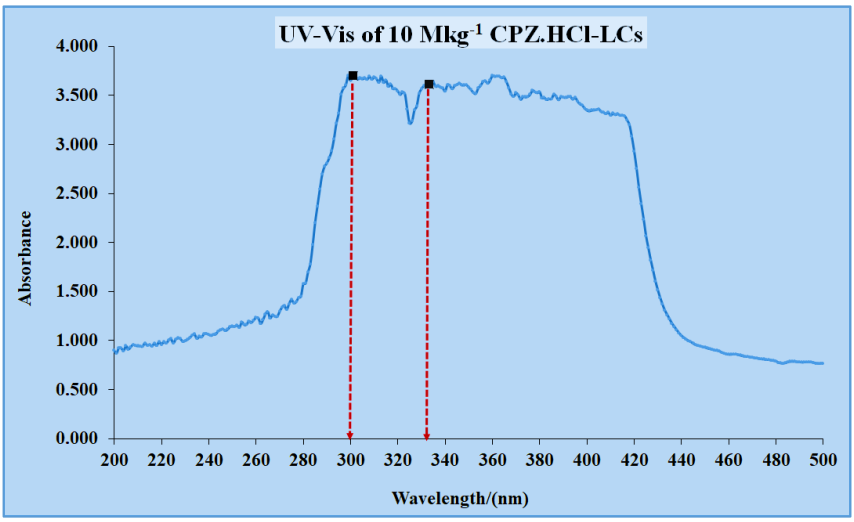

Figure 7.13: UV-Visible spectrum of 10 Mkg^{-1} CPZ.HCl-LCs

When examined under crossed polarisers, demonstrated long-lasting birefringence even in the presence of mechanical agitation of the phase, only for the highest of molalities studied (see figure 7.14 **b** for an example of the Schlieren textures observed). At low monomer molalities, the systems appeared dark when viewed through crossed-polarisers, as the monomer molality increased, birefringence started to appear, but this disappeared

through mechanical agitation of the material. This suggests liquid crystalline behaviour of the resulting CPZ.HCl/H_2O mixture at high CPZ.HCl molality. Moreover, given the mosaic, oily-streak texture of the image depicted in figure 7.14 **a**, the liquid crystal is suggested to be within the lamellar L_α phase.

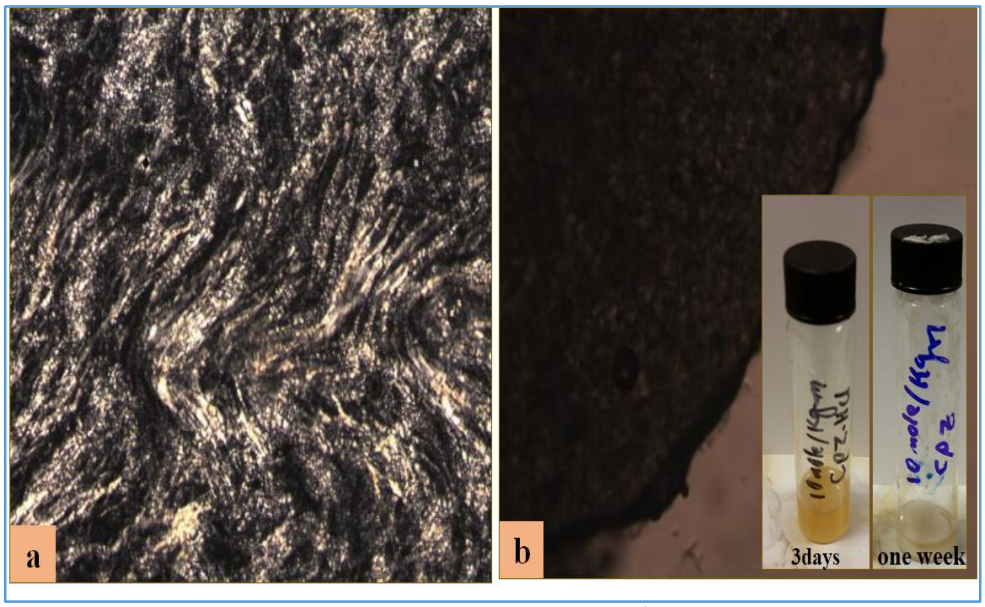

Figure 7.14: a. Polarising microscopy image of 10 M.Kg^{-1} CPZ.HCl-LCs in 1ml deionised water under cross polarisers, b. The image of the same solution after four months

The 10 mol kg^{-1} lyotropic liquid crystal was observed to be stable and retain its yellow colouration over a period of at least three months, provided it was kept in the dark and in the absence of any oxygen. In contrast, samples kept over the same timescale while exposed to light and oxygen were discoloured by a deep red material. The latter, when viewed through crossed polarisers under an optical microscope, did not exhibit birefringence (q.v. Figure 7.14), indicating the occurrence of mesomorphism – the system is now optically isotropic. Literature suggests the following mechanism for the formation of the deep red chlorpromazine sulfoxide[84]:

$$CPZ \xrightarrow{hv} CPZ^{*}\ (singlt)$$

$$CPZ^{*}\ (singlt) \rightarrow\ CPZ^{*}\ (triplet)$$

$$CPZ^{*}\ (triplet) +\ H^{+} + \frac{1}{2}O_2 \rightarrow\ CPZ^{\dot{+}} + \frac{1}{2}H_2O_2$$

$$CPZ^{\dot{+}} + \frac{1}{2}H_2O_2 +\ H^{+} \rightleftharpoons\ CPZ^{2+} +\ H_2O$$

$$CPZ^{2+} + CPZ \rightarrow 2CPZ^{\dot{+}}$$

$$CPZ^{2+} +\ H_2O \rightarrow CPZO + 2H^{+}$$

Mechanism 7-1: The mechanism of chlorpromazine sulfoxide

In order to examine this redox-induced mesomorphism more thoroughly, we next study the electrochemistry of this redox-active lyotropic liquid crystal.

7.3.2.2 Electrochemical characterisation of chlorpromazine/water lyotropic liquid crystals

The conductivity of the 10 mol kg^{-1} lyotropic system was observed to be 46.4 Ω cm at a temperature of 22.1℃. This is similar to 0.1 M KCL (12.2 Ω cm at 23℃), indicating that solution resistance at scan rates smaller than 1.0 Vs^{-1} is not likely to play a role in the voltammetric response of this material. The density of the liquid crystal was determined to be 1.4213 g cm^{-3}, suggesting that the liquid crystal is at a sufficient concentration of 2.9 mol dm^{-3}. This is very much similar to the sufficient concentration of many redox-active organic liquids. Accordingly, the voltammetric interrogation of the lyotropic phase may be understood in the light of body of literature concerning the voltammetry of concentrated organic liquids.[85-87] Viscosity Measurements of the formulated materials support this conclusion (see Figure 7.15): at a constant shear rate of 1.13 s^{-1}, it is clear that there is a marked increase in viscosity of the gel at 7.5 mol kg^{-1} and above. This

viscosity change corresponds to the aggregation of an isotropic solution of CPZ.HCl micelles to form a liquid crystalline phase.

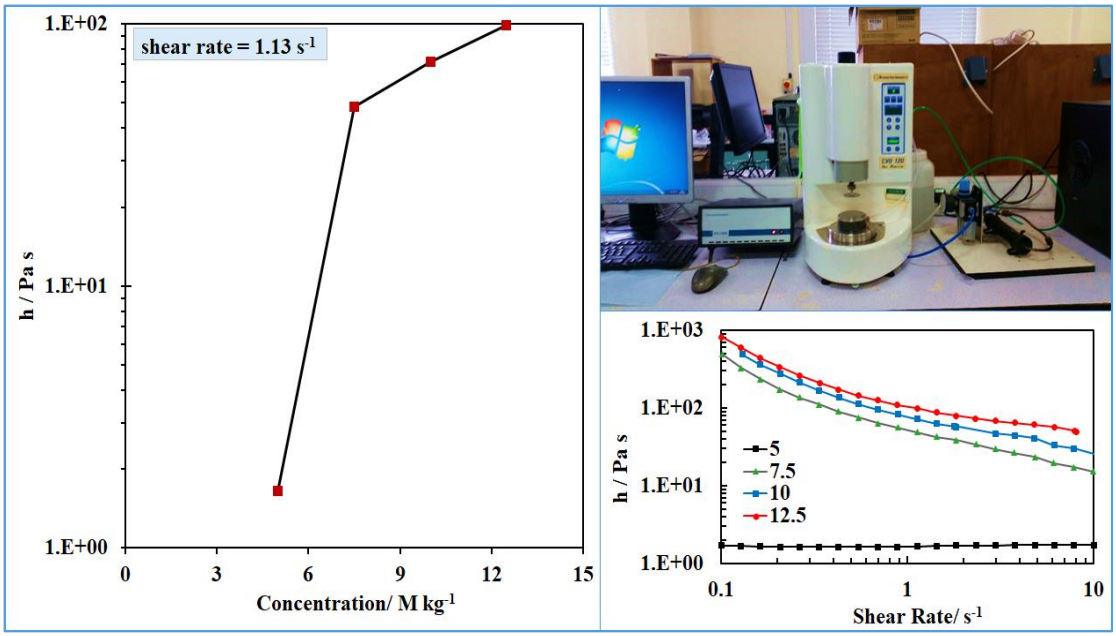

Figure 7.15: The left chart is the viscosity of different concentrations of CPZ.HCl, the top right side is the viscosity instrument, and the bottom right side is the Viscosity of different concentrations of CPZ.HCl vis Shear Rate

7.3.2.3 Effects of CPZ.HCl concentration

In chapter four, chlorpromazine was approved as a good mediator and an active molecule in aqueous solution with buffer solution (pH 4). Based on the fact that lyotropic liquid crystals are formed at high concentrations of the surfactant monomer in water through the thermal atmosphere. Wadhawan and co-workers have proved that CPZ.HCl solution was remained fluid and isotropic even at 0.1 M.[88] Thus, the development of lyotropic liquid crystal of CPZ.HCl in different concentrations (5, 7.5, 10 and 12.5 M kg^{-1}) was examined. This solution was prepared following the procedure in section 7.2.4; figure 7.16 illustrates CVs at scan rate 100 mV s^{-1} onto 12.5 µm AuE for various concentrations of CPZ.HCl.

It is noticed that as the concentration of CPZ.HCl increases the voltammogram moves along the potential scale, with no clear trend. Initial results showed that the increase in

CPZ.HCl concentrations were followed by the rise in the solution thickened, and colour changed from colourless to yellow gel up to 10 M kgm^{-1}, seen insert figure 7.16.

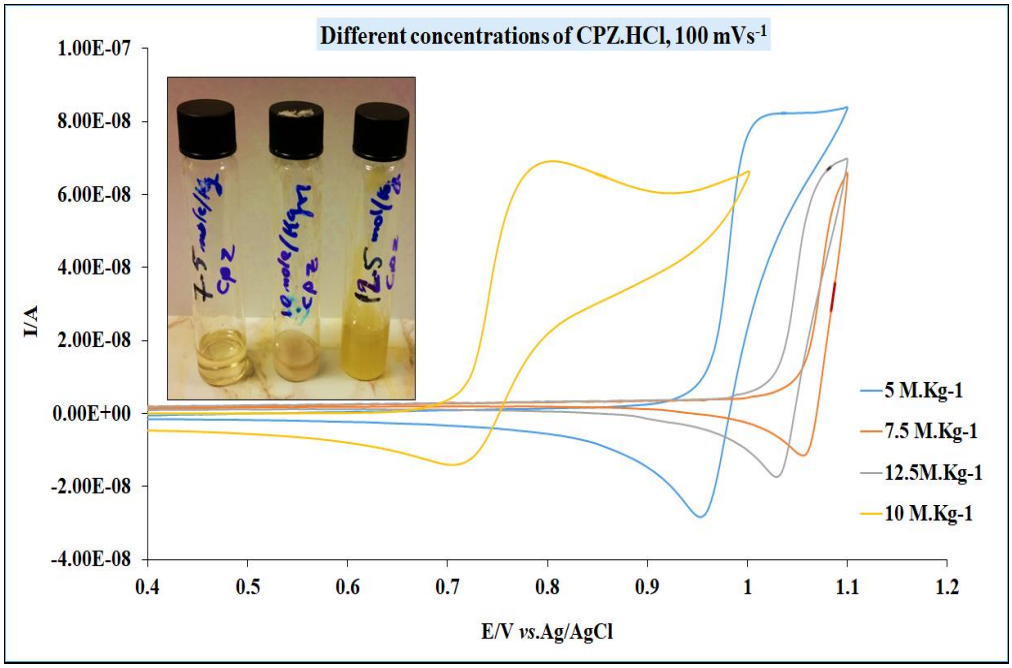

Figure 7.16: CVs at 100 mV s^{-1} for varying concentration of CPZ.HCl onto 12.5 µm AuE

The pH of the mixture falls to a minimum (see table 7.4) with increasing monomer molality, suggesting that the chloride *gegen* ions are mobile within the pseudo water phase of the resulting liquid crystal and that the extent of this dissociation is maximum when the monomer molality is 10 mol kg^{-1}. As we are interested in the electrochemical properties of this new material (*vide infra*), we kept further experiments restricted to this monomer composition.

Table 7.4: Various concentrations of CPZ.HCl with their state and pH

CPZ.HCl/M Kgm^{-1}	state	pH
5	Liquid	3.42
7.5	Liquid	3.17
10	Gel	2.18
12.5	Gel	2.50

7.3.2.4 Microscopic study X-ray scattering (XRD)

X-ray scattering measurements on the 10 mol kg^{-1} CPZ.HCl formulation (figure 7.17) using Cu K_α radiation (1.54 Å) of the 10 mol kg^{-1} lyotropic reveal several features. Particularly three Bragg spacings (strong first-order and second-order reflections, with a very weak third-order reflection) in the ratio 1: ½: ⅓, which is characteristic of a lamellar L_α arrangement, with a fundamental repeat distance (d) of 24.2 Å, corresponding to the combined thickness of the surfactant and the water layers. The thickness of the individual surfactant layers (d_s) is estimated from the equation 7.2,

$$d_s = \frac{d}{\left(1 + \frac{f_{water}}{f_{surf}}\right)}$$

Equation7.2

where ϕ_{water} is the volume fraction of the water phase and ϕ_{surf} is the volume fraction of the surfactant phase. For the 10 mol kg^{-1} (78 wt. %) formulation considered, these volume fractions correspond to 0.78 and 0.22, yielding a value of d_s = 18.8 Å. Considering the X-ray crystallographic data for CPZHCl in the solid state[89], this value is indicative of a surfactant bilayer. Following the Bragg equation, we suggest that the diffuse, wide-angle feature corresponds to the intra-aggregate spacings (d = 4.4 Å) between the alkyl chains attached to the N-X position on individual CPZHCl molecules, as similar values (4.5 Å) have been proposed for the spacings between alkyl chains within XYZ lyotropic liquid crystals.[90] Taken together with reported NMR data [91], this implies that the CPZ.HCl molecules aggregate together in a "cup-stack" arrangement and on top of each other, with the hydrophobic core comprising the aromatic rings, and the alkyl chains penetrating into the aqueous pseudo phase enabling the formation of a micellar palisade layer.

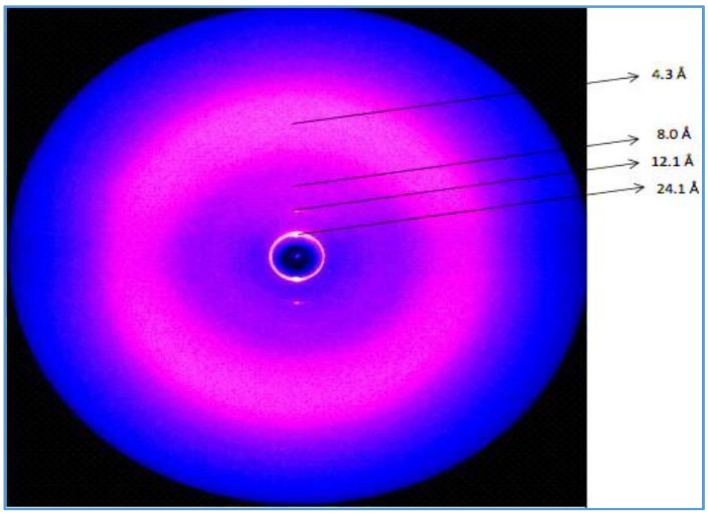

Figure 7.17: X-ray scattering pattern for 10 M kg^{-1} CPZ.HCl

7.3.2.5 Effects of WE material

Figure (7.18 **a)** depicts cyclic voltammograms at micro disc electrodes immersed within a 10 mol kg^{-1} CPZ.HCl/water lyotropic liquid crystal. It is clear that a single pair of well-defined oxidation and reduction signals are observable at high scan rates, corresponding to the oxidation of CPZ.HCl to the corresponding cation radical.

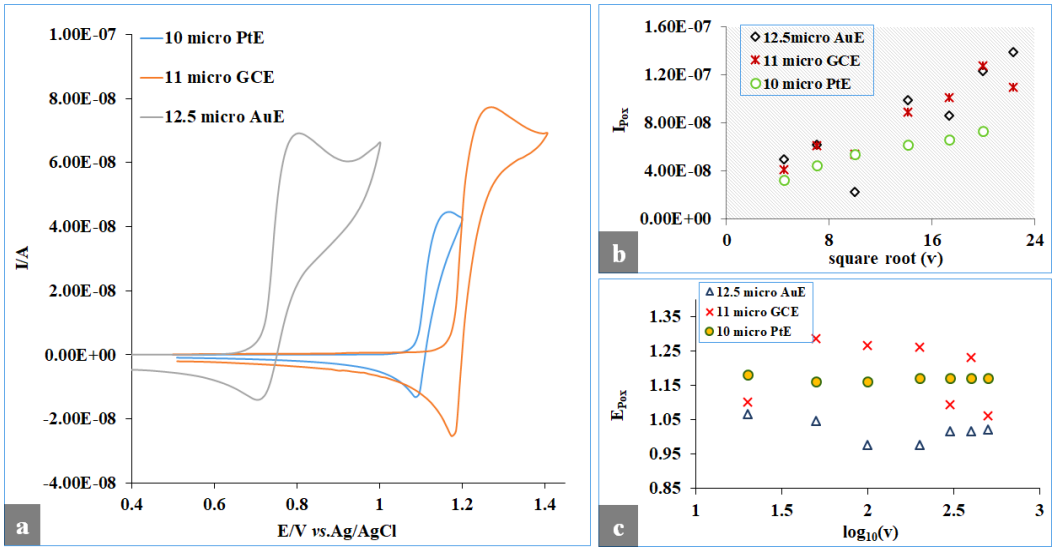

Figure 7.18: a: cyclic voltammograms of 10M.kg^{-1}CPZ.HCl-LCs dependence of working electrode material. Scan rate 100 mV s^{-1}, b: Oxidation peak currents for different micro WE against square roots of scan rates and c: Oxidation peaks potential for different micro WE against logarithms of scan rates

At higher potentials than those illustrated in Figure 7.18 **a**, a second oxidation wave is observable (figure 7.19), with peak typically around 200 mV more positive (at a scan rate of 100 mV s^{-1}). The latter corresponds to the oxidation of the cation radical to afford the

dication. As for the case in dilute, isotropic solution, this second oxidation wave is chemically irreversible, owing to nucleophilic attack by water on the dication.

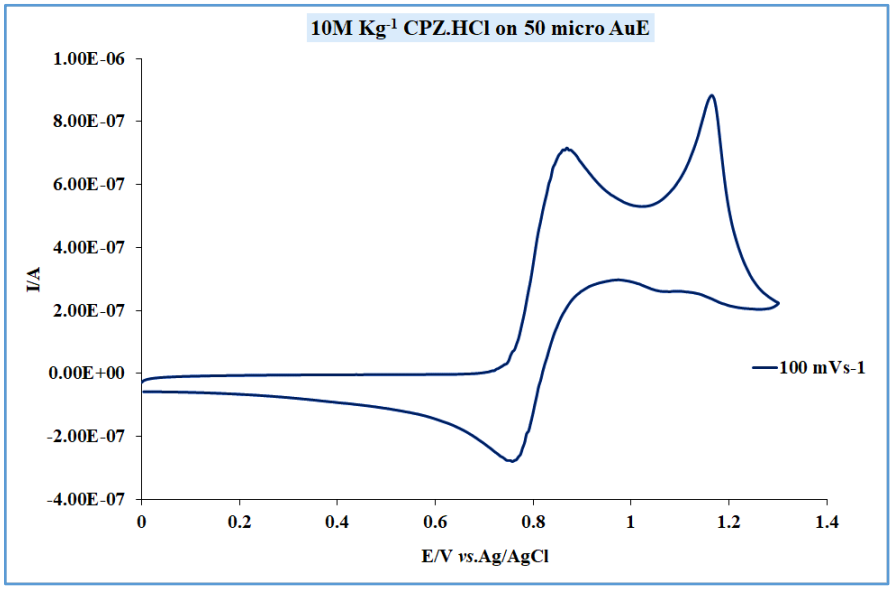

Figure 7.19: Cyclic voltammetry of CPZ.HCl on 50 micro AuE100mVs^{-1} scan rate

Surprisingly, unlike the case of dilute aqueous solution[92], the electrogenerated radical cation formed through oxidation of the CPZHCl/water lyotropic is not stable, as evident by the loss in the reverse peak on scanning the electrode more slowly (*q.v.* figures 7.20 and 7.21).

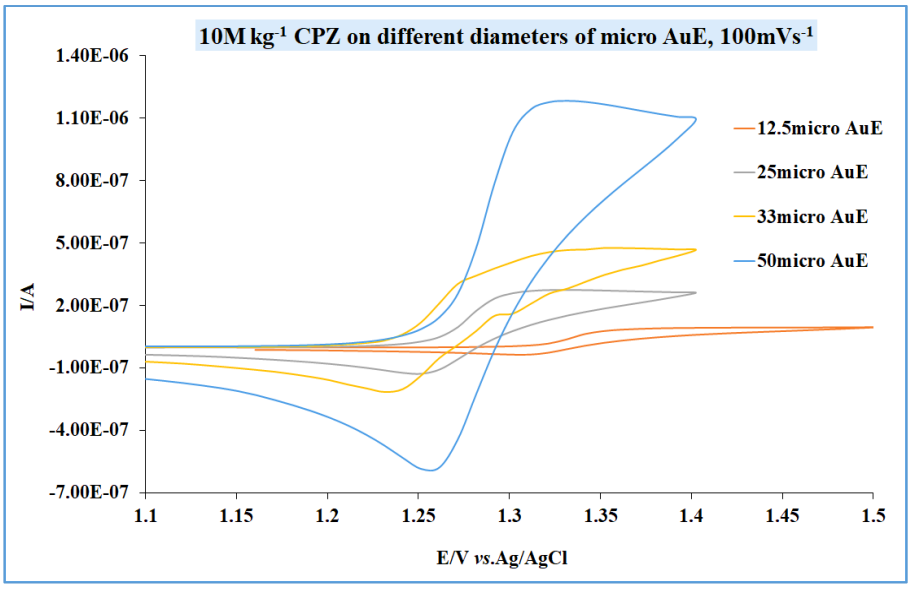

Figure 7.20: Cyclic voltammograms of CPZ.HCl-LCs on the various diameter of AuE (12.5, 25, 33 and 50 µm). Scan rate (100mV s^{-1})

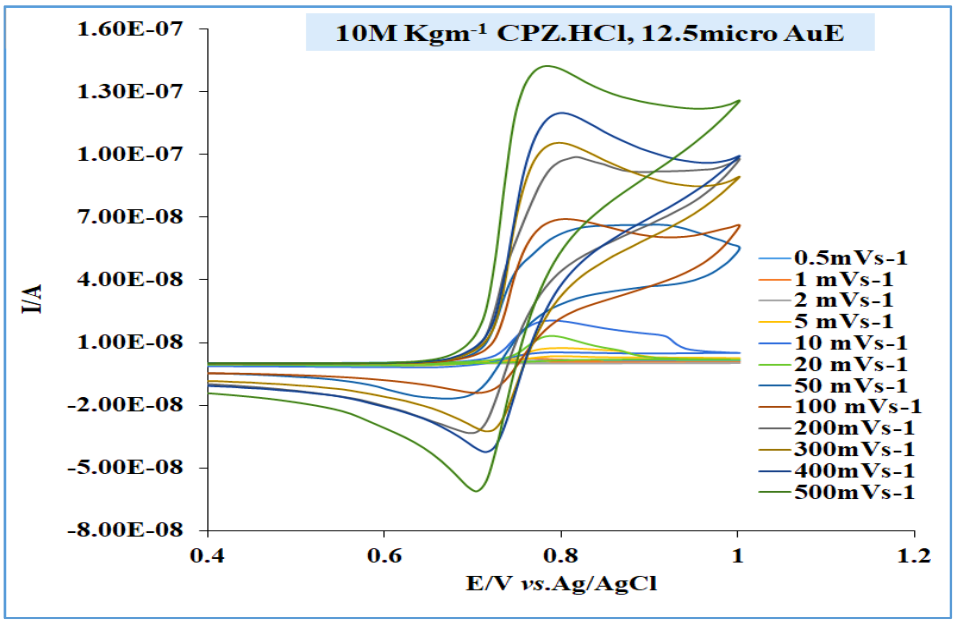

Figure 7.21: Cyclic voltammograms of 10 M.Kg^{-1}CPZ.HCl-LCs onto 12.5 µ AuE for scan rates (0.5, 1, 2, 5, 10, 20, 50, 100, 200, 300, 400 and 500 mV s^{-1})

Voltammetric peak current and potential data are presented in 7.18 **b** and **c**. These identify that as the scan rate decreases, the peaks shift towards more negative potentials by approximately 30 mV decade^{-1}, while the peak current exhibits a direct proportionality relationship with the square root of the scan rate, indicative of diffusive transport of material to the electrode surface. In previous work on electrochemistry within lyotropic liquid crystals[85], it has been demonstrated that it is difficult to interpret anisotropy in such systems through voltammetry alone.

Accordingly, for simplicity, we consider the liquid crystalline phase in this work to be electrochemically isotropic, characterised by an effective diffusion coefficient, D_{eff}. It has been shown previously that this parameter is the geometric mean of the diffusion coefficients in the directions normal and perpendicular to the electrode surface.[85] Moreover, routes for electron transfer to take place within concentrated lyotropic liquid crystals through a Dahms-Ruff-type mechanism have been illustrated.[85]At the highest of scan rates employed; the peak potential data demonstrate temporal independence, characteristic of fast electrode kinetics (electrochemical reversibility). This strongly

suggests that the irreversibility observed as the experimental timescale increas is due to chemical reaction taking place within the system. Based on chlorpromazine voltammetry in dilute solution, a DISP1 mechanism was considered.

DISP1 Mechanism

The reaction scheme considered is as follows.[93]

$$A + e^- \rightleftarrows B$$

$$B \underset{k_b}{\overset{k_f}{\rightleftarrows}} C$$

$$B + C \xrightarrow{k_D} A + D$$

Mechanism 7-2: The first-order disproportionation reaction

In which only species A and B exchange electrons at the electrode surface and the slow step is the first-order conversion of species B to C (rate constant k_f being very much smaller than rate constant k_b). Since the disproportionation reaction is considered irreversible ($K_{disp} >> 1$, strongly exoergic reaction), it follows that C is easier to reduce to D than A is to reduce to B, and occurs rapidly (large value of the rate constant k_D). We assume the heterogeneous electron transfer process is fast, allowing the Nernst equation to be upheld for species A and B.The relevant transport equations for this reaction scheme are as follows, under conditions of planar diffusion.

$$\frac{\partial c_A}{\partial t} = D\frac{\partial^2 c_A}{\partial x^2} + k_D c_B c_C$$

$$\frac{\partial c_B}{\partial t} = D\frac{\partial^2 c_B}{\partial x^2} - k_f c_B + k_b c_C - k_D c_B c_C$$

$$\frac{\partial c_C}{\partial t} = D\frac{\partial^2 c_C}{\partial x^2} + k_f c_B - k_b c_C - k_D c_B c_C$$

$$\frac{\partial c_D}{\partial t} = D\frac{\partial^2 c_C}{\partial x^2} + k_D c_B c_C$$

Equation7.3

where it is assumed that all species have the same diffusion coefficient (D), c_X refers to the concentration of species X, t is the temporal variable and x is the spatial variable. These diffusion-reaction equations need to be solved subject to the following boundary conditions, in which we recognise that there is no flux of species at the semi-infinite boundary, and the Nernstian boundary condition at the electrode surface (corresponding to fast electrode kinetics) is only upheld for species A and B, since the conversion of species C to D occurs only within the homogeneous solution.

$$
\begin{array}{ll}
t \le 0, \text{"}\, x & c_A = c_0; c_B = c_C = c_D = 0 \\
t > 0, x = 0 & \left(\frac{\partial c_A}{\partial x}\right)_{x=0} = -\left(\frac{\partial c_B}{\partial x}\right)_{x=0}; \left(c_A\right)_{x=0} = \left(c_B\right)_{x=0} e^{\frac{F}{RT}\left(E - E^0\right)}; \left(\frac{\partial c_C}{\partial x}\right)_{x=0} = -\left(\frac{\partial c_D}{\partial x}\right)_{x=0} \\
t > 0, x \to \infty & \left(\frac{\partial c_A}{\partial x}\right)_{x\to\infty} = \left(\frac{\partial c_B}{\partial x}\right)_{x\to\infty} = \left(\frac{\partial c_C}{\partial x}\right)_{x\to\infty} = \left(\frac{\partial c_D}{\partial x}\right)_{x\to\infty} = 0
\end{array}
$$

Equation7.4

In the above, F is the Faraday constant (96484.6 C mol^{-1}), R is the molar gas constant (8.3145 J mol^{-1} K^{-1}), T is the absolute temperature, E^o is the formal electrode potential corresponding to the A/B couple, and E is the applied potential. In cyclic voltammetry, E is a function of time:

$$
\begin{aligned}
&\textit{forward sweep}: \; E = E_{start} - vt \\
&\textit{return sweep}: \; E = 2E_{end} - E_{start} + vt
\end{aligned}
$$

Equation7.5

in which E_{start} is the initial potential applied, E_{end} is the most reducing potential used, and v is the potential scan rate (dE/dt). These reaction-transport equations can be simplified using the following dimensionless variables.

$$t = \frac{Fv}{RT}t\,;\;\; y = x\sqrt{\frac{Fv}{RTD}}$$

$$x = -\frac{F}{RT}\left(E - E^{0}\right)$$

$$a = \frac{c_A}{c_0}\,;\, b = \frac{c_B}{c_0}\,;\, c = \frac{c_C}{c_0}\,;\, d = \frac{c_D}{c_0}$$

$$\lambda_f = \frac{k_f RT}{Fv}\,;\, \lambda_b = \frac{k_b RT}{Fv}\,;\, \lambda_D = \frac{k_D c_0 RT}{Fv}$$

Equation7.6

The application of the steady-state hypothesis to species C:

$$\frac{\partial c}{\partial t} = \frac{\partial^2 c}{\partial y^2} = 0$$

Equation7.7

affords the following expression.

$$c = \frac{\lambda_f b}{\lambda_b + \lambda_D b}$$

Equation7.8

The case of the first-order disproportionation reaction (DISP1) requires the kinetics of the homogeneous electron transfer reaction to being vastly greater than the kinetics of the reverse conversion C → B. Under conditions of high concentration of species A, this is likely to uphold. It then follows that the reaction-transport equations may be simplified to the following, where we need only consider species A and B.

$$\frac{\partial a}{\partial t} = \frac{\partial^2 a}{\partial y^2} + \lambda_f b$$

$$\frac{\partial b}{\partial t} = \frac{\partial^2 b}{\partial y^2} - 2\lambda_f b$$

Equation7.9

The current flowing as a function of the applied potential is determined as follows. Since the current (i) is given by the expression

$$i = FSD\left(\frac{\partial c_A}{\partial x}\right)_{x=0}$$

Equation7.10

in which S is the electrode area, it may be recast in dimensionless terms (ψ) as:

$$y = \frac{i}{FSc_0\sqrt{\frac{DFv}{RT}}} = \left(\frac{\partial a}{\partial y}\right)_{y=0}$$

Equation7.11

The reaction-transport equations can be solved numerically using a finite difference grid, exploiting a pentadiagonal matrix algorithm[94], to account for the coupling of species A and B at the electrode surface and through the homogeneous reaction kinetics.

Numerical simulations were executed on a MacBook Air computer running with a 1.3 GHz Intel Core i5 processor with 4 GB of DDR3 RAM at 1600 MHz speed. Single cyclic voltammograms were computed within X min. This time-intensive computation occurred in order to achieve the required convergence of the concentration profiles; a closely spaced finite difference grid is comprising 150x150 spatial nodes, and 1000000 temporal notes were required. Figure 7.22 illustrates dimensionless voltammograms for the DISP1 reaction as the kinetic parameter λ_f is varied.

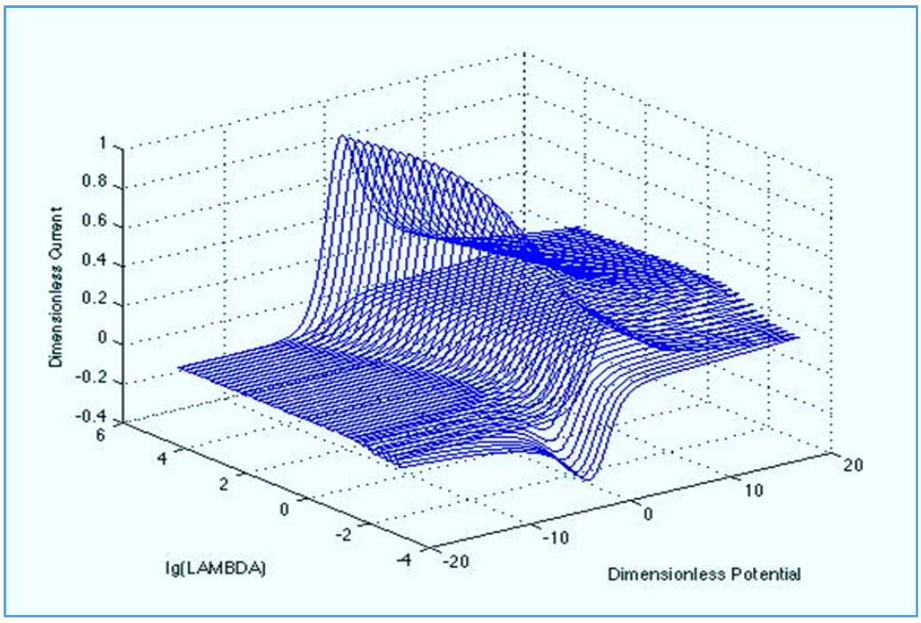

Figure 7.22: The dimensionless voltammograms of the first-order disproportionation reaction

Clearly, as the first-order loss of species B becomes faster, there is a loss in the reverse wave, an increase in the observed current and a shift in the peak potential for the reduction of species A. These three variables are quantified through the graphs plotted in figure 7.23, where it is seen that the shift in peak potentials only occurs towards more positive values when log > 0.

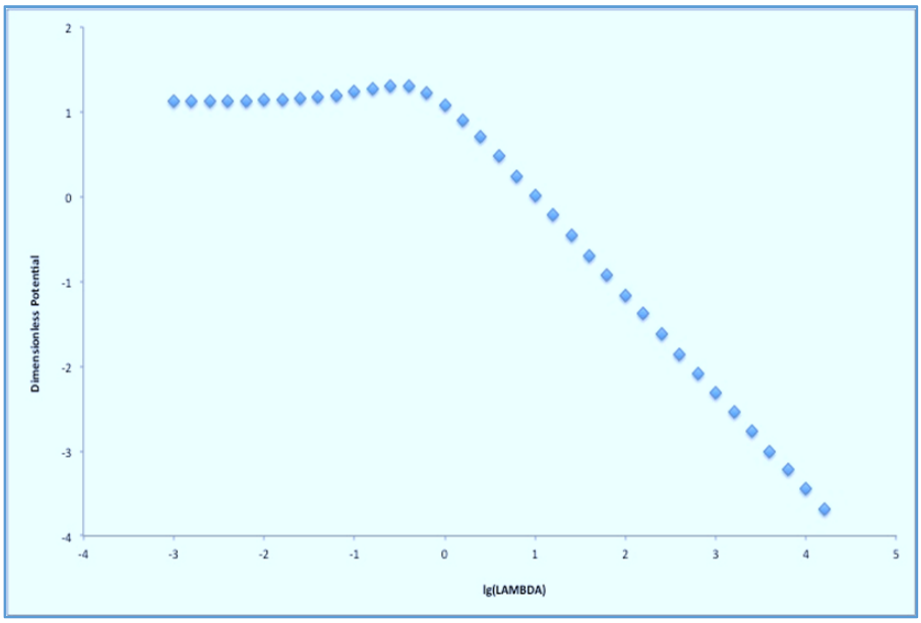

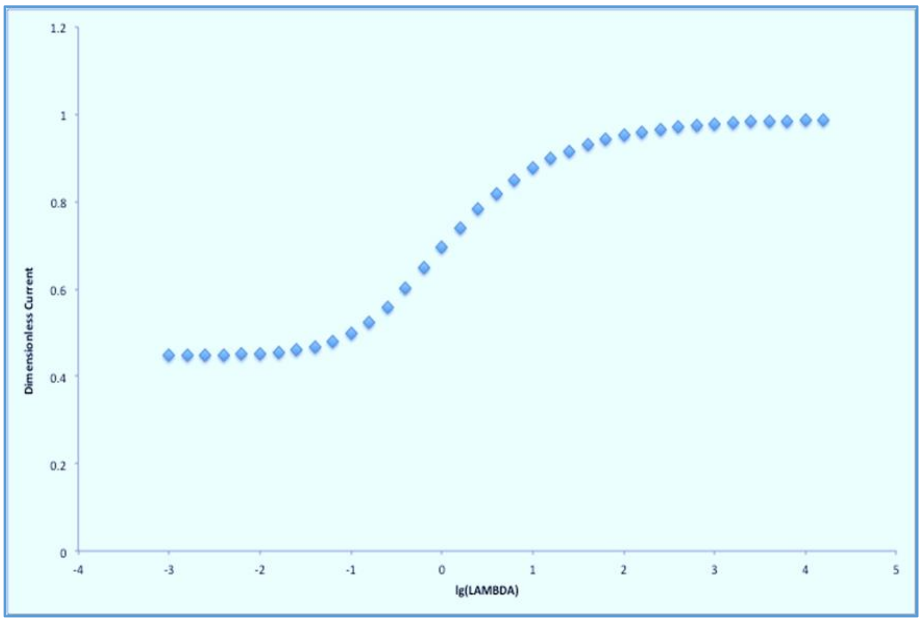

Figure 7.23: The diagrams for the DISP1 reaction of A. the dimensionless potential vs log LAMBDA and B: the dimensionless current vs log LAMBDA

These working curves can be used to extract both diffusion coefficient and rate constant for the first-order reaction from experimental data through the following process. First, experimental voltammograms are recorded corresponding to a particular analyte concentration, and over a wide range of scan rates (at least two or three orders of magnitude) at a well-defined electrode size geometry. This allows the experimental peak potential and peaks current data sets to be established.

Second, the experimental timescale is converted into dimensionless quantities by iterating through values of the first order rate constant within a relevant range (thereby mapping v $\rightarrow$ lgλ). The peak current is concurrently reduced to dimensionless form through iterating through the diffusion coefficient for the reduced species over a relevant range (thereby mapping $i_p \rightarrow \psi_p$). The optimum parameters for both k and D are then identified as those, which afford a minimum in the mean-scaled absolute deviation between experimental data and the working curves in figure 7.24. If the peak potential data are treated simultaneously with the peak current data, the value of k may be refined (if E^0) is known, or the value of k may be used to infer a value of the formal electrode potential for the

reduction of species A. Thus, the use of planar, one-dimensional diffusion regimes, where transport of species A is normal to the electrode surface, is an extremely useful limiting regime within which disproportionation reaction kinetics may be readily extracted from experimental voltammograms. For the voltammetry of the liquid crystal of chlorpromazine hydrochloride, the data were found to fit $D = 2 \times 10^{-12}$ m^2 s^{-1} with a first-order rate constant (k) for disproportionation being 0.6 s^{-1}, see figure 7.24.

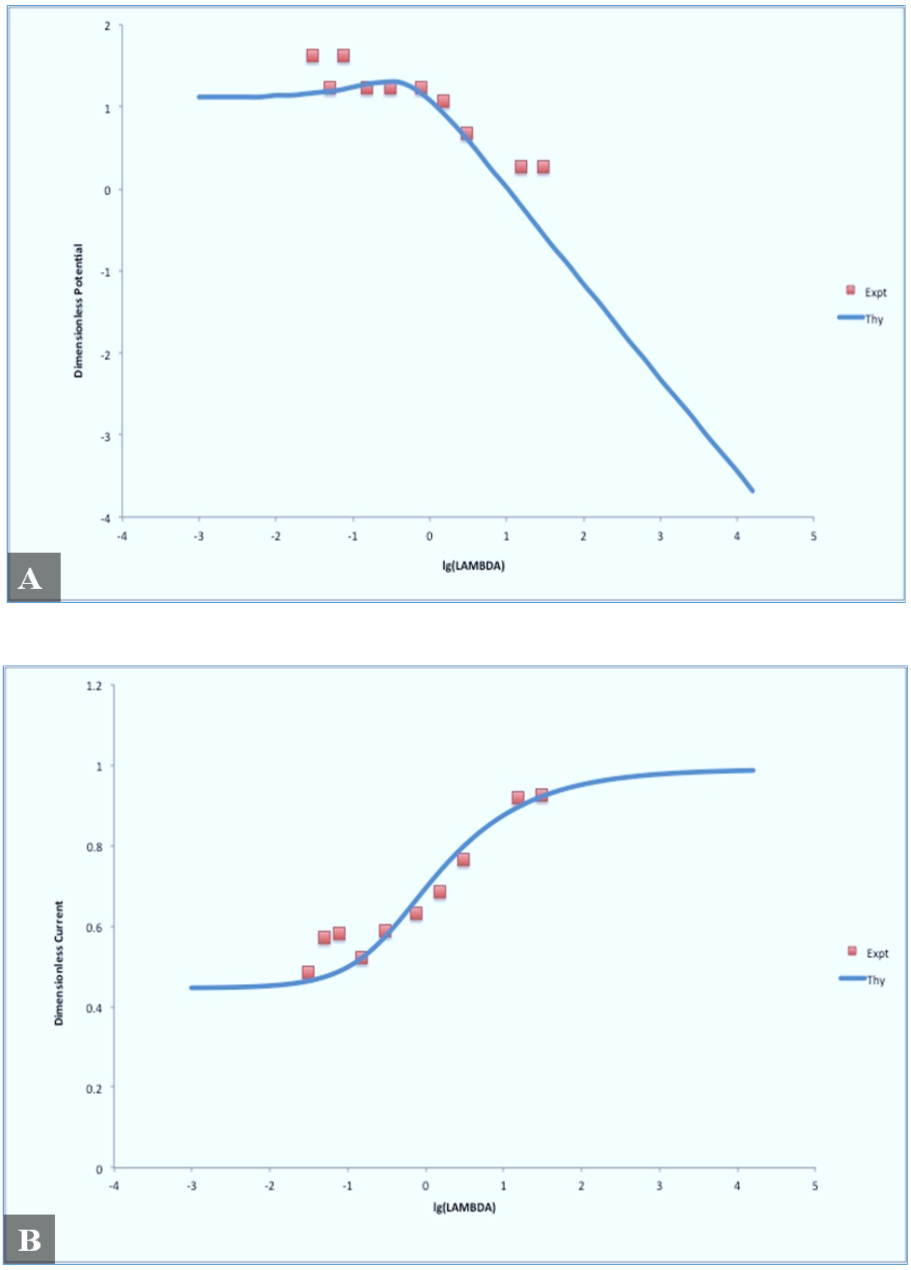

Figure 7.24: Fit of Experimental data to theory for the DISP1 process: A. potential and B. current

Given the characterisation of the transport, the liquid crystalline material was examined for use within a photogalvanic device.

❖ ***Perfect Photogalvanic Cell Model***

We seek here to characterise the system *via* a *perfect* photogalvanic cell as essentially depicted by a Randles equivalent circuit illustrated in figure 7.25.

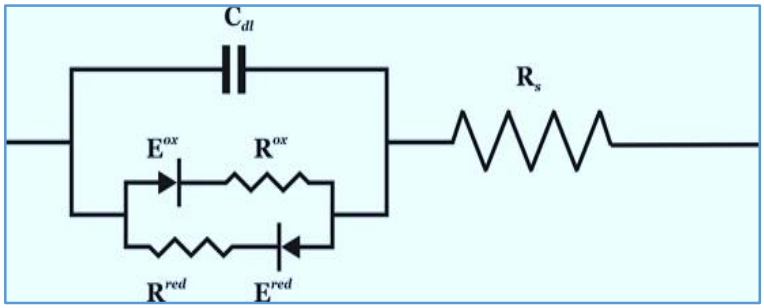

Figure 7.25: Randles equivalent electrical circuit for a perfect photogalvanic cell, which comprises voltage generation through the discharge of the Faradaic component (represented as involving a mass transfer resistance $R^{ox/red}$ and a kinetic polarisation $E^{ox/red}$) occurring in parallel with discharge of the interfacial capacitance, C_{dl}, and in series with the internal resistance, R_s. This galvanic cell is discharged through an external load resistor, R_{ext}, not shown

Here, the heterogeneous electron transfer processes at both electrodes are represented as a battery (existing only under illumination) which exhibits an internal resistance, R_s, and with the electromotive force of the photogalvanic cell, ξ, comprises of contributions due to the Faradaic charging of the battery redox chemistry, V_0, and the charging of the capacitances at each of the two electrodes, and across all the individual subphases, to afford a single value, C_{dl}. This system is discharged through a load resistance, R_{ext}, which is not depicted in figure 7.25. We assume that the cell is fully charged prior to discharge so that the initial charge on the capacitor is q_0:

$$q_0 = C_{dl} V_0$$

Equation7.12

Thus,

$$\xi = V_0 = \frac{q_0}{C_{dl}}$$

Equation7.13

During discharge of the cell *under constant illumination* (*viz.*, there is no Lambert-Beer attenuation of illumination across the pertinent diffusion length close to the illuminated electrode, and all photochemical reactions occur with unity quantum yield), the potential difference across the photogalvanic cell (*V*) decreases through the relationship,

$$V = \frac{q}{C_{dl}} - iR_s$$

Equation7.14

where we assume that neither activation nor concentration polarisation occurs within the battery. This is a reasonable assumption provided that both the reactant regeneration kinetics and the electrode are *fast*, that large currents flow, and that the transport lengths are restricted to values smaller than the diffusion length thickness. We assume there is no "leakage" current–all elements of the equivalent circuit are expected to behave perfectly. Since the passage of current *decreases* the charge on the capacitor, we may write,

$$i = -\frac{dq}{dt}$$

Equation7.15

and, thence, noting the boundary condition that $q = q_0$ when *t=0*,

$$\int_{q_0}^{q} \frac{dq}{\left(VC_{dl} - q\right)} = \int_0^t \frac{dt}{R_s C_{dl}}$$

Equation7.16

leads to the following expression for the charge on the capacitor,

$$q = VC_{dl}\left(1 - e^{-\frac{t}{R_s C_{dl}}}\right) + q_0 e^{-\frac{t}{R_s C_{dl}}}$$

Equation7.17

with the terminal potential difference being given by,

$$V = \frac{q_0}{C_{dl}} - iR_s e^{\frac{t}{R_s C_{dl}}} = \xi - iR_s e^{\frac{t}{R_s C_{dl}}} = iR_{ext}$$

Equation7.18

Which, satisfies the requirement for $V=\xi$ for $i=0$. The current flowing can then be deduced through the temporal derivative of the charge passed,

$$i = -\frac{dq}{dt} = \left(e^{-\frac{t}{R_s C_{dl}}} - 1 \right) \left(V \frac{dC_{dl}}{dt} + C_{dl} \frac{dV}{dt} \right) + \frac{1}{R_s} \left(\frac{q_0}{C_{dl}} - V \right) e^{-\frac{t}{R_s C_{dl}}} = \frac{\xi}{\left(R_{ext} + R_s e^{\frac{t}{R_s C_{dl}}} \right)}$$

Equation7.19

The current flowing in short circuit, i_{sc}, occurs when $V=0$, and therefore, $\frac{dV}{dt} = 0$, and corresponds to the case $R_{ext} \to 0$:

$$i_{sc} = \frac{q_0}{R_s C_{dl}} e^{-\frac{t}{R_s C_{dl}}} = \frac{\xi}{R_s} e^{-\frac{t}{R_s C_{dl}}}$$

Equation7.20

This expression reduces to

$$\left(i_{sc} \right)_{t=0} = \frac{\xi}{R_s}$$

Equation7.21

for the *instantaneous short circuit current*, as anticipated. These expressions permit the determination of the power generated across the load R_{ext}, p, as indicated as follows.

$$p = iV = i\xi - i^2 R_s e^{\frac{t}{R_s C_{dl}}}$$

Equation7.22

Since the power point occurs when the power generated is maximal, we differentiate the above expression concerning the current flowing through the circuit, and equate this expression to zero, under the assumption that the internal resistance is constant:

$$\left(\frac{\partial p}{\partial i}\right)_t = \xi - 2iR_s e^{\frac{t}{R_s C_{dl}}} = 0$$

Equation7.23

We note that the second derivative is negative, as expected for a maximum stationary point. Thus, solving equation 7.23, affords the current at the power point, i_{mp}

$$i_{mp} = \frac{1}{2R_s}\xi e^{-\frac{t}{R_s C_{dl}}} = \frac{1}{2} i_{sc}$$

Equation7.24

Stricto sensu, provided the internal resistance and capacitance are independent of the power characteristics, the conditions for maximum power require $\left(\frac{\partial p}{\partial i}\right)_t = \left(\frac{\partial p}{\partial t}\right)_i = 0$, with $\Gamma = \frac{\partial^2 p}{\partial i^2} + \frac{\partial^2 p}{\partial t^2} < 0$ and $\Delta = \frac{\partial^2 p}{\partial i^2}\frac{\partial^2 p}{\partial t^2} - \left(\frac{\partial^2 p}{\partial i \partial t}\right)^2 > 0$. It is readily verifiable that equation 7.24 fulfils all these conditions for non-zero current at all times. It thus follows that the terminal potential difference at the power point is,

$$V_{mp} = \frac{1}{2}\xi$$

Equation7.25

and that the maximum power delivered by the perfect photogalvanic cell, $p_{\max}$, is,

$$p_{\max} = i_{pp} V_{pp} = \frac{1}{4R_s}\xi^2 e^{-\frac{t}{R_s C_{dl}}} = \frac{1}{4} i_{sc}\xi$$

Equation7.26

Note that the optimum load in the external circuit, R_{ext}^{mp}, through which the maximum power may be dissipated, is:

$$R_{ext}^{mp} = R_s e^{\frac{t}{R_s C_{dl}}}$$

Equation7.27

In other words, impedance bridging requires $R_{ext}^{mp} \geq R_s$ at all times. *Thus, the fill factor (a measure of the quality of the device), defined by*

$$FF = \frac{p_{\max}}{i_{sc}\xi} \times 100$$

Equation7.28

is merely 25% for the perfect photogalvanic cell, *viz.* identical the case of an ideal photogalvanic cell (one in which there is no capacitative contribution).

7.3.2.6 Chlorpromazine lyotropic LC with an Experimental PG Cell

Having identified the current/voltage characteristics of a perfect PG cell, the experimental realisation of this was next examined. A PG cell was prepared as illustrated in figure 7.26, similar to those developed earlier.[95]

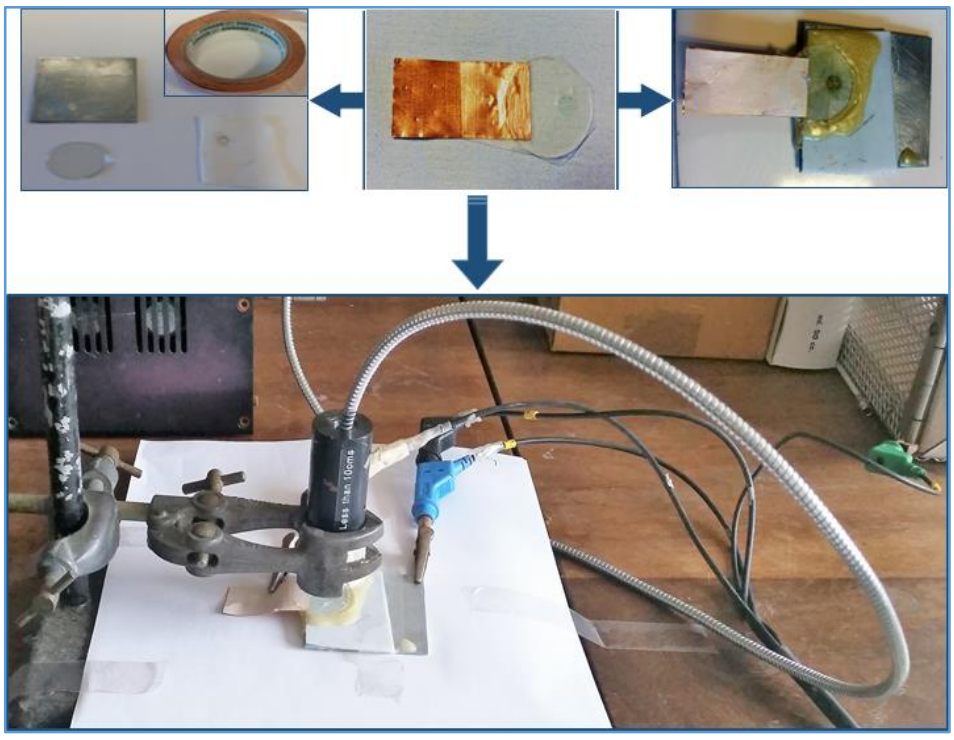

Figure 7.26: Photographs identifying the stages in preparing a PG cell and its deployment

Briefly, this involved glueing a 1 mm thick polytetrafluoroethylene (PTFE) space with 5 mm diameter hole onto a zinc plate. This hole was filled with 10 mol kg^{-1} CPZ-LLC and left to equilibrate overnight. Subsequent, an indium-tin oxide electrode with conductor-side connected with copper tape, and insulates with Magic Tape except for a 5 mm diameter hole, was carefully positional over the LLC, conductive-side down.

The cell was sealed so that the electrodes held in place using a low melting, cosmetic depilatory wax. The cell was left to equilibrate in the dark for two days prior to use. Illumination was achieved through a CAIRNS Xe wc lamp fitted with monochromator at 350 nm, and 1.0 mW cm^{-2} incident power. The experimental set up is shown in figure 7.27.

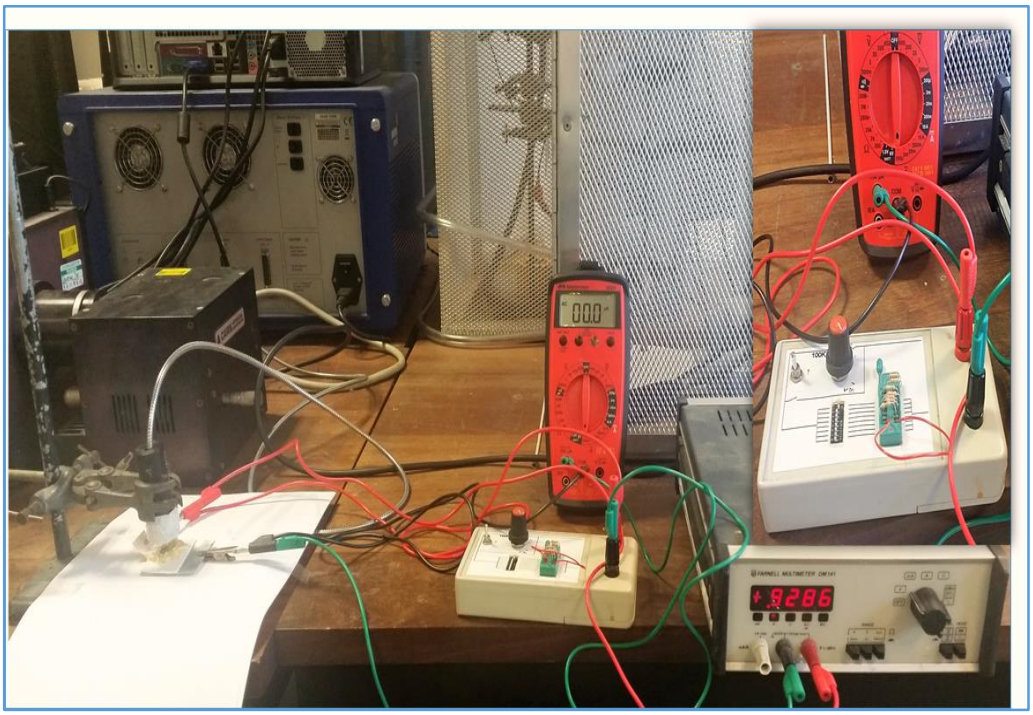

Figure 7.27: Energy power performance measurement

Zero-current potentiometry was undertaken in the dark and in the presence of chopped light, affording increases in cell voltage in the presence of light, see figure 7.28 photo potentiometry.

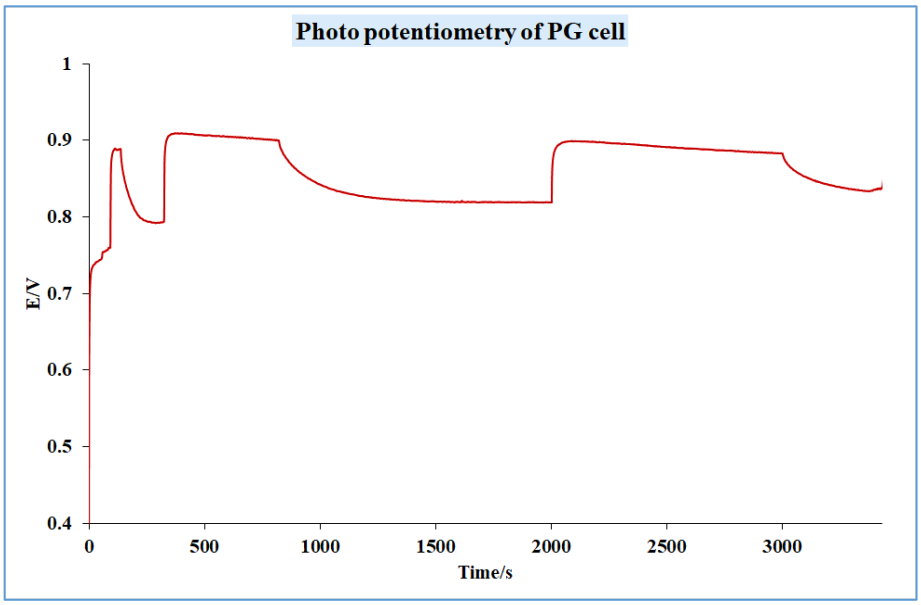

Figure 7.28: Photo potentiometry of the photogalvanic (PG) cell at zero current

This indicates that illumination gives rise to a reduction process at the illuminated electrode. Based on the mechanism given in mechanism 7.1, it is suggested that the non-steady photovoltages are due to a competition between the electrode scavenging the $CPZ^{\dot{+}}$cation radical and O_2/H^+ reaction with the $CPZ^{\dot{+}}$ species[84]:

$$CPZ_{(LLC)} \xrightarrow{hv} CPZ^*$$

$$CPZ^* + H^+ + \frac{1}{2}O_2 \rightarrow \frac{1}{2}H_2O_2 + CPZ^{\dot{+}}$$

$$CPZ^{\dot{+}} + e^- \rightleftarrows CPZ \qquad (ITO\ electrode)$$

$$CPZ^{\dot{+}} + \frac{1}{2}H_2O_2 \rightarrow CPZ^{2+} + H_2O$$

$$CPZ^{2+} + CPZ \rightarrow 2CPZ^{\dot{+}}$$

$$CPZ^{2+} + H_2O \rightarrow CPZO + 2H^+$$

Mechanism 7-3: The competition between electrode reaction and O_2 for CPZ cation radical

This competition between electrode reaction and chemical oxidation of $CPZ^{\dot{+}}$ means that the decay to the baseline when the light is removed is not rapid. It also means that the

occurrence of the addition chemical pathway reduces the efficiency of the PG cell (light energy is" wasted" in the photosynthesis rather than in conversion to electrical energy).

Nevertheless, the cell was examined to determine its performance as a PG system. In these experiments, the current flowing through the cell was recorded with the voltage across the cell under varying electrical loads over the cell on illumination. The results are reported in figure 7.29.

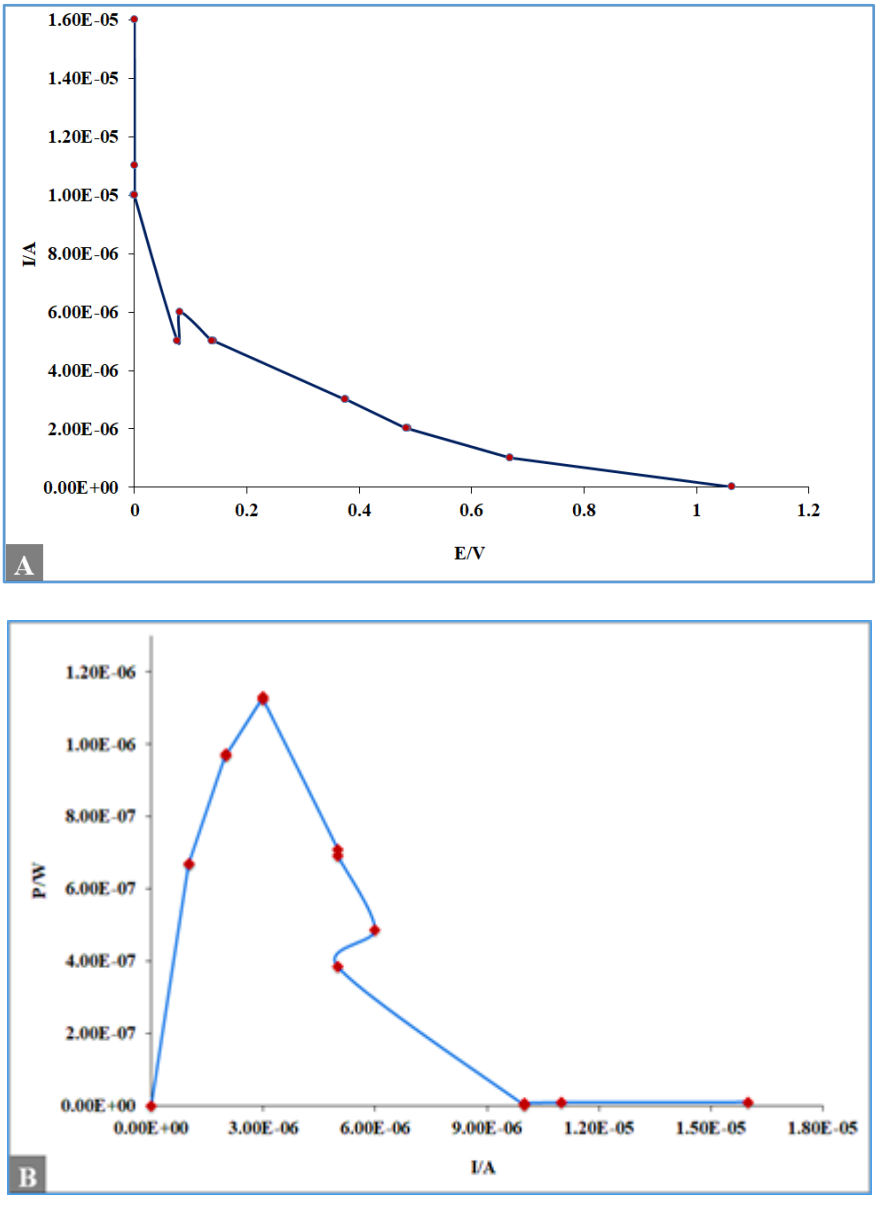

Figure 7.29: The voltammograms of electrical performance of the PG cell under illumination; A: current vis voltage and B: power vis current

It is clear that the cell characteristics result in those of a perfect PG cell (equation 7.14 *vis* figure 7.29 A). This graph 7.29 A has the approximate form of that reported in equation 7.14 for the perfect photogalvanic cell. On rearranging equation 7.14, it is observed that $i = \frac{q}{R_s C_{dl}} - \frac{V}{R_s}$. From this, it can be deduced that Rs = 100 kΩ and $\frac{q}{C_{dl}} = 7.5 \times 10^{-6} = 0.75\ V$, which is approx. the electromotive force (emf).

Ve The maximum power density (5.8 μW cm^{-2} occurs when the current flowing is 3μA. This power rating is sufficient to run only basic electronic devices. The power conversion efficiency (PCE) of this PG cell is:

$$PCE = 100 \times \frac{P_{max}}{P_{incident}} = 100 \times \frac{5.8 \times 10^{-6}}{1 \times 10^{-3}} = 0.58\%$$

This efficiency is amongst the best observed for photogalvanic cells. The fill factor for the system is given by equation 7.28.

$$FF = \frac{5.8 \times 10^{-6}}{(\frac{1.6 \times 10^{-5}}{0.1963})(1.064)} \times 100 = 6.6\%$$

This value is far from the perfect case of 25%. Hence, it follows that there is significant room for improving the performance of these cells, owing to the wastage of light through induced chemical reaction. One way to achieve a better performing cell is through the use of a CPZ derivatives that hinders (slow down) the rate of sulfoxide formation (oxidation), which is developing pathways to stabilise the CPZ^{+} species.

7.4 Conclusion

This chapter has examined the use of two different types of self-assembly for the development of electron transfer cascades: the first using droplets randomly sprinkled over the electrode surface; the second using lyotropic liquid crystals. The latter have been investigated for use in a photo-galvanic cell.

In the first part, two pigments chl a and Tchl were investigated in droplets immobilised onto different sizes and materials of WE. Also, the work examined many parameters of these pigments such as concentrations, solubility and electrolytes under the light and dark environment. Voltammetric results in this section have illustrated there is a clear anodic signal in the organic electrolyte, and there was a small anodic signal in the inorganic electrolyte. For the case of the oxidation of Tchl doped on macro GCE /light (on/off), vitamin K_1 and organic solution DCM, it has been seen that it affords a single oxidation peak regardless of VK_1 concentrations. No apparent light-induced effects have been observed, which means using the plant pigment in LCs need more study to meet requirements.

The results in the second section show for the first time that CPZ.HCl forms, at high monomer molality, a lamellar lyotropic liquid crystal; there are marked changes in the system on increasing the concentration of CPZ, leading to the formation of gel-like materials. These have been characterised by a number of methods including optical microscopy, X-ray scattering, viscosity and voltammetry. This phase is not photochemically stable-it changes colour on exposure to air and light from yellow to deep red, with loss of optical anisotropy. A single pair of well-defined oxidation/reduction signals were observed on different working electrode diameters. A scan rate voltammetric study indicated that this oxidation is consistent with a DISP1 process, with a first-order

rate constant and diffusion coefficient being extracted from the experimental data to be 0.6 s^{-1} and 2 x 10^{-12} m^2 s^{-1}, respectively. The application of this CPZ-LLC system in the photogalvanic cell was considered. As expected, given the first-order disproportionation process, non-steady photo-voltages were observed, as a result of competition between electrode reaction and chemical oxidation of CPZ^{+}. Thus, the efficiency of the PG cell was limited by photosynthesis rather than in conversion of light into electrical energy. The values of the power conversion efficiency and the fill factor for the system of this PG cell were 0.58% and 6.6%, respectively. The fill factor value is far from the perfect case of 25%. In terms of the consumptions light in this system, there are considerable opportunities to design the molecule to meet the requirement of efficient PG cells.

7.5 References

(1) Bahadur, B. editor.: *Liquid Crystals- Applications and Uses*; World scientific, **1990**; Vol. 1.

(2) Sluckin, T. J.; Dunmur, D. A.; Stegemeyer, H.: *Crystals that flow: Classic papers from the history of liquid crystals*; Taylor & Francis London, **2004**.

(3) Reinitzer, F. Beiträge zur kenntniss des cholesterins. *Monatshefte für Chemie/Chemical Monthly* **1888**, *9*, pp 421-441.

(4) Singh, S.; Dunmur, D. A.: *Liquid crystals: fundamentals*; World Scientific, **2002**.

(5) Geelhaar, T.; Griesar, K.; Reckmann, B. 125 Years of liquid crystals—a scientific revolution in the home. *Angew. Chem. Int. Ed.*, **2013**, *52*, pp 8798-8809.

(6) Kawamoto, H. The history of liquid-crystal displays. *P Ieee* **2002**, *90*, pp 460-500.

(7) Erdmann, D. Twenty years of liquid crystal research at Merck. *Gen. Rev.*, **1988**, pp 3-5.

(8) Kamei, H.; Katayama, Y.; Ozawa, T. Photovoltaic effect in the nematic liquid crystal. *Jpn. J. Appl. Phys.*, **1972**, *11*, pp 1385.

(9) Labes, S. K. a. M. M. Molecular Crystals and Liquid Crystals. **1969**, *7*, pp 11.

(10) Gray, G. W.; Harrison, K. J.; Nash, J. A. New Family of Nematic Liquid-Crystals for Displays. *Electron. Lett.* **1973**, *9*, pp 130-131.

(11) Chandrasekhar, S.; Sadashiva, B.; Suresh, K. Liquid crystals of disc-like molecules. *pramana.*, **1977**, *9*, pp 471-480.

(12) Akarslan, F.: Photovoltaic systems and applications. In *Modeling and Optimization of Renewable Energy Systems*; InTech, **2012**.

(13) Kippelen, B.; Yoo, S.; Haddock, J.; Domercq, B.; Barlow, S.; Minch, B.; Xia, W.; Marder, S.; Armstrong, N.: Liquid-Crystal Approaches to Organic Photovoltaics. In *Organic Photovoltaics*; Optical Science and Engineering; CRC Press, **2005**.

(14) Gregg, B. A.; Fox, M. A.; Bard, A. J. Photovoltaic effect in symmetrical cells of a liquid crystal porphyrin. *J. Phys. Chem. A.*, **1990**, *94*, pp 1586-1598.

(15) Adam, D.; Schuhmacher, P.; Simmerer, J.; Häussling, L.; Siemensmeyer, K.; Etzbachi, K.; Ringsdorf, H.; Haarer, D. Fast photoconduction in the highly ordered columnar phase of a discotic liquid crystal. *Nature.*, **1994**, *371*, pp 141-143.

(16) Carrasco‐Orozco, M.; Tsoi, W. C.; O'Neill, M.; Aldred, M. P.; Vlachos, P.; Kelly, S. M. New photovoltaic concept: liquid‐crystal solar cells using a nematic gel template. *Adv. Mater.*, **2006**, *18*, pp 1754-1758.

(17) Blake, P.; Brimicombe, P. D.; Nair, R. R.; Booth, T. J.; Jiang, D.; Schedin, F.; Ponomarenko, L. A.; Morozov, S. V.; Gleeson, H. F.; Hill, E. W. Graphene-based liquid crystal device. *Nano. lett.*, **2008**, *8*, pp 1704-1708.

(18) Stillings, C.; Pettau, R.; Wendorff, J. H.; Schmidt, H. W.; Kreger, K. Lamellar nano confinements effects in discotic liquid crystalline block copolymers. *Macromol. Chem. Phys.*, **2010**, *211*, pp 250-258.

(19) Hirai, T.; Osumi, S.; Ogawa, H.; Hayakawa, T.; Takahara, A.; Tanaka, K. Precise Synthesis and Surface Wettability of a Polymer with Liquid Crystalline Side Chains. *Macromolecules.*, **2014**, *47*, pp 4901-4907.

(20) Liu, Y.; Wu, W.; Wei, J.; Yu, Y. Visible Light Responsive Liquid Crystal Polymers Containing Reactive Moieties with Good Processability. *ACS Appl. Mater. Interfaces.*, **2016**, *9*, pp 782-789.

(21) Dierking, I. Chiral liquid crystals: Structures, phases, effects. *Symmetry.*, **2014**, *6*, pp 444-472.

(22) Jia, Y.-G.; Su, D.; Guo, Z.-H.; Hu, J.-S. Synthesis and characterisation of new nematic liquid crystalline compounds-based thiophene units. *Mol. Cryst. Liq. Cryst.*, **2016**, *624*, pp 91-102.

(23) Zhang, R.; Zeng, X.; Prehm, M.; Liu, F.; Grimm, S.; Geuss, M.; Steinhart, M.; Tschierske, C.; Ungar, G. Honeycombs in honeycombs: complex liquid crystal alumina composite mesostructures. *ACS nano.*, **2014**, *8*, pp 4500-4509.

(24) Soberats, B.; Yoshio, M.; Ichikawa, T.; Zeng, X.; Ohno, H.; Ungar, G.; Kato, T. Ionic Switch Induced by a Rectangular–Hexagonal Phase Transition in Benzenammonium Columnar Liquid Crystals. *J. Am. Chem. Soc.*, **2015**, *137*, pp 13212-13215.

(25) Fenzl, C.; Hirsch, T.; Wolfbeis, O. S. Photonic crystals for chemical sensing and biosensing. *J. Am. Chem. Soc.*, **2014**, *53*, pp 3318-3335.

(26) Xu, Z.; Gao, C. Graphene in macroscopic order: liquid crystals and wet-spun fibers. *Acc. Chem. Res.*, **2014**, *47*, pp 1267-1276.

(27) Zhou, S.: Elasticity, viscosity, and orientational fluctuations of a lyotropic chromonic nematic liquid crystal disodium cromoglycate. In *Lyotropic Chromonic Liquid Crystals*; *Springer*.,, **2017**; pp 51-75.

(28) Zhou, S., Shiyanovskii, S.V., Park, H.S. and Lavrentovich, O.D. Fine structure of the topological defect cores studied for disclinations in lyotropic chromonic liquid crystals. *Nat. Commun.*, **2017**, *8*.

(29) Zheng, Z.-g.; Li, Y.; Bisoyi, H. K.; Wang, L.; Bunning, T. J.; Li, Q. Three-dimensional control of the helical axis of a chiral nematic liquid crystal by light. *Nature.*, **2016**, *531*, pp 352-356.

(30) Goossens, K.; Lava, K.; Bielawski, C. W.; Binnemans, K. Ionic liquid crystals: versatile materials. *Chem. Rev.*, **2016**, *116*, pp 4643-4807.

(31) Zhu, C.; Tuchband, M. R.; Young, A.; Shuai, M.; Scarbrough, A.; Walba, D. M.; Maclennan, J. E.; Wang, C.; Hexemer, A.; Clark, N. A. Resonant carbon K-edge soft X-ray scattering from lattice-free heliconical molecular ordering: soft dilative elasticity of the twist-bend liquid crystal phase. *Phys. Rev. Lett.*, **2016**, *116*, pp 147803.

(32) Solanki, R.; Sharma, V.; Patel, R. Dependence of thermotropic mesomorphism on molecular flexibility of changing tail group. *Mol. Cryst. Liq. Cryst.*, **2016**, *631*, pp 107-115.

(33) An, J.-G.; Hina, S.; Yang, Y.; Xue, M.; Liu, Y. Characterization of Liquid Crystals: A Literature Review. *Rev. Adv. Mater. Sci.*, **2016**, *44*.

(34) Kelly, S.; O'Neill, M. Liquid crystals for electro-optic applications. University of Hull, **2000**.

(35) Middleman, S.; Hochberg, A. K.: *Process engineering analysis in semiconductor device fabrication*; Mcgraw-Hill College, **1993**.

(36) Richard, F. D.; Sally, J. D.: Organic chemistry Wm. C. Brown Publishers, **1996**.

(37) Kamat, P. V.; Tvrdy, K.; Baker, D. R.; Radich, J. G. Beyond photovoltaics: semiconductor nanoarchitectures for liquid-junction solar cells. *Chem. Rev.*, **2010**, *110*, pp 6664-6688.

(38) Schmidt-Mende, L.; Fechtenkötter, A.; Müllen, K.; Moons, E.; Friend, R. H.; MacKenzie, J. Self-organized discotic liquid crystals for high-efficiency organic photovoltaics. *Science.*, **2001**, *293*, pp 1119-1122.

(39) Collings, P. J.: *Liquid crystals: nature's delicate phase of matter*; Princeton University Press, **2002**.

(40) Tamhane, K. Formation of lyotropic liquid crystals through the self-assembly of bile acid building blocks. University of Central Florida, 2009.

(41) Goodby, J.; Görtz, V.; Cowling, S.; Mackenzie, G.; Martin, P.; Plusquellec, D.; Benvegnu, T.; Boullanger, P.; Lafont, D.; Queneau, Y. Thermotropic liquid crystalline glycolipids. *Chem. Soc. Rev.*, **2007**, *36*, pp 1971-2032.

(42) Hamley, I. W. Liquid crystal phase formation by biopolymers. *Soft Matter.*, **2010**, *6*, pp 1863-1871.

(43) Bahadur, B.: *Liquid Crystals—Applications and Uses:(Volume 1)*; World Scientific, **1990**; Vol. 1.

(44) Grzelczak, M.; Vermant, J.; Furst, E. M.; Liz-Marzán, L. M. Directed self-assembly of nanoparticles. *ACS. nano.*, **2010**, *4*, pp 3591-3605.

(45) Yun, S.-H.; Yoo, S. I.; Jung, J. C.; Zin, W.-C.; Sohn, B.-H. Highly ordered arrays of nanoparticles in large areas from diblock copolymer micelles in hexagonal self-assembly. *Chem. Mater.*, **2006**, *18*, pp 5646-5648.

(46) Cao, G.; Brinker, C. J.: *Annual review of nano research*; *World Sci.*, , **2006**; Vol. 1.

(47) Correia, A.; Pérez, M.; Sáenz, J.; Serena, P. Nanoscience and nanotechnology–driving research and applications. *Phys. Status Solidi (RRL)-Rapid Research Letters.*, **2007**, *1(4)*.

(48) Nath, D.; Banerjee, P. Green nanotechnology–A new hope for medical biology. *Environ. Toxicol. Pharmacol.*, **2013**, *36*, pp 997-1014.

(49) Roco MC, B. W. Societal implications of nanoscience and nanotechnology: Maximizing human benefit. *J. Nanopart. Res.*, **2005**, *1*, pp 1-3.

(50) Koltover, I.; Salditt, T.; Rädler, J. O.; Safinya, C. R. An inverted hexagonal phase of cationic liposome-DNA complexes related to DNA release and delivery. *Science.*, **1998**, *281*, pp 78-81.

(51) Pomerantz, W. C.; Yuwono, V. M.; Drake, R.; Hartgerink, J. D.; Abbott, N. L.; Gellman, S. H. Lyotropic liquid crystals formed from ACHC-rich β-peptides. *J. Amer. Chem. Soc.,* **2011**, *133*, pp 13604-13613.

(52) Zhou, S.: *Lyotropic chromonic liquid crystals: From viscoelastic properties to living liquid crystals*; Springer, **2017**.

(53) Abdulhalim, I.; Moses, R.; Sharon, R. Biomedical optical applications of liquid crystal devices. *Acta Phys. Pol. A.,* **2007**, *112*, pp 715.

(54) Dellinger, T. M.; Braun, P. V. Lyotropic liquid crystals as nanoreactors for nanoparticle synthesis. *Chem. Mater.,* **2004**, *16*, pp 2201-2207.

(55) Hegmann, T.; Qi, H.; Marx, V. M. Nanoparticles in liquid crystals: synthesis, self-assembly, defect formation and potential applications. *J Inorg Organomet Polym Mater.,* **2007**, *17*, pp 483-508.

(56) Wysocki, J.; Adams, J.; Haas, W. Electric-field-induced phase change in cholesteric liquid crystals. *Phys. Rev. Lett.,* **1968**, *20*, pp 1024.

(57) Bremer, M.; Kirsch, P.; Klasen‐Memmer, M.; Tarumi, K. The TV in Your Pocket: Development of Liquid‐Crystal Materials for the New Millennium. *Angew. Chem. Int. Ed.,* **2013**, *52*, pp 8880-8896.

(58) Pauluth, D.; Tarumi, K. Advanced liquid crystals for television. *J. Mater. Chem.,* **2004**, *14*, pp 1219-1227.

(59) Abu-Abed, A. S.; Lindquist, R. G. Capacitive transduction for liquid crystal based sensors, part II: Partially disordered system. *IEEE Sens. J.,* **2008**, *8*, pp 1557-1564.

(60) Yang, K.-L.; Cadwell, K.; Abbott, N. L. Use of self-assembled monolayers, metal ions and smectic liquid crystals to detect organophosphonates. *Sens. Actuator B-Chem.,* **2005**, *104*, pp 50-56.

(61) Matsui, T.; Ozaki, R.; Funamoto, K.; Ozaki, M.; Yoshino, K. Flexible mirrorless laser based on a free-standing film of photopolymerized cholesteric liquid crystal. *Appl. Phys Lett.,* **2002**, *81*, pp 3741-3743.

(62) Park, J.; Shin, M.; Lee, C. C. Measurement of temperature profiles on visible light-emitting diodes by use of a nematic liquid crystal and an infrared laser. *Opt. Lett.,* **2004**, *29*, pp 2656-2658.

(63) Moreira, M.; Carvalho, I.; Cao, W.; Bailey, C.; Taheri, B.; Palffy-Muhoray, P. Cholesteric liquid-crystal laser as an optic fiber-based temperature sensor. *Appl. Phys Lett.,* **2004**, *85*, pp 2691-2693.

(64) Smalyukh, I. I.; Kaputa, D. S.; Kachynski, A. V.; Kuzmin, A. N.; Prasad, P. N. Optical trapping of director structures and defects in liquid crystals using laser tweezers. *Opt. Express.,* **2007**, *15*, pp 4359-4371.

(65) Manzanera, S.; Prieto, P. M.; Ayala, D. B.; Lindacher, J. M.; Artal, P. Liquid crystal Adaptive Optics Visual Simulator: Application to testing and design of ophthalmic optical elements. *Opt. Express.,* **2007**, *15*, pp 16177-16188.

(66) Kim T, L. M.: Visual simulation of ice crystal growth. InProceedings of the 2003 ACM SIGGRAPH/Eurographics symposium on Computer animation. In *Proceedings of the 2003 ACM SIGGRAPH/Eurographics Symposium on Computer animation*; Eurographics Association, **2003**; pp 86-97.

(67) Maruyama, M. a. K., K., Nec Corporation., : Transmission liquid crystal display with a reduced dependency of a display quality upon a visual angle. United States patent US 5,600,456, **1997**.

(68) Suzuki, T.; Nakamura, M.; Sumida, H.; Shigeta, A. Liquid crystal make-up remover: conditions of formation and its cleansing mechanisms. *J. Soc Cosmet. Chem.*, **1992**, *43*, pp 21-36.

(69) Viswanath, I. K.; Murthy, Y.; Kondalarao, T. Mesophase behaviour of 1, 3-diacyloxy and 1, 4-diacyloxy esters. *Der Pharma Chemica.*, **2016**, *8*, pp 154-161.

(70) Yoneta, H.; Murouchi, S.; Watanabe, H.: Wholly aromatic polyester, composition thereof, and molded article made therefrom. Google Patents, **1997**.

(71) Xie, X.; Stueben, D.; Berner, Z. The application of microelectrodes for the measurements of trace metals in water. *Anal. Lett.*, **2005**, *38*, pp 2281-2300.

(72) Qureshi, A.; Kang, W. P.; Davidson, J. L.; Gurbuz, Y. Review on carbon-derived, solid-state, micro and nano sensors for electrochemical sensing applications. *Diam. Relat. Mater.*, **2009**, *18*, pp 1401-1420.

(73) Fleischmann, M.; Lasserre, F.; Robinson, J.; Swan, D. The application of microelectrodes to the study of homogeneous processes coupled to electrode reactions. *J.Electroanal.Chem.*, **1984**, *177*, pp 97-114.

(74) Zoski, C. G.; Simjee, N.; Guenat, O.; Koudelka-Hep, M. Addressable microelectrode arrays: Characterization by imaging with scanning electrochemical microscopy. *Anal. Chem.*, **2004**, *76*, pp 62-72.

(75) Bond, A. M.; Fleischmann, M.; Robinson, J. Electrochemistry in organic solvents without supporting electrolyte using platinum microelectrodes. *J.Electroanal. Chem. Interfac.*, **1984**, *168*, pp 299-312.

(76) Stett, A.; Egert, U.; Guenther, E.; Hofmann, F.; Meyer, T.; Nisch, W.; Haemmerle, H. Biological application of microelectrode arrays in drug discovery and basic research. *Anal. Bioanal. Chem.*, **2003**, *377*, pp 486-495.

(77) Evans, L. A.; Thomasson, M. J.; Kelly, S. M.; Wadhawan, J. Electrochemical Determination of Diffusion Anisotropy in Molecularly-Structured Materials. *J. Phys. Chem C.*, **2009**, *113*, pp 8901-8910.

(78) Ensafi, A. A.; Arabzadeh, A. A new sensor for electrochemical determination of captopril using chlorpromazine as a mediator at a glassy carbon electrode. *J. Anal. Chem.*, **2012**, *67*, pp 486-496.

(79) Ensafi, A. A.; Taei, M.; Khayamian, T.; Karimi-Maleh, H.; Hasanpour, F. Voltammetric measurement of trace amount of glutathione using multiwall carbon nanotubes as a sensor and chlorpromazine as a mediator. *J. Solid State. Chem.*, **2010**, *14*, pp 1415-1423.

(80) Novak, I.; Komorsky-Lovrić, Š. Square-Wave Voltammetry of Sodium Copper Chlorophyllin on Glassy-Carbon and Paraffin-Impregnated Graphite Electrode. *Electroanalysis.*, **2012**, *24*, pp 1957-1965.

(81) Attwood, D.; Florence, A.; Gillan, J. Micellar properties of drugs: properties of micellar aggregates of phenothiazines and their aqueous solutions. *J. Pharm. Sci.*, **1974**, *63*, pp 988-993.

(82) Beltran, D.; Chan, S.; Keyzer, H.: Anion Charge Transfer in Biologically Active Systems. In *Bioelectrochemistry*; Springer, **1980**; pp 185-207.

(83) Soltz, B. A.; Corey, J. Y.; Larsen, D. W. Molecular motion in chlorpromazine and chlorpromazine hydrochloride. *J. Phys. Chem.*, **1979**, *83*, pp 2162-2166.

(84) Ateş, S.; Somer, G. Photodegradation of chlorpromazine in aqueous solutions as studied by ultraviolet-visible spectrophotometry and voltammetry. *J. Chem. SOC., Faraday Trans.*, **1981**, *77*, pp 859-867.

(85) Halls, J. E.; Wright, K. J.; Pickersgill, J. E.; Smith, J. P.; Altalhi, A. A.; Bourne, R. W.; Alaei, P.; Ramakrishnappa, T.; Kelly, S. M.; Wadhawan, J. D. Voltammetry within structured liquid nanosystems: Towards the design of a flexible, three-dimensional framework for artificial photosystems. *Electrochim. Acta.*, **2012**, *70*, pp 215-227.

(86) Banks, C. E.; Davies, T. J.; Evans, R. G.; Hignett, G.; Wain, A. J.; Lawrence, N. S.; Wadhawan, J. D.; Marken, F.; Compton, R. G. Electrochemistry of immobilised redox droplets: Concepts and applications. *Phys. Chem. Chem. Phys.*, **2003**, *5*, pp 4053-4069.

(87) Wadhawan, J. D.; Wain, A. J.; Kirkham, A. N.; Walton, D. J.; Wood, B.; France, R. R.; Bull, S. D.; Compton, R. G. Electrocatalytic Reactions Mediated by N,N,N‘,N‘-Tetraalkyl-1,4-phenylenediamine Redox Liquid Microdroplet-Modified Electrodes: Chemical and Photochemical Reactions In, and At the Surface of, Femtoliter Droplets. *J. Am. Chem. Soc.*, **2003**, *125*, pp 11418-11429.

(88) Zhou, Y. Molecular Electrochemistry. The University of Hull. PhD thesis, **2012**.

(89) Hough, E.; Hjorth, M.; Dahl, S. The structures of (dimethylaminopropyl) phenothiazine drugs and their metabolites. II. Chlorpromazine sulphoxide, $C_{17}H_{19}ClN_2OS$, at 120 K. *Acta Crystallogr. C.*, **1985**, *41*, pp 383-386.

(90) Weihs, D.; Kesselman, E.; Schmidt, J.; Talmon, Y.; Sasuga, S.; Fujita, T.; Izawa, K.-I.; O’Connor, C. J.; Okabayashi, H.-F. Complex, Dynamic Behavior of Extremely Asymmetric Di-n-Alkylphosphate-Anion Aggregates, the Long-Chain Effect and the Role of a Limiting Size: Cryo-TEM, SANS, and X-Ray Diffraction Studies. *J. Phys. Chem. B.*, **2017**, *121*, pp 4099-4114.

(91) Attwood, D.; Waigh, R.; Blundell, R.; Bloor, D.; Thévand, A.; Boitard, E.; Dubès, J. P.; Tachoire, H. ^{1}H and ^{13}C NMR studies of the self‐association of chlorpromazine hydrochloride in aqueous solution. *Magn. Reson. Chem.*, **1994**, *32*, pp 468-472.

(92) Deputy, A.; HUAN-PING, W.; McCreery, R. L. Spatially resolved spectroelectrochemical examination of the oxidation of dopamine by chlorpromazine cation radical. *J. Phys. Chem.*, **1990**, *94*, pp 3620-3624.

(93) Amatore, C.; Savéant, J. ECE and disproportionation: Part VI. General resolution. Application to potential step chronoamperometry. *J. electro anal. chem. interfacial electrochem.*, **1979**, *102*, pp 21-40.

(94) Halls, J. E.; Hawthornthwaite, A.; Hepworth, R. J.; Roberts, N. A.; Wright, K. J.; Zhou, Y.; Haswell, S. J.; Haywood, S. K.; Kelly, S. M.; Lawrence, N. S.

Empowering the smart grid: can redox batteries be matched to renewable energy systems for energy storage? *Energy Environ. Sci.*, **2013**, *6*, pp 1026-1041.

(95) Halls, J. E.; Wadhawan, J. D. Photogalvanic cells based on lyotropic nanosystems: towards the use of liquid nanotechnology for personalised energy sources. *Energy Environ. Sci.*, **2012**, *5*, pp 6541-6551.

Chapter 8

Conclusions and Future works

8.1 Conclusion

Due to the enormous demand for energy, the attention has been focused on new and renewable energy resources. Artificial photosynthesis has been introduced to simulate and apply the principles of converting solar energy into chemical fuels that occur during natural photosynthesis. Although numerous attempts have been made to achieve high efficiencies of converting solar energy, no materials meet the all of the requirements, *i.e.*, electronic properties, band gap and band edge position. The overall aim of this study was to explore some electroactive species and then investigate their properties in the LCs system, which can be used as artificial solar cells. The characteristics and redox process for some electroactive species such as chlorpromazine hydrochloride in a buffer solution at glassy carbon electrode were studied.

The electroactive species such as L-cysteine and potassium iodide were used to investigate the electrocatalytic reduction of CPZ.HCl in bulk solution. Regarding the use of the working electrode, glassy carbon electrode provided a well-defined peak current upon the introduction of higher concentrations of these active species.

The electrochemical techniques that were used (voltammetry including at a rotating disk electrode) successfully explored the electrochemistry of CPZ.HCl. The environment of the electrocatalytic process was elucidated in solution, and the result showed that the electrocatalytic reaction of CPZ.HCl in present of L-Cys.H was EC' (primary reaction).

All the electrochemistry experiments demonstrated that the oxidative peaks current of CPZ.HCl at GCE are dependent on the concentration of species, and this affects the kinetic parameters of the electrocatalytic process through the changed diffusion coefficients of CPZ.HCl.

The electrochemical method showed that the cyclic voltammetry responses of adsorbing chlorophyllin pigment on the gold electrode were more efficient than glassy carbon electrode. In addition, the electrochemical reaction occurred more easily in the aqueous solution than the organic solution. For the case of the electroactive species potassium iodide, it was difficult to reproduce the electrochemistry.

Chlorophyllin preferentially adsorbs to gold electrode than glassy carbon electrode. Adsorbed chlorophyllin was able to participate in an electron transfer relay with iodide. The mechanism of the reaction was suggested to be a one-electron transfer.

Total chlorophyll (Tchl) pigment was identified in this work using various techniques (TLC, and UV-Visible). The electron transfer cascade of this pigment on the gold surface exhibited larger than glassy carbon surface. It was observed that there were increases in peak current and peak potential with an increase in the scan rates of Tchl combined with Triton X100, vitamin K_1 in aqueous solution (HCl), due to the role of the surfactant in the bulk solution. The two pigments chl a and Tchl were investigated in this thesis using coulometry and amperometry methods; there was a single oxidation peak in the system of the later pigment/VK_1.

This work developed a new liquid crystal: the L_α lamellar structure of chlorpromazine hydrochloride in water. This material was characterised including using X-ray scattering, pH meter, viscometer, conductivity meter, UV-Vis spectrometer and cyclic voltammetry. The material is stable and undergoes a slow, first order disproportionation on electrochemical oxidation.

Furthermore, the new L_α liquid crystal was used to generate electrical energy within a photogalvanic cell. The system CPZ.HCl-LCs was operated under the visible light showed a poor efficiency responding in the galvanic cell.

8.2 Future works

The thesis recommends that future studies are the following.

- Seeking to increase the efficiency of plant pigment/LC system through the introduction of other light-harvesting molecules such as hematochrome, carotene or xanthophyll to furnish photo-reductive chromonic liquid crystals, which may be exploited either light as sensors or as photogalvanic cells.
- Using high concentrations for some of the chlorpromazine derivatives, which may produce micelles and form L_{α} phase.
- Can be applied L_{α} phase of the liquid crystal in the photogalvanic cell (PG), which it compares later with CPZ.HCl-LCs using the same conditions.
- The efficiency of the cell is limited by the disproportionation reaction, therefore remove this it became better.
- Developing a new potential application of CPZ-LCs of its derivatives in the field of biosensors.

Chapter 9

Appendix

9.1 Conferences

- 5th PhD Experience Conference, (14-15th) April 2014, University of Hull, attending.
- 9th Post-Graduate Research Topics Meeting in Electroanalysis and Sensing, 4th December 2014 at Birkbeck, University of London, attending.
- 6th PhD Experience Conference, (7-8th) April 2015, University of Hull, poster.
- PhD Symposium – Lightning Talk, 8th of October 2015, University of Hull, poster presentation.
- SCI Electrochemistry Postgraduate Conference in partnership with ISE & RSC, 26th of May 2016, University College London, poster presentation.
- Chemistry Department Colloquium, 21st July 2016, Hull University, presentation.
- Analytical Research Forum (ARF) conference, 8th July 2016, Burlington House, Piccadilly, London, attending.
- 5th UK Solar Fuels Symposium and Postgraduate Afternoon Newcastle upon Tyne, (26-27th) January 2017, attending.

9.2 Memberships

- Royal Society of Chemistry (RSC).
- Science Chemistry Innovation (SCI).